TRACE METAL GEOCHEMISTRY OF BRACHIOPOD CALCITE: A NEW WINDOW TO THE PAST

SCOTT BUTLER

Submitted in partial fulfilment of the requirements for the degree of PhD

March 2015

DECLARATION

This work has not been submitted in substance for any other degree or award at this or any other university or place of learning, nor is being submitted concurrently in candidature for any degree or other award.

Signed …… (candidate) Date ……

This thesis is being submitted in partial fulfillment of the requirements for the degree of ……(insert MCh, MD, MPhil, PhD etc, as appropriate)

Signed …… (candidate) Date ……

This thesis is the result of my own independent work/investigation, except where otherwise stated.

Other sources are acknowledged by explicit references. The views expressed are my own.

Signed …… (candidate) Date ……

I hereby give consent for my thesis, if accepted, to be available online in the University's Open Access repository and for inter-library loan, and for the title and summary to be made available to outside organisations.

Signed …… (candidate) Date ……

I hereby give consent for my thesis, if accepted, to be available online in the University's Open Access repository and for inter-library loans **after expiry of a bar on access previously approved by the Academic Standards & Quality Committee.**

Signed …… (candidate) Date

……

ABSTRACT

The Mg/Ca temperature proxy was applied for the first time to seasonality records in calcitic brachiopod shells, using a laser ablation tracking technique on both Recent and fossil material. Seawater temperature calibrations were established using modern *Terebratulina retusa* from Scottish waters with annual temperature variations ~7 °C, and *Liothyrella neozelanica* from a water depth transect (168–1488 m) off New Zealand. Comparison of intra-shell Mg/Ca with shell $\delta^{18}O$ confirms a temperature control on brachiopod Mg/Ca. Preliminary temperature calibrations are:

T. retusa $Mg/Ca=1.76\pm0.27e^{(0.16 \pm 0.03)T}$, $R^2=0.75$

L. neozelanica $Mg/Ca=0.49 \pm 1.27e^{(0.2 \pm 0.11)T}$, $R^2=0.32$.

The Eocene-Oligocene Transition (EOT) is the first time during the Cenozoic that Antarctica was permanently glaciated. Mg/Ca and $\delta^{18}O$ of brachiopod calcite from two New Zealand sites, one Late Eocene and one Early Oligocene, were sampled to assess seasonality over the EOT. Mg/Ca data identify no statistically significant change in seasonality in this area over the EOT. A 1.3 ‰ positive excursion in $\delta^{18}O$ is identified: 0.6 ‰ is attributed to global change in $\delta^{18}O_{seawater}$ and 0.7 ‰ to regional change in $\delta^{18}O_{seawater}$. Surface currents remained the same around New Zealand across the EOT. Summer Mg/Ca seawater temperatures (~21-24°C) in New Zealand are similar to temperatures derived from TEX_{86} (Site 1172).

The Silurian Ireviken Excursion (~428 Ma) is a worldwide $\delta^{13}C$ and $\delta^{18}O$ isotopic excursion. *Atrypa* from Gotland, Sweden was sampled from before and after this Llandovery/Wenlock excursion. Mg/Ca and $\delta^{18}O$ data indicate no significant change in seawater temperature over this excursion, against a shift of 1.29 ‰ in $\delta^{13}C$. Relative temperature changes between summer and winter Mg/Ca suggest seasonality of 3.5–5.4 °C. Estimated seawater temperature ~37 °C agrees with a recent clumped isotope study. High temperatures obtained in another study may be attributable to sampling that incorporated the outer side half of the secondary layer.

ACKNOWLEDGMENTS

I would like to start by thanking my three supervisors; from Cardiff University, Carrie Lear and Lesley Cherns and from the National Museum of Wales, Trevor Bailey. It is fair to say that without your help, guidance and support I would not have been able to complete this thesis. I will forever be grateful to all of you. You have all helped immensely in your own ways. Carrie; you always pushed me to improve my work and I thank you for your countless hours of reading and re-reading it. Trevor; you helped me with the analytical side of my PhD and I thank you for the many hours spent toiling over perfecting the Laser Ablation technique. Lesley; you have been my sounding board not just throughout the PhD but for the last 7 years and I thank you for everything you have done for me. I'd also like to mention that the support all three of you gave me when I first became ill with glandular fever was immense and it really helped me see that there would be light at the end of what felt like a very long tunnel.

I also want to thank Gordon Curry from the University of Glasgow. The specimens you donated to this project were invaluable and formed much of the early calibration work. The chats in Glasgow regarding brachiopods also showed me that I had a lot to learn and quickly. Jeffrey Robinson and Daphne Lee from the University of Otago are also thanked for their time, assistance and hospitable nature. Lesley and I would never have found those localities in North Otago let alone identify the brachiopods if both of you were not there helping us. In addition thanks go to Kareen Schanbel and Sadie Mills from NIWA who were unbelievably helpful in donating specimens and helping us sift through their fantastic invertebrate collection. I will never forget

watching The Best Exotic Marigold Hotel with you both in Wellington, such a fun evening.

I extend my thanks to Amanda Valentine-Baars from the National Museum of Wales. The time you spent teaching me how to set my shells properly in resin was a huge help to me. You also made the hours in the windowless lab more fun. Iain McDonald is also thanked for setting up the laser ablation equipment and for being there when I managed to knock the plasma off, I'm still sorry.

As for thanking friends; there are way too many of you to start naming people individually. However, the football lads of Bough Justice, Rock Bottom and Ideal Standard along with the football girls of Rock Solid made my four years in Cardiff so memorable and I know I've made friends for life. The good people I've met over the last 6 months at David Lloyd Worcester have helped me not only become a semi-decent tennis player but also helped me recover from my illness and have helped to give me a break from my thesis.

Finally a huge thank you to my family, you've always been there for me. You've put up with me for 26 years and I can't thank you enough for everything you've done. You've made my life easier than it should have been and when I became ill you helped me back to health, notably with my shoulder operation and most recently with glandular fever. I love you all. I can't write anymore or I fear I may cry.

AUTHOR'S NOTE

Chapter 4 and the Laser Ablation methodology outlined in Chapter 3 have been published:

Butler, S., T. R. Bailey, C. H. Lear, G. B. Curry, L. Cherns and I. McDonald (2015). "The Mg/Ca–temperature relationship in brachiopod shells: Calibrating a potential palaeoseasonality proxy." Chemical Geology **397**(0): 106-117.

As this work is a multi-author paper the roles of other authors are summarised here. Trevor Bailey provided help with the calibration equations and method development. Caroline Lear and Lesley Cherns contributed towards how best to sample the brachiopod shells and general discussion. Gordon Curry provided th

e *Terebratulina retusa* shells and initial discussion. Iain McDonald helped identify the best parameters for laser ablation and correct standards.

LIST OF CONTENTS

1. INTRODUCTION

1.1 Objectives

This thesis has three primary objectives:

1) Refine (quantify) the Mg/Ca-temperature calibration for brachiopod calcite of individual species or genera.
2) Construct brachiopod intra-shell Mg/Ca records to determine changes in temperature and seasonality in the South Pacific associated with the formation of the Antarctic ice sheet over the Eocene-Oligocene climate transition.
3) Use the Mg/Ca-temperature relationship in brachiopod calcite to test the hypothesis that the Ireviken $\delta^{13}C$ and $\delta^{18}O$ excursions (Llandovery-Wenlock) are associated with an icehouse-greenhouse transition.

1.2 Introduction

Brachiopods have a long geological history, Cambrian – Recent, providing huge potential to use brachiopods for palaeoclimatic research throughout the Phanerozoic. Much of the information we have on Palaeozoic environmental change is derived from quantitative or semi-quantitative data gathered from stable isotopes of brachiopod calcite. Two periods in particular have been the focus of study; Carboniferous glaciations (e.g. Grossman et al., 1993; Mii et al., 1999; Grossman et al., 2008) and the Ireviken Event in the Silurian (e.g. Munnecke et al., 2003; Brand et al., 2006). Whilst $\delta^{18}O$ is a useful proxy, the signal can reflect changes in temperature, changes in $\delta^{18}O$ of the seawater due to ice sheets, changes in local salinity or a combination of these factors. Mg/Ca of biogenic calcite is a widely used palaeotemperature proxy. For example, Mg/Ca and $\delta^{18}O$ of foraminifera have been used effectively to study seawater temperature and seawater $\delta^{18}O$ changes over the

Eocene Oligocene Transition (e.g. Lear et al., 2008). They have also been used to look at rapid warming events such as the Palaeocene Eocene Thermal Maximum (PETM) (e.g. Zachos et al., 2003; Tripati and Elderfield 2005; Zachos et al., 2006; Hollis et al., 2012). One complication in benthic foraminiferal Mg/Ca palaeothermometry is the effect of carbonate saturation state (e.g.,Elderfield et al., 2006; Lear et al., 2010). However this is associated with deep waters and should not affect Mg/Ca in brachiopods from shallow depths. Furthermore, the brachiopod shell is made of the most diagenetically stable form of calcium carbonate, low Mg calcite, meaning that it has the potential to remain unaltered by diagenesis given the right burial conditions.

Using brachiopod Mg/Ca to deconvolve the temperature component of $\delta^{18}O$ excursions therefore provides vast potential for research. Despite this, brachiopod calcite has not fulfilled its potential as a carrier for trace metal proxies due to lack of quantitative calibrations. Only recently has the potential of brachiopod calcite in Mg/Ca as a temperature proxy begun to be investigated in detail (Perez-Huerta et al., 2008; Perez-Huerta et al., 2011; Brand et al., 2013).

In preliminary work for this thesis, a record of published Mg concentration data was compiled from modern terebratulid brachiopod shells from world-wide locations (Lowenstam, 1961; Brand et al., 2003) which indicate that brachiopod shell Mg/Ca potentially increases exponentially with increasing temperature (Figure 1.2-1). The sensitivity was close to that observed in other calcitic organisms, such as foraminifera, e.g. (Lear et al., 2002; Anand et al., 2003). However some of the data, displaying very high Mg/Ca, in the compilation clearly needed to be addressed; a possibility is that these results represent extreme vital effects which influenced the incorporation of Mg into the crystal latttice in certain species or there could be

incorporation of the magnesium-rich primary layer into the analysis (Perez-Huerta et al., 2008).

The trace metal compositions of calcite marine fossils have been used to successfully reconstruct palaeoclimate and environmental conditions over a range of timescales from daily to long-term (m.y.) changes in the Cenozoic (e.g. Lear et al., 2000; Lear & Rosenthal, 2006; Lear et al., 2008; Montagna et al., 2007; Mouchi et al., 2013 and Sosdian et al., 2006). Different organisms are capable of capturing temperature variations on differing time scales. Bivalves, specifically oyster shells have successful been used to calculate temperatures from Mg/Ca at daily (Mouchi et al., 2013) and subweekly resolution (Takesue and Van Geen, 2004). Temperatures at weekly resolution have been resolved in scleractinian corals (Montagna et al., 2007). Seasonal temperature variability has been assessed using Sr/Ca in modern and fossil gastropods (Sosdian et al., 2006; Sosdian et al., 2012) and Mg/Ca in fish otolith bones over the EOT (Ivany et al., 2000). Corals (Mitsuguchi et al., 2008) and bivalves (Carroll et al., 2009) have also been used to assess climate on a decadal scale. Over longer timescales, foraminifera from drift sites with high sedimentation rates have been used to produce trace metal temperature records with decadal-millenial resolution, (e.g. Williams et al., 2010). Foraminifera are more commonly used to produce records with 10kyr-Myr resolution (e.g. Lear et al., 2000; Lear et al., 2004). However foraminifera have no possibility of being used to assess even long term environmental change in most of the Palaeozoic because the earliest foraminifera had organic walls or agglutinated tests; calcareous tests did not evolve until the Carboniferous (Pawlowski et al., 2003).

Brachiopods are a perfect candidate to develop as a palaeoseasonality proxy, their ability to grow all year round enables the trace metals in their shells to capture both

summer and winter temperatures signals (Butler et al., 2015). This allows for reliable seasonality studies to be carried out over the Cenozoic. Even more exciting is the prospect of using brachiopods from the Palaeozoic as both indicators of long term (> million year) climate change and short term (seasonal) climate variability.

Here I set out a general introduction and overview of brachiopods, the EOT and the Ireviken Event in the Silurian. I will deal with specific introductions and background on a chapter by chapter basis.

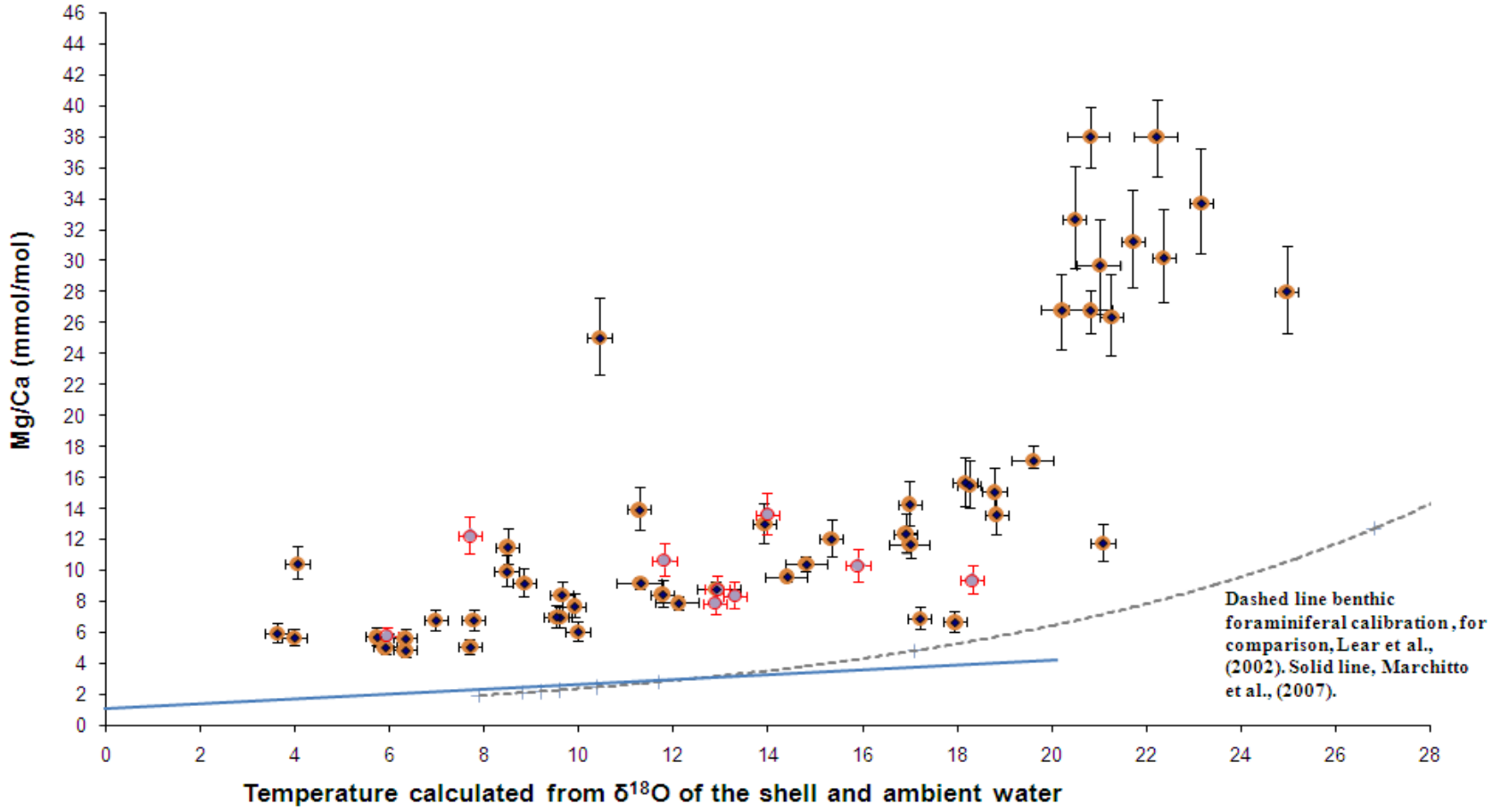

Figure 1.2-1. Initial evidence that brachiopod calcite may have an exponential relationship with temperature Data from Lowensteim 1961 and Brand et al., 2003).

1.3 Brachiopod overview

Brachiopods are sessile marine invertebrates belonging to the phylum Brachiopoda, which are most closely related to other lophophorates, the Bryozoa and Phoronida. The three different types of classification are shown in Table 1.3-1. The brachiopods that are of interest here are the Rhynchonelliformea, formerly known as the Articulata and part of the Calciata. The traditional classification (Huxley, 1869) is based on the presence or absence of teeth and sockets for the articulation of the valves. The Calciata classification was adopted for the original treatise by Williams (1956) and is based on the secretion, shell structure and growth of the calcitic shell. The three-part classification used in the latest treatise was first constructed by cladistics in Williams et al. (1996) and is based on very detailed internal and external morphology. Presently there are two orders of the Rhynchonelliformea, the Terebratulida and the Rhynchonellida, in the Palaeozoic however there was much greater diversity. The Rhynchonelliformea have shells that are composed of low

Traditional Classification	Inarticulata		Articulata
Calciata Classification	Lingulata	Calciata	
Three-Part Classification	Linguliformea	Craniformea	Rhynchonelliformea

Table 1.3-1. Showing three different classifications of brachiopods. The currently used system is the three part classification.

magnesium calcite (Williams, 1956), the most diagenetically stable form of $CaCO_3$ and are therefore the only brachiopods discussed here.

1.4 Brachiopod morphology and ecology

Brachiopods have bilateral symmetry that bisects two valves of different morphology, Figure 1.4-1. Living Terebratulide and Rhynchonellide brachiopods are

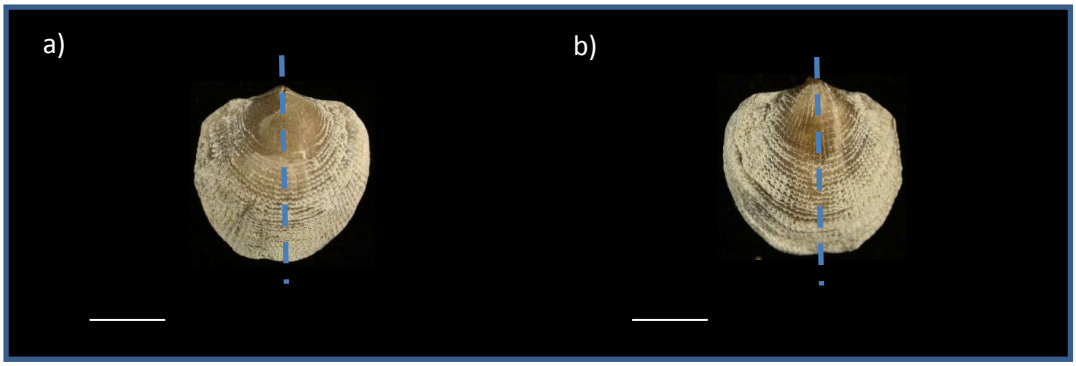

Figure 1.4-1. Bilateral symmetry marked by blue dashed line in fossil *Atrypa*. a) brachial/dorsal valve b) pedicle/ventral valve. Scale bars 0.5 cm.

epifaunal and attached to the substrate by a fleshy pedicle. The pedicle enters the pedicle valve through a posterior opening, the pedicle foramen, at the umbo. The brachial valve is usually, but not always, smaller than the pedicle valve and houses supports for the lophophore used for feeding and respiration. Modern brachiopods live in clustered populations on rocky sea floors. There are fossil examples from the Cambrian Chengjiang fauna, which have been exceptionally preserved, where the brachiopods can be seen to be attaching themselves to each other via their pedicles effectively forming a small colony. The umbo represents the part of the shell that grew in the juvenile stage of life. It lies at the posterior, and is characterised by high convexity and growth lines that are notably close together. Ribs on brachiopods can be indicative of the type of environment that the species live in. This is due to the

fact that ribbed brachiopods are known to live above the wave base; an important factor for looking at palaeo-water depth.

On the internal surface of the shell are the muscle scars, which represent muscles used for opening and closing the valves (adductor, diductor muscles) and attachment of the pedicle (adjustor muscles; Figure 1.4-2). The muscle scars migrate towards

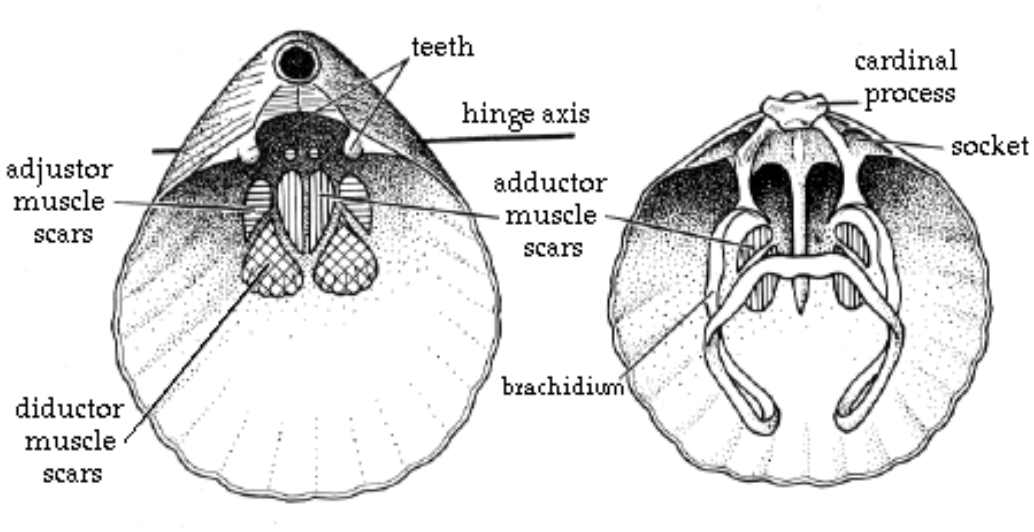

Figure 1.4-2. The internal morphology of a rhynchonelliformean brachiopod shell, Clarkson (1998).

the anterior end of the shell through ontogeny. Teeth and sockets form a hinge mechanism to articulate the two valves in rhynchonelliformean brachiopods. The brachidium is a calcareous support for the lophophore in some but not all brachiopods. The cardinal process is variably shaped secondary shell situated medially in the posterior end of the brachial valve for attachment of the diductor muscles.

1.5 Brachiopod shell growth

The growth bands are only found in the primary layer of the shell, they are thought to be formed biannually and show terminations of shell growth at times of pronounced environmental or physiological disturbance, such as reproduction

(Curry, 1982). I5n *Terebratulina retusa*, from the Firth of Lorne, Scotland occurs regularly in late spring and late autumn in response to water temperatures falling between 10-11 °C (Curry, 1982). The summer growth band is much more substantial than the winter growth band due to the favourable conditions for shell precipitation during these months.

1.6 Brachiopod shell ultrastructure

The shell comprises three or four layers, depending on the species of brachiopod (Williams and Rowell, 1965). The outermost layer is a thin organic layer, the periostracum, which is rarely preserved in fossils. Organics are destroyed early in the taphonomic process except in very exceptional circumstances.

The primary shell layer is the outermost inorganic layer, Figure 1.6-1. It is composed of low magnesium calcite, is very thin (< 50 μm), granular in texture and is easily distinguished from the secondary fibres. Growth lines can be seen in this layer of the shell but not in the secondary or tertiary layers. The primary layer is out of equilibrium with the ambient sea water, which may be because the anterior mantle that secretes the primary layer respires aerobically at four times the rate of the posterior mantle that secretes the secondary layer (Hughes et al., 1988; Rosenburg et al., 1988). This gradient in metabolic activity can be directly correlated with the marked fractionation of oxygen and carbon isotopes in the primary layer calcite, and the more modest vital effects in the secondary layer calcite (Carpenter and Lohmann, 1995). The higher metabolic activity associated with primary layer precipitation may be linked to a larger kinetic fractionation of both oxygen and carbon isotopes during hydroxylation of CO_2 and/or rapid precipitation of the calcite (Carpenter and Lohmann, 1995). Carpenter and Lohmann (1995) suggested that the relatively high

precipitation rates could be related to low $\delta^{18}O$ and $\delta^{13}C$. Similarly, Sosdian et al. (2006) showed that growth rates in the aragonitic gastropod *Conus ermineus* affected the calibration for Sr/Ca. It should therefore be noted that growth rate could potentially affect the distribution of trace elements in the brachiopod shell.

The secondary layer, Figure 1.6-1, is densely packed low Mg calcite fibres bound by cytoplasmic sheaths, which are each secreted by the outer mantle lobes. It is generally in equilibrium with the ambient seawater with regards to Mg/Ca ratios (Perez-Huerta et al., 2008) and $\delta^{18}O$ and $\delta^{13}C$ (Carpenter and Lohmann, 1995). The outermost section of the secondary layer is out of equilibrium with the ambient seawater, possibly because of the proximity to the primary layer. Due to the absence of growth lines within the secondary layer, relating the exact age of the area being sampled to a specific growth line of the primary layer is difficult (Figure 1.6-1). However, it is possible to see the direction of growth in the secondary layer fibres.

In *Terebratulina retusa,* atomic force microscopy (AFM) shows that the secondary layer shell fibres have a complex granular structure, and in low magnification images the juxtaposition of the fibres is apparent (Cusack et al., 2008a). AFM also shows that within each fibre there are lineations perpendicular to the fibre axis, thought to be growth increments. Low Mg calcite fibres act as a single crystal with a common crystallographic orientation along each fibre length (Cusack et al., 2008a). The crystallographic orientation of calcite in rhynchonelliformean brachiopods, with the c-axis perpendicular to the shell exterior, ensures that the cleavage planes of the calcite are as far as possible away from the edge of the shell, to minimise the chances of the shell breaking on impact (Schmahl et al., 2004).

The tertiary layer, Figure 1.6-1, is comprised of prismatic calcite crystals precipitated from points within the mantle where several cells have coalesced. Growth bands are not visible in this layer of the shell. The tertiary layer is in oxygen isotopic equilibrium with the ambient sea water (Yamamoto et al., 2010a; Yamamoto et al., 2010b), and unlike the secondary layer gives consistent values throughout. As both the tertiary layer of the shell and the secondary layer (Parkinson et al., 2005) are in oxygen isotopic equilibrium with the ambient seawater then they can both be used for sampling. In this study the *Terebratulina* specimens do not have a tertiary layer and therefore the innermost part of secondary layer has been sampled in this species. In the genus *Liothyrella* there is a tertiary layer and this area of the shell has been sampled.

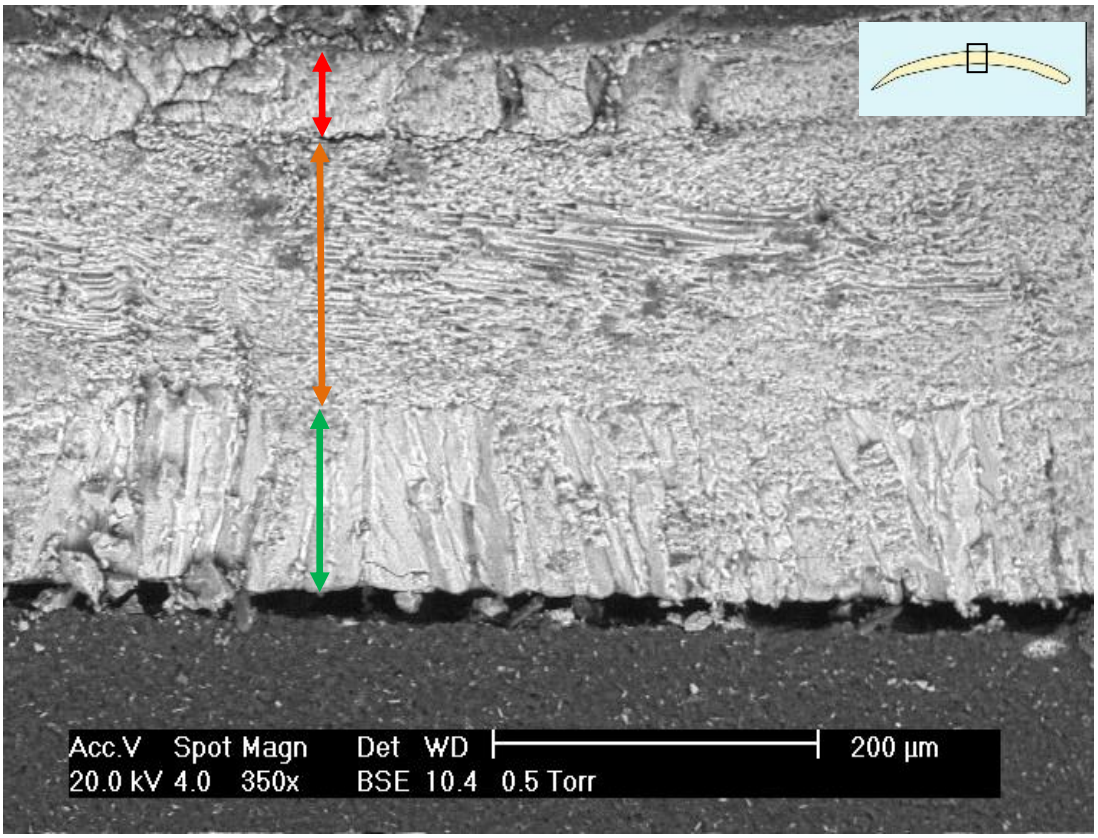

Figure 1.6-1. Ultrastructure of *Liothyrella neozelanica*. Red arrow indicates primary layer, orange arrow the secondary layer and the green arrow shows the tertiary layer. Modern shell J691 from Latitude -37.55, Longitude 176.98. Inset show approximate position in transverse section.

1.7 Vital effects in brachiopods

Lowenstam (1961) concluded that rhynchonelliform brachiopods precipitate shell calcite in oxygen isotopic equilibrium with the ambient seawater. There are however parts of the shell that are not in oxygen isotopic equilibrium with the ambient seawater and this is thought to be due to vital effects. Vital effects need to be taken into account when calculating calibrations for palaeothermometry. These biological controls can alter the shell chemistry and hence the Mg/Ca ratio by a number of processes. In a multispecies calibration if the vital effect of one species is constant then a correction can be applied to the calibration to compensate for the offset from expected values.

The muscle scars (Figure 1.4-2) are one of several areas in the shell where vital effects are known to affect the shell chemistry. The muscle scar migrates towards the anterior shell with ontogeny. It is thought that this migration may lead to constant dissolution and reprecipitation of the shell in this area, this biological processes could explain why the muscle scar is out of equilibrium with the ambient seawater (Hughes et al., 1988).

The umbo region of the shell shows $\delta^{18}O$ values (Parkinson et al., 2005) and Mg/Ca ratios (Perez-Huerta et al. 2008; Perez-Huerta et al., 2011) that are out of equilibrium with the ambient sea water. One possible explanation is that the growth rate of the shell has an effect on the $\delta^{18}O$ values and the Mg/Ca ratio, as the fast growth rate may not allow time for the shell to reach equilibrium with the ambient sea water. It could also be due to the metabolic rate of the brachiopod being different just after larval settling (Curry, 1982).

The shell closest to the anterior margin is also known to show vital effects. This is relatively easily explained in comparison to the other vital effects, because it represents the terminal stage of life when the brachiopod is likely to be experiencing disease or external stress (Gordon Curry pers. comm., 2010).

1.8 Brachiopod shell Mg distribution

Biological control of Mg incorporation into brachiopod calcite was first proposed by Lowenstam (1961) because the partition coefficient was lower in the shell of rhynchonelliformeans than in the sea water. England et al. (2007) have since proposed that low Mg calcite brachiopods have a biological mechanism that controls the distribution of Mg at different structural levels. Perez-Huerta et al. (2008) set out to test this by analysing laser ablation spots in different parts of the shell. They found that Mg is distributed unevenly across the length and depth of the brachiopod shell. The primary layer of the shell has generally between 2 and 2.5 times the amount of Mg than the secondary layer (Perez-Huerta et al., 2008). A sharp decrease in Mg from the primary to the secondary layer shows that the outermost part of the secondary layer is out of equilibrium with the ambient seawater. The amount of Mg seems to decrease gradually towards the centre of the secondary layer. The equilibrium zone for secondary layer calcite starts at approximately one third or one half of the distance from the outer edge of the valve and continues through to the inner edge (Perez-Huerta et al., 2008). The equilibrium zone of the secondary layer as defined by the Mg concentrations agrees with the $\delta^{18}O$ record of *Terebratalia transversa*, which shows that the innermost secondary layer is in isotopic equilibrium with the ambient seawater (Cusack et al., 2008b). This applies to the central and anterior parts of the shell, the values for the umbo are considered too sporadic to be in equilibrium, possibly due to rapid juvenile growth (Buening and

Carlson, 1992). Buening and Carlson (1992) demonstrated that in addition to the ontogenetic influences, there is also interspecies differentiation, showing that species specific calibrations would probably be more attainable than a multi species calibration.

1.9 Brachiopods through Time

The Brachiopoda have their first occurrence in the Cambrian Explosion 570 Ma and continue right through the Phanerozoic until Recent, see Figure 1.9-1. Brachiopod generic diversity reached an acme in the Devonian. Following this brachiopod genera declined though the Frasnian-Famennian extinction events which also saw the extinction of many reef building organisms such as rugose corals, tabulate corals and stromatoporoids. The numbers of genera also decreased during the end Permian mass extinction where over 90% of marine species became extinct. Until the end Permian the brachiopods were the dominant shallow benthic marine invertebrates. In Post-Palaeozoic times the brachiopods have remained at a relatively low diversity but have not declined.

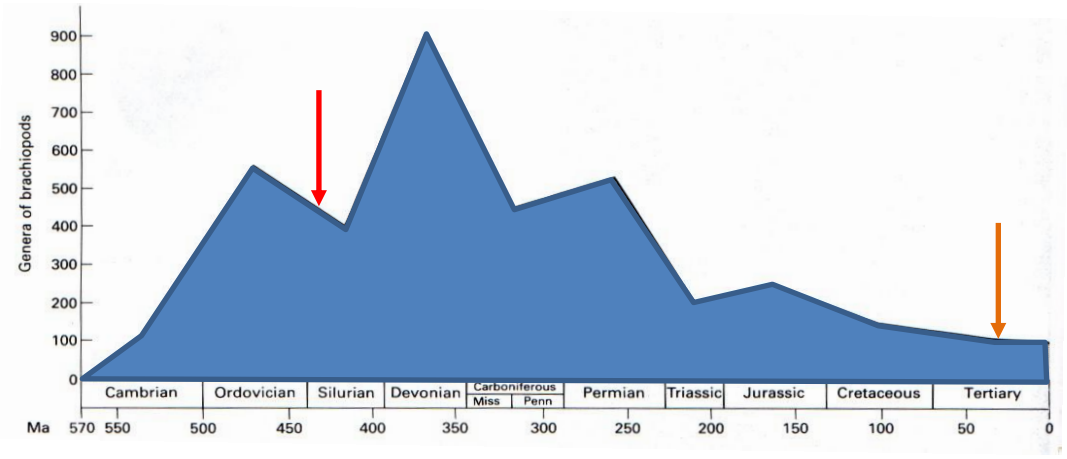

Figure 1.9-1 Number of brachiopod genera throughout the Phanerozoic, red arrow marks the Ireviken Excursion of the Silurian and the orange arrow represents the Eocene-Oligocene Transition, adapted from Rowell and Grant (1987).

Brachiopods are important in regards to studying past climate in the Palaeozoic, firstly because of their relatively large abundance and secondly because the Rhynchonelliformea are composed of low Mg calcite which is the most diagenetically stable form of calcium carbonate. This means that the brachiopod has a better chance of preserving calcite that has not been diagenetically altered. The benefits of using brachiopods to study climate in the Cenozoic are entirely different, for instance they are not as abundant as other low Mg calcite organisms such as foraminifera. As macrofossils brachiopods are much larger than foraminifera and retain a record of incremental growth throughout their life span, this means that brachiopods could be used to study seasonality as the winter and summer growth increments can be directly sampled. This is something that cannot easily be done with foraminifera, if at all. It should be possible to produce an effective temperature calibration for Mg/Ca of Rhynchonelliformean brachiopods due to the fact that although they are not as abundant today they still have a wide latitudinal and geographical range spanning -1 °C to ~30 °C.

1.10 Introduction to the Eocene-Oligocene Transition

Atmospheric CO_2 is thought to have fallen below the threshold that allowed significant ice volume to build up on Antarctica for the first time in the Cenozoic (Pagani et al., 2005; Pearson et al., 2009; Zhang et al., 2013; DeConto et al., 2003). Although there is a possibility that smaller or semi-permanent ice sheets may have sporadically been in place from the mid to late Eocene (Westerhold et al., 2014). Associated with this glaciation is a contemporaneous deepening of the carbonate compensation depth (CCD), which has led to complications when trying to assess Mg/Ca ratios of foraminifera from deep ocean sites (e.g. Lear et al., 2004). Without knowledge of this deepening of the CCD, Mg/Ca ratios seem to indicate a warming

over this transition. However, this is not the case and although there is no true consensus on how temperatures responded over this period it is thought that a minimum 1-2 °C temperature decrease is likely (Coxall et al., 2005) There is potential for this temperature decrease to be up to 4 °C for deep oceans and 2.5 °C for low latitude sea surface temperatures (Lear et al., 2008). The 4 °C cooling is consistent with a model in Liu et al. (2009).

Most temperature data from the Cenozoic come from proxies used on foraminifera as they are ubiquitous and abundant. Due to their microscopic size they are difficult to utilise for seasonality studies, which look at the difference between summer and winter temperatures, this is one reason why relatively few seasonality studies have taken place. As seasonality studies are important to show how the different seasons were influenced by the growth of the Antarctic ice sheet other organisms have been used to try and assess seasonality over this period. Ivany et al. (2000) studied fish otoliths and Wade et al. (2012) used a multi-proxy approach on foraminifera, both in the Gulf of Mexico. These two studies showed a decrease of 4 °C in winter temperatures and are supported by palynological evidence which suggests a ~5 °C cooling around Greenland (Eldrett et al., 2009). Another study on rodent teeth from the UK (Grimes et al., 2005) show no change in seasonality over the EOT whilst, a study on horse teeth shows a much greater cooling of ~8 °C in mean annual temperatures but not change in seasonality (Zanazzi et al., 2007). All of these seasonality studies have taken place in the northern hemisphere. This study will give valuable insight into how seasonality was influenced in the southern Pacific over the EOT. The one seasonality study from the Southern Hemisphere deals with changes in seasonality in the mid to late Eocene, and found that seasonality decreased on Seymour Island near Antarctica in the run up to the EOT (Dutton et al., 2002). It is

not known whether the southern and northern hemisphere sea water temperatures responded in the same way to the glaciation.

1.11 Introduction to the Ireviken Event of the Silurian

The $\delta^{13}C$ and $\delta^{18}O$ Ireviken Excursion close to the Llandovery-Wenlock boundary of

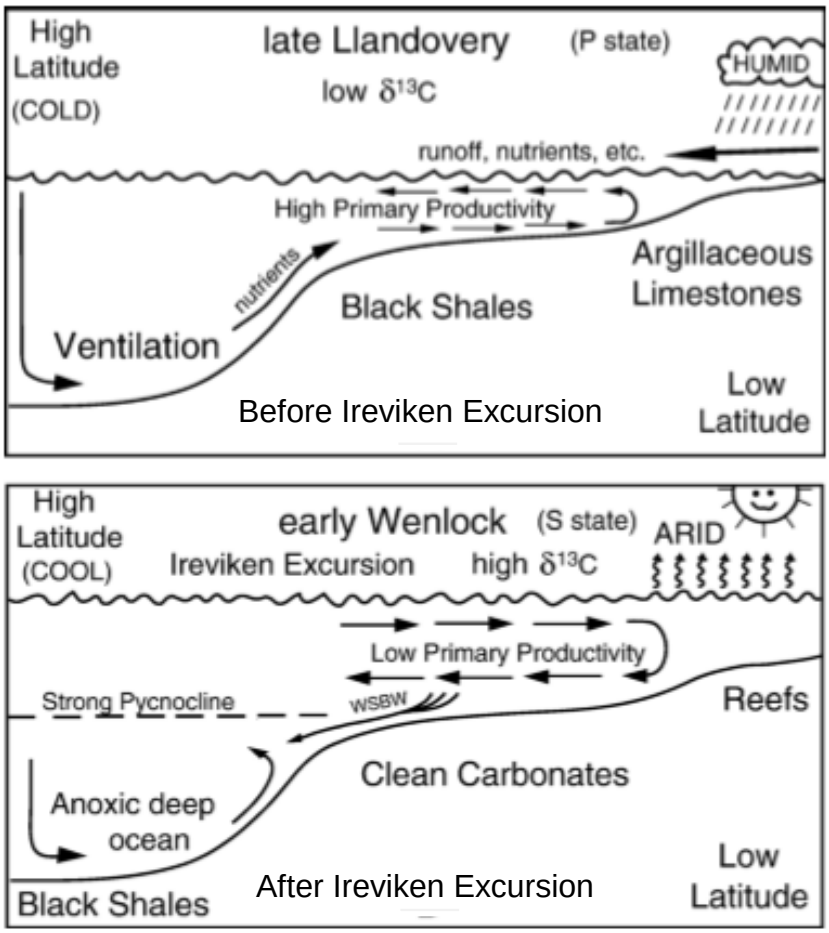

Figure 1.11-1. Climate states for the Silurian first proposed by Jeppsson (1990) and adapted by Cramer and Saltzman (2007). Adapted from Cramer and Saltzman (2007).

the Silurian is an objective horizon for this project. At this point in the Silurian there is a globally recognised positive $\delta^{13}C$ excursion. The values of the excursion are different depending where in the world studies are located (Munnecke et al., 2003; Brand et al., 2006). No definitive driving force behind this excursion is known, however the consensus is that increased burial of carbonate matter plays a large role (Kump et al., 1999; Cramer and Saltzman 2007a and 2007b). There is also a less

well defined positive excursion in $\delta^{18}O$ of ~0.4 ‰ at low latitudes (Munnecke et al., 2003) and a much larger ~2.5 ‰ excursion at higher latitudes (Brand et al., 2006). However, subsequent work found no $\delta^{18}O$ excursion at low latitude sites (Cummins et al., 2014).

Two climate states are identified for the Silurian Primo (P) and Secundo (S) (Jeppsson, 1990; also Aldridge et al., 1993; Jeppsson 1996; Cramer and Saltzman, 2005; Cramer and Saltzman, 2007a) (see Section 6.1.6 for descriptions, Figure 1.11-1) The Ireviken Excursion lies in the transition between two of these climate states and is also associated with the start the Sheinwoodian glaciation, partly identified by glacial deposits in Brazil (Grahn and Caputo, 1992). Using Mg/Ca ratios to investigate this period will help to assess whether or not a temperature change at low latitudes occurred over the Ireviken Excursion.

1.12 Thesis chapters

- Chapter 2: A description of the materials, localities and age models used in this thesis.

- Chapter 3: A new sampling technique is explained that captures seasonal geochemical cycles from the secondary layer of the brachiopod shell in *Terebratulina retusa* and the secondary and tertiary layers of *Liothyrella neozelanica*.

- Chapter 4: Data are presented from *Terebratulina retusa* and *Liothyrella neozelanica* to construct the first two brachiopod Mg/Ca-temperature calibrations. This work has been published (Butler et al., 2015) in *Chemical Geology*.

- Chapter 5: Brachiopod Mg/Ca-temperature calibrations are applied to the Eocene Oligocene transition to assess seasonality before and after the transition. This chapter also attempts to deconvolve the $\delta^{18}O$ signal and assess South Pacific Ocean reorganisation associated with the glaciation event.
- Chapter 6: Mg/Ca ratios are used to look at temperature changes over the Ireviken Excursion and $\delta^{18}O$ values are used to calculate mean temperatures for the early Silurian.
- Chapter 7: Synthesis and suggestions for future research.

2. MATERIALS

2.1 Mg/Ca in modern brachiopods from known water temperatures

Terebratulina was chosen for this study as this genus ranges from the Upper Jurassic to Recent (Lee et al., 2006). The modern species *T. retusa* has a depth range of 18 – 2157 m and is patchily distributed around the central and eastern North Atlantic as

Figure 2.1-1. Map of the British Isles with a close up of the area around the Firth of Lorne (56°26'N, 5°38'W). Orange star marks the collection locality for specimens of *Terebratulina retusa*.

far north as the Barents Sea and as far south as Cape Verde, and is also present in the Mediterranean (Logan, 2007). Three co-existing specimens of *T. retusa* were taken from the large population studied by Curry (1982). These were collected alive in March 1977, by the R/V *Calanus* or *Seol Mara*, using a conventional 'clam-dredge'

from a 150 - 200 m deep depression in the Firth of Lorne, Scotland (Figure 2.1-1) where they are predominantly attached to a substrate of horse mussels (*Modiolus modiolus)* (Curry, 1982). Bottom water temperatures at this locality were measured using insulated sampling bottles and range from 6.5 – 13 °C throughout the year (Curry, 1982). Bottom water $\delta^{18}O$ at this locality was measured by Parkinson et al. (2005), and is 0.06 ‰ VSMOW.

Ten salinity measurements taken between February 1982 and February 1983 from 120 – 200 m deep from three sites within 10km of the sampling site (Grantham 1983a&b; Grantham et al., 1983a&b) showed no significant seasonal variation, having a February average of 33.8 +/- 0.2 psu (1sd, n=6), and a July average of 33.7 +/- 0.1 psu (1sd, n=4).

2.2 Mg/Ca of modern brachiopods from a depth transect of known water temperatures

2.2.1 Selection of location

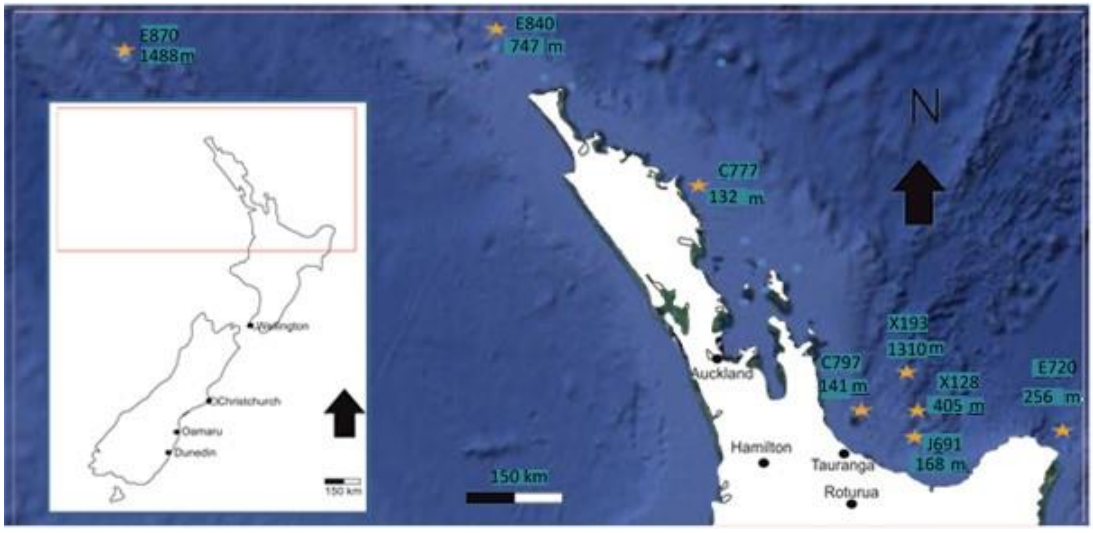

Figure 2.2.1-1. Map of New Zealand; stars identify localities from which individual brachiopods were collected and blue dots indicate CTD localities.

A depth transect was sought to investigate the relationship between Mg/Ca and

temperature in modern shells. This enabled brachiopods which lived in slightly higher temperatures than the Firth of Lorne brachiopods to be studied and allowed an investigation of the Mg/Ca temperature relationship in a different modern genus. Several requirements needed to be fulfilled for a location to be considered suitable for a depth transect. The first being that brachiopods needed to be relatively abundant in the potential area. The second requirement was that the surface water must be warmer than 13 °C as this would allow study of Mg/Ca in brachiopods at higher temperatures than the samples collected from the Firth Of Lorne. Finally ocean data needed to be available for the area.

Brachiopods are generally uncommon in modern seas but in the waters around New Zealand it is possible to study living populations and obtain recent specimens (Richardson, 1981). Off the north coast of North Island, New Zealand, surface temperatures reach 20 °C in the summer months and with the other criteria met it was the obvious place to obtain specimens for a depth transect, Figure 2.2.1-1.

A depth transect would also help look at the lower end of the ocean temperature range because off the North Coast of New Zealand the species *Liothyrella neozelanica* has a sampled depth range of ~100 m to ~1500 m, other brachiopod genera were present in the collections but were limited to much narrower range of water depths and therefore temperatures. At a depth of 1500 m the average temperature for this area is 3.4 °C, giving the potential to obtain a temperature calibration for *L. neozelanica* which ranged from 3.4 °C through to 20 °C. This turned out to be unobtainable as explained in section 4.1.

2.2.2 Specimen selection

The specimens in Figures 2.2.2-1 and 2.2.2-2 were chosen from the Invertebrate Collection of the National Institute of Water and Atmospheric Research (NIWA), based in Wellington. Brachiopod specimens had been collected on research cruises from 1962 to 1989 from the sites highlighted in Figure 2.2.1-1. These brachiopods were then stored dry in the collection and identified by Daphne Lee and Jeffrey Robinson, from the University of Otago. The sample selection process was restricted by the number of specimens NIWA had in their collections, if only one specimen was available from a specific location and depth, it was not offered for analysis. In locations where two or more specimens were available, the least complete specimen was offered for analysis. All specimens are named after the site they were collected from, Figure 2.2.1-1.

Eight *Liothyrella neozelanica* specimens were collected from NIWA, these had depths ranging from 133 m to 1488 m. All of these specimens were either complete valves, slightly broken valves, or broken valves with the anterior third of the shell completely intact. Collection details are shown in Table 2.2.2-1 and the properties of the hand specimens and the specimens under SEM are detailed in Appendix 1.

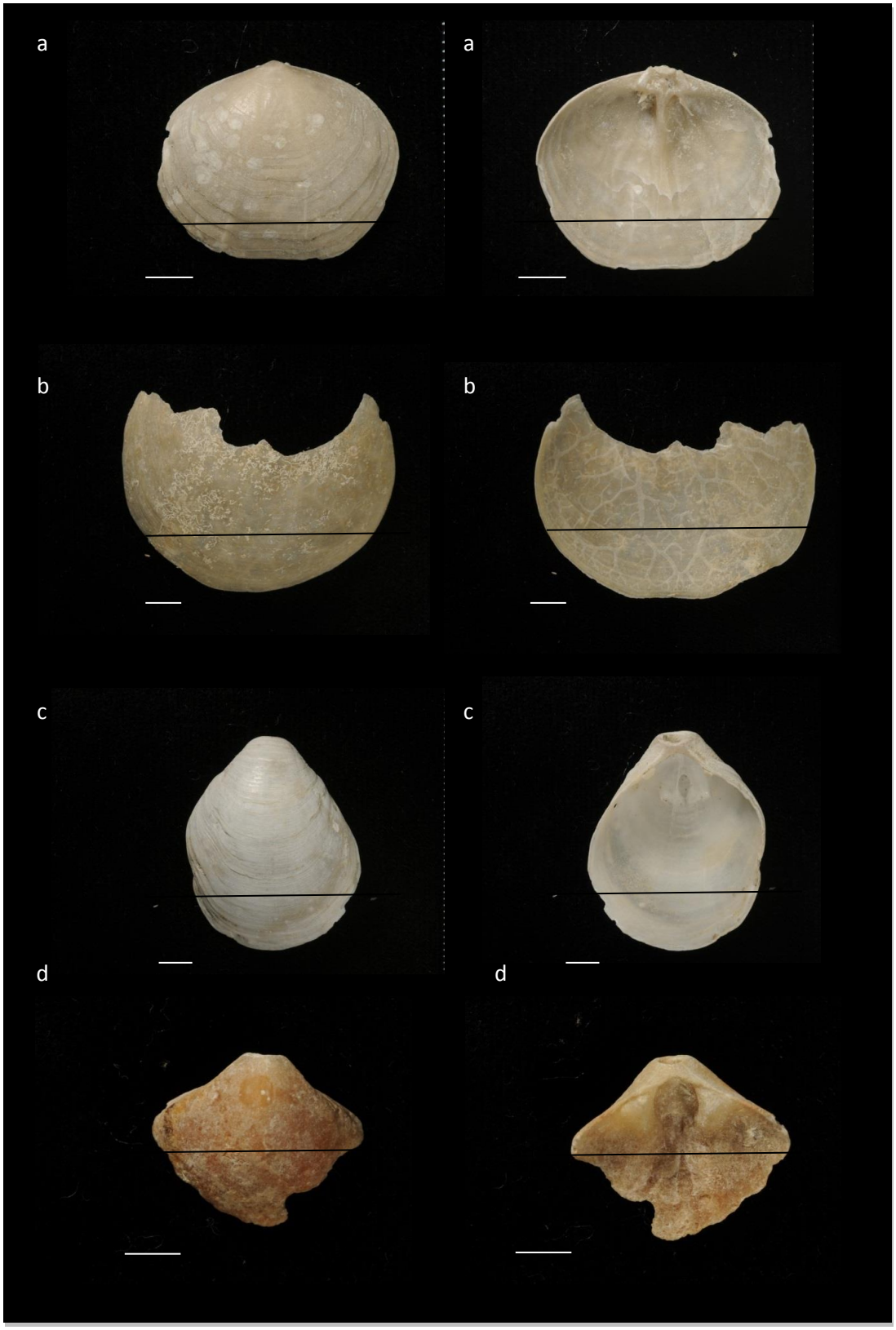

Depth Transect Figure 2.2.2-1. *Liothyrella neozelanica*. All scale bars. 0.5 cm, a= X128, b= J691, c= E720 d= C797. Black line denotes line of section.

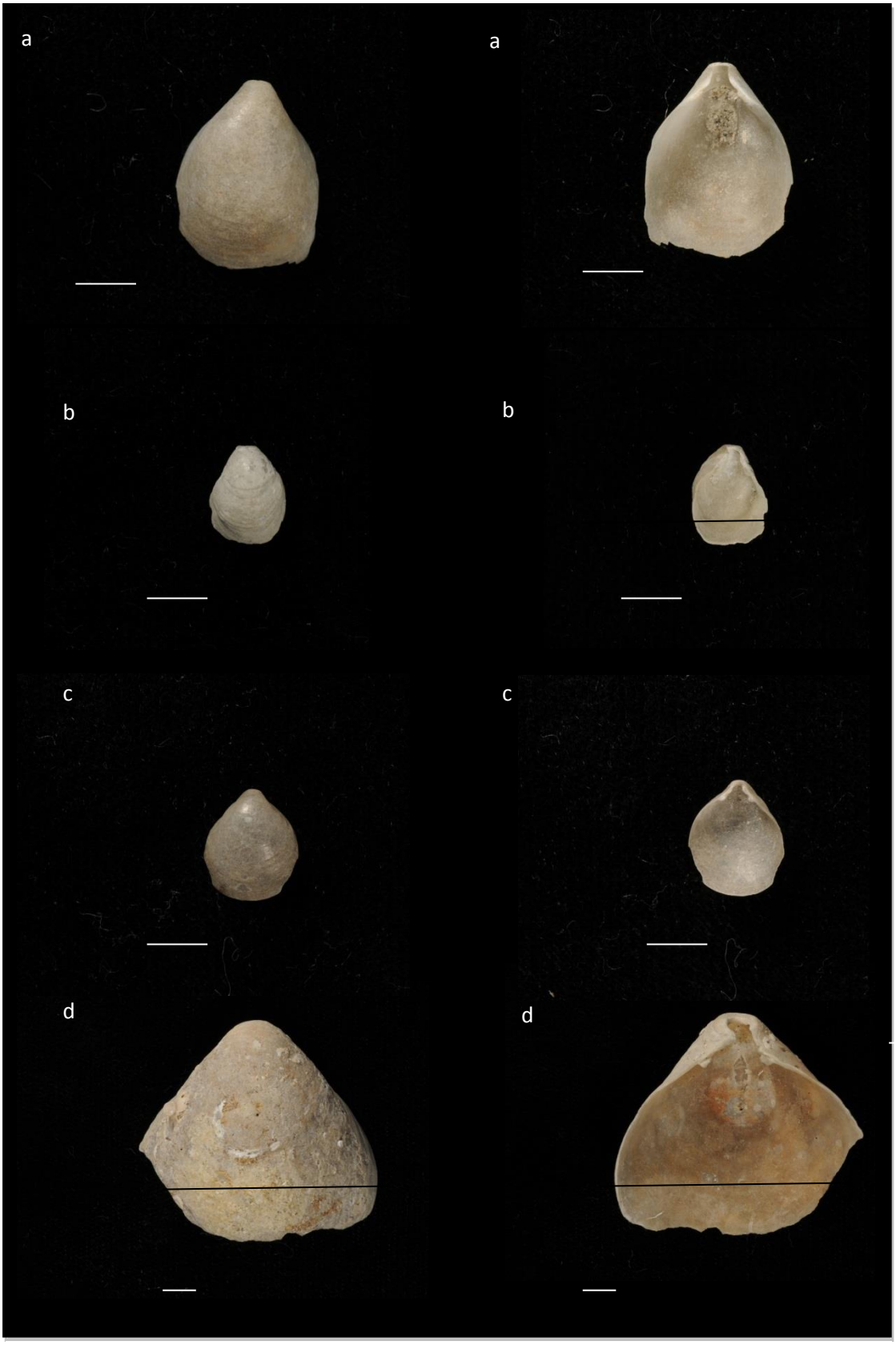

Depth Transect Figure 2.2.2-2. *Liothyrella neozelanica.* All scale bars. 0.5 cm, a= X193, b= C777, c= E870 d= E840. Black line denotes line of section.

Station ID	Depth (m)	Latitude	Longitude	Nearest CTD Temperature Data, Latitude	Nearest CTD Temperature Data, Longitude	Date Collected
C777	132	-35.32	174.54	-35.81	175.06	20/02/1962
C797	141	-37.33	176.30	-36.00	175.76	23/02/1962
J691	168	-37.55	176.98	-36.00	175.76	09/09/1974
E720	256	-37.55	178.58	-36.00	175.76	24/03/1967
X128	405	-37.41	176.99	-36.00	175.76	25/11/1989
E840	757	-33.87	172.27	-34.18	172.14	16/03/1968
X193	1310	-37.04	176.89	-36.00	175.76	5/12/1989
E870	1488	-34.08	168.17	-34.08	168.17	20/03/1968

Table 2.2.2-1. Collection details for *Liothyrella neozelanica* from offshore North Island, New Zealand.

2.2.3 Temperature data

The temperature data were supplied by NIWA and come from the World Ocean Atlas (2001). The recording stations used to supply the data for this study are from the stations closest to the locations that the brachiopods were collected from. These stations recorded seasonal temperatures and salinities up to a maximum water depth of 500 m. The precision of the data is 0.5 °C and 0.1 psu. Data was collected all year round and as a result an accurate representation of the seasonality in this area can be established. Monthly average temperature data were only available to a depth of 500 m, therefore for specimens collected from below 500 m the average temperature was used. It is also assumed that at intermediate depths there is little annual variation in the temperature of seawater, due to the fact that little annual temperature variation exists at 500 m.

2.3 Study of Mg/Ca in brachiopods over the Eocene-Oligocene Transition

2.3.1 Localities

As with modern brachiopods, finding populations of fossilised brachiopods from the Late Eocene and Early Oligocene is limited to very few places. One of these places is North Otago, South Island, New Zealand. Here many brachiopods have been described; the locations at which they are found are often the type localities for one or more species. A study by Buening et al., (1998) used several of the sites in this area for a study of oxygen and carbon isotopes over the Eocene-Oligocene transition. Brachiopod specimens were collected from sites of Late Eocene and Early Oligocene age. No single locality actually spanned the transition.

2.3.1.1 McDonalds Quarry (-45° 09’ 57” N, 170° 54’ 15” E)

This early Oligocene locality, Figure 2.3.1-1, is composed of limestone from the Ototara Limestone Formation, originally the McDonald Limestone Formation (Gage, 1957) which generally has a depositional environment of 30-60 m (Edwards, 1991). Brachiopods are not ubiquitous at this locality. The limestone in the quarry is massive and homogenous on the whole, with very few brachiopod fossils. As the site is an active quarry many of the faces that are seen do not remain in place for any long period of time. The brachiopods were not collected in situ from this section; they were collected from the fossiliferous boulders that were found at the foot of the quarry walls. Field observations suggested that the brachiopods from this locality were mainly quite well preserved, with the fossils being a bright cream colour; the majority of which were still articulated. There were however some shells that had undergone a different taphonomic process as there were brachiopods which were preserved only as internal moulds. These were easily distinguished by the presence of Fe oxide in the sediment.

The lack of cross bedding, the complete nature of the fossils and the massive homogenous appearance of the limestone suggests that it was deposited in a low-energy environment. The limestone is bioclastic often composed of bryozoan fragments, mainly open-textured and soft but in some places is semi-crystalline and hard, these hard areas are mostly associated with fossiliferous brachiopod beds (Gage, 1957).

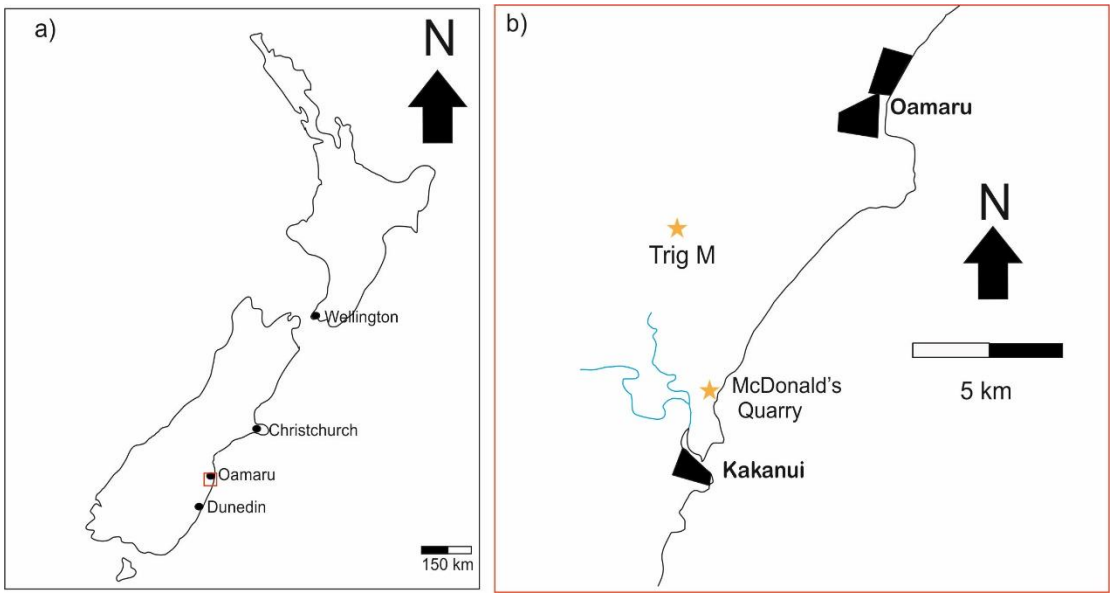

Figure 2.3.1-1. a) Map of New Zealand, with red area highlighting the area shown in b). b) Map of Oamaru area of North Otago where the two sites used in this study are located and marked by orange stars, adapted from Buening et al. 1998.

2.3.1.2 Trig M (-45° 07’ 44” N, 170° 53’ 50” E)

A Late Eocene locality, Figure 2.3.1-1, originally identified as the Totara Limestone which was later incorporated into the Ototara Limestone Formation (Edwards et al., 1991). The site is situated topographically slightly lower than the Trig point after which it is named. The locality is ~50 m west of the trig point and has an outcrop that is well exposed in places and grass covered in others. The total extent of the outcrop covers an area approximately 20 m by 10 m. The sediment is a very well cemented cream and orange/brown limestone, which has volcanic tuff making up some of the matrix. The orange/brown sediment weathers out much more easily than

the more carbonate rich areas. The level of preservation, when viewed in the field, generally seemed good. There were small veins of iron oxide on some of the fossils, but these appeared to be superficial.

This site is thought to be of similar depth to McDonalds quarry, potentially slightly deeper (Daphne Lee Pers. Comm. 2012). The robust and thicker nature of both the *Liothyrella* and *Terebratulina* shells could indicate that this depositional environment was more turbulent than that represented by the sediments at McDonalds Quarry.

2.3.2 Selection of species for Mg/Ca analysis over the Eocene-Oligocene Transition

Liothyrella and *Terebratulina* specimens were chosen as the species to use for this study as they were the genera used for the modern calibration work, Chapter 4. The sites detailed above were chosen because species of *Liothyrella* and *Terebratulina* were found in large numbers at each locality. *Terebratulina suessi* and *Liothyrella oamarutica* were collected from McDonalds Quarry, see Figures 2.3.2-1, 2.3.2-2 and 2.3.2-3. *Terebratulina suessi* and *Liothyrella concentrica* were collected from Trig M, see Figures 2.3.2-4 and 2.3.2-5. *Terebratulina suessi* was far less common at Trig M than Mcdonalds Quarry, washing and sieving 3kg of bulk sediment, yielded only three specimens. The size of the two species is very different; *L. oamarutica* is a large brachiopod, with specimens from these sites reaching 6-7 cm in length, whereas no samples of *T. suessi* used in this study are larger than 2 cm.

Note that whilst *Liothyrella concentrica* is described as a different species some taxonomists believe that this is the same species as *Liothyrella oamarutica* (Jeffrey Robinson Pers. Comm. 2012) whilst others believe it is a very close relative (Allan, 1932). Comparing the shell chemistries of *Liothyrella concentrica* and *oamarutica*

would therefore at worst only have minor contributions from species specific vital effects.

Two species were studied to allow comparison between the data sets and increase the reliability of estimates of Mg/Ca change across the Eocene-Oligocene boundary. As the species are both epifaunal and from the same localities, it is reasonable to expect that both species will have lived in similar habitats and experienced the same environmental conditions, making a direct comparison possible. The specimens are named after the sites they were collected from and species they represent. The prefixes TMTER and TMLIO are given to *Terebratulina* and *Liothyrella* specimens collected from Trig M (Eocene). The prefixes MCTER and MCLIO are given to *Terebratulina* and *Liothyrella* collected from McDonalds Quarry (Oligocene).

Figure 2.3.2-1. McDonalds Quarry: Oligocene. *Liothyrella oamarutica* a= MCLIO1, b= MCLIO2, c=MCLIO3, d= MCLIO4. All scale bars 1cm.

Figure 2.3.2-2, McDonalds Quarry: Oligocene. *Liothyrella oamarutica* a=MCLIO5; *Terebratulina suessi*, b= MCTER1 c= MCTER2, d= MCTER3. All scale bars 1 cm.

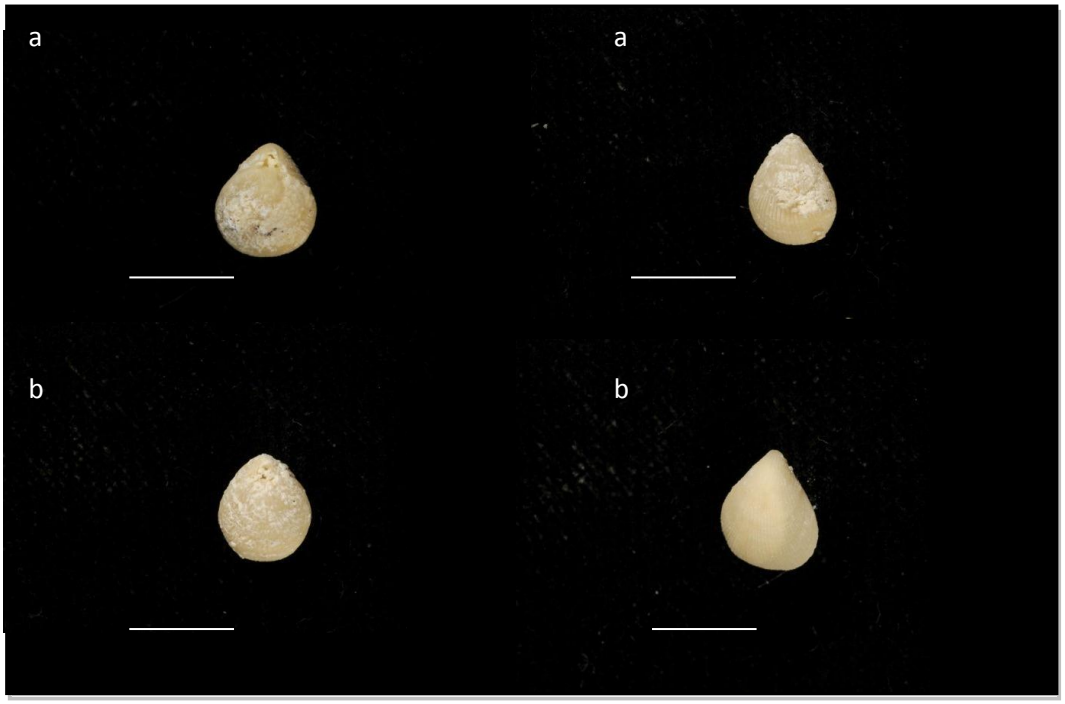

Figure 2.3.2-3. McDonalds Quarry: Oligocene. *Terebratulina suessi* a=MCTER4, b=MCTER5. All scale bars 5mm.

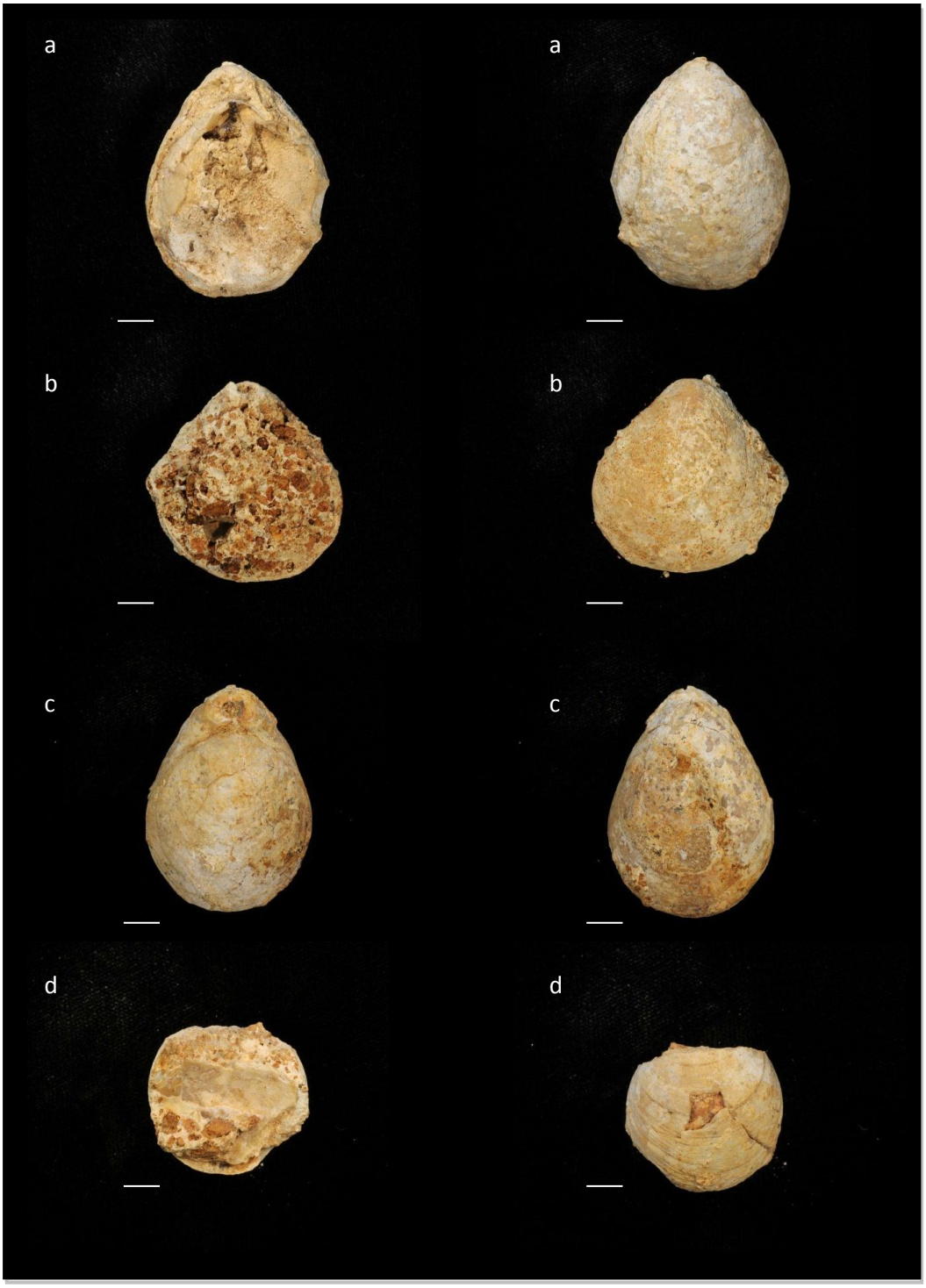

Figure 2.3.2-4. Trig M: Eocene. *Liothyrella concentrica* a= TMLIO1 b= TMLIO2 c= TMLIO3 d= TMLIO4. All scale bars 1cm.

Figure 2.3.2-5. Trig M: Eocene. Liothyrella concentrica a= TMLIO5, b= TMTER1, c= TMTER2, d= TMTER3. All scale bars 0.5 cm

2.4 Mg/Ca over the Ireviken Event of the Silurian

2.4.1 Sample selection

The specimens used in this work are of the genus *Atrypa* (Dalman, 1828). This is an extinct Rhyconelliformean genus, ranging from the Silurian (upper Llandovery) to the Upper Devonian (Frasnian), that had a worldwide distribution (Moore et al., 1965). This genus was used because it is common in these sediments, and there was high availability in the collections of the National Museum of Wales.

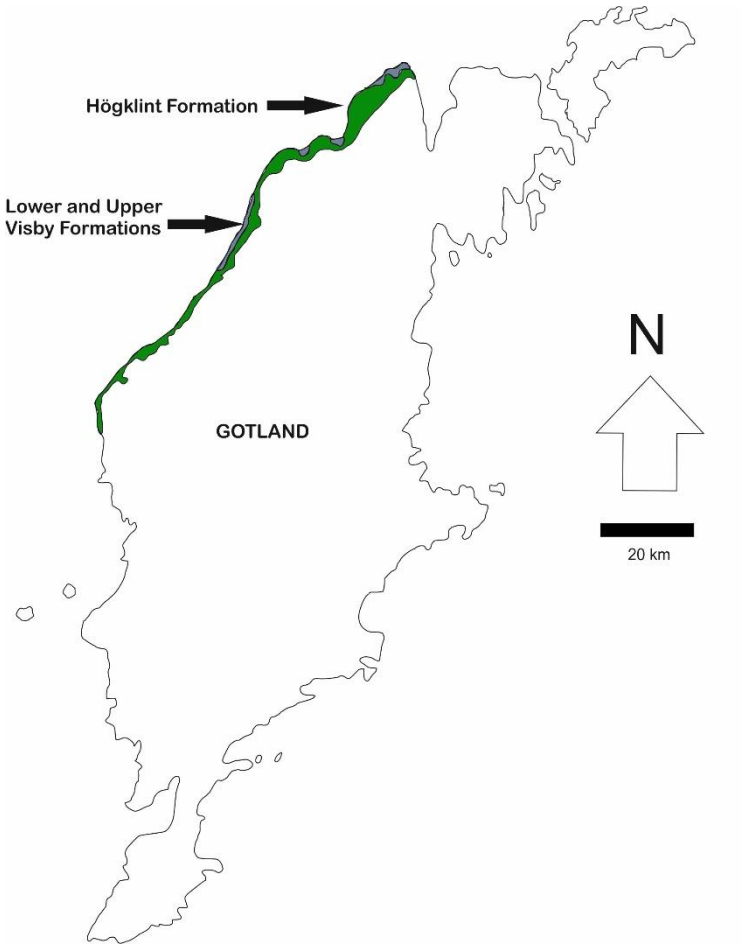

Figure 2.4.2-1. Map of Gotland, Sweden, showing the formations associated with Llandovery-Wenlock succession.

2.4.2 Site selection

The Swedish island of Gotland (Figure 2.4.2-1) was chosen as the source for brachiopod specimens as there is extremely good exposure spanning 10 million years of the Silurian, starting in the upper Llandovery and going through to upper Ludlow (Calner et al., 2004). The preservation of the brachiopods is excellent with shells showing no major signs of diagenetic alteration (Calner et al., 2004). This leads to a greater chance that there was no secondary recrystallisation of calcite which is potentially a problem when dealing with fossils which are Silurian in age. This recrystallision can reset the original biogenic calcite trace metal signals. Diagenetic alteration of original shell chemistry can cause incorporation of Fe and Mn in the crystal lattice, whilst selectively removing Sr; it can also change original Mg concentrations in either direction depending on the circumstances (Brand and Veizer, 1980).

Four sites were used for this study, two below the Ireviken Isotope Excursion these being Nyhamn and North of Nyhamn and two above the isotope excursion, Ygne and Ireviken 3. These sites were chosen for their close stratigraphic proximity to the $\delta^{13}C$ isotope excursion, Figure 6.1.6, all falling within ten metres of the event.

2.4.3 Individual specimens

The specimens from Ireviken, Ygne, North of Nyhamn and Nyhamn are shown in Figures 2.4.3-1, 2.4.3-2, 2.4.3-3 and 2.4.3-4 respectively. The specimens are named after the site they were collected from. All are *Atrypa* and specimens from Ireviken, Ygne, Nyhamn and North Nyhamn are given the prefixes IRE. YGNE, NHY and NNY, respectively.

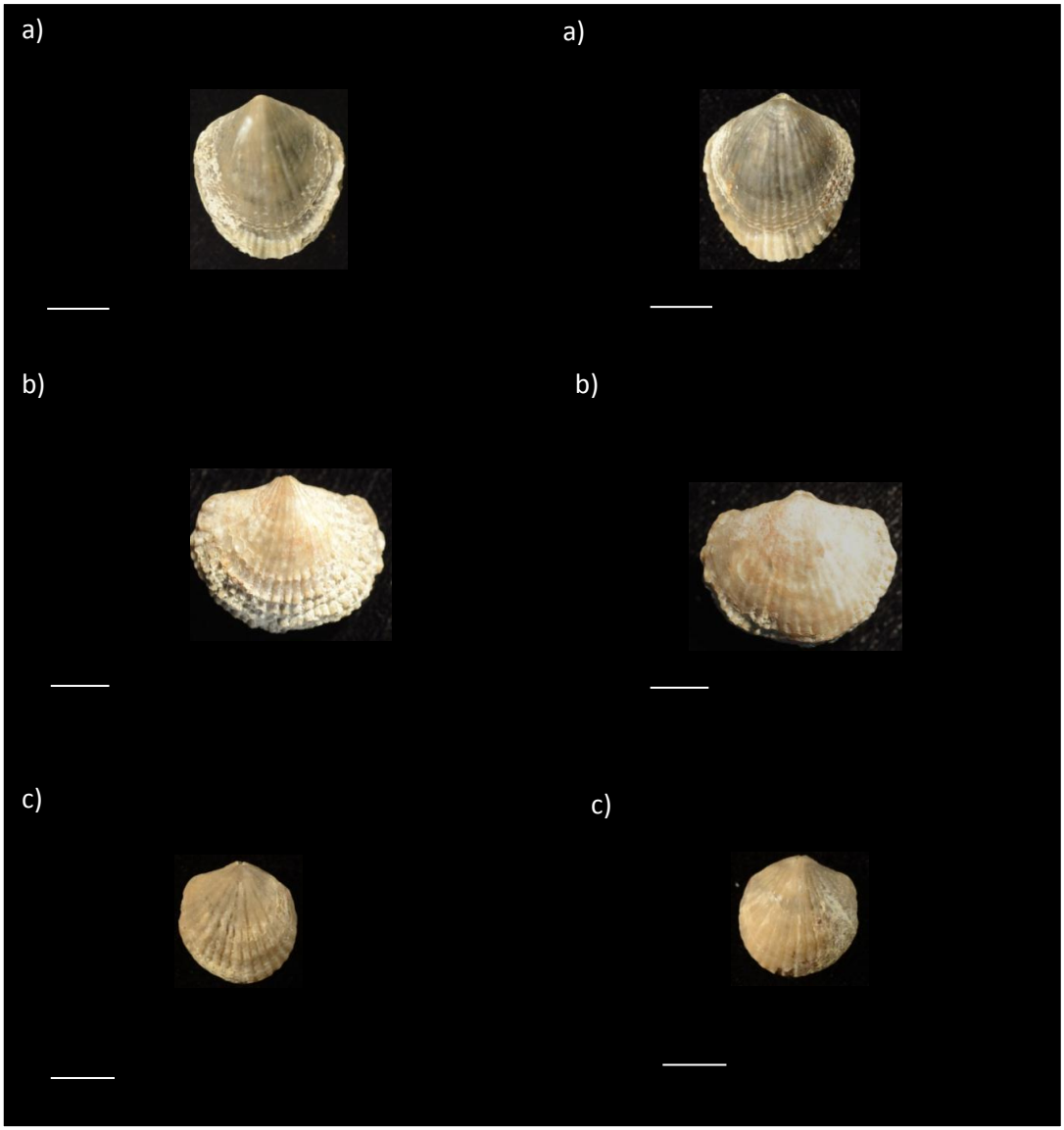

Figure 2.4.3-1 Dorsal and ventral views *Atrypa sp*, from Ireviken. a) IRE1 b) IRE2 c) IRE3. Scale bars 0.5 cm.

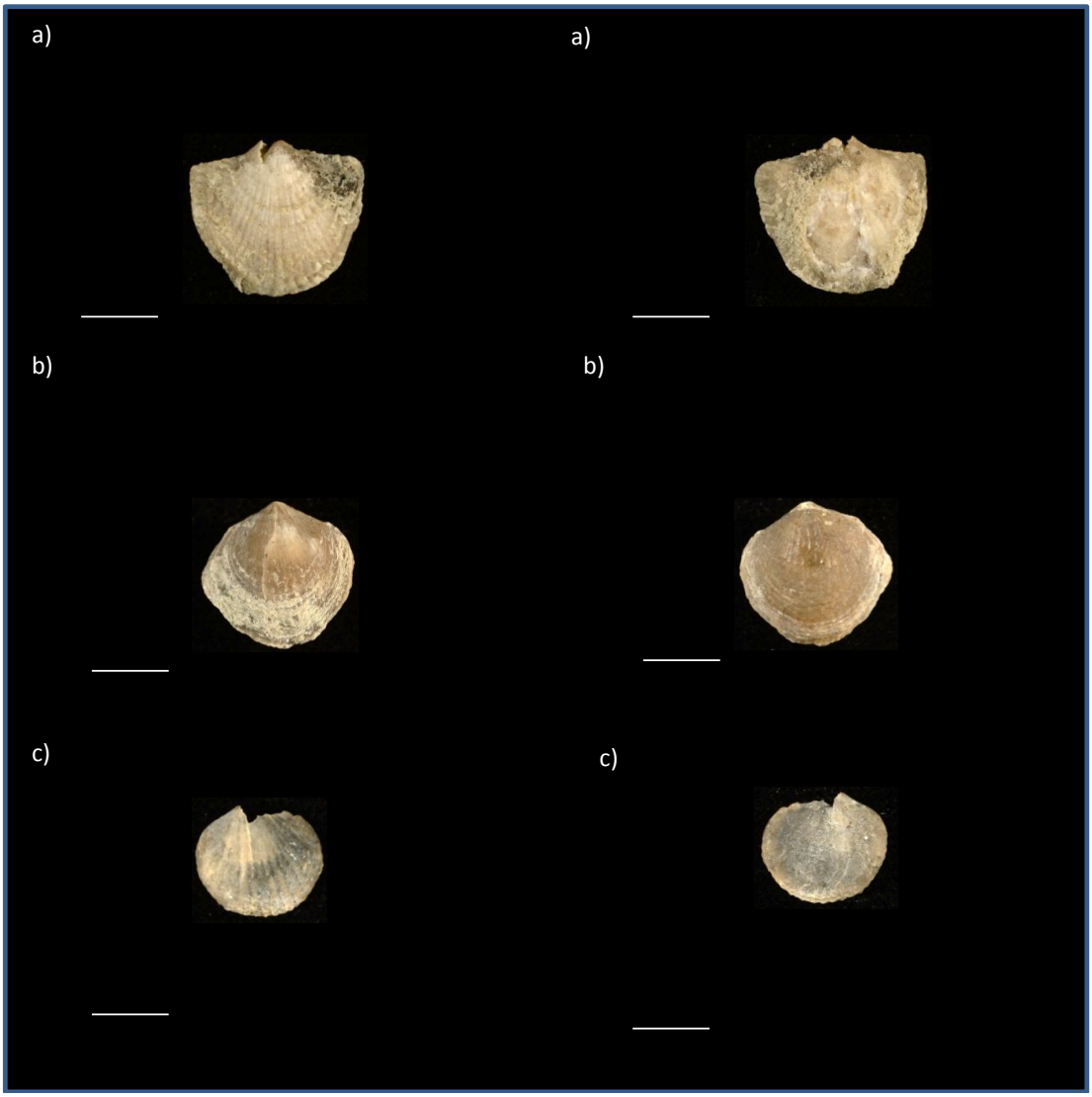

Figure 2.3.4-2. Dorsal and ventral views of *Atrypa sp*. specimens from Ygne. a) YGNE1 b) YGNE2 c) YGNE3. All scale bars 0.5 cm.

Figure 2.3.4-3. Dorsal and ventral views of *Atrypa sp*. specimens from site North of Nyhamn. a) NNY1 b) NNY2 c) NNY3. All scale bars 0.5 cm.

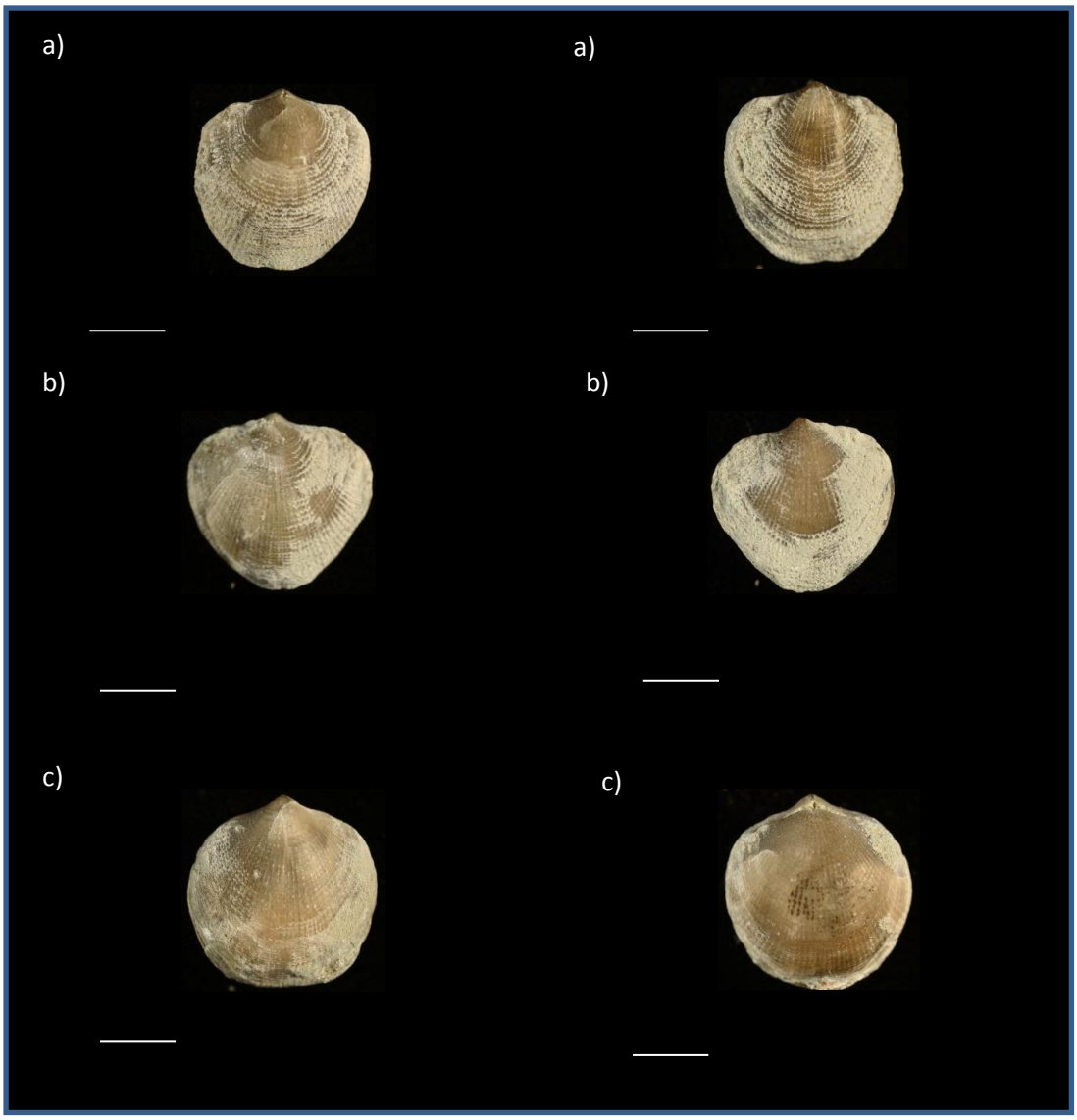

Figure 2.3.4-4. Dorala and ventral views of *Atrypa sp*. specimens from Nyham. a) NYH1 b) NYH2 c) NYH3. All scale bars 0.5 cm.

3 METHODOLOGY

3.1 Preparation of shells for Laser Ablation sampling of element to calcium ratios in modern brachiopods from known water temperatures and fossilised brachiopods from unknown water temperatures

Valves were manually separated and cleaned by ultrasonicating in deionised water and removing sediment with a fine brush. They were then set in a polyester resin with a methyl ethyl ketone peroxide catalyst, sectioned with a diamond wafering saw, lapped with silicon carbide and finally rinsed in deionised water.

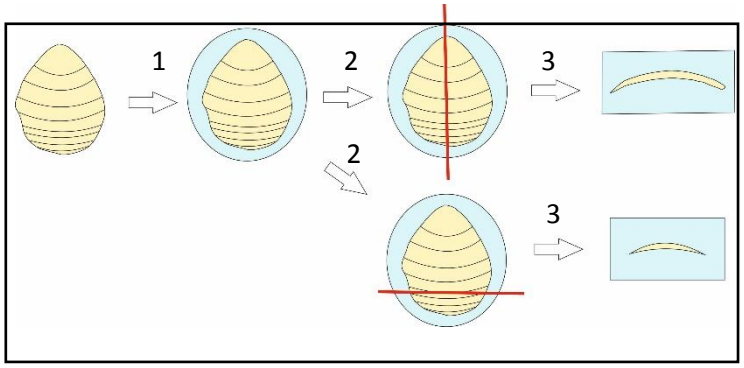

Figure 3.1-1. The process of setting a brachiopod valve in resin. 1) Plan view of the valve being set in resin. 2a) Red line indicates ontogenetic line of section. 2b) Red lines indicates transverse line of section. 3a and b) Ontogenetic and transverse sections in cross section after sectioning.

In *Terebratulina retusa* shell 1, the ventral valve (hereafter called 1V) was sectioned longitudinally to investigate ontogenetic effects, Figure 3.1-1, and the dorsal valve (hereafter called 1D) was sectioned transversely ~ 6mm from the anterior margin, Figure 3.1-1. All valves of *T.retusa* shell 2 (2D & 2V) and *T.retusa* shell 3 (3D & 3V) were sectioned transversely ~5mm from the anterior margin to avoid potential crystallographic effects present in the posterior region (Perez-Huerta, 2011).

All the modern *Liothyrella neozelanica* shells from New Zealand were sectioned transversely except specimen E720 which was sectioned transversely first and then ontogenetically.

Shells from the Eocene-Oligocene of New Zealand were all sectioned transversely to allow profiles from either side of the mid-line to be compared. This helps to verify that profiles have not been altered through diagenesis, see Chapter 5 for full discussion.

For the Silurian study three specimens were used from each locality. Two specimens from each locality were sectioned longitudinally (ontogenetically), down the long axis of the brachiopod. The other specimen from each locality was sectioned transversely, to assess diagenetic effects and potentially seasonality within the shell. The shells that were sectioned transversely were cut in the adult third of the shell to avoid the potential of any crystallographic effects on the data (Perez-Huerta et al., 2008).

3.2 Analysis by Laser Ablation-ICP-MS

The method described below was used for the following Chapters: 4 ('Investigating the Mg/Ca: Temperature Relationship in Modern Brachiopods. Calibrating *Terebratulina retusa* and *Liothyrella neozelanica* from Known Water Temperatures') and 5 ('Seasonality and Temperature Change across the Eocene-Oligocene Transition from Brachiopod Mg/Ca'). Elemental analysis was performed using a New Wave Research 213nm Laser Ablation system, coupled to a Thermo X Series2 Inductively Coupled Plasma Mass Spectrometer (LA-ICP-MS) at Cardiff University using the parameters shown in Table 3.2-1. The sample was moved under the laser at 11 μm/s. At higher speeds fragments of shell were seen to break off,

Laser Model	New Wave Research UP213 UV
Energy density (fluence)	3.0 Jcm^{-2}
Focus	Fixed at surface
Repetition rate	10 Hz
Track width	~ 40 µm
Acquisition mode	Time resolved analysis
Duration of gas blank	35 s

Table 3.2-1. Parameters used for laser ablation.

causing undesired spikes in signal intensity on ionisation. At slower laser speeds, signal intensity was attenuated as less material escaped the deeper laser ablation pits. Laser tracks were run as close to the inside of the shell as possible to stay within the inner half of the secondary layer calcite (Figure 3.2-1) as this has been shown to be precipitated in oxygen isotopic and Mg/Ca equilibrium with the ambient seawater (Parkinson et al., 2005; Perez-Huerta et al., 2008). Laser tracks were curved so that

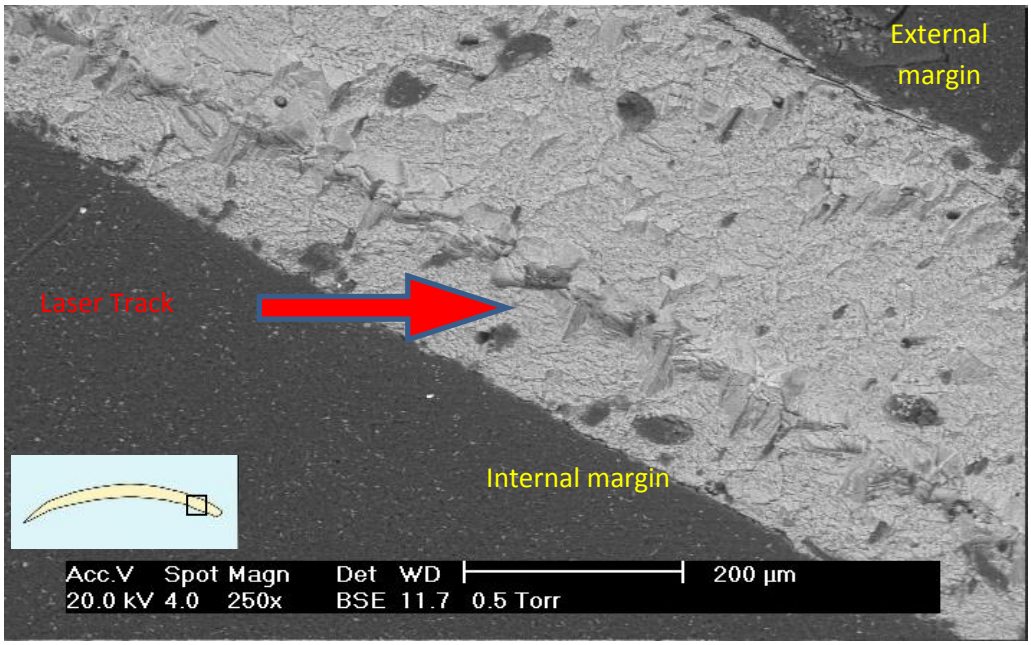

Figure 3.2-1. SEM image of ablated shell, with the position of laser track within the brachiopod shell highlighted. Inset shows approximate image location.

they remained at the same distance from the inner margin of the shell.

^{24}Mg, ^{25}Mg, ^{27}Al, ^{43}Ca, ^{44}Ca, ^{48}Ca, ^{55}Mn, ^{57}Fe, ^{84}Sr, ^{86}Sr and ^{88}Sr peaks were averaged by the mass spectrometer every 0.5 seconds. The isotope ^{25}Mg was used as it gives more reproducible results than ^{24}Mg, possibly due to interference of doubly charged ^{48}Ca on mass 24. ^{86}Sr was chosen over ^{88}Sr to avoid overloading the detector at higher signal levels. NIST 610 glass was analysed as a standard between each sample track, as similar concentrations of Mg are found within modern brachiopod shells and this glass (466 μg/g, Pearce et al., 1997). A gas blank was measured for the first twenty seconds of each ablation, the laser was not firing during this period and therefore this gas blank can be used to monitor the background levels of the isotopes being detected. Standards were measured approximately every 7 minutes and show a high level of reproducibility throughout each day of analysis <8 % RSD for ^{25}Mg/^{43}Ca, and <4 % RSD for ^{86}Sr/^{43}Ca and ^{43}Ca/^{48}Ca. All data reduction was performed offline in spreadsheets. The gas blank measured prior to ablation of the sample was first deducted from the sample raw counts. The sample elemental ratios were calculated; for example by dividing Mg^{25} by Ca^{43} to produce an Mg/Ca ratio. These elemental ratios were then corrected by dividing the elemental ratios by the elemental ratio given from the standard ablated directly before the sample. A carbonate standard would have been preferable to a glass standard but when this work commenced no reliable carbonate standard was available. MACS 3 has since been developed by the USGS and used in several studies (e.g. Chen et al., 2011 and Hughes et al., 2014). The NIST 610 glass was persisted with for the sake of continuity.

In the laser ablation element to calcium profiles, each individual data point represents an averaged signal from material ablated by a 40 μm laser spot that moved

5.5 μm along the laser track; the spatial resolution is therefore ~ 50 μm. Valve profiles were constructed from several individual tracks subsequently stitched together. Adjoining tracks were overlapped by 60 μm, due to a 5 second time delay between firing the laser and obtaining a stable signal, to ensure continuous data profiles across the shell. This overlap meant that for a new track, the first ~11 data points after the gas blank were omitted from the results as they were obtained from the previously ablated track. Depending on their size, sectioned valves were sampled in a differing number of laser tracks ~ 3mm long and stitched together. The exception to this is the longitudinal section of *T.retusa* valve 1V which was sampled in 16 laser tracks around 1.5mm long. The total analysis time for a 3 cm traverse of a valve was approximately 2.5 hours.

Alongside Mg and Sr data, the isotopes ^{27}Al, ^{55}Mn and ^{57}Fe were collected for the purpose of screening for diagenetic alteration. Diagenetic alteration of original shell chemistry can cause incorporation of Fe and Mn in the crystal lattice, whilst selectively removing Sr, and can change original Mg concentrations in either direction depending on the circumstances (Brand and Veizer, 1980, Brand 2004). Aluminium was also measured as an indicator of contamination by clay minerals, which can cause elevated Mg/Ca values (Barker et al., 2003). As the shells in the study of *T.retusa* from the Firth of Lorne were collected alive, the effects of post-mortem diagenesis are absent. The data in this study represent the natural levels of elemental incorporation into the shell before death. It should be noted however that incorporation of clays into punctae or sub-millimetre scale cracks within the shell may cause elevated values of Mg, Sr and Al.

For the specimens used in Chapter 6 (‘Using Mg/Ca Ratios to Assess Seawater Temperatures across the Silurian ‘Ireviken Excursion’ on Gotland, Sweden’) the

method used for the laser ablation was that same as all other chapters with one exception. The frequency of the laser was changed from 10 Hz to 20 Hz, this was because in a chance experiment showed that 20 Hz provided a more consistent and powerful signal than 10Hz.

3.3 Stable isotope analysis

3.3.1 Firth of Lorne

Powder for stable isotope analyses was drilled using a New Wave Research Micromill. For *T.retusa* valve 1D the stable isotope trenches were drilled to a depth of 200 μm, length of 460 μm and width of ~ 60 μm. In the ontogenetic sampling of *T.retusa* valve 1V the dimensions of the trench were 1 mm long, 100 μm deep and ~60 μm wide. This was changed as the valves were slightly thinner in places and the longer, shallower trench minimised the risk of incorporating calcium carbonate from the primary layer. Trenches with smaller dimensions did not produce enough powder for accurate stable isotope analysis. After each trench was drilled and the powdered sample transferred to a plastic vial, the trench, sample surface and drill bit were cleaned with deionised water and a brush to ensure no cross contamination of powder between trenches. Trenches were drilled as close to the inner margin of the shell as possible, as only the inner half to two thirds of the shell thickness are known to be in oxygen isotopic equilibrium with the ambient sea water (Parkinson et al., 2005). Samples were analysed at Cardiff University on a Thermo MAT 253 with a Kiel IV carbonate preparation device. Analytical precision was determined by use of in-house Carrara marble calibrated against international (NBS19) carbonate standards with a precision of 0.07 ‰ for $\delta^{18}O$ and 0.04 ‰ for $\delta^{13}C$. All results are reported relative to the PDB scale.

3.3.2 New Zealand depth transect

Except for *L. neozelanica* E720 which was drilled down the entire length of an ontogenetic section, stable isotope sampling was carried out using a slightly different technique to that used for the Scottish *T. retusa*. For the other New Zealand shells a single trench, 1 mm long, 100 μm deep and 60 μm wide was drilled in each shell using a New Wave Research Micromill. The specimen was drilled as close to the interior margin as possible and in the thickest section available. Using the thickest part of the section was implemented to avoid drilling any of the primary layer, which is shown to be out of oxygen isotopic equilibrium with ambient sea water (Parkinson, 2005). This technique was used to produce an average value for the shell by drilling a trench which had a length long enough to incorporate both potential winter and summer signals.

The $\delta^{18}O$ temperature calculation was done using an adapted version of the Brand et al. (2013) equation, equation 1 below:

Equation 1. $$T = 16.89 - 4.18(\delta^{18}O_{calcite} - \delta^{18}O_{seawater}) + 0.18(\delta^{18}O_{calcite} - \delta^{18}O_{seawater})^2$$

This equation is based upon the thorough delineation of the relationship between $\delta^{18}O$ and seawater temperature in modern brachiopod calcite recently provided by Brand et al. (2013); it is a second order polynomial fit to data from their supplementary data Table S2. Unlike Brand et al. (2013), it was chosen not to include a correction for the effect of Mg on $\delta^{18}O$, as this is derived from a study of synthetic magnesian calcite, where it is required for Mg/Ca values above 100mmol/mol (Jiménez-López et al., 2004). The $\delta^{18}O$ values for seawater for the South Pacific are taken from LeGrande and Schmidt (2006).

3.3.3 Eocene-Oligocene Transition

Followed the technique outlined in section 3.3.2.

3.3.4 Silurian Ireviken Excursion

The method of section preparation was the same as all other shells. However, all shells that were sectioned longitudinally were drilled in two separate places for stable isotopes. One trench ~1 mm long, 100 μm wide and 150 μm deep was drilled in the umbo section of the shell as this has before been used to collect powder for stable isotopes or the part of the shell used has not been specified (e.g. Brand et al., 2006). This is because this area of the shell is generally the thickest, easiest to drill and most likely to be preserved. However, Parkinson et al. (2005) suggested that the umbo area of the shell may lead to erroneous temperatures being calculated from the stable isotopes as it is out of oxygen isotopic equilibrium with the ambient seawater. Therefore, to test if there is any marked difference between the umbo and the rest of the shell, a second trench ~1 mm long, 100 μm wide and 150 μm deep was drilled in the adult third of the shell avoiding the primary layer. The thickest part of this area of shell was chosen as this gives the greatest distance between the area sampled and the primary layer of the shell. The shell was too thin to drill the whole shell for stable isotopes.

On the transversely sectioned shells only one trench was drilled ~1 mm long, 100 μm wide and 150 μm deep. This trench was drilled in the thickest section available, as far away from the primary layer as possible.

CHAPTER 4: INVESTIGATING THE Mg/Ca : TEMPERATURE RELATIONSHIP IN MODERN BRACHIOPODS. CALIBRATING *Terebratulina retusa* AND *Liothyrella neozelanica* FROM KNOWN WATER TEMPERATURES.

4.1 Introduction

The basis for the Mg/Ca proxy for palaeotemperature is founded in laboratory experiments by Katz (1973) who showed that the partition coefficient of Mg^{2+} into inorganic calcite correlates extremely well with temperature. The equation below shows how Mg^{2+} substitutes for Ca^{2+} in the calcite lattice.

$$CaCO_3 + Mg^{2+} \rightarrow MgCO_3 + Ca^{2+}$$

Magnesium to calcium ratios (Mg/Ca) have been established as proxies for marine temperatures in a range of calcite shells, e.g. benthic and planktonic foraminifera and ostracodes (Chivas et al., 1986; Dwyer et al., 1995; Nürnberg et al., 1996; Rosenthal et al., 1997). Although the Mg/Ca-temperature relationship in biogenic carbonates likely represents a combination of thermodynamic and physiological effects (Rosenthal et al., 1997), initial studies by Lee et al. (2004), Perez-Huerta et al. (2008) and Brand et al. (2013) suggest that a consistent Mg/Ca-temperature dependence may also be found in brachiopod calcite. This consistent temperature dependence allows study of temperature change but vital or physiological effects may make comparison between species somewhat difficult.

As a tool for obtaining palaeoclimate data rhynchonelliform brachiopods have several benefits when compared to other fauna recording palaeoclimate signals. All shells of the subphylum Rhynchonelliformea have a fibrous secondary layer of low

magnesium calcite (Williams et al., 1996), which is the most diagenetically stable form of $CaCO_3$ (e.g. Lowenstam, 1961; Veizer et al., 1986). Rhynchonelliform brachiopod shells are present from the Early Cambrian to the present (Zhang et al., 2008). This long fossil record offers the potential to collect palaeoclimate data as far back as the early Palaeozoic, and to calibrate fossil data against modern observations. Excluding the pelagic larval stage, brachiopods stay in one place on the ocean floor throughout their life, and are therefore static recorders of their environment. Brachiopod shells also have distinct growth lines. Although poorly understood, these possibly represent seasonal change (Buening and Carlson, 1992), and may also form biannually at times of physiological and environmental stress, such as spawning (Curry 1982). Therefore brachiopods may represent an untapped archive of past seasonality.

A recent study of Mg in rhynchonelliform brachiopod shells using synchrotron X-ray absorption near edge spectroscopy has confirmed that Mg resides within the calcite lattice and is therefore suitable for use as a temperature proxy (Cusack et al., 2008). Modern rhynchonelliform brachiopod shells all have an outer primary layer of prismatic calcite and an inner secondary layer of fibrous calcite, and some species have an additional tertiary layer of prismatic calcite (Williams & Cusack, 2007). Previous laser ablation studies of rhynchonelliform brachiopods using spot analyses have shown that the primary layer displays high and variable Mg concentrations (Perez-Huerta et al., 2008). Mg concentrations within the secondary layer however, are reproducible (Perez-Huerta et al., 2008), and symmetrical in transects perpendicular to the main axis of growth (Lee et al., 2004). Both these studies suggest that secondary layer calcite might record seawater temperature signals. In addition, it has been shown that secondary layer calcite is precipitated in oxygen

isotopic equilibrium with the ambient seawater, when sampling has avoided shell parts subject to resorption and renewed calcification during life (the muscle scars, loop and teeth) (Parkinson et al., 2005; Yamamoto et al., 2010a, 2010b, 2011; Brand et al. 2014). Unlike oxygen isotopes in carbonate Mg/Ca is independent of the influence of salinity (Lear et al., 2000).

A study of the Recent rhynchonelliform, *Laqueus rubellus* demonstrated that Mg/Ca maxima coincide with seasonal periods of shell growth evidenced by the morpho-statistical approach of calculating deviations from a spiral shell growth curve (Pérez-Huerta et al., 2014).

In light of the above studies, the current chapter aims to test the hypothesis that the cyclic variations in intra-shell Mg/Ca profiles represent seasonal temperature variations.

Section 3.2.1 describes a laser ablation method that retrieves profiles of trace element to calcium ratios from brachiopod shells which are reproducible on the sub-mm scale. The current chapter compares laser trace element and micro-drilled stable isotope data to determine whether seasonal temperature variations are recorded in Mg/Ca profiles of modern shells of *T. retusa* (Linnaeus, 1758) and *L. neozelanica* (Thomson, 1918) (shells described in Chapter 2). Mean shell Mg/Ca of modern *L. neozelanica* specimens from a water depth transect are also investigated. The combined approach of using measured water temperatures as well as $\delta^{18}O$ calculated temperatures enables preliminary calibration of the Mg/Ca:temperature relationship.

4.2 Results

4.2.1 Diagenetic assessment of specimens from a modern depth transect off the north coast North Island, New Zealand.

As the *T. retusa* shells in this study are modern and were collected alive, the effects of post-mortem diagenesis are absent. The data in this study represent the natural levels of incorporation of elements into the shell before death. In contrast, the dredged *L. neozelanica* samples each experienced variable unknown lengths of time on the sea-floor after death. The *L. neozelanica*; ranged from complete valves (X128) to specimens with large sections of the valve missing (J691). There was however no correlation between completeness of the valve and their geochemical preservation.

Five of the *Liothyrella* shells, C777, C797, X128, X193 and E840 showed evidence

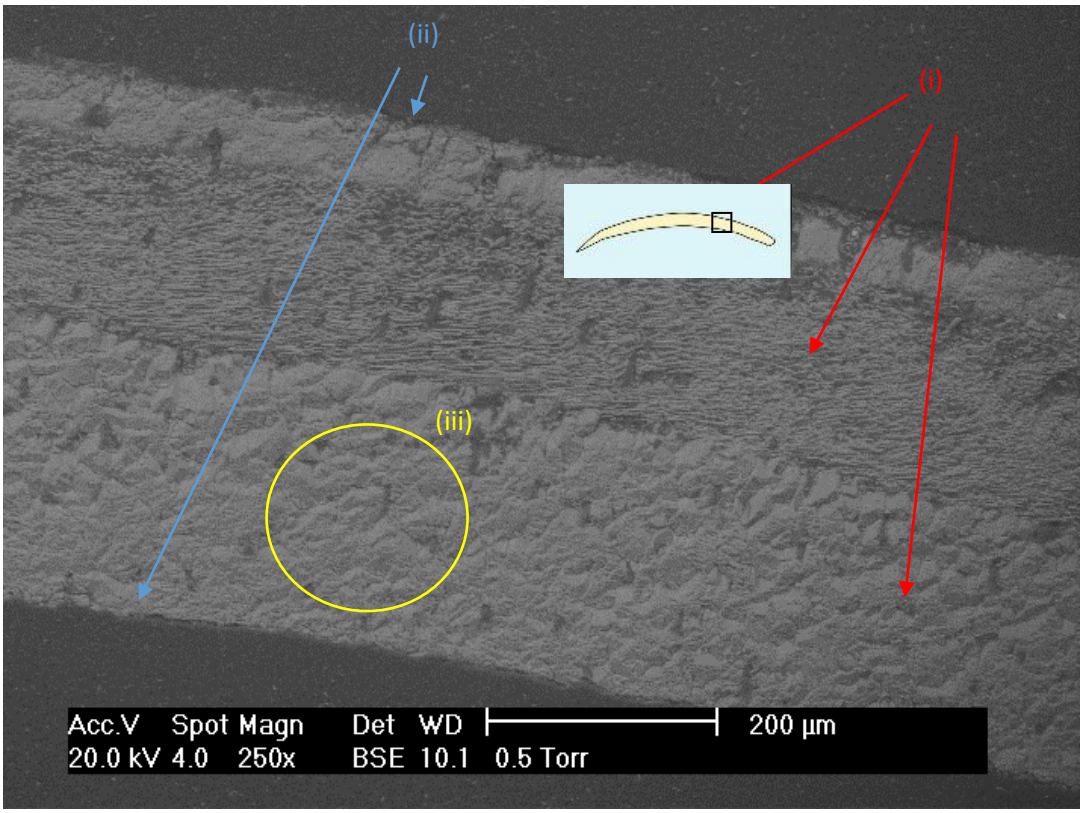

Figure 4.2.1-1 Specimen E720, a well preserved *L.neozelanica* under SEM. (i) Layers of ultrastructure (ii) Contact between resin and shell material (iii) Representative area of similar tone. Inset shows area of SEM image,

of diagenetic alteration. Firstly, hand specimen observations suggested discolouration of valves (Appendix 1, photos in figures 2.2.2-1 and 2.2.2-2). Characteristics of all specimens viewed in hand specimen can also be seen in Appendix 1. However the main differences between the specimens rejected for further analysis, highlighted red in Table 4.2.1-1, and those highlighted blue in Table 4.2.1.-1 will be summarised here. The unaltered specimens generally had a semi-translucent appearance, creamy-white colour and had little sign of any encrusting organisms on the valve. The diagenetically altered specimens were opaque, orangey-brown in colour and occasionally had a pocked or marked surface where encrusting organisms or diagenesis had altered the texture of the shell.

SEM and laser ablation data were used to investigate altered versus pristine samples. These observations show that some valves had been resting on the sea bed long enough for organisms to start boring into the valves. SEM imagery showed that the pristine nature of the ultrastructure, in these five shells, was in many places no longer intact due to boring or alteration (Appendix 1; SEM images for specimens C777, C797, E840, E720, E870 and J691). However the general differences between the altered specimens and the unaltered specimens are as follows. Pristine ultrastructure in *L. neozelanica*, Figure 4.2.1-1, is simple to recognise under SEM:

i. Primary, secondary and tertiary ultrastructural layers are present, well defined and complete without any large cracks, holes or borings.
ii. The edges of the shell have a sharp contact to the resin surrounding the shell.
iii. When using the backscatter electron detector the calcite is all of a similar ‘tone’ with few dark areas which may indicate infilling resin or clays.

Each of the four shells rejected were shown to have one or a combination of the

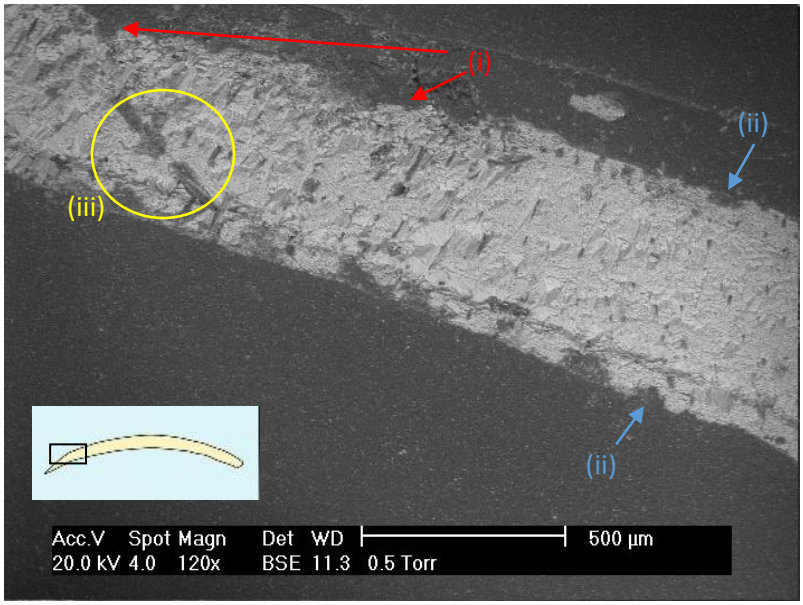

Figure 4.1.2-2 Specimen E840, areas of poor preservation in a *L.neozelanica* under SEM. Inset image shows SEM image location.

following properties under SEM: (Figure 4.2.1-2).

i. Sections of the primary layer partly or completely missing.

ii. Borings into the internal or external surface of the valve continue up to 50 µm into the valve.

iii. Transitions between ultrastructural layers are poorly defined,

    a. Original structure is poorly defined.

    b. Within individual layers the tone of the image is not uniform and as a result dark areas which may be resin or clay infills are present.

Laser ablation ICP-MS analysis, using the method detailed in Chapter 3.1.2, shows that the specimens have very high levels of Al/Ca in the profile compared to pristine specimens, and slightly elevated Mn/Ca, Table 4.2.1-1. The five shells showing diagenetic alteration show a strong correlation between Al/Ca and Mg/Ca, R^2 values

are between 0.45 and 0.95 for these specimens (Figure 4.2.1-3) whilst the pristine specimens from New Zealand and the live specimens have R^2 values lower than 0.12 (Figure 4.1.2-3).

Specimen	Average Al/Ca (mmol/mol)	Average Mn/Ca (mmol/mol)
C777	39.7 ± 3.7	0.05 ± 0.003
C797	5.8 ± 0.54	0.1 ± 0.01
X128	8.8 ± 0.92	0.61 ± 0.005
E840	15.2 ±1.71	0.4 ± 0.02
X193	5.3 ± 0.62	0.3 ± 0.03
E720	0.2 ± 0.01	0.02 ± 0.000
E870	0.2 ± 0.05	0.04 ± 0.000
J691	0.1 ± 0.01	0.04 ± 0.001

Table 4.2.1-1 Average values of Al/Ca and Mn/Ca in *L.neozelanica* shells from New Zealand. Specimens highlighted red represent poorly preserved shells rejected due to high levels of Al/Ca. E840 highlighted orange shows a moderate level of preservation and was still used for analysis after diagenetic screening. Specimens highlighted blue show good levels of preservation. Error is shown at two standard error.

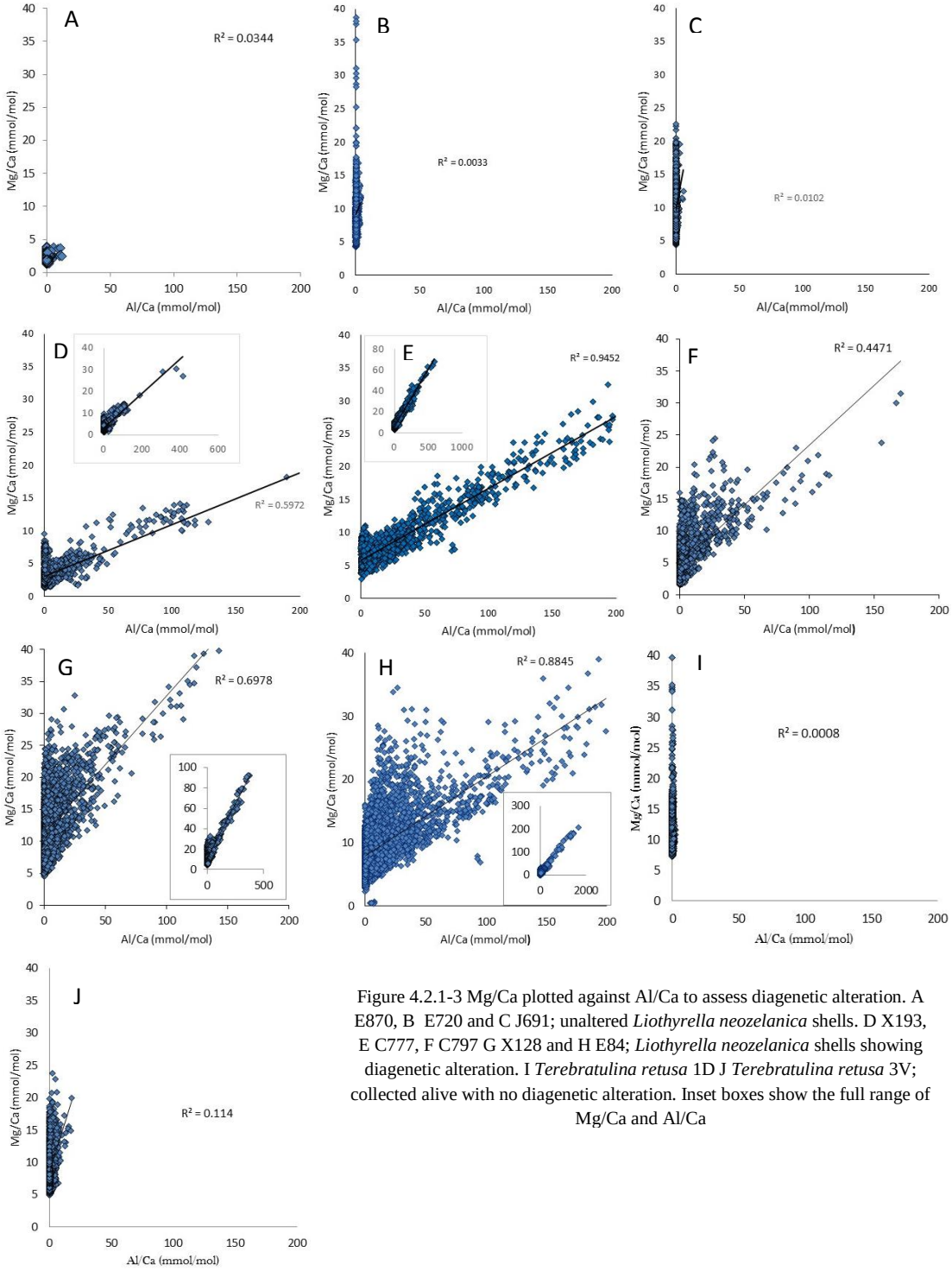

Figure 4.2.1-3 Mg/Ca plotted against Al/Ca to assess diagenetic alteration. A E870, B E720 and C J691; unaltered *Liothyrella neozelanica* shells. D X193, E C777, F C797 G X128 and H E84; *Liothyrella neozelanica* shells showing diagenetic alteration. I *Terebratulina retusa* 1D J *Terebratulina retusa* 3V; collected alive with no diagenetic alteration. Inset boxes show the full range of Mg/Ca and Al/Ca

The diagenetically altered specimens were screened to 4 mmol/mol as Mg/Ca and Al/Ca data below this threshold showed no correlation, $R^2 < 0.05$ in all specimens. C777, C797, X128 and X193 all show large signs of diagenetic alteration and were rejected from for further analysis whilst after screening E840 produced a geochemical profile deemed to be reliable and as such was considered for further analysis (Figure 4.1.2-4). All diagenetically screened transverse profiles are in Appendix 2.

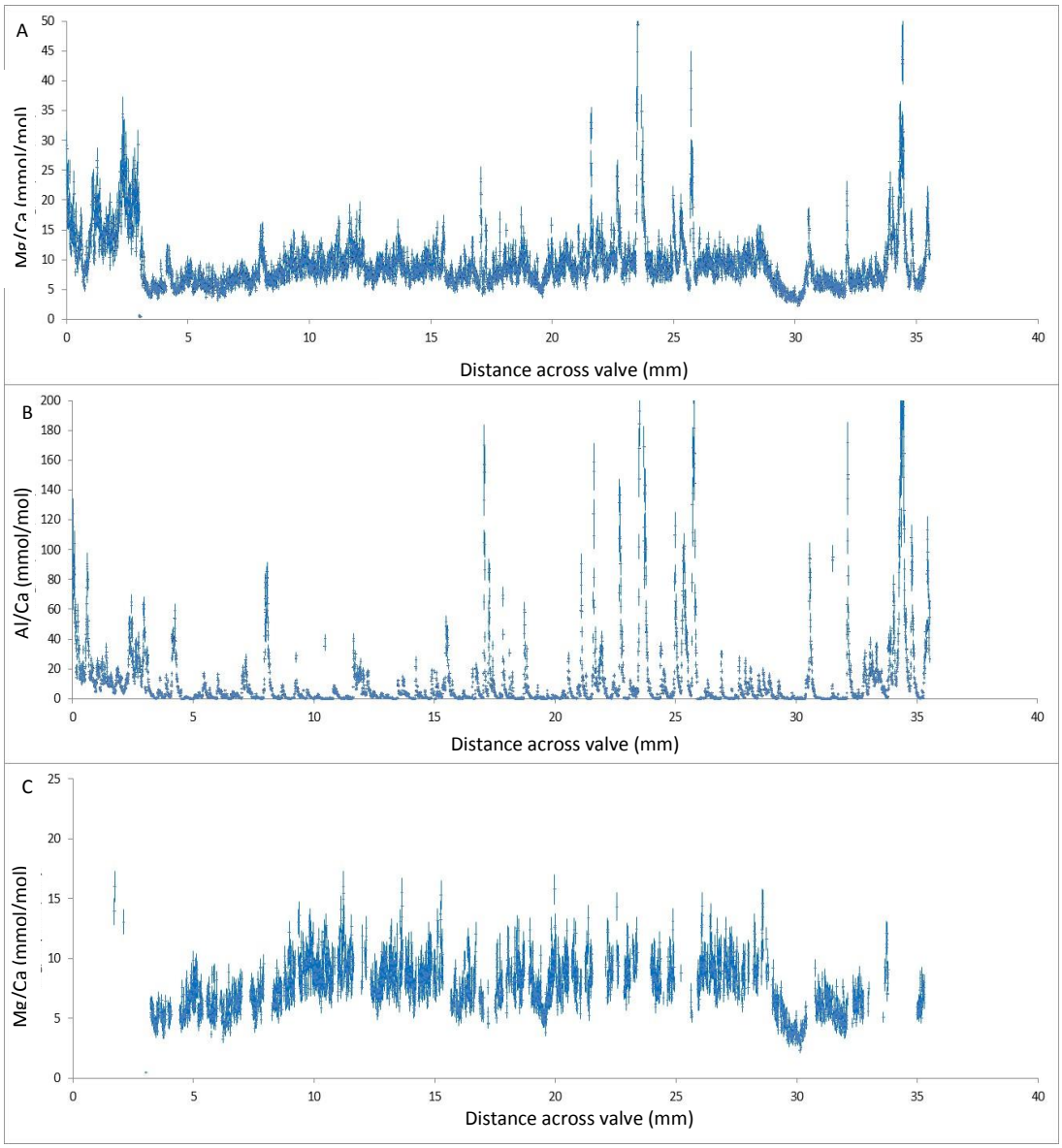

Figure 4.2.1-4 Mg/Ca plotted against Al/Ca to assess diagenetic alteration in *Liothyrella neozelanica* E840. A Mg/Ca pre-screening, B Al/Ca and C Mg/Ca after screening..

4.2.2 Reproducibility of intra-shell element/calcium profiles

To assess the reproducibility of LA-ICP-MS intra-shell profiles, we ran repeat analyses on two different short tracks from the dorsal valve of *T. retusa* shell 1 (see inset, Figure 4.2.2-1). Identical elemental profiles are not expected as subsequent traverses sample slightly deeper in the valve on each run. However, Mg/Ca profiles of repeated tracks have reassuringly similar shaped profiles and Mg/Ca ranges (Figure 4.2.2-1). Furthermore, the Mg/Ca values of a run are positively correlated with subsequent runs, with R^2 values between 0.70 and 0.81. Where the Mg/Ca of Track 1 reaches > 20 mmol/mol at ~ 0.3 mm, it is likely that the laser began sampling material from the primary layer. Mg/Ca values are closely comparable to the data of Perez-Huerta et al. (2008) who produced profiles using five laser spots across the width of *T. retusa* valves from the same locality. Three repeated runs of Track 2, parallel to the inner margin of the valve, also yield consistent Mg/Ca

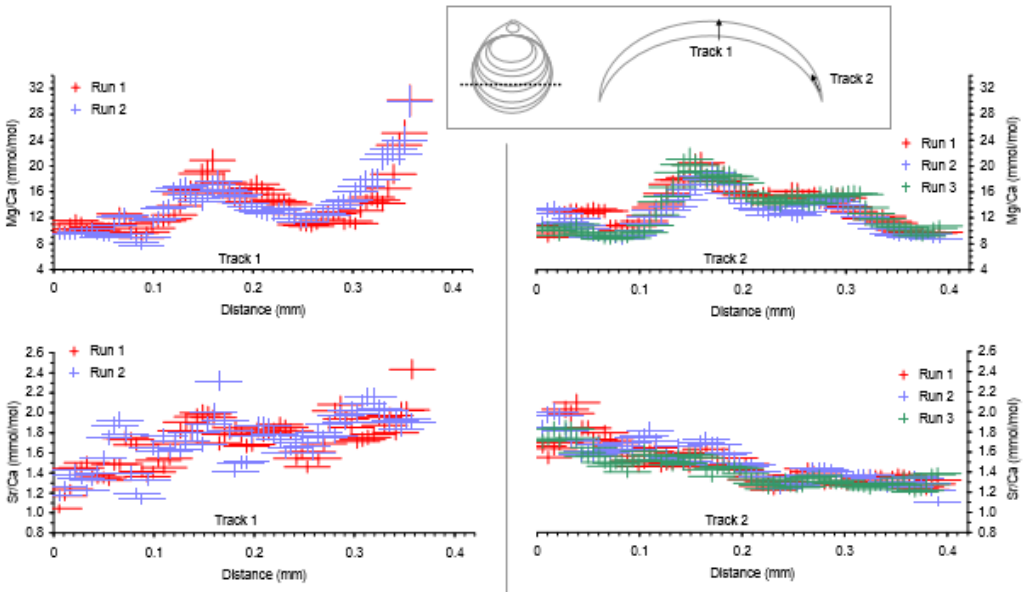

Figure 4.2.2-1Repeat Mg/Ca and Sr/Ca profiles from *T. retusa* dorsal valve 1D: Track 1, across the sectioned valve from interior to exterior margin, Track 2, in the middle of the sectioned valve parallel to the interior margin. The *x* error bars reflect the spatial resolution of the sampling, and the *y* error bars reflect analytical uncertainty based on standards run throughout the day (8% RSD for Mg/Ca and 4% RSD for Sr/Ca). For this and all subsequent figures, the dashed line in the inset box indicates the approximate line of section, and the arrowed lines show the position of the laser tracks.

Sr/Ca values of a run and subsequent runs are more weakly correlated (R^2 between

0.35 and 0.72) than is the case for Mg/Ca. Both runs of track 1 have a Sr/Ca range of ~ 1.4 mmol/mol. The repeated runs of Track 2 have a Sr/Ca range of 0.9 ± 0.1 mmol/mol. Mg/Ca and Sr/Ca do not co-vary in Track 2, parallel to the shell margin, although appear to be weakly correlated in Track 1, across the shell width (R^2 of 0.41 and 0.55), which includes both the primary and secondary calcite layers (Figure 4.2.2-1).

4.2.3 Geochemical variability along an ontogenetic section of T. retusa

Element profiles were taken from the posterior to the anterior margin of the ventral valve of *T. retusa* shell 1 (1V, Figure 4.2.3-1) to examine variations in shell chemistry from the juvenile to adult portions of the valve. The full range of Mg/Ca variation in valve 1V reaches up to 120 mmol/mol in the youngest shell material, an enrichment of ~10 times the average value of the adult shell (Figure 4.2.3-1, 1V inset). Including this large peak, the Mg/Ca profile of 1V shows 9 pairs of Mg/Ca peaks and troughs spaced ~2 – 3 mm apart, with all except the youngest two being between 6 and 12 mmol/mol in peak-to-trough magnitude (Figure 4.2.3-1).

To allow comparison of $\delta^{18}O$ and Mg/Ca data on the same spatial scale, I plot laser Mg/Ca data averaged over the same distances as the trenches drilled for $\delta^{18}O$ analysis ('Averaged Mg/Ca'). In the youngest part of valve 1V, the profiles of $\delta^{18}O$ and averaged Mg/Ca do not co-vary (0 – 7.5mm from the posterior edge of the valve, shaded grey). However, Mg/Ca maxima and minima correspond with lighter and heavier $\delta^{18}O$ respectively, from 7.5mm onwards, the adult portion of the valve.

The ontogenetic Sr/Ca profile (1V) displays values as high as 2.8 mmol/mol at 0 – 1.2 mm, which is around twice the average value of the rest of the valve. Between 2 – 15 mm Sr/Ca show fluctuations with peak-to-trough magnitudes of up to 0.5

mmol/mol. Sr/Ca maxima generally correspond to Mg/Ca maxima, however Sr/Ca variations are more poorly defined than the Mg/Ca peaks and troughs (Figure 4.2.3-1).

Laser $^{43}Ca/^{48}Ca$ profiles are included as a monitor of instrument performance and an indicator of the possible inclusion of non-carbonate material in the shell. There is no significant variation in this ratio on profile 1V except for a small increase in scatter centred around 1mm.

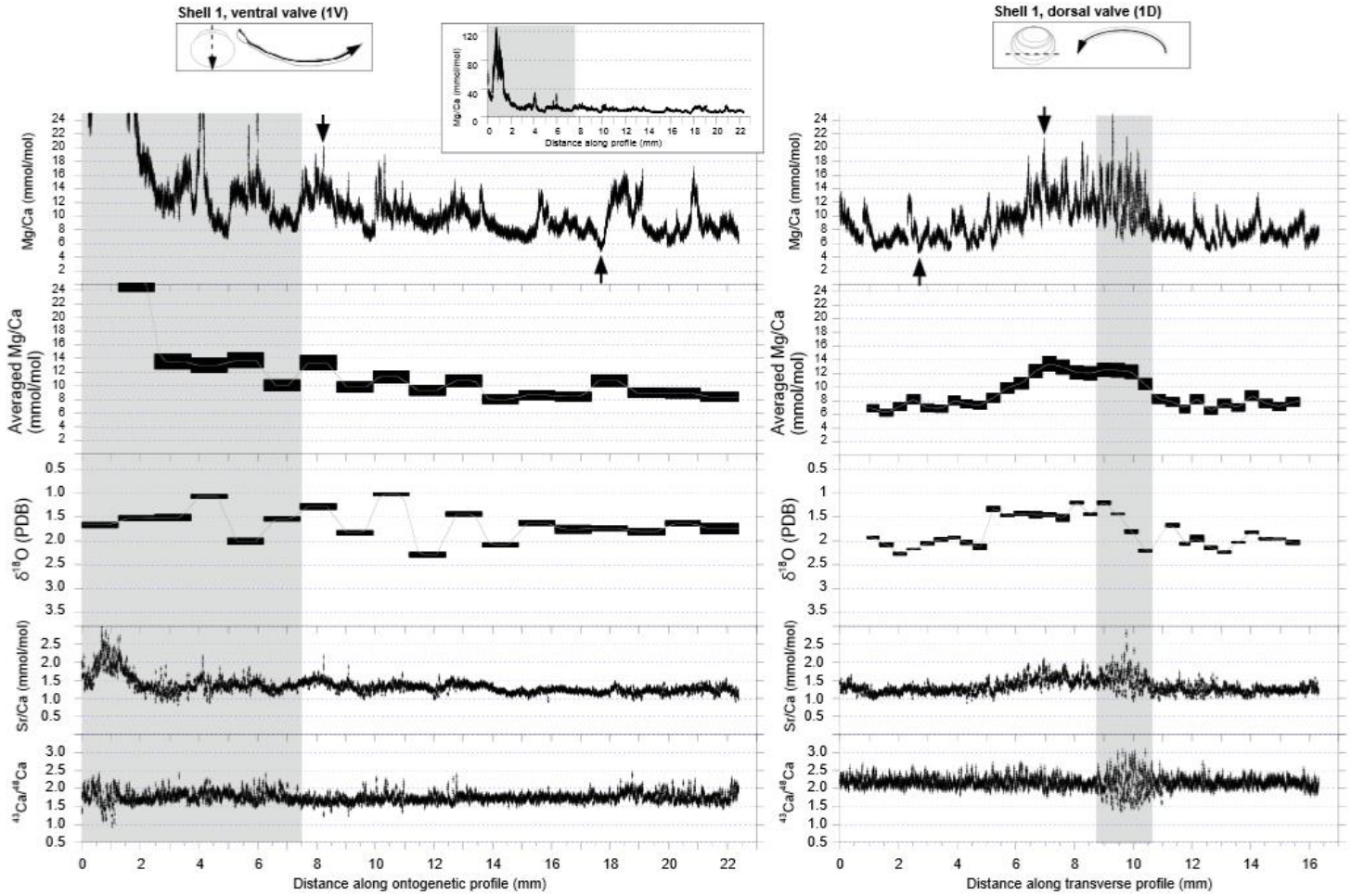

Figure 4.2.3-1 Profiles of laser Mg/Ca, Sr/Ca and $^{43}Ca/^{48}Ca$ intensity data, and microdrilled $\delta^{18}O$ data from *T. retusa* shell 1. 'Averaged Mg/Ca' is a plot of the laser Mg/Ca data averaged over the same distances as the trenches drilled for $\delta^{18}O$ analysis. 1V is an ontogenetic section, from the posterior to anterior margin of the ventral valve. The inset box shows the full range of Mg/Ca values, and grey shading denotes where $\delta^{18}O$ and averaged Mg/Ca do not co-vary. 1D is a transverse section, the grey shading denotes a portion removed through data screening due to the coincidence of high Mg/Ca and Sr/Ca with scattered $^{43}Ca/^{48}Ca$. The maximum and minimum values of the adult portions of the laser Mg/Ca profiles are indicated by arrows. For laser data, Y error bars reflect analytical uncertainty based on standards run throughout the day (+/- 8% RSD for Mg/Ca, and +/- 4% RSD for Sr/Ca and $^{43}Ca/^{48}Ca$). For $\delta^{18}O$, the Y error bars represent +/- 1sd of the individual measurements.

4.2.4 Geochemical variability along a transverse section of T. retusa

Profile 1D of Figure 4.2.3-1 reports data obtained from a transverse section of the dorsal valve of *T. retusa* shell 1. This section was cut at approximately two thirds of the distance from the shell posterior margin to avoid potential crystallographic effects present in the posterior region (Perez-Huerta et al., 2011), and to allow comparison between ventral (1V) and dorsal (1D) valves of the same shell.

The $^{43}Ca/^{48}Ca$ ratio is constant at 2.2 +/- 0.4 across this transverse profile, except for a short portion with more variable ratios (~ 9 – 10.5 mm), which correspond to more noisey Mg/Ca and Sr/Ca values (1D, Figure 4.2.3-1, shaded grey). The cause of this increased scatter is unknown, but is likely to be either contamination by clay minerals, non-shell carbonate or resin causing isobaric interference in the Ca mass range. These shaded data are not considered in further discussion, although they highlight the usefulness of the $^{43}Ca/^{48}Ca$ ratio as a preliminary screen of data quality. Disregarding this small portion, the Mg/Ca data delineate a profile that is approximately symmetrical about the mid-line in terms of the magnitude and spacing of the peaks (cf. Lee et al., 2004). At the edges of the valve, 0 – 6 mm and 11 – 16 mm, which grew when the brachiopod was older, Mg/Ca displays narrow peaks reaching ~ 13 mmol/mol and broader minima of ~ 5 mmol/mol. In the centre of the valve, 6 – 9 mm, which grew when the brachiopod was younger, values are higher and more scattered between ~7 – 21 mmol/mol. The Mg/Ca variations of this transverse profile (1D) have similar peak-to-trough magnitudes (6 – 12 mmol/mol), and similar absolute maxima and minima (arrowed) as the data from the adult part of the ontogenetic profile from the corresponding ventral valve (Figure 4.2.3-1, 1V, unshaded).

There is a good overall similarity between the $\delta^{18}O$ and averaged Mg/Ca profiles of valve 1D, with higher Mg/Ca and lighter $\delta^{18}O$ in the centre of the valve. Maximum and minimum $\delta^{18}O$ values of valve 1D (2.28 ‰ and 1.33 ‰) are very similar to those recorded in valve 1V (2.29 ‰ and 1.02 ‰). Sr/Ca data are approximately 0.5 mmol/mol higher in the centre of the transverse profile (6 – 9 mm) than the edges of the valve (0 – 6 mm and 11 – 16 mm) (Figure 4.2.3-1, 1D).

4.2.5 Variation in shell chemistry between three T. retusa shells (six valves)

Profiles of laser data from the remaining transversely sectioned *T. retusa*, shells 2 and 3, are presented in Figure 4.2.5-1. All four profiles are approximately symmetrical about the mid-line, with deviation resulting from the difficulty in cutting a section exactly perpendicular to the growth axis. Sr/Ca data vary by less than 0.5 mmol/mol in all valves, and the $^{43}Ca/^{48}Ca$ ratio is constant between and across all valves. Mg/Ca peak-to-trough magnitudes are closely comparable to those seen in shell 1 (Figure 4.2.3-1), with the highest magnitude, 14 mmol/mol, also seen in valves 2D and 3D. Absolute maximum and minimum Mg/Ca values are consistent between both valves of the same shell, and between all valves of three individual shells (Table 4.2.5-1).

Shell	Section	Valve (D=Dorsal, V=Ventral)	Minimum Mg/Ca (mmol/mol)	Maximum Mg/Ca (mmol/mol)	(Mg/Ca_{Max}-Mg/Ca_{Min}) /ΔT (mmol/mol / ˚C)
1	Ontogenetic	V (excluding grey shaded region on Fig.4)	5.1	18.8	2.1
1	Transverse	D (excluding grey shaded region on Fig.4)	5.0	19.8	2.3
2	Transverse	V	6.1	18.6	1.9
2	Transverse	D	6.2	18.4	1.9
3	Transverse	V	7.3	18.6	1.7
3	Transverse	D	4.6	16.5	1.8
Mean			**5.7 +/- 0.8 (2se)**	**18.5 +/- 0.9 (2se)**	**2.0 +/- 0.2 (2se)**

Table 4.2.5-1. Maximum and minimum Mg/Ca seen in *T. retusa* valves collected live from the Firth of Lorne, which has a measured temperature range of 6.5 – 13˚C (Curry, 1982).

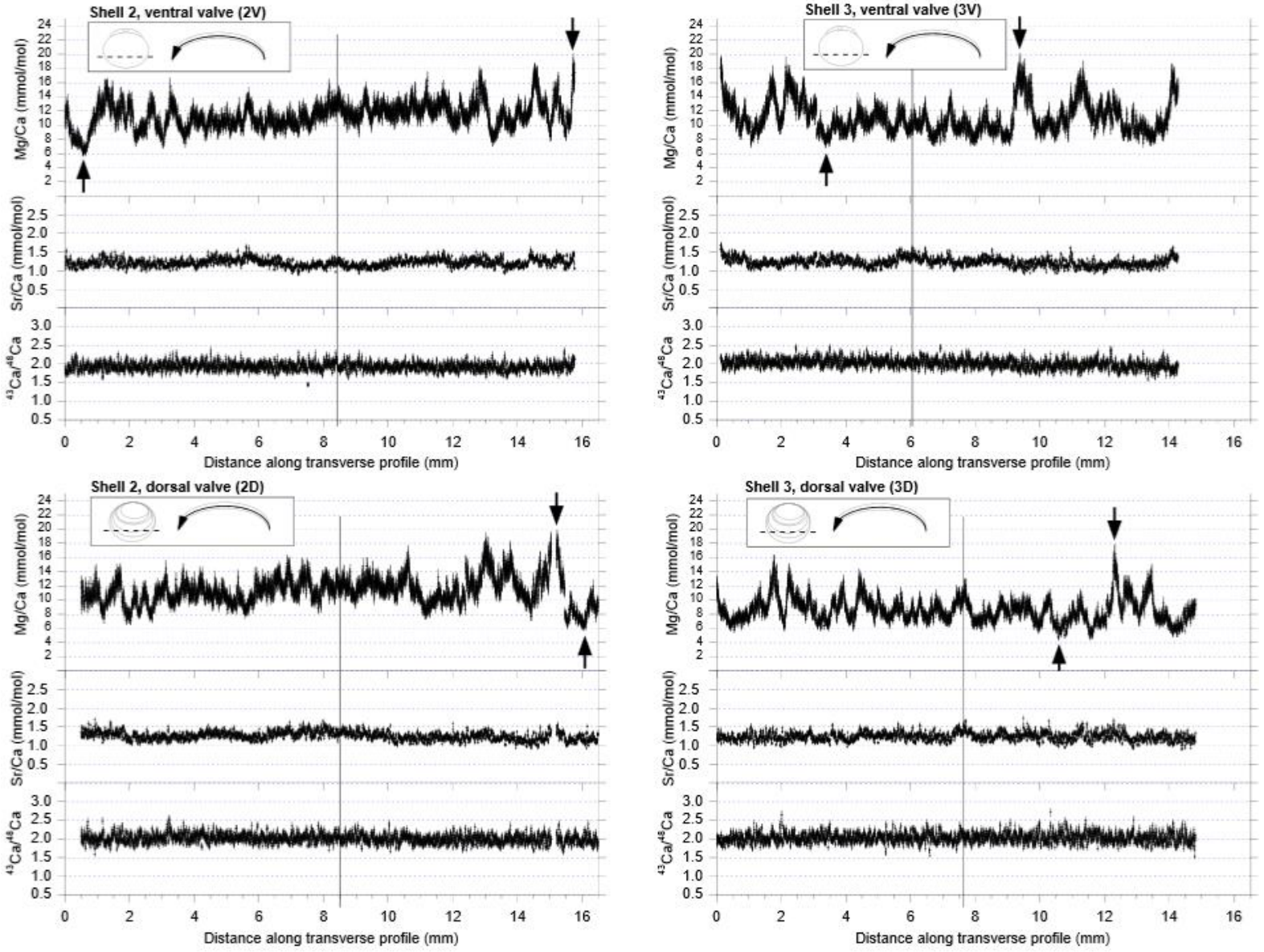

Figure 4.2.5-1. Transverse profiles of laser Mg/Ca, Sr/Ca and $^{43}Ca/^{48}Ca$ intensity data from *T. retusa* shells 2 and 3. Maximum and minimum values of the Mg/Ca profiles are indicated by arrows. Vertical lines show the suggested mid-line of the valve. Y error bars reflect analytical uncertainty based on standards run throughout the day, +/- 8% RSD for Mg/Ca and +/- 4% RSD for Sr/Ca and $^{43}Ca/^{48}Ca$.

4.2.6 Geochemical variability along an ontogenetic section of L. neozelanica

Like the *T. retusa* data, the *L. neozelanica* ontogenetic section (valve E720) has its highest Mg/Ca values (up to 25 mmol/mol) in the most juvenile (posterior) part (0 - 2.5 mm, shaded grey) (Figure 4.2.5-1). The remainder of the valve displays Mg/Ca variations with peak-to-trough magnitude between 3 and 12 mmol/mol, on spatial scales of ~1mm. As observed for *T. retusa*, Mg/Ca and $\delta^{18}O$ do not co-vary in the juvenile portion of the ontogenetic section. However, the $\delta^{18}O$ and averaged Mg/Ca profiles of this *L. neozelanica* shell show a high degree of co-variation from ~2.5mm onwards. $\delta^{18}O$ ranges from 1.3 to 1.9 ‰. The largest Sr/Ca variations seen in the adult part of the valve are ~0.7 mmol/mol in magnitude and coincide with large Mg/Ca variations (at ~24 - 26mm). The maximum, minimum and peak-to-trough amplitudes of the Mg/Ca variations seen in the adult calcite are similar to those seen in the transverse section of this shell (Figure 4.2.6-1, E720).

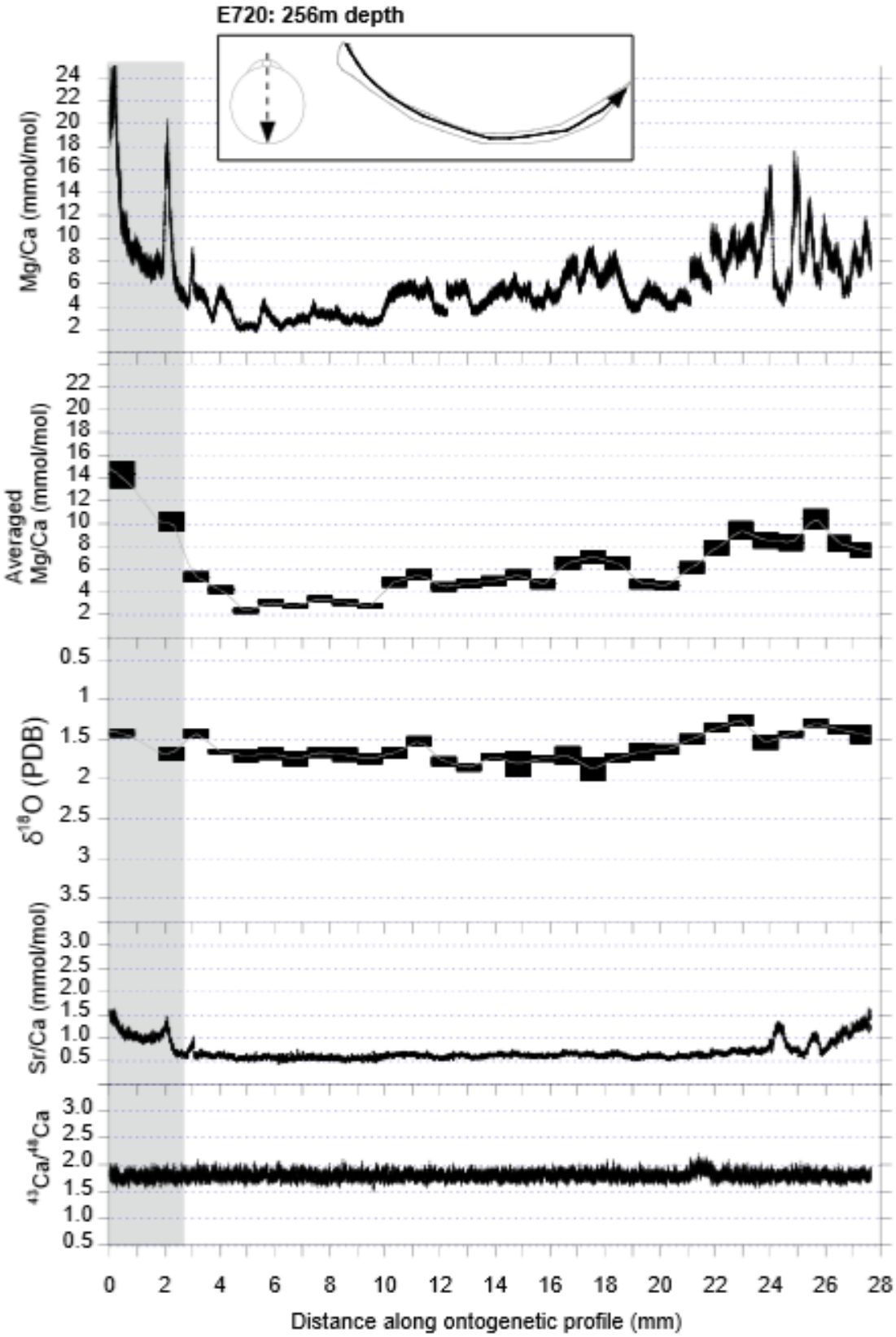

Figure 4.2.6-1. Ontogenetic profile of laser Mg/Ca, Sr/Ca and $^{43}Ca/^{48}Ca$ intensity data, and microdrilled $\delta^{18}O$ data from *L. neozelanica* shell E720. 'Averaged Mg/Ca' is a plot of the laser Mg/Ca data averaged over the same distances as the trenches drilled for $\delta^{18}O$ analysis. Grey shading denotes where $\delta^{18}O$ and averaged Mg/Ca do not co-vary. For laser data, Y error bars reflect analytical uncertainty based on standards run throughout the day (+/- 8% RSD for Mg/Ca, and +/- 4% RSD for Sr/Ca and $^{43}Ca/^{48}Ca$). For $\delta^{18}O$, the Y error bars represent +/- 1sd of the individual measurements.

4.2.7 Liothyrella neozelanica from a modern water depth transect

Four *L. neozelanica* shells from the New Zealand water depth transect (168m – 1488m) were sectioned transversely (Figure 4.2.7-1). With increasing water depth of recovery, the valve profiles show a reduction in the mean Mg/Ca, as well as reduced

Valve	Depth of recovery (m)	$\delta^{18}O$ (‰VPBD)	$\delta^{18}O$ temperature from Equation 1 (˚C)	Min. Mg/Ca (mmol/mol)	Max. Mg/Ca (mmol/mol)	Temperature at Depth of Recovery from Closest CTD Site (°C)
J691	168	1.31 +/- 0.07	13.6	~ 4	~24	15.0
E720 Ontogenetic section **'coldest'** **'warmest'**	256	1.88 +/- 0.15 1.26 +/- 0.07	11.2 13.5	~2	~17	13.5
E720 Transverse section	256	1.64 +/- 0.04	12.1	~ 4	~20	13.5
E840 Transported downslope?	757	1.68 +/- 0.03	11.0	~ 3	~17	7.5
E870 Transported downslope?	1488	2.93 +/- 0.05	6.6	~ 2	~4	3.0

Table 4.2.7-1. Mg/Ca signals and $\delta^{18}O$ measurements from *L. neozelanica* valves from four different depths.

Mg/Ca peak-to-trough amplitudes (Figure 4.2.7-1, Table 4.2.7-1). Intra-shell Mg/Ca variation is barely discernible in valve E870, which was recovered from 1488m water depth. The largest variation in Sr/Ca seen in these profiles is around 0.5

mmol/mol, occurring in the two valves from the shallowest depth, and the mean value of Sr/Ca decreases with increasing depth. $^{43}Ca/^{48}Ca$ profiles show no significant variation but have a larger degree of scatter in valve E840 (the valve which had the most data removed through screening for contamination by borings, as described in section 4.2.1). Measurements of $\delta^{18}O$ using powder drilled from the hatched regions on Figure 4.2.7-1, become heavier with increasing depth (Table 4.2.7-1).

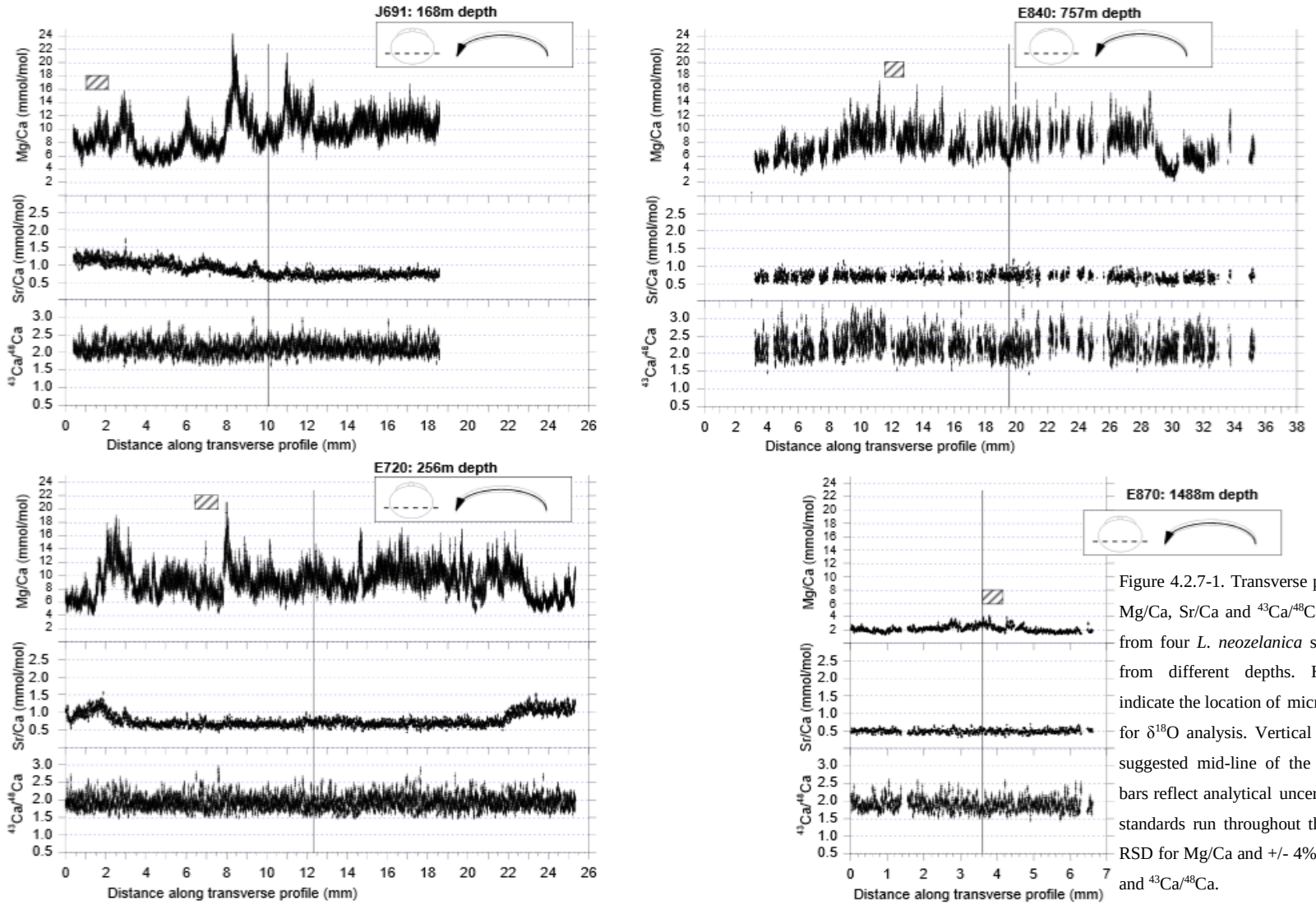

Figure 4.2.7-1. Transverse profiles of laser Mg/Ca, Sr/Ca and $^{43}Ca/^{48}Ca$ intensity data from four *L. neozelanica* shells recovered from different depths. Hatched boxes indicate the location of microdrill sampling for $\delta^{18}O$ analysis. Vertical lines show the suggested mid-line of the valve. Y error bars reflect analytical uncertainty based on standards run throughout the day, +/- 8% RSD for Mg/Ca and +/- 4% RSD for Sr/Ca and $^{43}Ca/^{48}Ca$.

4.3 Discussion

4.3.1 Elevated Mg/Ca in posterior regions of valves

In ontogenetic sections, the posterior regions of both *T.retusa* and *L. neozelanica* have strongly elevated Mg/Ca compared to the rest of the valves (Figures 4.2.3-1 & 4.2.6-1). These are likely caused by the crystallographic orientation effect as observed in *T. retusa* by Perez-Huerta et al. (2011); in the posterior region where the c-axes of calcite crystals are randomly oriented, high and variable Mg/Ca values were reported. The remainder of the valve's secondary layer calcite, where regular fibres have c-axes perpendicular to the inner shell margin, yielded lower and less scattered Mg/Ca values (Perez-Huerta et al., 2011). This feature could possibly be a result of very fast shell growth in young brachiopods (Buening and Carlson, 1992), and is consistent with a growth band study showing that *T.retusa* are immature and fast growing up to 3 years of age (Curry, 1982). It follows that the most reliable portion of brachiopod secondary layer calcite to use for reconstructing seasonality comes from the older parts of the shell (Buening and Carlson, 1992; Pérez-Huerta et al., 2011). Chemical profiles obtained from such regions of fossil brachiopod shells can be successfully interpreted as recording seasonal changes in palaeoenvironment (Mii & Grossman, 1994; Grossman et al., 1996; Powell et al., 2009).

4.3.2 Do brachiopod intra-shell Mg/Ca variations reflect temperature?

All of the *T. retusa* shells selected for this study experienced the same environmental conditions as they were collected alive simultaneously from one locality. Each transverse section was cut at a similar shell-age, about two thirds of the distance from the posterior margin to avoid the crystallographic effects mentioned above. The inter-shell maximum and minimum Mg/Ca values from each profile are consistent,

and average 18.5±0.9 mmol/mol and 5.7±0.8 mmol/mol respectively (Table 4.2.5-1). The annual temperature range at the sample site is 6.5˚C. Therefore, if the intra-shell Mg/Ca variations are assumed to be a direct result of this seasonal temperature range, these data suggest a Mg/Ca-temperature sensitivity of 2.0 mmol/mol/˚C (Table 4.2.5-1). The shape of the Mg/Ca cycles in the adult portion of the *T. retusa* ontogenetic section (Figure 4.2.3-1, ~7.5mm onwards) is saw-toothed with a steeper increase than decrease. This suggests that the brachiopod grew slowly in the winter / spring and faster in the summer / autumn. This is consistent with observations of *T. retusa* growth lines by Curry (1982) which suggest that two thirds of the annual growth occurs in the 6 months of summer / autumn with one third of the annual growth occurring in the 6 months of winter / spring. However, different minima are seen in different years in the ontogenetic profile (Figure 4.2.3-1) suggesting there was no minimum temperature at which growth shut down, which would otherwise bias our calculated Mg/Ca-temperature sensitivity. Our assumption that intra-shell brachiopod shell Mg/Ca variations reflect seasonal temperature variations can be tested using intra-shell $\delta^{18}O$ data to provide an independent measure of the temperature variation recorded within valves.

Our *T. retusa* $\delta^{18}O$ values are similar to previously published data from this species from the Firth of Lorne (1.0 - 2.5‰ Parkinson et al., 2005), which is also the range of expected equilibrium values for this seawater (Parkinson et al., 2005). There is no significant annual salinity variation at this locality (Grantham, 1983; Grantham et al. 1983a&b) as a result $\delta^{18}O$ data are interpreted solely in terms of seawater temperature. When compared on similar spatial scales of sampling, the close co-variation of $\delta^{18}O$ and averaged Mg/Ca in the adult portions of the valve (non-shaded region in Figure 4.2.3-1), support a temperature control on Mg/Ca. Using a

$\delta^{18}O_{seawater}$ value of 0.06‰ VSMOW for this locality (Parkinson et al., 2005), we use the following equation to convert $\delta^{18}O$ to temperature.

Equation 1. $T = 16.89 - 4.18(\delta^{18}O_{calcite} - \delta^{18}O_{seawater}) + 0.18(\delta^{18}O_{calcite} - \delta^{18}O_{seawater})^2$

This equation is based upon the thorough delineation of the relationship between $\delta^{18}O$ and seawater temperature in modern brachiopod calcite recently provided by Brand et al. (2013); it is a second order polynomial fit to data from their supplementary data Table S2. Unlike Brand et al. (2013), a correction for the effect of Mg on $\delta^{18}O$ was not included, as this is derived from a study of synthetic magnesian calcite, where it is required for Mg/Ca values above 100mmol/mol (Jiménez-López et al., 2004). The $\delta^{18}O$-based temperatures range from ~8.5 to 13˚C. These values do not encompass the coldest measured seawater temperatures (6.5˚C), likely because the calcite was drilled from trenches, and the brachiopods grow more slowly in the winter months. 'Averaged Mg/Ca' from the region of the microdrill trenches (black boxes in Figure 4.2.3-1) are plotted versus their corresponding $\delta^{18}O$ temperatures on Figure 4.3.2-1 (open triangles). Owing to the reduced spatial sampling resolution of this technique, the data lie between the points representing laser-ablation Mg/Ca maxima and minima and *in situ* measured seawater temperatures. These two end members defined by measured seawater temperatures lie within the 95% confidence intervals of an exponential fit to the data defined by $\delta^{18}O$ temperatures (equation 2) (Figure 4.3.2-2).

Equation 2. $Mg/Ca = 2.35 \pm 0.46\ e^{(0.13 \pm 0.04)T}$

This agreement between the two approaches suggests that in the secondary layer calcite of *T. retusa*, Mg/Ca is a faithful recorder of seawater temperature. Combining the data from the two methods defines a Mg/Ca-temperature relationship (Figure

4.3.2-2), which can be approximated by an exponential fit with an R^2 value of = 0.75 (equation 3).

Equation 3. $Mg/Ca = 1.76 \pm 0.27\ e^{(0.16 \pm 0.03)T}$ (errors are 95% confidence intervals)

A similar Mg/Ca-temperature relationship is also seen within intra-shell $\delta^{18}O$ and Mg/Ca data from the ontogenetic section of *L. neozelanica* shell E720. Laser ablation Mg/Ca data were averaged over the $\delta^{18}O$ sampling trench and plotted versus their corresponding $\delta^{18}O$ temperatures (open circles, Figure 4.3.2-1). $\delta^{18}O$-temperatures were calculated using Equation 1, using estimates for the $\delta^{18}O$ of seawater obtained from the salinity:$\delta^{18}O$ relationship of LeGrande and Schmidt (2006), with salinity at depth taken from the closest available CTD cast (WOCE, 2002). The impact of uncertainty in $\delta^{18}O_{seawater}$ on calculated temperatures is shown by the right hand x error bars (dashed) on Figure 4.3.2-1, which denote the range of temperatures obtained when assuming up to 500m post-mortem downslope transport.

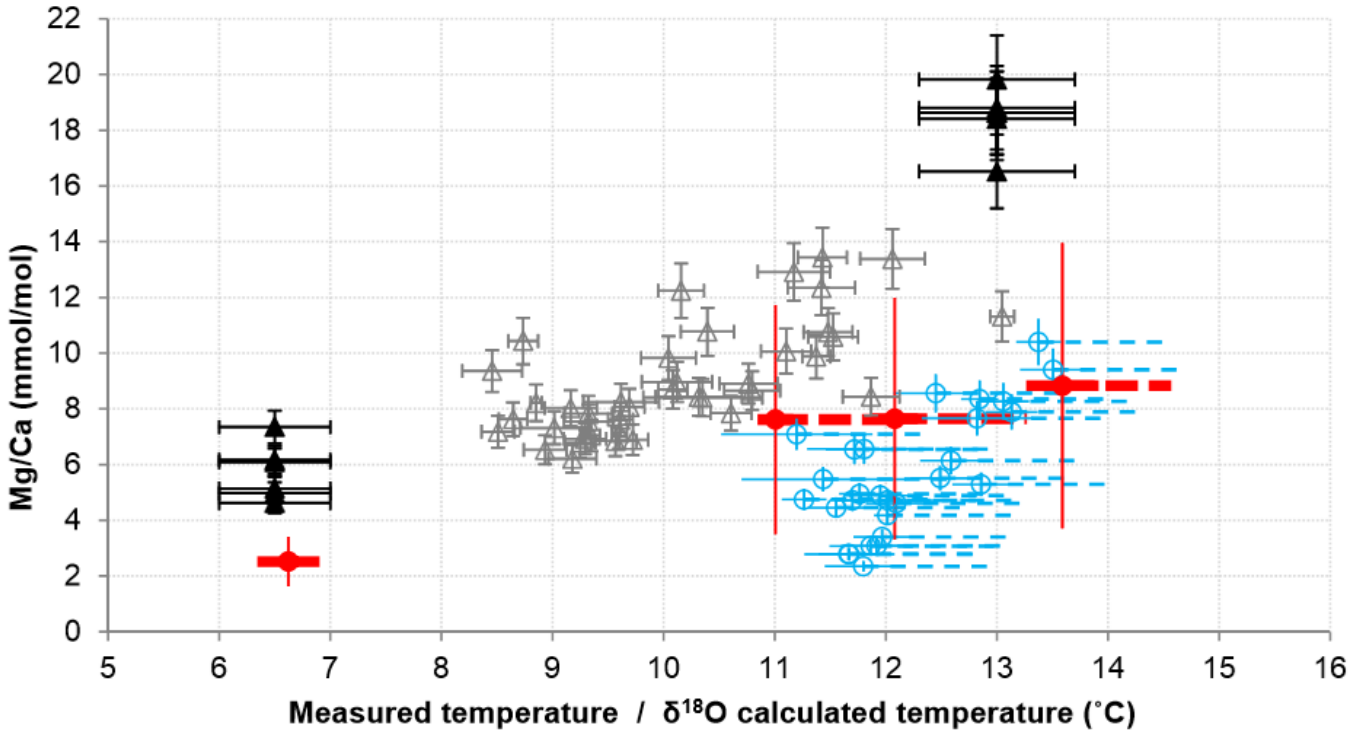

Figure 4.3.2-1. Mg/Ca-temperature relationships in *T. retusa* and *L. neozelanica*. Filled triangles (*T. retusa*) plot maximum and minimum Mg/Ca values from the laser profiles of shells 1 to 3 (Figs. 4&5, Table 3) versus measured seawater temperature. X error bars indicate the possible error in measured seawater temperature by showing the difference between seawater temperatures at depth measured in CTD casts from two subsequent summers and winters, +/- 0.5˚C (Grantham, 1983, Grantham et al. 1983a&b). Open triangles (*T. retusa)* plot 'Averaged Mg/Ca' from Figure 4 versus their corresponding $\delta^{18}O$ temperatures (calculated as described in section 5.2) for the ontogenetic and transverse sections of shell 1. Closed circles (*L. neozelanica*) plot averaged laser Mg/Ca from the same region of the valve as the δ18O sampling (hatched on Figure 4.2.7-1), versus the corresponding $\delta^{18}O$ temperature (calculated as described in section 5.2) for valves from different depths. Y error bars show +/- 2sd of the Mg/Ca data from the laser profiles of each valve (Fig. 4.2.7-17).Open circles (*L. neozelanica*) plot 'Averaged Mg/Ca' versus their corresponding $\delta^{18}O$ temperatures (as described in section 5.2) for the ontogenetic section of shell E720 (Figure 4.2.6-1).

Unless otherwise noted, all other x error bars come from the substitution of +/- 1sd of the $\delta^{18}O$ measurement into the temperature calculation (Equation 1) and all other y error bars reflect the analytical uncertainty in Mg/Ca based on standards run throughout the day, +/- 8% RSD.

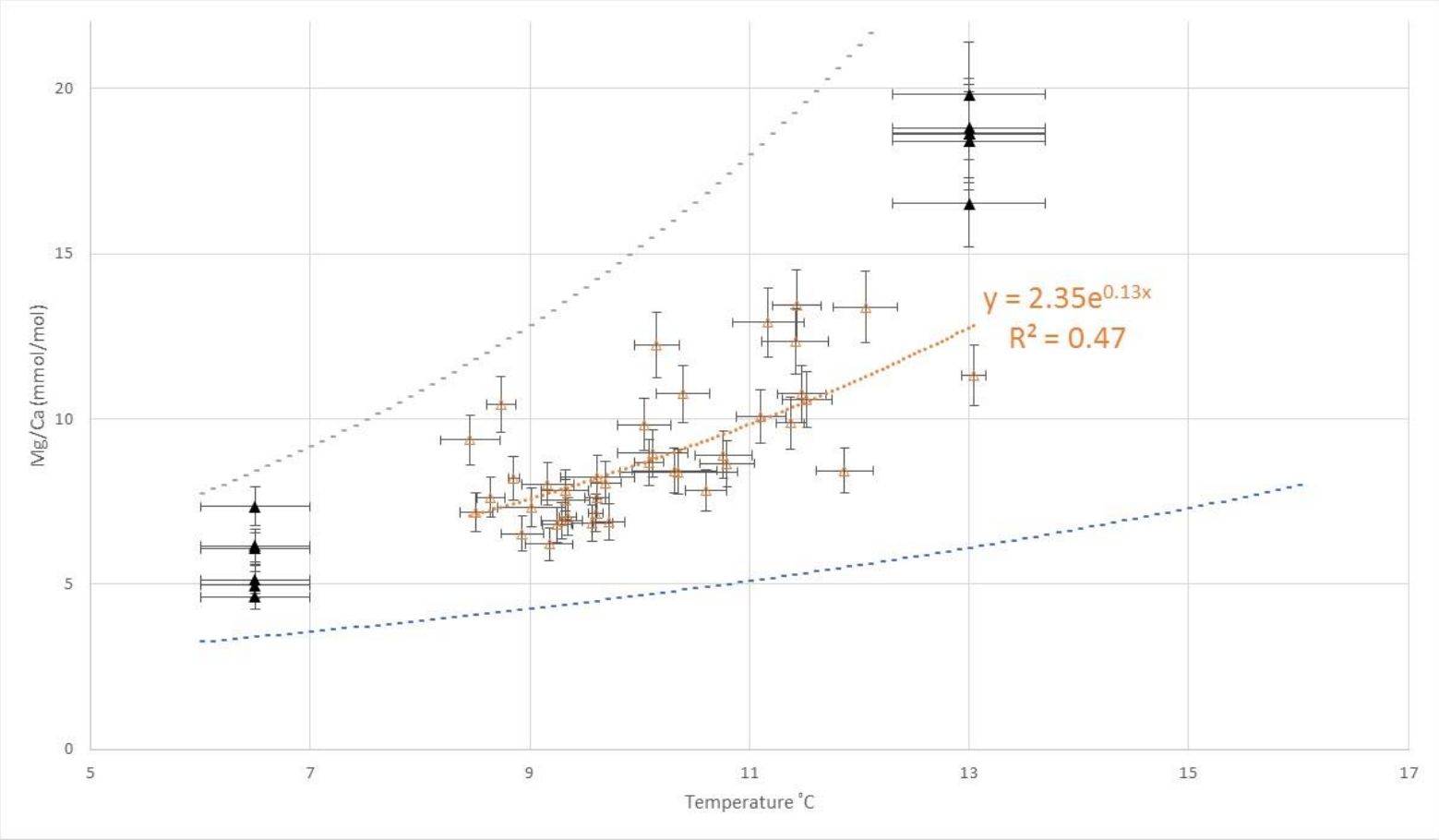

Figure 4.3.2-2. Exponential fit, dashed orange line, applied to temperatures calculated from $\delta^{18}O$ of brachiopod calcite, open orange triangles. Closed black triangles show measured seawater temperatures and the dashed blue lines represent plus and minus envelopes of two standard error of exponential fit slope and intercept.

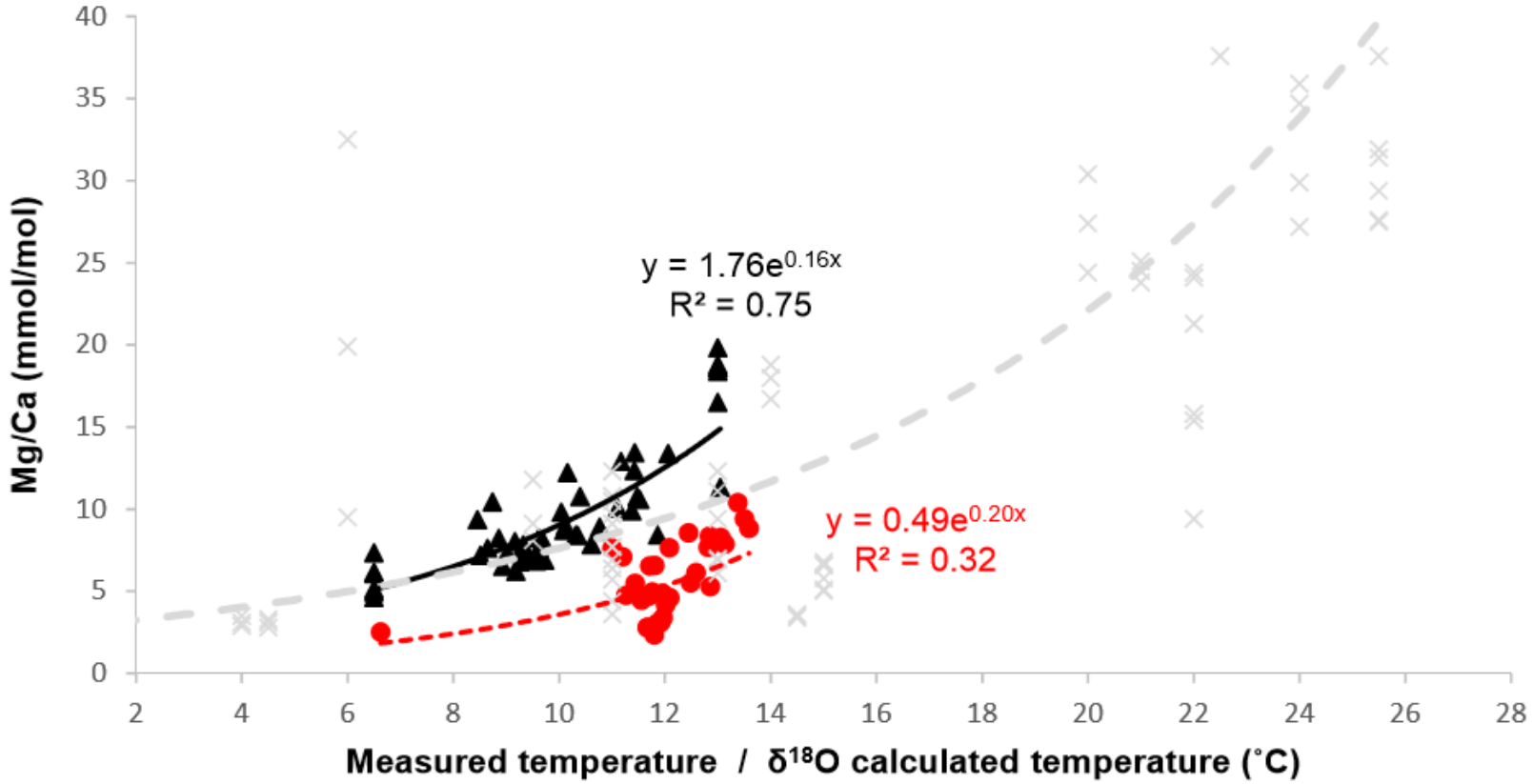

Figure 4.3.2-3. Exponential curve fits for all *T.retusa* data (triangles) and all *L. neozelanica* data (circles) from Figure 4.3.3-1, compared to an exponential fit through the data of Brand et al. (2013) obtained from drilled or crushed and powdered valves from multiple species from worldwide localities (squares).

4.3.3 Brachiopod Mg/Ca and $\delta^{18}O$ from a modern water depth transect

In general the overall trend of increasing *L. neozelanica* $\delta^{18}O$ with water depth is consistent with water column temperature profiles (Table 4.2.7-1), and the measurements are broadly comparable to published data from this species in different shallow water settings off the South Island of New Zealand (1.1 - 1.44 ‰ for Doubtful Sound (Brand et al., 2013), and 0.7-1.7 ‰ for the Otago Shelf (Parkinson et al., 2005). Unfortunately it is not known whether the shells have been transported after death prior to collection. We therefore chose to use the shell $\delta^{18}O$ as the most robust means of evaluating the *in situ* temperature during the brachiopod's lifetime. Although this approach requires an assumed value for seawater $\delta^{18}O$, the variation of this parameter with water depth is less significant than temperature. Equation 1 is used to calculate temperature, in combination with the salinity:$\delta^{18}O$ relationship of LeGrande and Schmidt (2006), with salinity at depth taken from the closest available CTD cast (WOCE, 2002). A maximum post-mortem downslope transport of 500m is assumed, which translates into a $\delta^{18}O_{seawater}$-related uncertainty of + 1.19˚C on our calculated temperatures (Figure 4.3.2-1). Plotting averaged Mg/Ca versus calculated $\delta^{18}O$-temperature on Figure 4.3.2-1 (filled circles), defines a similar Mg/Ca-temperature sensitivity to those defined by intra-shell data from both *L.neozelanica* and *T.retusa* (described in section 4.3.2).

An exponential fit through all measurements from *L. neozelanica* (intra-shell and depth profile) (Figure 4.3.2-3) defines the following Mg/Ca-temperature relationship:

Equation 4. $Mg/Ca = 0.49 \pm 1.27\ e^{(0.2 \pm 0.11)T}$ (errors are 95% confidence intervals)

This equation and its large error margins are strongly influenced by the scarcity of data from low temperatures, so an aim of future work on this species should be to further constrain this initial relationship. A comparison of this initial *L. neozelanica* Mg/Ca-temperature relationship to that of *T.retusa* highlights the presence of a taxonomic offset of around 5 mmol/mol (Figure 4.3.2-3), which is similar to the taxonomic differences observed in fossil brachiopods by Popp et al. (1986) and Grossman et al. (1996). Further investigation of taxonomic offsets are recommended for future work.

The Mg/Ca sensitivity to temperature for both *T. retusa* and *L. neozelanica* is similar to the overall trend obtained from drilled or crushed and powdered valves from multiple species from worldwide localities (Brand et al. 2013; Figure 4.3.2-3). However, the laser ablation data are less scattered, supporting its use in better defining the Mg/Ca-temperature relationship in brachiopod shell calcite.

4.3.4 A potential proxy for reconstructing past seasonality?

To gain an initial insight into how many fossil valves might need to be studied to obtain meaningful estimates of seasonality for the geological past, we treated the six *T. retusa* valves as if they were fossil unknowns. For the adult portions of each valve, deemed unaffected by the crystallographic effect, we converted the difference between maximum and minimum Mg/Ca into a difference between maximum and minimum temperature (seasonality) using Equation 3. This yields an estimate of the seasonal temperature range (7.4˚C) with a confidence in the mean of +/- 0.8 ˚C (2se, n=6) (Table 4.2.5-1). Although this level of precision reflects the ideal situation of at least six pristinely preserved fossil valves of identical age, it is small enough to encourage development of the proxy.

4.4 Conclusions

Laser-ablation sampling is an ideal means of identifying the full amplitude of brachiopod intra-shell trace metal variations. The results strongly support a temperature (seasonality) control on brachiopod intra-shell Mg/Ca cycles in the adult portion of the brachiopod shell. Laser ablation sampling of brachiopod shells also defines the shape of seasonal cycles in Mg/Ca, allowing assessment of whether the full seasonal temperature range is captured in a shell. Two different profile-sectioning techniques were also compared. Sectioning brachiopod shells longitudinally has the advantage of capturing an increased number of seasonal cycles, which may be useful for estimating past seasonality, although care must be taken to avoid sampling the juvenile material in the posterior part of the shell. Sectioning brachiopods transversely, about two-thirds of the shell length from the posterior margin avoids this problem. Furthermore, this traverse produces an approximately symmetrical seasonal signal either side of the axis of symmetry, which could be a useful constraint on assessing the robustness of seasonal Mg/Ca cycles observed in fossil shells that may have undergone more diagenetic processes.

The estimated Mg/Ca-temperature sensitivity is higher than that for inorganic calcite, but similar to other biogenic calcites, suggesting a combined thermodynamic and physiological control on the uptake of Mg into brachiopod shell calcite. The sensitivity is similar for both *T. retusa* and *L. neozelanica*, and is higher than the linear Mg/Ca-temperature calibrations for the calcite layers of the bivalves *Mytilus trossulus* (Klein et al., 1996), and *Mytilus edulis* (Vander Putten et al., 2000) which has previously been applied to fossil brachiopod Mg/Ca data (Powell et al., 2009).

In summary, laser-ablation Mg/Ca profiles of brachiopod calcite have great potential as a palaeothermometer, capturing both secular variations in bottom water temperatures and also past changes in the degree of seasonality.

CHAPTER 5: SEASONALITY AND TEMPERATURE CHANGE ACROSS THE EOCENE-OLIGOCENE TRANSITION FROM BRACHIOPOD Mg/Ca

5.1 Introduction

Understanding how seasonality changed in the years preceding, across and after the Eocene-Oligocene Transition (EOT) is key to understanding how the Earth's climate system came to develop high latitude southern hemisphere glaciation ~34 Ma (Figure 5.1-1) and how the climate system subsequently responded. This study sets

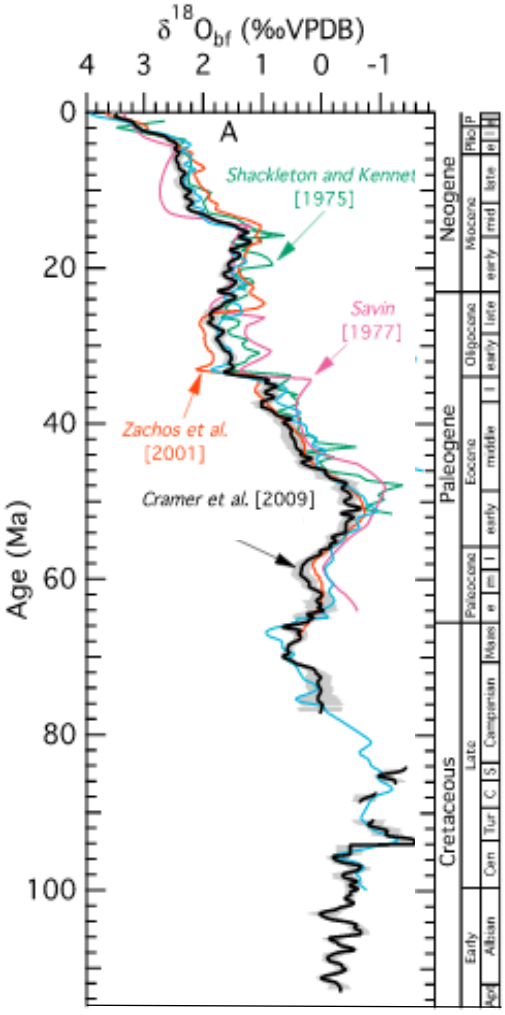

Figure 5.1-1. Cenozoic benthic foraminiferal $\delta^{18}O$. The Eocene-Oligocene transition is highlighted by the blue bar. Adapted from Cramer et al., (2011). Featuring data used in previous studies (Shackleton and Kennet, 1975; Savin, 1977; Zachos et al., 2001; Cramer et al., 2009)

out to assess seasonality from the Late Eocene and Early Oligocene of New Zealand.

5.1.1 Eocene-Oligocene Transition

Broadly the Cenozoic shows a pattern of large scale cooling from end Cretaceous greenhouse conditions, 65 Ma, to the modern day icehouse environment, (Figure 5.1-1). This long term cooling is thought to have been the result of a combination of factors which has altered the amount of heat and subsequent distribution of it over Earth's surface (Zachos et al., 2001). Large scale cooling is potentially thought to be a response to variations in the Earth's albedo, changes in atmospheric composition of greenhouse gases (principally CO_2), orogenies, and ocean circulation patterns, which are thought to be influenced by the opening and closing of ocean gateways (Zachos et al., 2001). The Eocene-Oligocene transition took place ~34 Ma and is widely thought to be the first time in the Cenozoic there was semi-permanent continental ice on Antarctica (Zachos et al., 1996). Coupled ocean atmosphere modelling suggests that CO_2 drawdown at this time rather than the opening of ocean gateways, such as the Drake Passage and the Tasman Gateway, and subsequent formation of a strong Antarctic circumpolar current (ACC) caused the abrupt increase in Antarctic icesheet growth. This growth contributed considerably to reorganising ocean circulation (Goldner et al., 2014), this is supported by modelling work which shows that a strong and coherent ACC was not possible in the Oligocene due to Australasian palaeogeography (Hill et al., 2013). Conversely modelling work including the opening of the Panama Seaway as well as the Drake Passage suggests that tectonics and palaeogeography may have played in role in this large scale glaciation (Yang et al., 2014).

The Early Oligocene Glacial Maximum (EOGM) is a 500 kyr period which post-dates the Eocene-Oligocene boundary. This is not to be confused with Oi-1 which many authors have used in regards to this glaciation event. Oi-1 was first defined by Miller et al. (1991) and spans 35.8 Ma to 32.5 Ma using the timescale of Berggren et al. (1985). The EOGM is at the base of Oi-1 (Coxall and Pearson 2007) and begins at 33.6 Ma whilst the EOGM is marked by the heaviest $\delta^{18}O$ values and occurs at a similar time (Figure 5.1.1-1). The absolute ages are slightly different from those given by Miller et al. (1991) as Coxall et al. (2005) used the ODP Leg 199 orbitally tuned age model which has been revised by Pälike et al. (2006). Here instead of using Oi1, reference to the highest $\delta^{18}O$ values ~33.6 Ma will be referred to as the

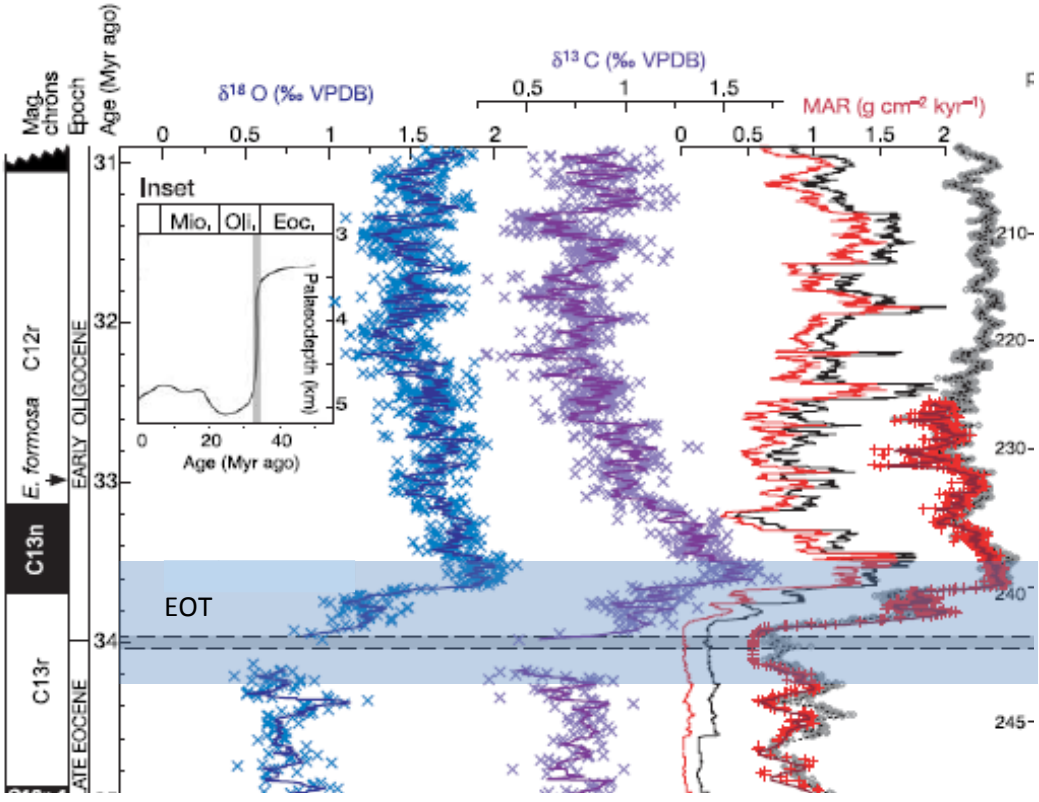

Figure 5.1.1-1. Trends in $\delta^{18}O$, $\delta^{13}C$, MAR and bulk sediment over the Eocene-Oligocene transition. The EOGM is represented by the heaviest $\delta^{18}O$ close to 33.5 Myr ago. Adapted from Coxall et al., (2005).

EOGM.

The large scale glaciation occurred in the latest Eocene and earliest Oligocene. A benthic foraminiferal $\delta^{18}O$ record from the central Pacific show a 1.5 ‰ shift towards more positive values (Coxall et al., 2005). This shift represents a combination of cooling and ice sheet expansion on Antarctica. This increase takes place over a period of 500 kyrs with the positive shifts occurring in two 40 kyr periods, separated by a 200 kyr plateau. The first step in the record, which accounts for less than half of the total shift, occurs in magnetic chron interval C13r, the second step took place at the base of C13n (Zachos et al., 1996). The step like pattern of the $\delta^{18}O$ records is very similar to early GCM-ice sheet model simulations of the climate transition (DeConto and Pollard 2003 a, b) although this stepped feature is absent in more recent models (Gasson et al., 2014).

The initiation of step change within the $\delta^{18}O$ records occurs during an interval of low eccentricity and low amplitude change in obliquity; these are conditions that favour dampened seasonality (Coxall et al., 2005). This is in accordance with modelling work by DeConto and Pollard (2003a) that suggests it is the absence of warm summers, not the occurrence of cold winters that led to the first ice sheets being present on Antarctica. The ice sheet was able to expand during the winter without regression in the summer. Following the end of the EOGM the benthic foraminiferal $\delta^{18}O$ values became fairly constant and were on average 1 ‰ higher than the late Eocene, this is thought to suggest deglaciation and subsequent stabilisation of ice volumes in the early Oligocene (Coxall and Pearson, 2007).

GCM modelling studies suggest that Antarctic glaciation may warm the Southern Ocean (Knorr and Lohmann 2014; Goldner et al., 2014). Hence the reason for studying brachiopods from the South Island of New Zealand. The proximity of South

Island to the Southern Ocean allows for a detailed study of temperatures across the EOT in an area that may have been influenced by the potential warming associated with glaciation. Relative temperature data provide the most robust results in terms of changes in seawater temperature and add to the debate surrounding deconvolving the $\delta^{18}O$ signal over the EOT. This study also attempts to quantitatively assess temperatures across the EOT.

5.1.2 Decreasing CO_2 as the cause of the Eocene-Oligocene glaciation

It is thought that falling CO_2 levels were the main driver of glaciation across the EOT (e.g. DeConto and Pollard, 2003a and b; Pagani et al., 2005; DeConto et al., 2008; Zhang et al., 2013). Records of pCO_2^{atm} derived from di-unsaturated alkenones extracted from deep sea cores show a generally decreasing trend from the late Eocene, with the majority of the drawdown in pCO_2 occurring just after the Eocene-Oligocene boundary (Pagani et al., 2005; Zhang et al., 2013), Figure 5.1.2-1. Boron

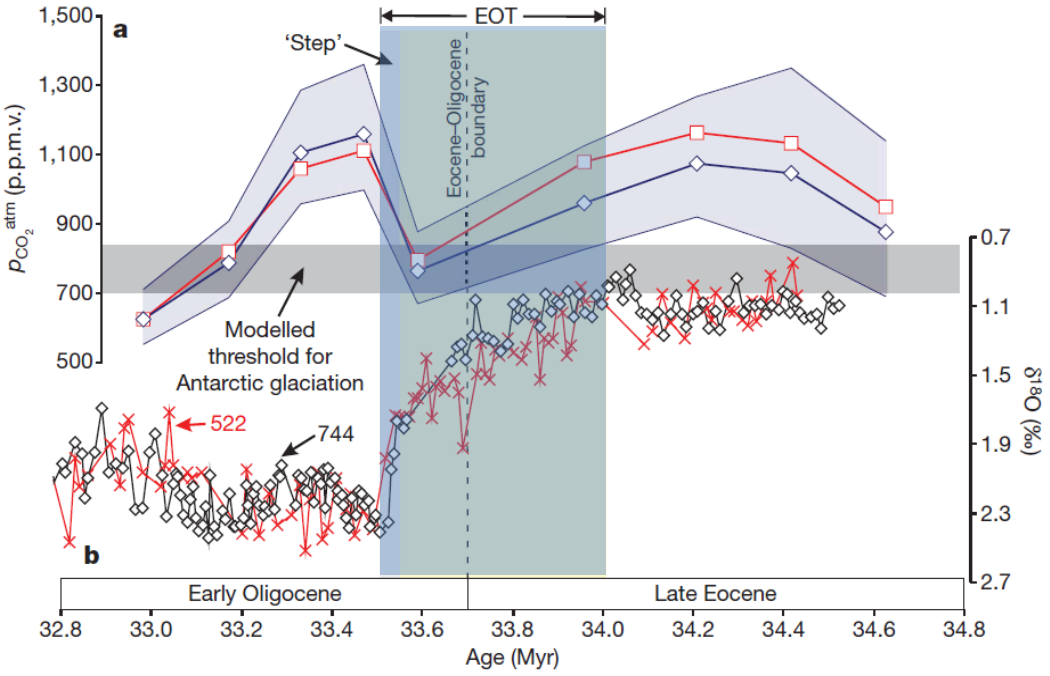

Figure 5.1.2-1. The change in pCO_2^{atm} over the Eocene-Oligocene transition this is shown alongside the $\delta^{18}O$ curve. Figure adapted from Pearson et al., (2009)

isotopes ($\delta^{11}B$) from carbonate shells of upper-ocean planktonic foraminifera can be used to infer the palaeo-surface ocean pH and thus can be used to infer the dissolved CO_2 concentration, $[CO_2]_{aq}$ provided an additional parameter of the carbonate system can be estimated (Hemming and Hanson, 1992; Foster, 2008). In oligotrophic conditions this $[CO_2]_{aq}$ is in approximate equilibrium with the pCO_2^{atm}.

Although greenhouse gases, other than CO_2, such as methane, may have contributed to changing pCO_2^{atm} it is likely that CO_2 has the greatest forcing over pCO_2^{atm} as changes in other gases are relatively minor in comparison (Hansen, 2008) and can therefore be used as a representation of CO_2^{atm}. Just after the Eocene Oligocene boundary there was a fall in the level of pCO_2^{atm} to the modelled threshold for Antarctic glaciation (Figure 5.1.2-2) (DeConto and Pollard 2003a). Although values cannot be pinpointed entirely accurately even the approximate values shown suggest that the glaciation was probably unipolar as these values are at least twice the modelled threshold for northern hemisphere glaciation (Deconto et al., 2008).

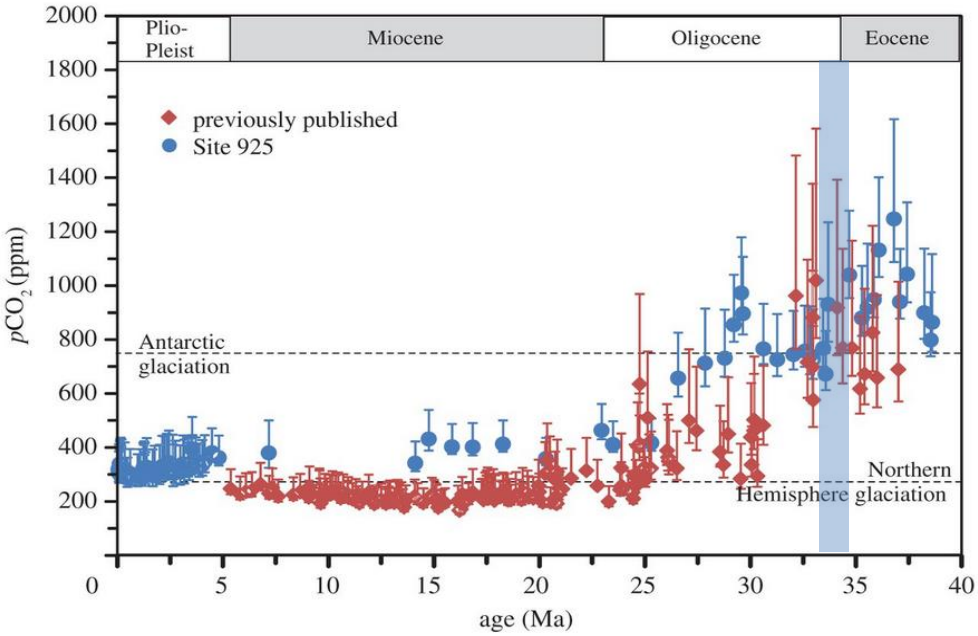

Figure 5.1.2-2. Derived pCO_2 from the Eocene to Recent. The blue box marks the EOT. Figure adapted from Zhang et al., (2005).

Possible reasons for the drawdown in CO_2 across the EOT are increased siliciclastic weathering associated with the Himalayan orogeny (Sarkar et al., 2003; Zachos and Kump, 2005) and an increase in primary production manifested mainly in an increase in diatom abundance which would have increased the level of organic carbon burial (Zachos and Kump 2005; Egan et al., 2013).

5.1.3 Deconvolving the temperature and ice volume components of the $\delta^{18}O$ shift.

$\delta^{18}O$ is a reliable proxy for mean temperature however, the ice sheet and salinity component makes any $\delta^{18}O$ record difficult to interpret in isolation. The most recent version of the brachiopod $\delta^{18}O$:temperature equation is shown in equation 1 (adapted from Brand et al., 2013).

Equation 1. $$T = 16.89 - 4.18(\delta^{18}O_{calcite} - \delta^{18}O_{seawater}) + 0.18(\delta^{18}O_{calcite} - \delta^{18}O_{seawater})^2$$

The main organisms used for collecting mean temperatures of the oceans are planktonic and benthic foraminifera. This is due to their relative abundance and global distribution throughout the Cenozoic. The benthic foraminifera represent the temperatures of bottom and deep ocean waters, whilst the planktonic foraminifera give an average representation of the different depths of sea surface water that they lived in over their life cycle (e.g. Creech et al., 2010). Mg/Ca palaeothermometry helps to deconvolve $\delta^{18}O$ records as it is a proxy which is salinity and ice sheet independent.

When taken at face value the benthic deep sea foraminiferal Mg/Ca records over the EOGM from DSDP Site 522 seem to show no cooling trend (Lear et al., 2000), whilst at ODP site 1218 they show a 2 °C increase in temperature (Lear et al., 2004). A means of reconciling the apparent warming in the Mg/Ca temperature records with

our understanding of climate dynamics is via the 'snowgun hypothesis' (Prentice and Matthews, 1991), Lear et al. (2000) suggested that this could be the reason for ice accumulation across the EOT. The theory is that warmer surface waters around Antarctica led to an increase in evaporation and subsequent precipitation over the continent, which leads to an increase in the size of the ice sheet through increased accumulation. This holds true up to a critical threshold in the water temperature, where the waters become too warm and ice sheet instability is triggered. This is also interesting with regards to seasonality as this is a process that would not require cool summers for ice sheet expansion.

This early work therefore attributed the entire $\delta^{18}O$ shift to glaciation. In this scenario, the magnitude of ice growth is unrealistic for Antarctica alone (Coxall et al., 2005), which led to the suggestion of possible contemporaneous northern hemisphere glaciation. However, large scale northern hemisphere glaciation is now thought to be unlikely based on the magnitude of the CO_2 draw down required to pass both thresholds (a decrease from >800ppm to ~280ppm in less than 500 kyr) (DeConto et al., 2008). Palynological evidence from off the coast of Greenland suggests relatively warm temperatures over the EOT and as such implies that Northern Hemisphere glaciation was probably restricted to ephemeral alpine outlet glaciers (Eldrett et al., 2009). As Northern Hemisphere glaciation is thought unlikely it can be assumed that the majority of glaciation is associated with Antarctic ice sheets.

Recent work demonstrates that the most likely reason for the apparent warming in the benthic foraminiferal Mg/Ca records across the EOT is the contemporaneous increase in carbonate saturation state associated with the deepening of calcite

compensation depth (CCD) by 1 km (Lear et al., 2004; Lear et al., 2010). One possible explanation for the deepening of the CCD over the EOT is that increased chemical weathering of Antarctica's carbonate basement rock led to changes in ocean alkalinity (Basak and Martin, 2013). There have been several attempts to deconvolve the temperature and saturation state signals in the benthic foraminiferal Mg/Ca records, and recent progress has been made using other trace metal proxies such as Li/Ca (Lear et al., 2010).

Planktonic foraminifera from Tanzania, TDP Sites 12 and 17, are far enough above the CCD that carbonate saturation state has little effect (Lear et al., 2008). Planktonic $\delta^{18}O$ values at these sites increase across the EOT (Lear et al., 2008), and broadly follow the two-step increase in benthic $\delta^{18}O$ from ODP site 1218 (Coxall et al., 2005). An initial ~0.7 ‰ increase in the planktonic $\delta^{18}O$ coincides with a decrease in planktonic Mg/Ca, aragonite benthic foraminifera Sr/Ca and the calcitic benthic Mg/Ca values, which is equivalent to an ~2.5 °C cooling at the start of the EOT (Lear et al., 2008). This implies that the temperature component could account for an ~0.5 ‰ shift whilst the remaining 0.2 ‰ shift of the first step can be accounted for by an increase in continental ice volume (Lear et al., 2008). The second step in planktonic $\delta^{18}O$ values is not mirrored by a decrease in surface water temperatures suggesting that this shift is associated with an increase in $\delta^{18}O_{seawater}$ of ~0.4 ‰. In total over the EOT there is an ~0.6 ‰ increase of $\delta^{18}O_{seawater}$, when translating this value to volume of continental ice an ice volume approximately equivalent to the modern day Antarctic ice sheet is suggested (Lear et al., 2008). It can be inferred that the majority of the ice growth occurred in step 2 of the EOT. The data from the

Tanzanian Drilling Project suggest that the deepening of the CCD and associated increase in saturation state has masked the cooling at ODP site 1218.

An 8 box ocean and 4 box atmospheric model by Tigchelaar et al. (2010) suggests that the two-step transition can be partially explained by changes in the meridional overturning circulation (MOC). They suggest that a change from sinking in southern high latitudes and upwelling in northern high latitudes, to sinking at both northern and southern high latitudes was triggered by a small density perturbation and propose that this change in overturning state leads to cooling of the deep sea and a positive excursion in $\delta^{18}O$ values. The second part of the excursion they attribute to rapid glaciation of the Antarctic ice sheet. This shows that the mechanisms behind the glaciation are not fully understood.

The increase in ice volume during the EOGM produced a global sea level drop of approximately 70m, the associated Antarctic ice sheet was similar in size or slightly larger than the modern day ice sheet (Lear et al., 2008; Pusz et al., 2011). A 3-D ice sheet-shelf model by Wilson et al. (2013) includes topography of the Late Eocene. In previous modelling work modern day topography corrected for ice loading was assumed (e.g. DeConto and Pollard, 2003b), Wilson et al's (2013) model shows that modern day Antarctic land area has decreased by 20 % due to glacial erosion compared with the Eocene land mass. The implication of this is that the total calculated volume of East and West Antarctic ice could be 1.4 times greater than previously assumed (e.g. DeConto and Pollard 2003b; Jamieson et al., 2010) this level of modelled ice volume is consistent with a cooling of 1-2 °C across the EOT (Wilson et al., 2013).

A palaeotemperature proxy based on the paleosol weathering index, developed by Gallagher and Sheldon (2013), was used to assess the mean annual temperatures from the mid-Eocene (45 Ma) through to the Quaternary of western Oregon and southeast Washington. This record shows a temperature decrease over the EOT of 2.8 °C, very similar to that shown by the marine records. Other terrestrial proxies show a significant cooling over the Eocene-Oligocene transition. A $\delta^{18}O$ study on the freshwater gastropod *Viviparus lentus* from the Hampshire basin shows a cooling of 4-6 °C in mean annual air temperatures of northern Europe (Hren et al., 2013).

The evidence for a two-step glaciation is strong. This study cannot look at this aspect of the EOT, however, the New Zealand brachiopod Mg/Ca and $\delta^{18}O$ data provide new information into the evolution of temperature and $\delta^{18}O_{seawater}$ in the south Pacific.

5.1.4 Previous studies on Eocene-Oligocene seasonality

Mean annual temperature studies on foraminifera identify general temperature changes that occurred but give no specific detail in regards to winter and summer temperatures. However, seasonality is difficult to assess from foraminifera as they are microscopic. Therefore, studies have utilised various other organisms to try to decipher seasonality over the EOT. Seasonality on Seymour Island (100 km east of the Antarctic Peninsula, Figure 5.1.4-1) fell during the Early-Middle Eocene from ~4-9 °C to 2.5 °C in the Late Eocene (Dutton et al., 2002). This supports modelling work; as cooler summers are thought to be a prerequisite for significant ice accumulation (DeConto and Pollard, 2003), however it is the winter temperatures that most notably fell on Seymour Island, although it is noted that this shift may not capture the true change in seasonality as growth cessation in bivalves at low

temperatures was problematic (Dutton et al., 2002). Minimum seasonality should occur at the beginning of the EOT as this point ~34 Ma is associated with low-eccentricity obliquity 'node' conditions which lead to dampened seasonality (Coxall et al., 2005). However factors other than seasonality must also have influenced the ice sheet expansion as there is no evidence that this period of low-eccentricity and obliquity was any more extreme than eccentricity minima and obliquity minima that occur every 2.4 and 1.2 Myr respectively (Coxall et al., 2005). Seasonality studies are therefore vital as they give an insight into how the climate responded when all factors, such as decreasing CO_2 levels, the expansion of the Antarctic ice sheet and changing ocean circulation, not just Milankovitch cycles are taken into consideration.

Seasonality studies for the EOT have concentrated on the northern hemisphere (Figure 5.1.4-1). Ivany et al. (2000) in a study of fish otoliths (ear bones) from the Gulf Coast of the United States showed that the range of temperatures for the late Eocene is generally between 15 °C and 20 °C, with winter minima never falling below 13.5 °C. Their records for the Oligocene show warm month temperatures still to be around 20 °C, however the winter temperatures are much lower than the Eocene winters with values for some samples as low as 11 °C. As there were extinctions of many warm water taxa at this time, on the Gulf Coast, it is theorised that this extinction was not due to the minimal mean temperature change. Instead, it is thought that it was due to the change in winter temperatures. This means that the harsher winters are thought to account for this turnover in molluscan fauna (Ivany et al., 2000). It is also possible that the coldest months are not recorded in the otoliths due to growth cessation at even lower temperatures (Ivany et al., 2000). A change in

seasonality, associated with a decrease primarily in winter temperatures, over the EOT is also supported by evidence from a borehole study (Wade et al., 2012) at St. Stephens Quarry Alabama, USA. They presented $\delta^{18}O$ data from a species of planktonic foraminifera, *Pseudohastigerina naguewichiensis* which have a suggested summer growth season and upper mixed-layer calcification (Wade and Pearson, 2008) and therefore a $\delta^{18}O$ signal that reflects summer sea surface temperature. This was compared to $\delta^{18}O$ of *Turborotalia ampliapertura* which is thought to represent mean annual sea surface temperature. However, this is an assumption and *Turborotalia ampliapertura* may have calcified in a deeper mixed layer habitat. The two species had similar $\delta^{18}O$ trends between 34 – 33.7 Ma, however from 33.7 Ma the disparity between the $\delta^{18}O$ of the two species increases to a maximum of 1 ‰ at 33.55 Ma, which represents a temperature difference of 4 °C, attributed to winter cooling. This shows increased seasonality after the Eocene-Oligocene boundary as mean annual sea surface temperature declined whilst summer sea surface temperatures remained the same (Wade et al., 2012). Although the absolute values are different in the Ivany et al. (2000) and Wade et al. (2012) studies, the amount of cooling shown by both over the EOT is similar. In addition to this, palynological evidence from the Northern Hemisphere also shows increased seasonality over the EOT. This is largely due to an ~5 °C cooling in the winter month mean temperatures. The summers stayed relatively warm and as a result there would not have been any way to form continental ice on East Greenland, glaciation was probably restricted to ephemeral alpine outlet glaciers (Eldrett et al., 2009).

In contrast to the findings of Ivany et al. (2000), Eldrett et al. (2009) and Wade et al. (2012), mammal teeth from North America show no evidence of a systematic shift in

winter month mean temperatures (Zanazzi et al., 2007). There is a drop in mean annual temperature of ~8 °C; this is greater than the 2-3 °C shift seen in many marine records. Zanazzi et al., (2007) conclude that a decrease in the mean annual temperatures rather than an increase in seasonality or aridity to be the main cause of gastropod, amphibian and reptile extinctions associated with the EOT. The more modest temperature changes shown by Ivany et al. (2000), Eldrett et al. (2009) and Wade et al. (2012) are more convincing than the cooling shown by Zanazzi et al. (2007) as the reliability of their data and associated large temperature change has been questioned by Sheldon et al. (2009). Palaeosol and sedimentological data has suggested that this apparent drop in temperature over the EOT ascertained from $\delta^{18}O$ of horse teeth may be an artefact of the drinking water due to changes in the $\delta^{18}O$ of precipitation (Sheldon et al., 2009). Comparisons across the EOT will be made in relation to the more modest 4 °C temperature change.

Other studies show a negligible change in seasonality over the EOT. Grimes et al.

Figure 5.1.4-1. Global distribution of studied sites with regards to temperature or seasonality across the Eocene-Oligocene Transition. The black star represents site 1218 (*e.g.* Coxall et al., 2005), blue star (Zanazzi, 2007), red star (Katz et al., 2008; Wade et al., 2012), orange star (Ivany et al., 2000), pink star (Eldrett et al., 2009), yellow star (*e.g.* Lear et al, 2008), grey star (Grimes et al., 2005) turquoise star (Dutton et al., 2002) and the green star represents the New Zealand section used in this study and that of Buening et al., (1998).

(2005) studied fresh water $\delta^{18}O$ values derived from rodent tooth enamel, molluscs and otoliths, from the Isle of Wight, UK, and were able to correlate a minor cooling

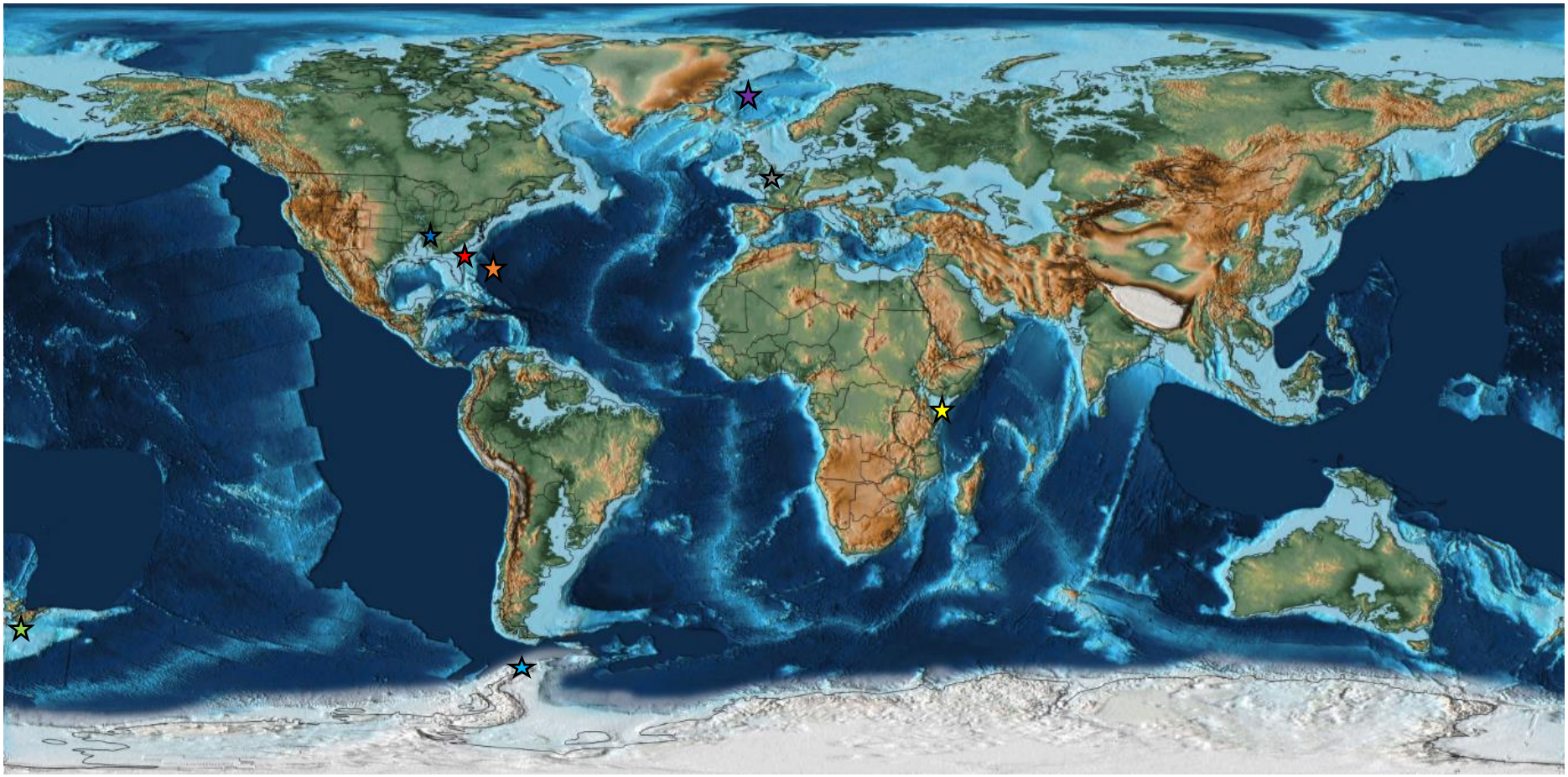

Figure 5.1.4-2. Global distribution of studied sites with regards to temperature or seasonality across the Eocene-Oligocene Transition on an Early Oligocene palaeogeographic map. The black star represents site 1218 (*e.g.* Coxall et al., 2005), blue star (Zanazzi, 2007), red star (Katz et al., 2008; Wade et al., 2012), orange star (Ivany et al., 2000), pink star (Eldrett et al., 2009), yellow star (*e.g.* Lear et al, 2008), grey star (Grimes et al., 2005) turquoise star (Dutton et al., 2002) and the green star represents the New Zealand section used in this study and that of Buening et al., (1998). Map from Sctoese (2008a).

phase seen in their record with the build-up to the EOGM. They also identify one other minor cooling phase and two other minor warming phases. As a result their record shows no average change in temperature over the EOT. With regards to seasonality they argue that the data show a fluctuating mesothermal climate. These studies (Ivany et al., 2000; Grimes et al., 2005; Zanazzi et al., 2007; Eldrett et al., 2009; Wade et al., 2012) most likely document the response to glaciation across the EOT. Distribution of sites which have already been used for seasonality and temperature studies over the EOT can be found in Figure 5.1.4-1 and on an Early Oligocene palaeogeographic map in Figure 5.1.4-2.

Identifying whether or not there was a change in seasonality over the EOT will add to the knowledge of how Earth's climate responded to decreasing levels of atmospheric CO_2 and to having a permanent ice sheet on Antarctica. The majority of sites used to study EOT seasonality so far have been situated in the northern hemisphere. The New Zealand section studied here will give a much needed insight into seasonality in the south Pacific as modelling has shown that Antarctic glaciation may in fact warm the Southern Ocean and surrounding water masses (Knorr and Lohmann, 2014). This is thought to be due to changes in the wind field associated with ice sheet expansion inducing changes in ocean circulation, deep water formation and sea ice cover which result in sea surface warming and deep water cooling (Knorr and Lohmann, 2014).

5.1.5 Shallow marine carbonate systems and eustatic sea level changes

Often shallow marine successions can be effectively used to reconstruct relative local or regional sea level, as a sea level change is often associated with a change in sedimentation. However, using fossils from shallow marine systems to study the

change in temperatures over the EOT comes with its own set of complications. When using neritic environments the records from individual localities are often incomplete or do not span the transition due to hiatuses and changes in sedimentation. Jaramillo-Vogel et al. (2013) tried to combat this by integrating lithofacies analysis with biostratigraphic data obtained from two shallow marine successions of Late Eocene to Early Oligocene age from Northern Italy and then producing a high resolution correlation between their data and pelagic successions from Tethys, Tanzania and the southern Indian Ocean (ODP Site 744).

Several shifts in the $\delta^{18}O$ from ODP Site 744 are correlated with facies changes in the Calcare di Nago Formation, Italy (Jaramillo-Vogel et al., 2013). A 0.4 ‰ negative shift occurs in the late Eocene at ODP Site 744, this correlates with a marine transgression in the Calcare di Nago Formation, which is attributed to a change in eustatic sea level through deglaciation. This is interpreted as evidence for medium scale continental ice-sheets being in place before the Eocene-Oligocene transition (Jaramillo-Vogel et al., 2013). A positive isotope shift that leads to the onset of the EOT-1 event (defined as the first $\delta^{18}O$ increase across the EOT) as seen at TDP Sites 12 and 17 (Pearson et al., 2008) and is associated with a period of stepwise shallowing of the environment; interpreted to be caused by the waxing of ice sheets over EOT-1 (Jaramillo-Vogel et al., 2013). Following EOT-1 there is another 0.4 ‰ negative shift recorded from Tanzania this corresponds to a deepening of the facies in Northern Italy and suggests that there was at least a small deglaciation pulse between EOT-1 and Oi-1. To study specific parts of the EOT such as those in Jaramillo-Vogel et al. (2013) it is key to have a very well constrained age

model and a site that spans the transition; in New Zealand. This is not possible as no one site spans the transition.

Here issues associates with periods of non-deposition and changes in eustatic sea level have been negated by using two different localities in the North Otago region of New Zealand, (Pers. Comm. Daphne Lee 2012; Section 2.3.1). For full description of sites see section 2.3.1.

5.1.6 Eocene-Oligocene of New Zealand

Brachiopod $\delta^{18}O$ data from eastern New Zealand have been interpreted to suggest a cooling of the water to ~6 °C in the earliest Oligocene from 12 °C in the latest Eocene (Buening et al., 1998). $\delta^{18}O$ values from the west coast of New Zealand suggest warmer waters at 13-15 °C compared to the ~6 °C on the east coast (Buening et al., 1998). This leads to the suggestion that there was a change in the palaeocurrent associated with the onset of glaciation with cold waters from close to Antarctica being driven up the east coast of New Zealand (Buening et al., 1998). This is partially supported by a Community Climate System Model (CCSM) produced by Huber et al. (2004) which shows cold waters being driven up the west and east coast of New Zealand in the Eocene. Huber et al. (2004) claim that their CCSM is supported by Buening et al's (1998) data, however the model and the data seem to be in slight disagreement with the model showing the cool Antarctic waters being driven up the western and eastern coasts of New Zealand, see Figure 5.1.6-1. This is in direct contrast to the flora and fauna found on the island which are indicative of warmer environments in both the late Eocene and early Oligocene (Adam et al., 1990 Buening et al., 1998).

It is possible to make inferences about the climate around New Zealand using ODP Site 1172, as TEX86 data from the Eocene of east and west New Zealand (Burgess et al., 2008; Hollis et al., 2009; Bijl et al., 2009) match extremely well with the data from this site. The data are in support of the flora and fauna with sea surface temperatures, which may be biased towards the summer, displaying a late Eocene average of ~21 °C (Bijl et al., 2009)

The brachiopods of New Zealand are largely present in the geological record both before and after the EOT. Whilst finding sites with similar species requires several localities to be sampled, both *Terebratulina suessi* and *Liothyrella oamarutica/conentrica* were collected from the Eocene and Oligocene of NZ. This shows the importance of NZ as a location for Cenozoic seasonality studies as the effects of extinction are not overly problematic.

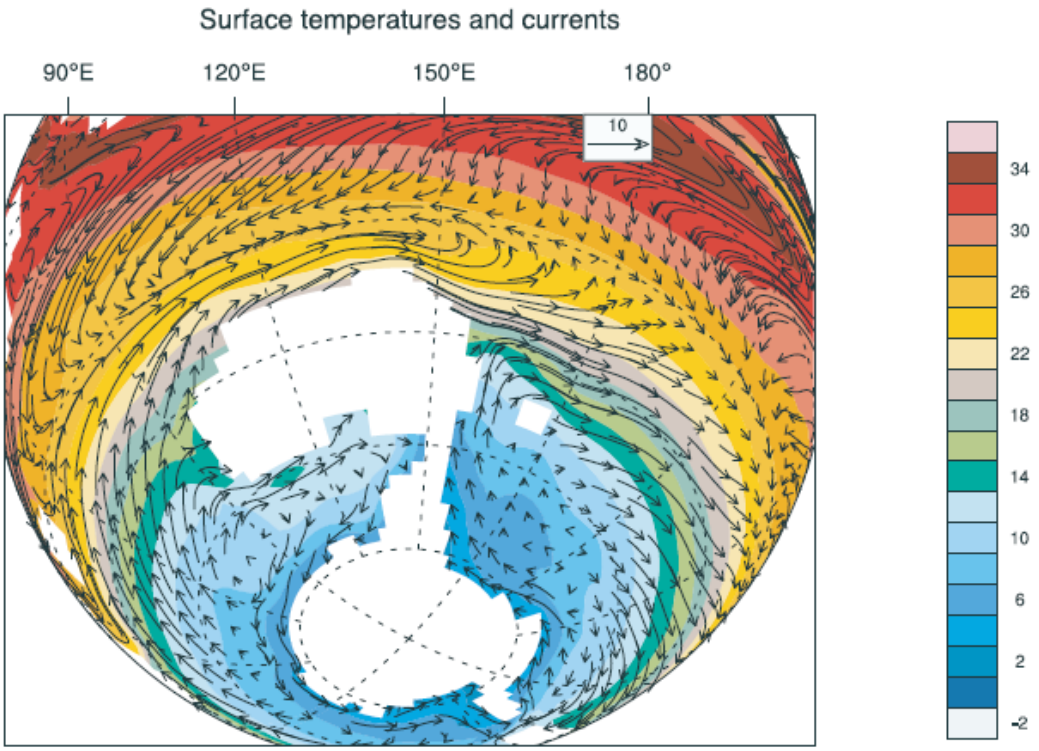

Figure 5.1.6-1. CCSM produced by Huber et al. (2004) showing cool Antarctic waters being driven up the east coast of New Zealand. Middle-Late Eocene.

The New Zealand brachiopods studied here add to the knowledge of seasonality prior to and after the EOT, in the South Pacific. This is made possible by continuous growth of the brachiopod throughout the year with growth not ceasing, at least, above temperatures of 6 °C (Butler et al., 2015; Chapter 4). Therefore mean summer and winter temperatures from either side of the transition have been assessed. The location of these brachiopods, in the South Pacific add a much needed Southern Hemisphere data set to the otherwise Northern Hemisphere dominated studies of seasonality.

5.2 Methodology

For full materials and methodology, see Chapters 2 and 3 respectively. However a brief summary of site and species selection is provided here along with uncertainties and assumptions for the sites used. This is followed by the analytical methods used to assess diagenesis, shell symmetry and palaeoseasonality.

5.2.1 Rationale for site and species selection

There is no single section in North Otago New Zealand which spans the EOT. As a result of this two sites of similar palaeowater depth (based on Edwards et al., 1991), from the Ototara Limestone Formation were selected to compare relative changes across the EOT. These sites are Trig M from the Late Eocene; McDonalds Quarry from the Early Oligocene and are ~5 km apart (Figure 2.3.1-1). Two species were analysed for trace metals, $\delta^{18}O$ and $\delta^{13}C$ from each site. Three *Terebratulina suessi* and five *Liothyrella concentrica* from Trig M and five *Terebratulina suessi* and five *Liothyrella oamarutica* from McDonalds Quarry were analysed for trace metals, $\delta^{18}O$ and $\delta^{13}C$.

There are several uncertainties and assumptions surrounding these two sites. Firstly it is assumed that both Trig M and McDonalds Quarry fall within the palaeowater depth of 30-60 m attributed to the Ototara Limestone Formation outlined in Edwards et al. (1991). Trig M is Latest Eocene whilst McDonalds Quarry is thought to be Early Oligocene (Daphne Lee Pers. Comm. March 2012). McDonalds Quarry has been placed at ~33 Ma at the base of magnetic chron 12 (Buening et al., 1998) whilst Trig M is contemporaneous to Weston Quarry which was placed at between 34 and 34.5 Ma (Buening et al., 1998). The date of ~33 Ma given to McDonalds quarry

places this site as post-EOGM. The implications of this are that seasonality across the EOGM will not be known and any calculations involving ice volume are likely to not show the full extent as globally the highest $\delta^{18}O$ values are shown over the EOGM.

5.2.2 Diagenetic and analytical checks

Diagenetic and ontogenetic effects must be identified before fossil brachiopod Mg/Ca profiles can be interpreted in terms of palaeoseasonality. In this study known ontogenetic effects were avoided by sectioning brachiopods transversely in the most anterior third of the shell, the third furthest from the umbo. In this region the secondary layer of the shell is known to be precipitated in isotopic equilibrium with the ambient seawater (Parkinson, et al., 2005, Perez-Huerta et al., 2008). This sectioning also allows for an assessment of the geochemical preservation of the brachiopod calcite, as it allows a comparison from one half of the shell to the other. The midline of the shell should act like a mirror, as the shell is symmetrical about this point.

5.2.2.1 Al/Ca Screening

Data were collected for the isotopes Mg^{24}, Mg^{25}, Al^{27}, Mn^{55}, Ca^{43}, Ca^{48}, Sr^{84}, Sr^{86} and Sr^{88}. Al and Mn were collected to screen against diagenesis and incorporation of clays in punctae or holes present within the shell. Ca^{43} and Ca^{48} were collected to assess the laser (New Wave Research 213nm Laser Ablation system) and instrument (Thermo X Series2 Inductively Coupled Plasma Mass Spectrometer) performance throughout the analysis of the laser tracks. Two different Al/Ca values were used for diagenetic screening. At McDonalds Quarry (Oligocene) there is a correlation

between Mg/Ca and Al/Ca when Al/Ca values are above 1 mmol/mol; in MCLIO1 above 1 mmol/mol R^2= 0.63 and below 1 mmol/mol R^2= 0.03. At Trig M (Eocene) there is a correlation between Mg/Ca and Al/Ca at values over 5 mmol/mol; in TMLIO4 above 5 mmol/mol R^2= 0.52 and below 5 mmol/mol R^2= 0.02. As a result data points with Al/Ca over 1 mmol/mol, at McDonalds Quarry, and 5 mmol/mol, at Trig M, were screened out. The differences are probably a reflection of differing Al and Mg values in the clay minerals at the two sites.

Mg/Ca from a poorly preserved *Liothyrella* from Trig M is shown before (Figure 5.2.2.1-1A) and after the screening process (Figure 5.2.2.1-1C). In Figure 5.2.2.1-1B, there are thin peaks in the Al/Ca data, which are at the same distance across the valve as thin peaks in the Mg/Ca data, Figure 5.2.2.1-1A. In Figure 5.2.2.1-1C, once the screening has taken place, these peaks are no longer present in the Mg/Ca data and the data profile becomes fragmentary due a relatively high proportion of the shell having levels of Al/Ca above 5 mmol/mol. Figure 5.2.2.1-2A shows a poorly preserved *Terebratulina* from McDonalds quarry and the associated Al/Ca profile Figure 5.2.2.1-2B, all bar one data point in this shell was above the screening threshold of 1 mmol/mol (Figure 5.2.2.1-2C) and as a result this shell was excluded from all further trace metal analysis.

When a shell is well preserved the diagenetic screening process has little influence on the data profile; an example of a well preserved *Liothyrella oamarutica* and a well preserved *Terebratulina suessi*, from McDonalds Quarry are shown in Figures 5.2.2.1-3 and 5.2.2.1-4 respectively. There is little difference between the original profiles in Figures 5.2.2.1-3A and 5.2.2.1-4A and the screened profiles in Figures

5.2.2.1-3C and 5.2.2.1-4C. The results of the Al/Ca screening process are summarised for species from each locality below.

5.2.2.1.1 *Liothyrella oamarutica* (McDonalds Quarry, Oligocene)

These specimens are generally very well preserved, although there is a positive correlation, between Mg/Ca and Al/Ca when Al/Ca levels are over 1 mmol/mol, R^2= 0.63 in MCLIO1. Three shells produced data with limited evidence of diagenetic alteration; these are MCLIO1, MCLIO2 and MCLIO4. Two produced poorer profiles where diagenesis had influenced some values, MCLIO3 and MCLIO5. MCLIO3 has two data gaps on the left hand side of the geochemical profile which would correspond to the peaks on the right hand side (Figure 5.3.2-2). As no peaks for one half of the shell were captured this shell was excluded from further analysis. MCLIO5 has data gaps on the left hand side of the geochemical profile which correspond to all of the minimum values on the right hand side of the geochemical profile (Figure 5.3.2-4). As minimum values were not captured on both sides of the shell it was excluded from further analysis.

5.2.2.1.2 Terebratulina suessi (McDonalds Quarry, Oligocene)

Two of the specimens had levels of Al/Ca that were too high to use (above 1 mmol/mol). MCTER1 has levels too high right across the shell, except for one data point and was therefore excluded from further analysis. MCTER2 was also high in Al/Ca and is also excluded from further analysis, (Appendix 3). MCTER3, MCTER4 and MCTER5 all produced data that showed limited evidence of diagenetic alteration.

5.2.2.1.3 *Liothyrella concentrica* (Trig M, Eocene)

TMLIO2 had high levels of Al/Ca but in some areas peaks and troughs in the data were still obtainable and the comparison between the two halves of the profile match well where there are sufficient data (Section 5.2.3). All other shells showed little diagenetic alteration based on Al/Ca.

5.2.2.1.4 *Terebratulina suessi* (Trig M, Eocene)

This species is very rare at this locality and only three specimens were collected. They are all well preserved with low levels of Al/Ca. All three specimens were included in the trace metal analysis. These specimens are slightly larger, ~0.5 cm, than the *Terebratulina suessi* from McDonalds quarry.

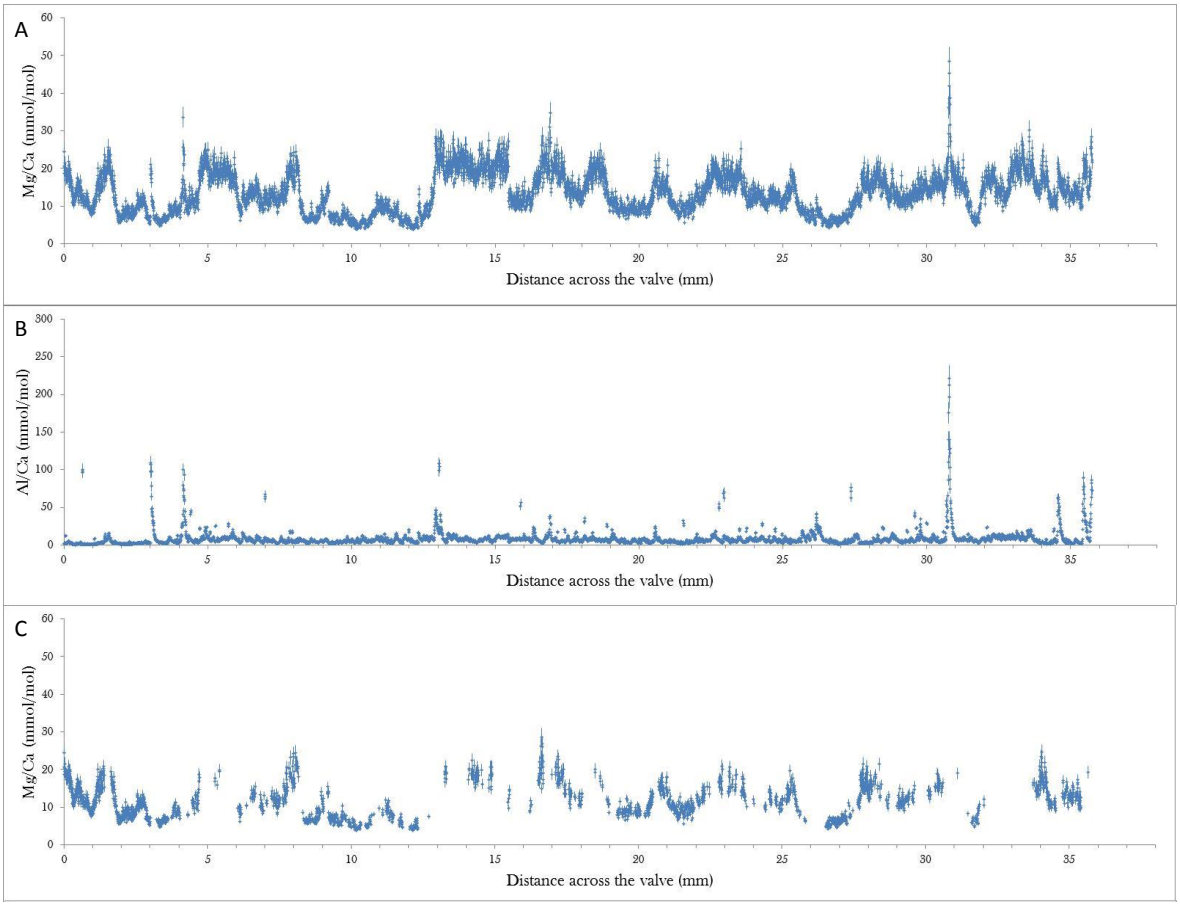

Figure 5.2.2.1-1. Data from poorly preserved *Liothyrella concentrica*, TMLIO2, from Trig M. A) Mg/Ca data before screening to 5 mmol/mol Al/Ca, B) Al/Ca data before screening and C) Mg/Ca data after screening to 5 mmol/mol Al/Ca.

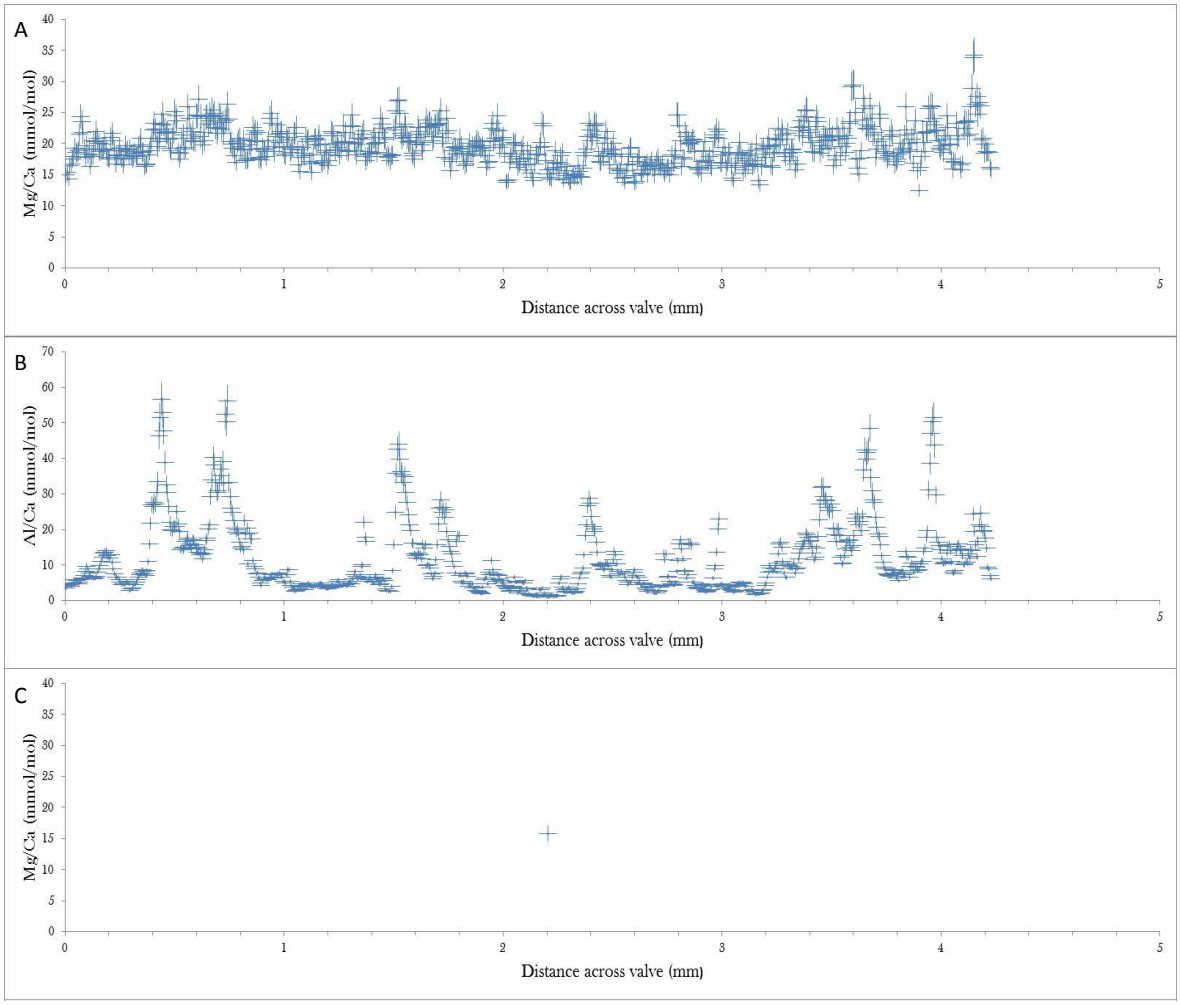

Figure 5.2.2.1-2. Data from poorly preserved *Terebratulina suessi*, MCTER1, from McDonalds Quarry. A) Mg/Ca data before screening to 1 mmol/mol Al/Ca, B) Al/Ca data before screening and C) Mg/Ca data after screening to 1 mmol/mol Al/Ca.

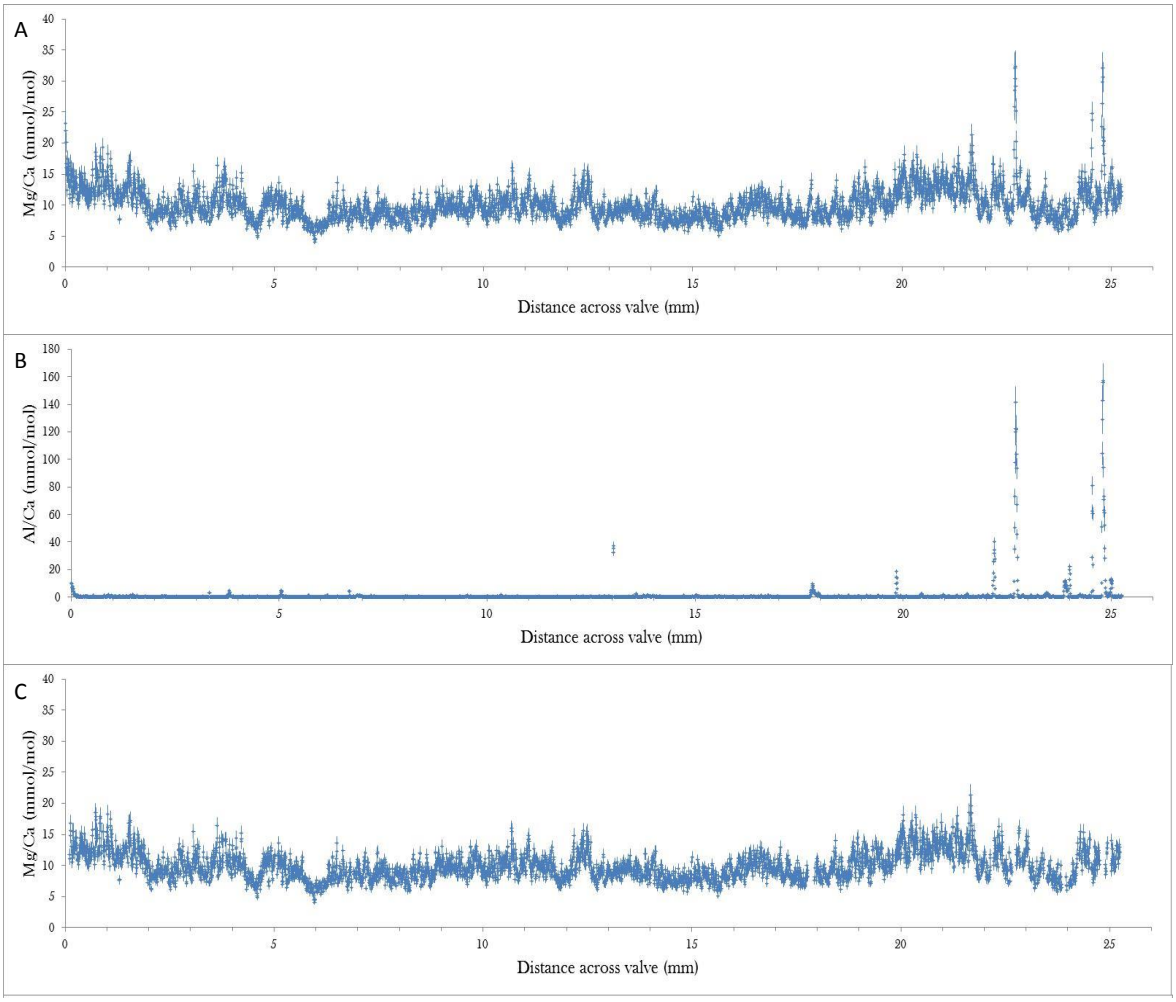

Figure 5.2.2.1-3. Data from a well preserved *Liothyrella oamarutica*, MCLIO2, from McDonalds Quarry. A) Mg/Ca data before screening to 1 mmol/mol Al/Ca, B) Al/Ca data before screening and C) Mg/Ca data after screening to 1 mmol/mol Al/Ca.

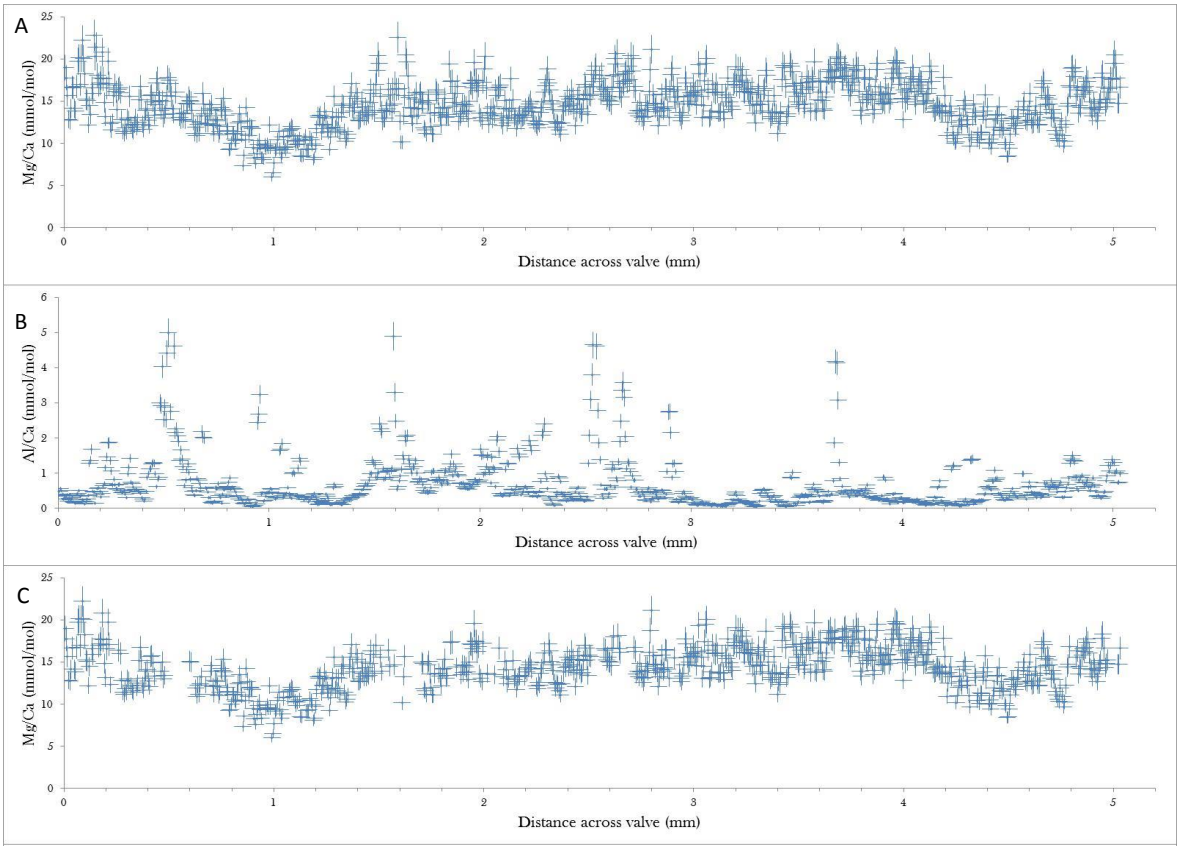

Figure 5.2.2.1-4. Data from a well preserved *Terebratulina suessi*, MCTER5 from McDonalds Quarry. A) Mg/Ca data before screening to 1 mmol/mol Al/Ca, B) Al/Ca data before screening and C) Mg/Ca data after screening to 1 mmol/mol Al/Ca.

5.2.2.2 Mn/Ca screening

After the Al/Ca screening was complete, the shell Mn/Ca ratios were assessed for indications of diagenetic alteration. If a strong positive covariation above 0.2 mmol/mol between Mn/Ca and Mg/Ca was observed, the data were screened as described below. Sixteen shells passed this test (a typical cross plot is shown in Figure 5.2.2.2-1) whilst two shells (MCLIO5 and TMTER3) failed this test.

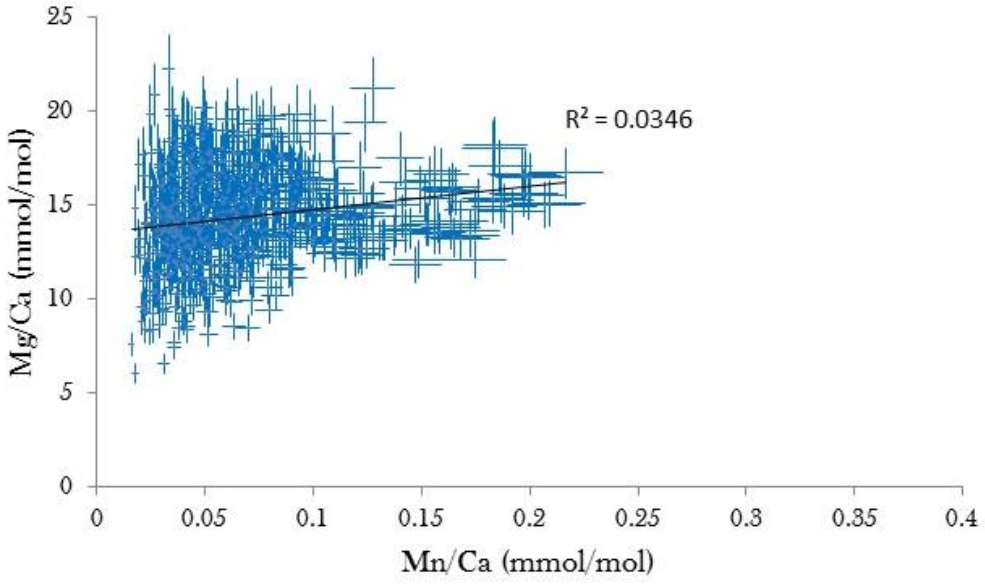

Figure 5.2.2.2-1. Cross plot of Mg/Ca v Mn/Ca, with 8% error bars from specimen MCTER5. This shell is considered to be well preserved and passed the Mn/Ca screening test.

Within TMTER3 Mn/Ca ratios over 0.2 mmol/mol were associated with elevated Mg/Ca values (Figure 5.2.2.2-2). This shell was therefore screened to 0.2 mmol/mol Mn/Ca as well as 5 mmol/mol Al/Ca.

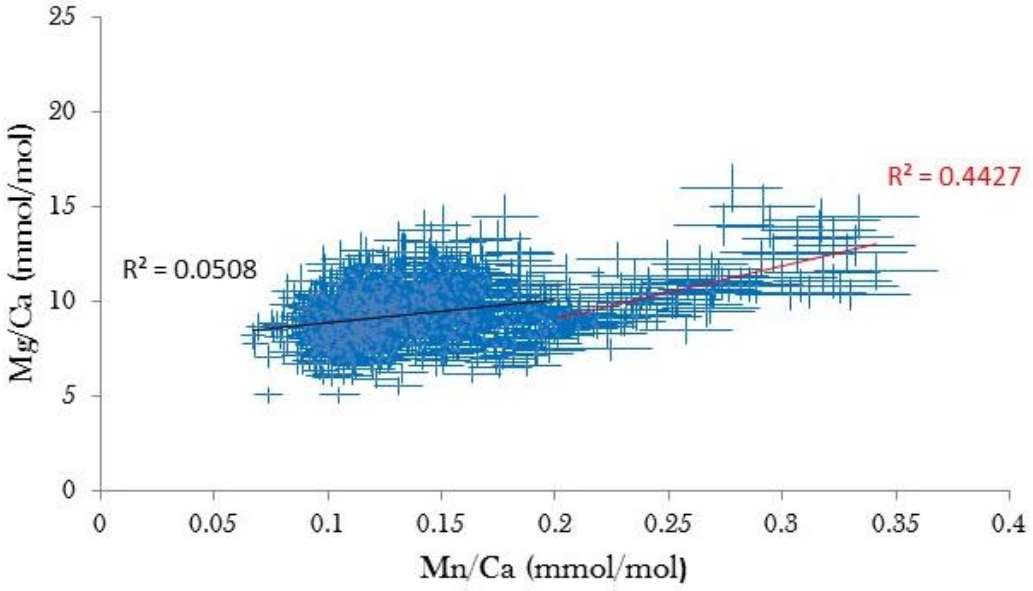

Figure 5.2.2.2-2. Cross plot of Mg/Ca v Mn/Ca, with 8% error bars from specimen TMTER3. This shell is considered to be well preserved but was screened to 0.2 mmol/mol for Mn/Ca. The black linear fit represents data below Mn/Ca values of 0.2 mmol/mol and the red linear fit represents data above Mn/Ca values of 0.2 mmol/mol.

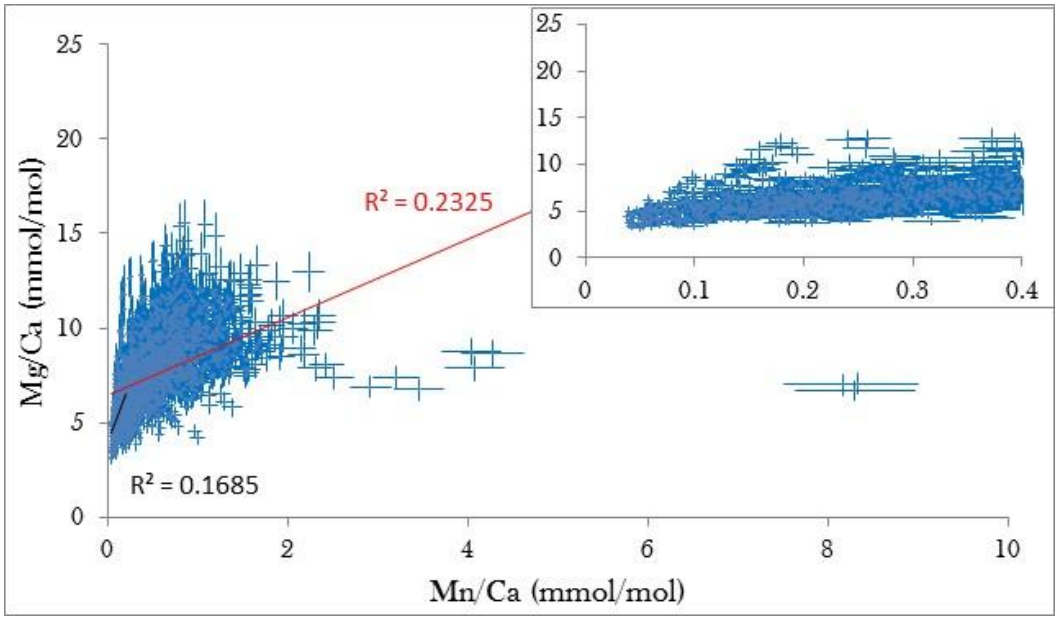

Figure 5.2.2.2-3. Cross plot of Mg/Ca v Mn/Ca, with 8% error bars from specimen TMLIO5. Inset box showing data at the same scale as the Mn/Ca cross plots in Figure 5.3.1-5 and 5.3.1-6.

One *Liothyrella oamarutica* (TMLIO5) shell from Trig M had average Mn/Ca that was much higher than other shells from Trig M (Table 5.2.3-1). There was also a positive correlation, R^2=0.23, between Mn/Ca and Mg/Ca in TMLIO5 (Figure 5.2.2.2-3). The region of elevated Mn/Ca was concentrated in the right hand side of

the geochemical profile (Figure 5.3.1-8), which lead to an ureliable profile and as such this shell was excluded from further analysis.

5.2.3 Assessing shell symmetry as an internal check on the brachiopod Mg/Ca palaeothermometer

Once the shells have been screened for diagenetic alteration assessing shell symmetry is of critical importance when studying palaeoseasonality in brachiopods. Similar Mg/Ca values on either side of the shell symmetry add confidence to the theory that these values are representative of water temperatures that the brachiopod was experiencing at a given time and not representative of area specific vital effects.

Criteria for assessing shell symmetry are based on reproducibility studies carried out on a modern *Terebratulina retusa* collected live from the Firth of Lorne, (Chapter 4). To assess the reliability of the laser ablation method, two identical laser ablation analyses were performed on one trench whilst three laser ablation analyses were carried out on another. Data from these analyses should be almost identical as this is the closest laser ablation analysis can come to sampling the same calcite twice. Therefore this is directly comparable to assessing the symmetry of a shell; as calcite the same distance from the midline of the valve would have been secreted at the same time and in theory have the same values. Cross plots of these analyses show that all of the data points fall within a defined envelope of y= 0.667x and y= 1.5x (Figure 5.2.3-1).

As a result the criteria for assessing symmetry in fossils brachiopods is similar. An error envelope of y= 0.667x and y= 1.5x was applied to all cross plots made from the fossil data Figures 5.3.2-2, 3, 4 and 5. These cross plots were made by taking values

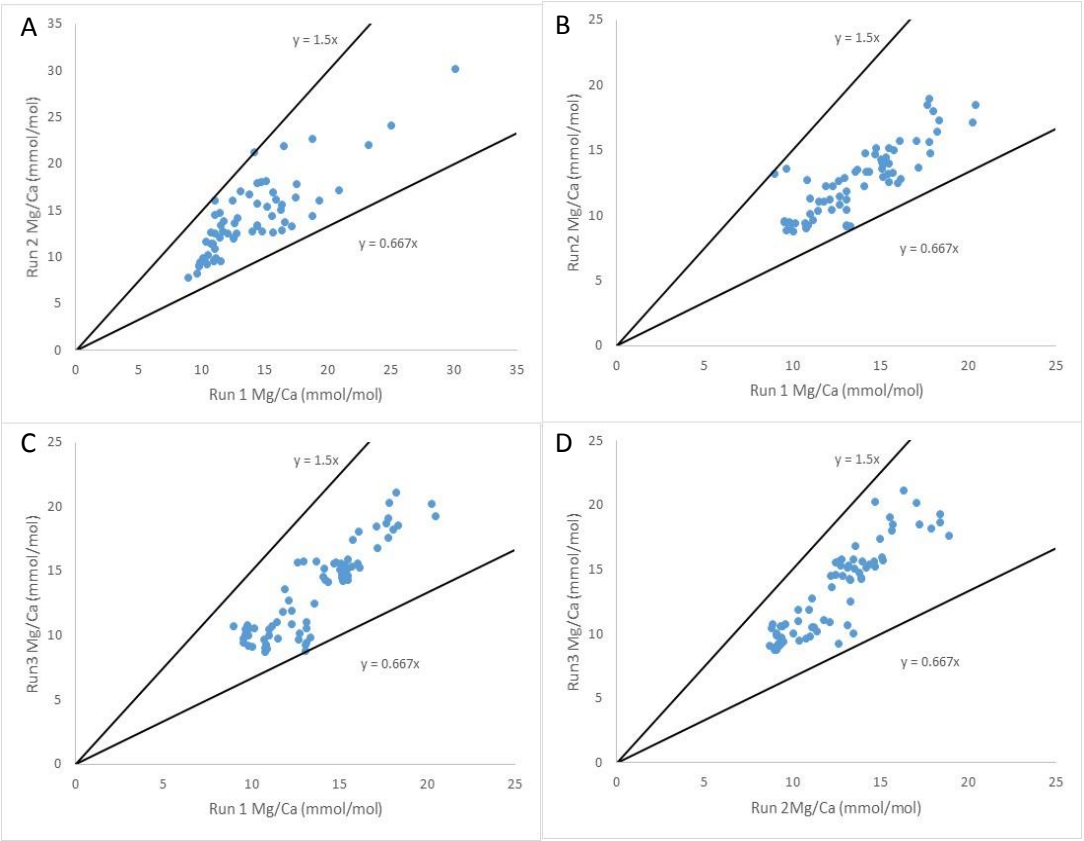

Figure 5.2.3-1 Reproducibility studies of the laser ablation method. A is from reproducibility trench 1, taken across the valve width; B, C and D are from reproducibility trench 2, run perpendicular to the inside of the valve. Black lines represent envelope of y=1.5x and y=0.667x which all data plot inside of.

of indentical distance from the midline and plotting them against each other. It is reasonable to assume that the data will not be as closely matching as the ones from the reliability studies in *Terebratulina retusa* as symmetry in the shells is unlikely to be perfect, there are several reasons why this may be the case. Even when the greatest care is taken, sometimes, a shell may not be cut directly perpendicular to the maximum growth direction or shell symmetry. As a result when the Mg/Ca profile of the shell is viewed the midpoint of the profile may not represent the midline of the shell. An example of this is specimen MCLIO2, (Figure 5.3.1-1C and 1D). As some

brachiopods grow in colonies, space can be a limiting factor in their growth. It is reasonable to believe that if a brachiopod is growing in crowded conditions then growth itself may not be symmetrical about the midline of the shell as the brachiopod may grow in a different shape, making the shell slightly asymmetrical. It is not always possible to identify if this is the case by viewing the specimen itself as they can be fragmented. Also this difference in symmetry of 1 – 2 mm may be difficult to detect when viewed in hand specimen. Asymmetrical growth is highlighted by the white areas marked with a question mark in Figure 5.3.1-1C. As a result of these other issues influencing shell symmetry if > 66 % of the data plotted within the defined envelope then the shell was considered to have retained its symmetry. Seventeen shells passed this test; one shell (TMLIO5) failed this symmetry test, due to the concentration of Mn/Ca influencing Mg/Ca across the transverse geochemical profile (Figures 5.3.1.3-2, 3, 4, 5, 6, 7, 8 and 9). Although not considered further due to part of the shell not capturing the full range of values MCLIO3 and MCLIO5 are both symmetrical where data are available.

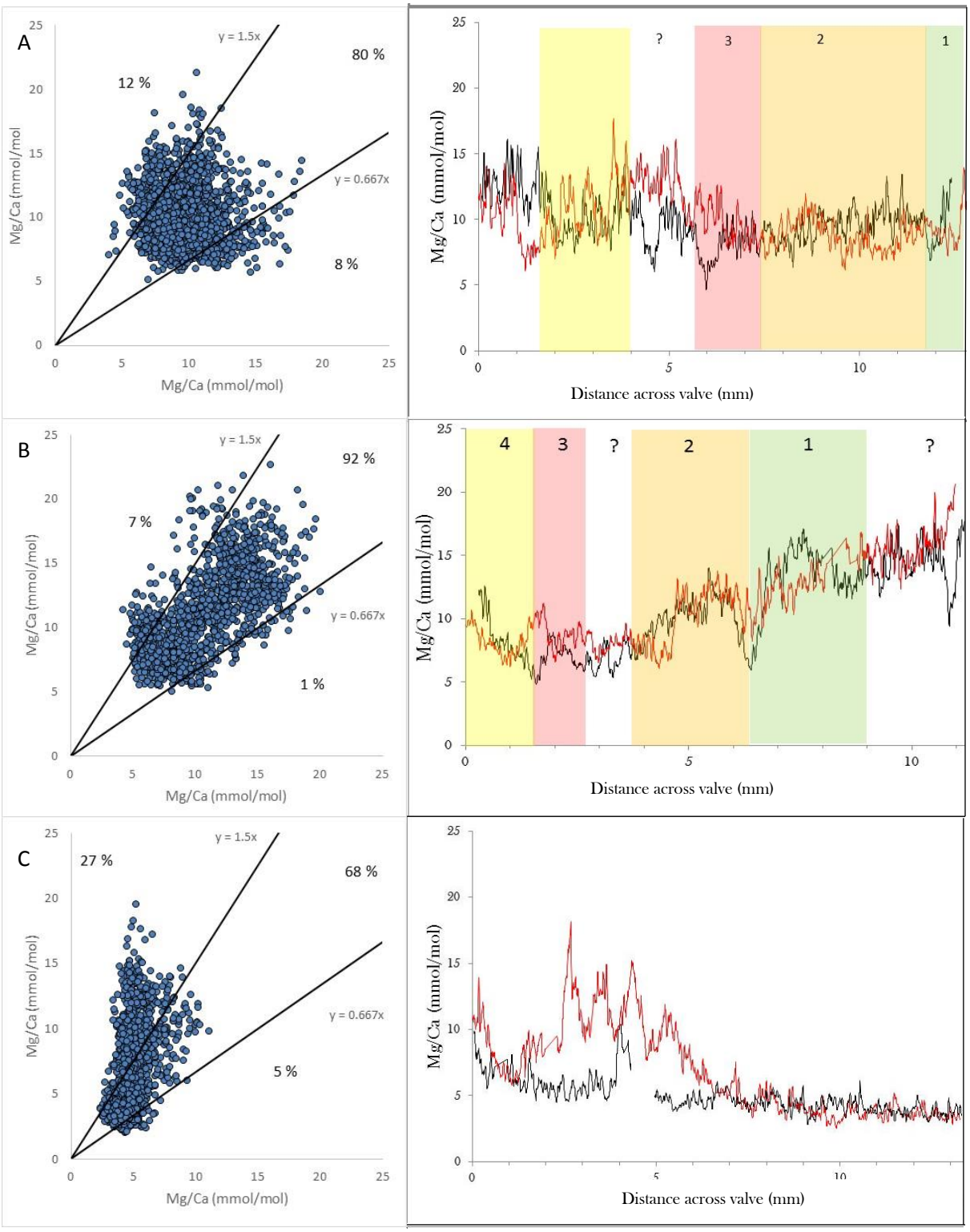

Figure 5.2.3-2 Right half of the transverse geochemical profile plotted against the left half of the transverse geochemical profile for A MCLIO1, B MCLIO2 and C MCLIO3. Black lines display error envelope of y=1.5x and y=0.667x. Percentages mark data that plot above y=1.5, below y=0.667x and in between y=1.5x and y=0.667x. A', B' and C' corresponding 8 point moving average data plotted with right half of the shell as a red line and left half as a black line, outside edge of the shell starts at 0 mm. All three shells passed the symmetry test.

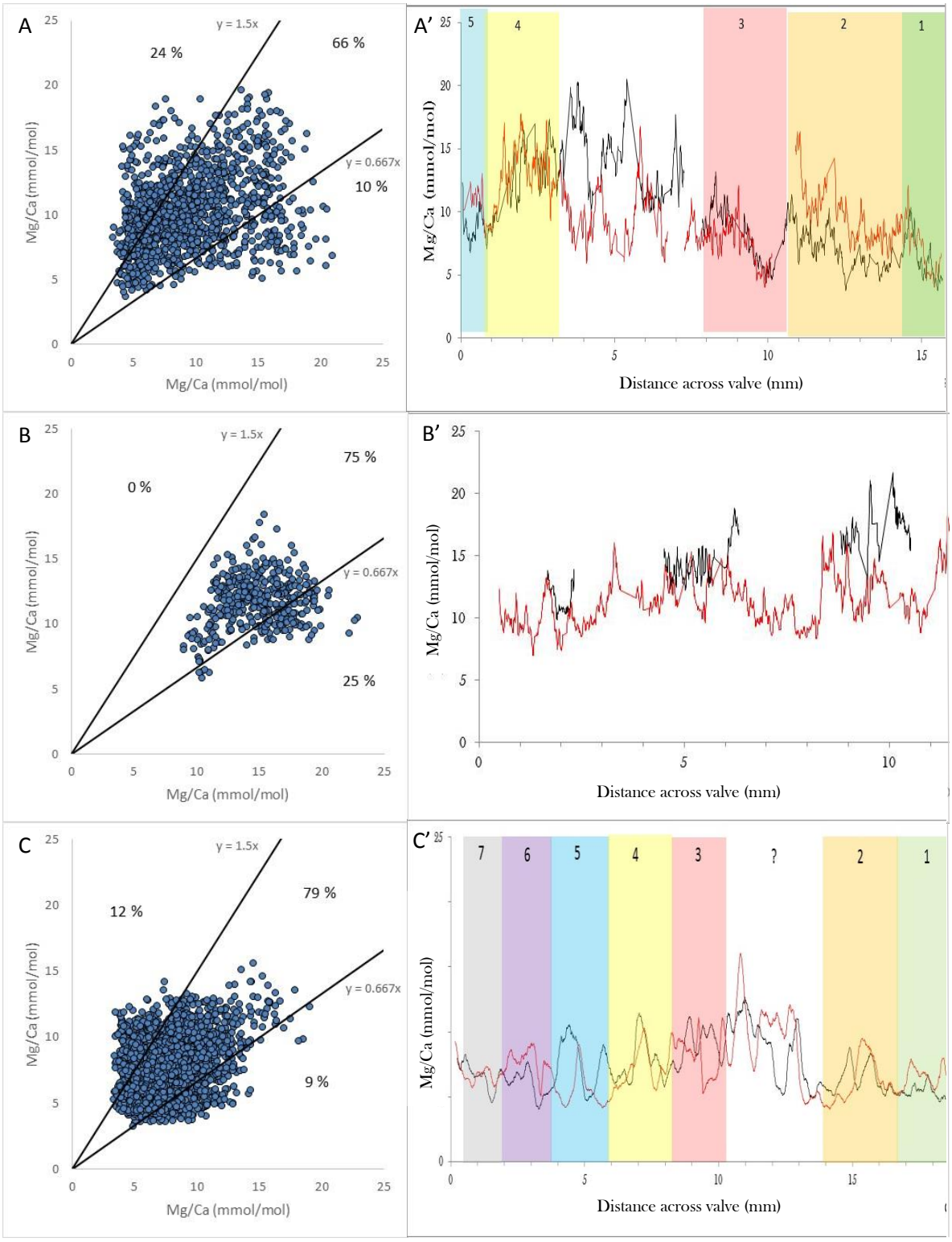

Figure 5.2.3-3 Right half of the transverse geochemical profile plotted against the left half of the transverse geochemical profile for A MCLIO4, B MCLIO5 and C TMLIO1. Black lines display error envelope of y=1.5x and y=0.667x. Percentages mark data that plot above y=1.5, below y=0.667x and in between y=1.5x and y=0.667x. A', B' and C' corresponding 8 point moving average data plotted with right half of the shell as a red line and left half as a black line, outside edge of the shell starts at 0 mm. All three shells passed the symmetry test.

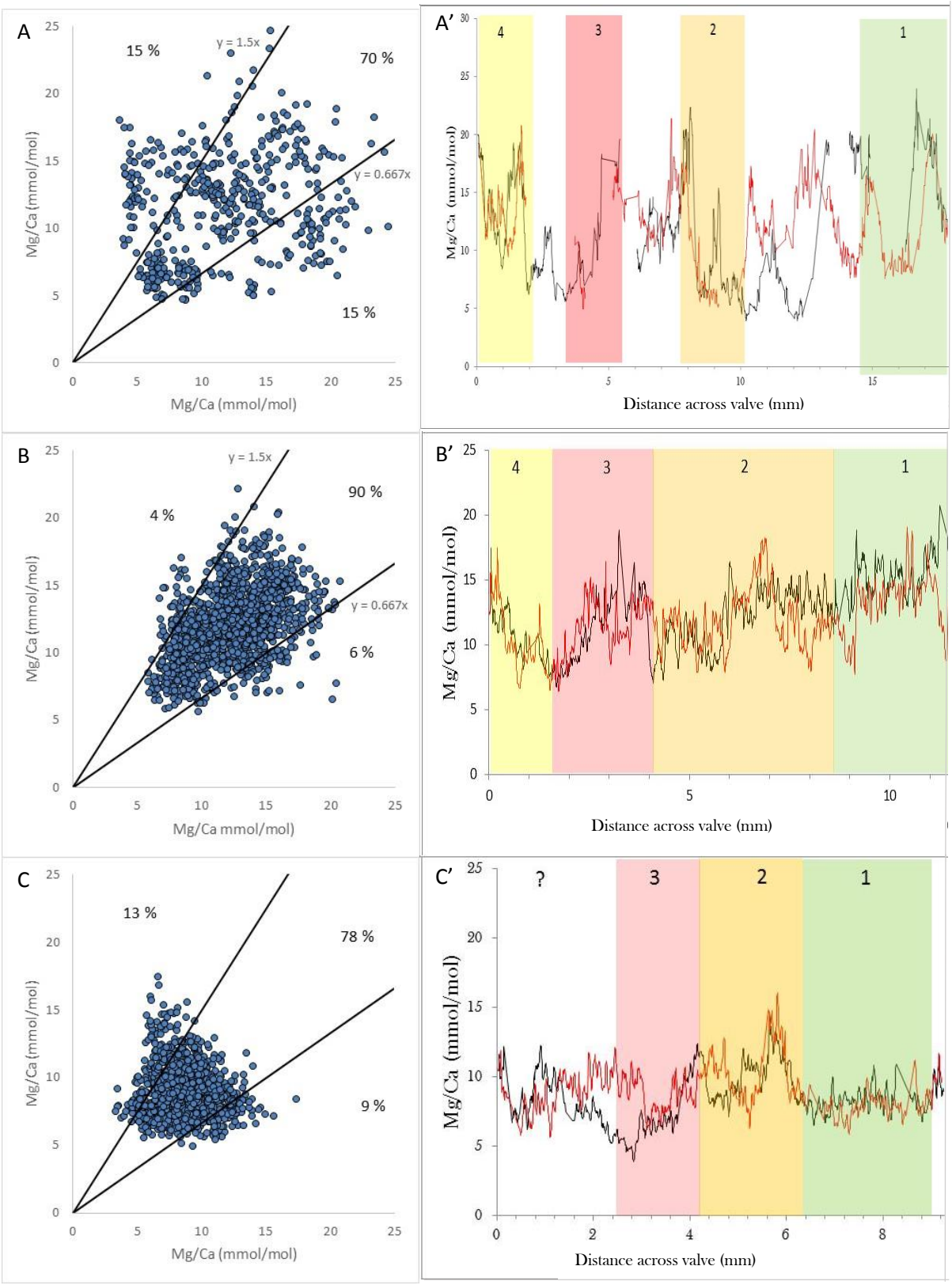

Figure 5.2.3-4 Right half of the transverse geochemical profile plotted against the left half of the transverse geochemical profile for A TMLIO2, B TMLIO3 and C TMLIO4. Black lines display error envelope of y=1.5x and y=0.667x. Percentages mark data that plot above y=1.5, below y=0.667x and in between y=1.5x and y=0.667x. A', B' and C' corresponding 8 point moving average data plotted with right half of the shell as a red line and left half as a black line, outside edge of the shell starts at 0 mm. All three shells passed the symmetry test.

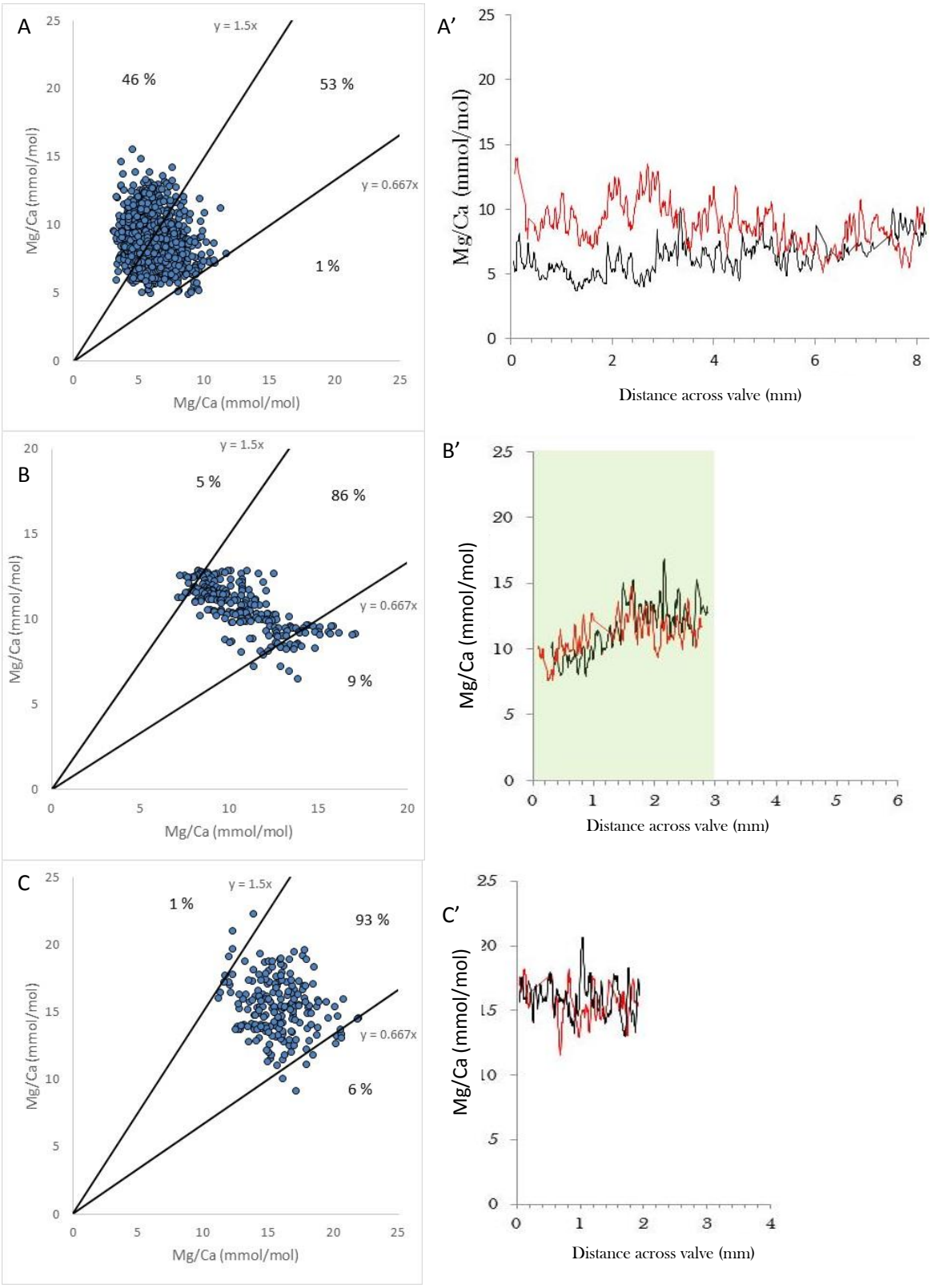

Figure 5.2.3-6 Right half of the transverse geochemical profile plotted against the left half of the transverse geochemical profile for A TMLIO5, B MCTER3 and C MCTER4. Black lines display error envelope of y=1.5x and y=0.667x. Percentages mark data that plot above y=1.5, below y=0.667x and in between y=1.5x and y=0.667x. A', B' and C' corresponding 8 point moving average data plotted with right half of the shell as a red line and left half as a black line, outside edge of the shell starts at 0 mm. TMLIO5 failed the symmetry test, MCTER3 and MCTER4 passed.

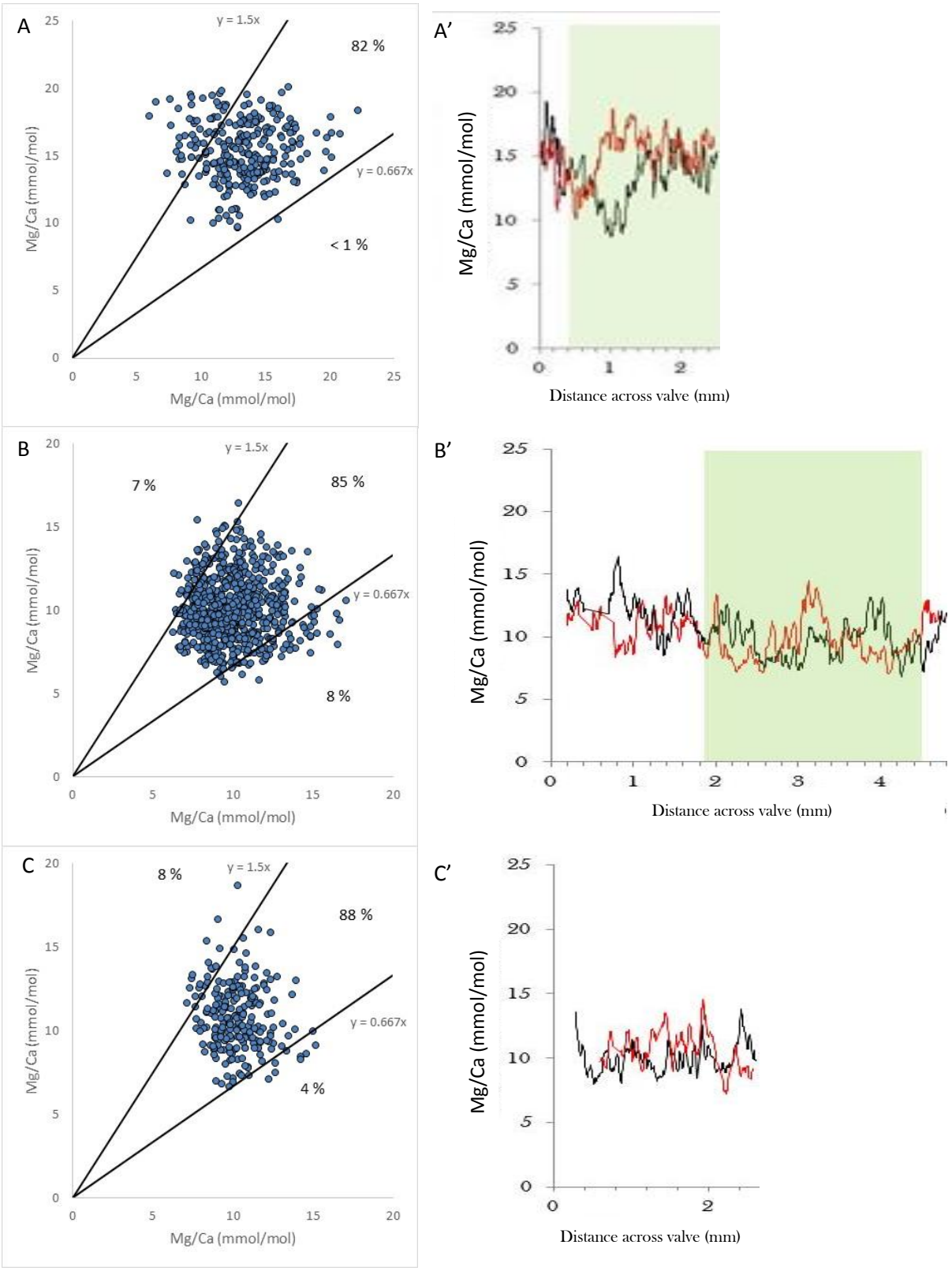

Figure 5.2.3-8 Right half of the transverse geochemical profile plotted against the left half of the transverse geochemical profile for A MCTER5, B TMTER1 and C TMTER2. Black lines display error envelope of y=1.5x and y=0.667x. Percentages mark data that plot above y=1.5, below y=0.667x and in between y=1.5x and y=0.667x. A', B' and C' corresponding 8 point moving average data plotted with right half of the shell as a red line and left half as a black line, outside edge of the shell starts at 0 mm. All three shells passed the symmetry test.

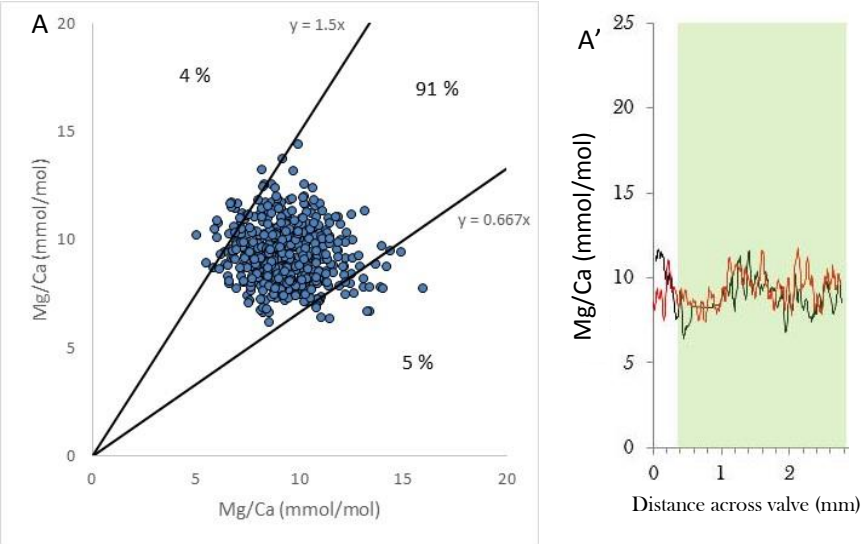

Figure 5.2.3-9. Right half of the transverse geochemical profile plotted against the left half of the transverse geochemical profile for TMTER3. Black lines display error envelope of y=1.5x and y=0.667x. Percentages mark data that plot above y=1.5, below y=0.667x and in between y=1.5x and y=0.667x. TMTER3 passed this symmetry test. A' corresponding 8 point moving average data plotted with right half of the shell as a red line and left half as a black line, outside edge of the shell starts at 0 mm. All three shells passed the symmetry test.

Specimen	Species	Average Ca^{43}/Ca^{48} (mmol/mol)	Average Pre-screening Al/Ca (mmol/mol)	Max Pre-screening Al/Ca (mmol/mol)	Average Mn/Ca (mmol/mol)	Max Mn/Ca (mmol/mol)	Are Mg/Ca profiles symmetrical where data have not been screened out?	Shell used in interpretations?
MCLIO1	*Liothyrella oamarutica*	1.91	1.05	157.37	0.04	2.63	Yes	Yes
MCLIO2	*Liothyrella oamarutica*	1.93	0.72	52.65	0.05	2.48	Yes	Yes
MCLIO3	*Liothyrella oamarutica*	1.96	1	100.95	0.07	1.32	Yes	No
MCLIO4	*Liothyrella oamarutica*	1.93	2.18	57.22	0.08	7.18	Yes	Yes
MCLIO5	*Liothyrella oamarutica*	1.85	10.49	218.87	0.41	47.57	Yes	No
MCTER1	*Terebratulina suessi*	1.74	11.64	56.86	0.25	0.95	-	No
MCTER2	*Terebratulina suessi*	1.76	12.11	305.76	0.06	0.41	-	No
MCTER3	*Terebratulina suessi*	1.86	0.88	4.96	0.06	0.15	Yes	Yes

MCTER4	*Terebratulina suessi*	**1.89**	**2.21**	**5**	**0.06**	**0.22**	**Yes**	**Yes**
MCTER5	*Terebratulina suessi*	**1.89**	**0.67**	**4.99**	**0.07**	**0.3**	**Yes**	**Yes**
TMLIO1	*Liothyrella concentrica*	**2.16**	**1.11**	**61.5**	**0.61**	**8.91**	**Yes**	**Yes**
TMLIO2	*Liothyrella concentrica*	**1.58**	**8.22**	**220.91**	**0.56**	**28.98**	**Yes**	**Yes**
TMLIO3	*Liothyrella concentrica*	**1.82**	**3.42**	**44**	**0.25**	**3.61**	**Yes**	**Yes**
TMLIO4	*Liothyrella concentrica*	**1.78**	**5.49**	**325.67**	**0.11**	**4.05**	**Yes**	**Yes**
TMLIO5	*Liothyrella concentrica*	**1.79**	**3.81**	**149.99**	**0.54**	**8.33**	**No**	**No**
TMTER1	*Terebratulina suessi*	**2.04**	**1.21**	**133.21**	**0.22**	**2.03**	**Yes**	**Yes**
TMTER2	*Terebratulina suessi*	**1.84**	**7.51**	**67.43**	**0.38**	**1.13**	**Mostly**	**Yes**
TMTER3	*Terebratulina suessi*	**2**	**0.74**	**4.68**	**0.15**	**0.34**	**Mostly**	**Yes**

Table 5.2.3-1. Outcomes of diagenetic screening checks. Red text highlights altered shells, blue text highlights unaltered shells.

5.2.4 Estimating palaeoseasonality from intra-shell Mg/Ca profiles

Laser Ablation Mg/Ca profiles were used to identify annual bands (marked as the coloured boxes in Figures 5.3.1-1, 2, 3, 4, 5, 6, 7, 8, 9 and 10). These bands were identified by superimposing the moving average of the left half of the valve on top of the right half of the valve (Figures 5.3.1-1, 2, 3, 4, 5, 6, 7, 8, 9 and 10). Where data were available for both halves of the valve; the starting points for annual bands were selected by identifying areas in the moving average profiles where the each side of the shell displayed a trough. The end of a band was identified by selecting the next trough in both halves of the moving average data, therefore these bands represent one full year. This was not always possible due to data gaps.

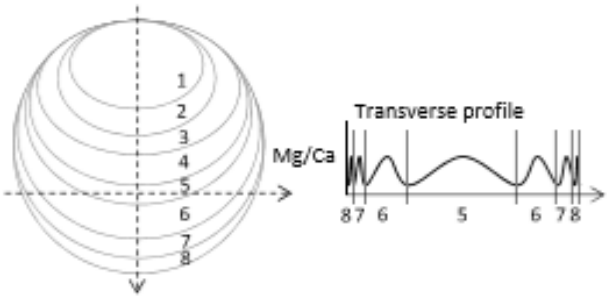

Figure 5.2.4-1. Idealised geochemical profile from a transverse section of a brachiopod

There is evidence for these bands representing annual seasonal cycles: The size of the bands generally decreases towards the lateral margin of the shell as expected if shells are showing seasonal patterns (Figure 5.2.4-1). The band in the centre marked '1' varies in size, as often the complete extent of this band has not been sampled as that band is located slightly further towards the umbo and is therefore not possible to sample (band 5 in Figure 5.2.4-1). There are some exceptions to this, Figure 5.3.1-3, where band 4 is larger than band 3. This change represents a change in growth rate and could be brought around by an increase in nutrient supply or less demands on

space for the brachiopod. The general decrease in band width is what would be expected to be seen as the rate of growth gradually slows in adult brachiopods (Curry, 1982). This gives confidence towards these truly being annual cycles. If bands on each side of the shell have slightly different sized bands this is not a concern for the reasons stated above. If however they have vastly differing absolute values then that would suggest diagenetic alteration.

There are some problems with assessing annual bands; areas of uncertainty or non-matching data are highlighted in Figures 5.3.1-1, 2, 3, 4, 5, 6, 7, 8, 9 and 10 by white spaces marked with '?', they represent areas where no matching data were available, in many cases this is because one of the sides had data screened out because the Mg/Ca data were influenced by clays associated with elevated Al/Ca (Figure 5.3.1-6). Another reason is because the data that are present have moving averages with different shaped profiles in certain areas (for example a peak on one half of the shell and a trough on the other Figures 5.3.1.1B and 5.3.1.5B) or have areas where the moving average is consistently more than 5 mmol/mol apart (Figure 5.3.1-3). This could be due to a number of reasons. One of which is that vital effects may influence the Mg/Ca ratios differently in specific areas of the shell and thus override any temperature signal. An alternative reason is because growth may have ceased on one side of the shell for a period of time, possibly due to injury or spatial pressures exerted by surrounding organisms or sediment. This is apparent in specimen TMLIO1, Figure 5.3.1-5, the '?' band is much larger on the left than the right. When viewing this area from band 2 and moving towards band 3 the pattern is similar however the closer to band 3 that is viewed the more disparate the data become, with a large peak on the left half that is not seen in the right. This could potentially be due

to additional growth on the left side that is not on the right side. This is supported by the return to a similar pattern from band 3 onwards.

Seasonality has been assessed here by taking the mean of the Mg/Ca maxima and the mean of the Mg/Ca minima identified in all annual bands, on both sides of the valve symmetry, this provided the summer and winter Mg/Ca for each shell. For example if a shell had eight annual bands, eight maxima and eight minima were averaged to give summer and winter Mg/Ca respectively. These values represent the maximum and minimum temperatures the shell experienced during one year, giving an idea of the possible seasonality that was present in the Eocene and Oligocene on the east of coast of modern day New Zealand. Summaries of these values for *Terebratulina* can be found in Table 5.3.1-1, and *Liothyrella* in Tables 5.3.1-2 and 5.3.1-3. The highest and lowest Mg/Ca from the annual bands are marked by the dashed red and blue arrows respectively in Figures 5.3.1-1, 2, 3, 4, 5, 6, 7, 8, 9 and 10.

5.3 Results

5.3.1 Mg/Ca from Liothyrella and Terebratulina across the EOT

The highest Mg/Ca from the Eocene *Terebratulina suessi* specimens is 17.1 mmol/mol. The average of annual maxima (the average of the highest values in the annual bands across the entire length of the transverse geochemical profile) from all 3 shells is 15.5 mmol/mol. The lowest minimum in any of the *Terebratulina suessi* shells from the Eocene is 5.1. The average annual minima (the lowest values in the annual bands across the entire length of the transverse geochemical profile) is 6.1 mmol/mol, (Table 5.3.1-1).

Specimen	Species	Age	Max Mg/Ca Left Half	Max Mg/Ca Right Half	Min Mg/Ca Left Half	Min Mg/Ca Right Half
MCTER1	*Terebratulina suessi*	Early Oligocene	Altered	Altered	Altered	Altered
MCTER2	*Terebratulina suessi*	Early Oligocene	21.4	22.7	11.7	12.1
MCTER3	*Terebratulina suessi*	Early Oligocene	17.8	16.6	7.1	6.5
MCTER4	*Terebratulina suessi*	Early Oligocene	22.0	22.9	11.2	11.1
TMTER1	*Terebratulina suessi*	Late Eocene	17.1	16.4	6.5	5.7
TMTER2	*Terebratulina suessi*	Late Eocene	15.2	18.7	6.76	6.63
TMTER3	*Terebratulina suessi*	Late Eocene	13.96	14.41	5.05	6.16

Table 5.3.1-1. Maximum and minimum Mg/Ca values from the right and left halves of each individual specimen. Red values indicate potentially unreliable results (see section 5.2 for details).

MCLIO1 (Oligocene)		**MCLIO2 (Oligocene)**		**MCLIO4 (Oligocene)**	
Summer and Winter Mg/Ca (mmol/mol)	Seasonal Difference Mg/Ca (mmol/mol)	Summer and Winter Mg/Ca (mmol/mol)	Seasonal Difference Mg/Ca (mmol/mol)	Summer and Winter Mg/Ca (mmol/mol)	Seasonal Difference Mg/Ca (mmol/mol)
6.4	10.0	13.3	-	5.7	7.0
16.4	-	4.3	9.0	12.7	6.0
-	-	10.0	5.7	6.7	12.2
4.1	9.5	5.3	4.7	18.9	-
13.6	7.7	14.9	9.6	-	-
5.9	10.1	5.3	9.6	14.2	-
16.0	9.3	20.0	14.7	4.5	9.7
6.7	8.1	-	-	13.7	9.2
14.8	-	19.0	-	3.9	9.8
-	-	8.1	10.9	12.0	8.1
15.1	-	16.5	8.4	3.7	8.3
6.2	8.9	5.4	11.1	-	-
11.9	5.7	12.5	7.1	3.7	8.4
5.1	6.8	5.6	6.9	12.1	6.7
13.0	6.5	12.2	6.6	5.4	12.7
6.5	14.8			18.1	12.4
21.3	13.7			5.7	9.7
7.6				15.4	
				-	
				7.5	12.1
				19.6	14.0
				5.6	9.1
				14.7	

Table 5.3.1-2 Summer and winter Mg/Ca values from annual bands of Oligocene brachiopods. Summer temperatures are in red, winter temperatures in blue and differences in black. A dash indicates a gap in the data and as a result where a gap is found no determination of seasonal difference can be made.

The highest Mg/Ca value from the annual bands of Eocene *Liothyrella concentrica* specimens is 28.6 mmol/mol and the average of the annual maxima from the four shells used is 16.5 mmol/mol. The lowest Mg/Ca value from annual bands in the same specimens is 3.5 mmol/mol and the average of the annual minima is 5.3 mmol/mol, (Table 5.3.1-3).

The maximum Mg/Ca value from the Oligocene *Terebratulina suessi* specimens is 22.9 mmol/mol and the average of annual maxima across 3 shells is 19.8 mmol/mol. The lowest Mg/Ca value from the same specimens is 6.0 mmol/mol and the average annual minima across 3 shells is 8.4 mmol/mol, (Table 5.3.1-1).

The highest Mg/Ca value from the annual bands of Oligocene *Liothyrella oamarutica* specimens is 21.3 mmol/mol and the average of the annual maxima from 3 shells is 15.1 mmol/mol. The lowest Mg/Ca value from annual bands in the same specimens is 3.7 mmol/mol and the average of the annual minima is 5.6 mmol/mol, (Table 5.3.1-2).

TMLIO1 (Eocene)		**TMLIO2 (Eocene)**		**TMLIO3 (Eocene)**		**TMLIO4 (Eocene)**	
Summer and Winter Mg/Ca (mmol/mol)	Seasonal Difference Mg/Ca (mmol/mol)	Summer and Winter Mg/Ca (mmol/mol)	Seasonal Difference Mg/Ca (mmol/mol)	Summer and Winter Mg/Ca (mmol/mol)	Seasonal Difference Mg/Ca (mmol/mol)	Summer and Winter Mg/Ca (mmol/mol)	Seasonal Difference Mg/Ca (mmol/mol)
4.7	4.4	7.4	13.4	20.2		3.6	9.8
9.1	4.6	20.8	-	5.9	14.3	13.4	7.7
4.5	6.2	-	-	19.0	13.1	5.7	11.6
10.7	7.2	4.7	14.7	6.4	12.6	17.3	11.4
3.5	6.9	19.4	-	18.5	12.1	5.9	7.8
10.4	6.3	-	-	10.1	8.4	13.7	-
4.1	7.5	24.5	-	20.3	10.2	-	-
11.6	6.8	3.9	20.6	-	-	12.9	-
4.8	8.0	-	-	22.1	-	4.9	8.0
12.8	8.6	22.4	-	6.6	15.5	18.5	13.6
4.2	-	8.8	13.6	20.4	13.8	5.7	12.8
-	-	28.6	19.9	6.8	13.6	15.9	10.2
15.3	11.2	6.6	22.0	18.4	11.6	5.4	10.5
4.1	-	17.9	11.3	5.6	12.8		

-	-	-	-				
3.9	5.9	4.2	17.2				
9.8	6.1	21.4	-				
3.7	6.2	-	-				
9.9	5.8	18.6	-				
4.1	8.8	4.8	13.8				
12.9	-	-	-				
-	-	24.7	-				
6.1	6.6	9.1	15.6				
12.7	7.8						
4.9	7.0						
11.9	7.6						
4.3	7.6						
11.9	8.3						
3.6	5.4						
9.0	5.4						
3.6	6.8						
10.4							

Table 5.3.1-3 Summer and winter Mg/Ca values from annual bands of Eocene brachiopods. Summer temperatures are in red, winter temperatures in blue and differences in black. A dash indicates a gap in the data and as a result where a gap is found no determination of seasonal difference can be made.

	MCLIO1 (Oligocene)	MCLIO2 (Oligocene)	MCLIO4 (Oligocene)	Oligocene Combined	TMLIO1 (Eocene)	TMLIO2 (Eocene)	TMLIO3 (Eocene)	TMLIO4 (Eocene)	Eocene Combined
Average Annual Summer Mg/Ca (mmol/mol)	15.3	14.8	15.1	**15.1 SD = (2.9)**	11.3	22.0	19.99	15.3	**16.5 SD = (5.1)**
Average Annual Winter Mg/Ca (mmol/mol)	6.1	5.7	5.2	**5.6 SD = (1.2)**	4.3	6.2	6.9	5.2	**5.3 SD = (1.6)**
Maximum Annual Summer Mg/Ca (mmol/mol)	21.3	20.0	19.6	**21.3**	15.3	28.6	22.1	18.5	**28.6**
Minimum Annual Summer Mg/Ca (mmol/mol)	11.9	10.0	12.0	**10.0**	9.0	17.9	18.4	12.9	**9.0**
Maximum Annual Winter Mg/Ca (mmol/mol)	7.6	8.1	7.5	**8.1**	6.1	9.1	10.1	5.9	**10.1**

Minimum Annual Winter Mg/Ca (mmol/mol)	4.1	4.3	3.7	**3.7**	3.5	3.9	5.6	3.6	**3.5**
Average Seasonal Difference Mg/Ca (mmol/mol)	9.2	8.7	9.7	**9.2** **SD = (2.6)**	6.9	16.2	12.5	10.3	**10.3** **SD = (4.1)**
Maximum Seasonal Difference Mg/Ca (mmol/mol)	14.8	14.8	14.0	**14.8**	11.2	22.0	15.6	13.6	**22.0**
Minimum Seasonal Difference Mg/Ca (mmol/mol)	5.7	4.6	6.0	**4.6**	4.4	11.3	8.4	6.7	**4.4**

Table 5.3.1-4. Average, maximum and minimum summer and winter Mg/Ca values from annual bands of Oligocene and Eocene brachiopods, along with average, maximum and minimum seasonal differences in Mg/Ca. Summer temperatures are in red, winter temperatures in blue and differences in black.

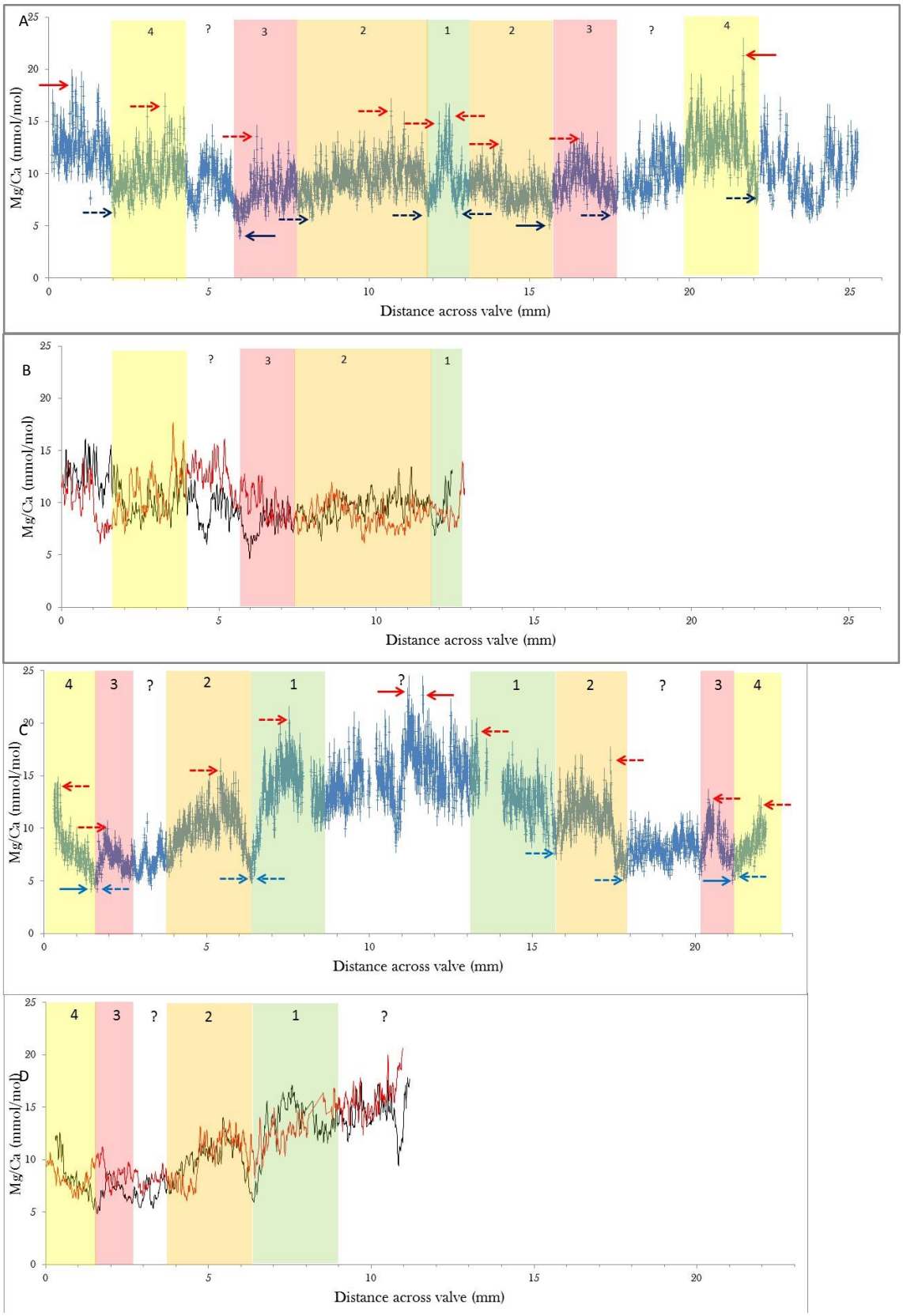

Figure 5.3.1-1. Mg/Ca data from MCLIO1 (A and B) and MCLIO2 (C and D). A and C show the laser ablation data with 8 % y-axis error bars and 40 µm x-axis error bars. The solid red and blue arrows indicate the highest Mg/Ca and lowest Mg/Ca respectively on one half of the profile. The dashed red and blue arrows indicate the respective highest and lowest Mg/Ca in each band, bands are identified by the numbered colour boxes. B and D show an 8 point moving average of the same data from A and C. The two lines show the left (black) and right (red) halves of the valves starting with the outside of the shell at 0 mm moving towards the centre of the shell.

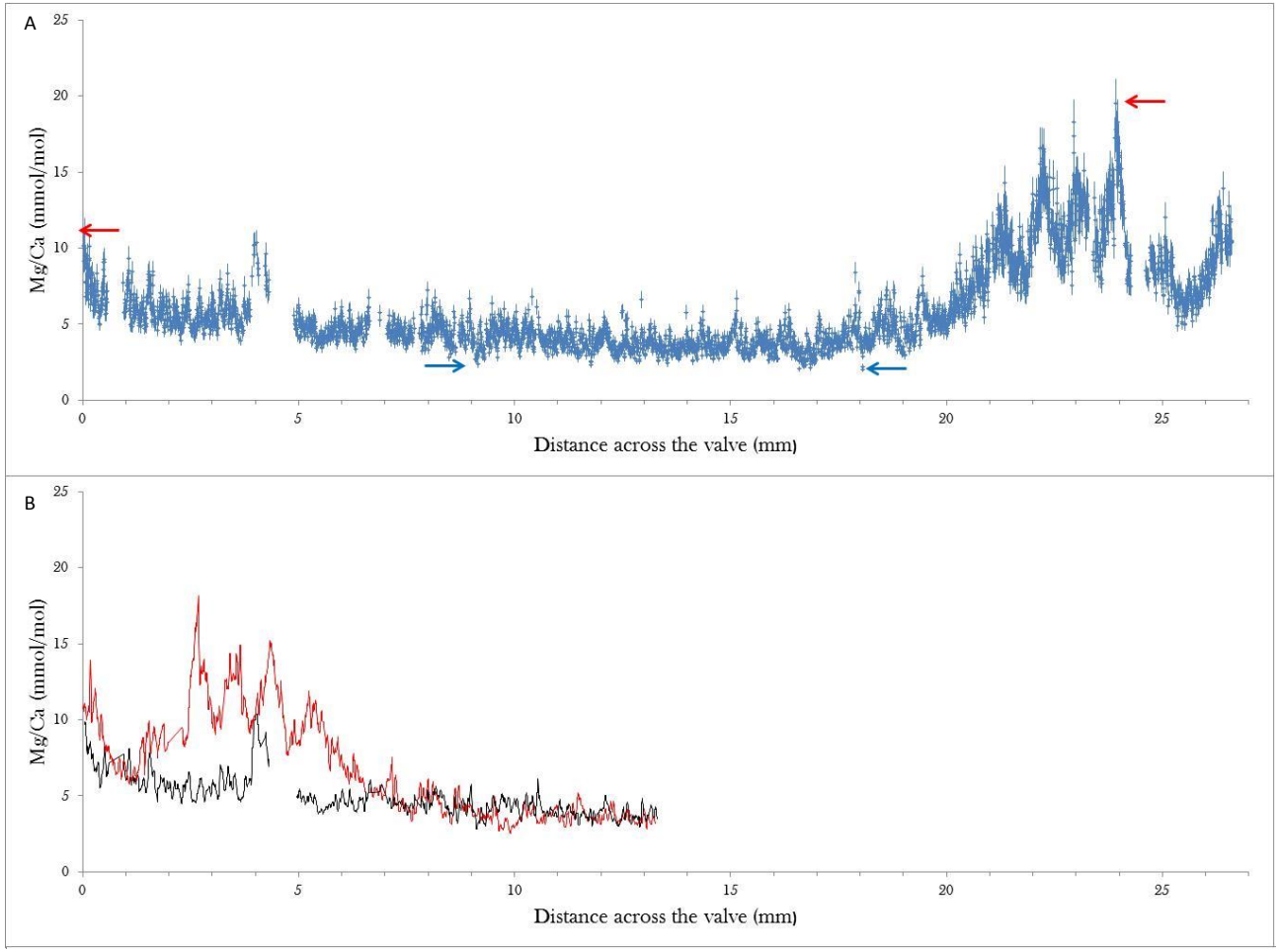

Figure 5.3.1-2. Mg/Ca data from MCLIO3. A shows the laser ablation data with 8 % y-axis error bars and 40 μm x-axis error bars. The solid red and blue arrows indicate the highest Mg/Ca and lowest Mg/Ca respectively on one half of the profile. B shows an 8 point moving average of the same data from A. The two lines show the left (black) and right (red) halves of the valves starting with the outside of the shell at 0 mm moving towards the centre of the shell. Valve not used in interpretations due to asymmetrical nature of the profile.

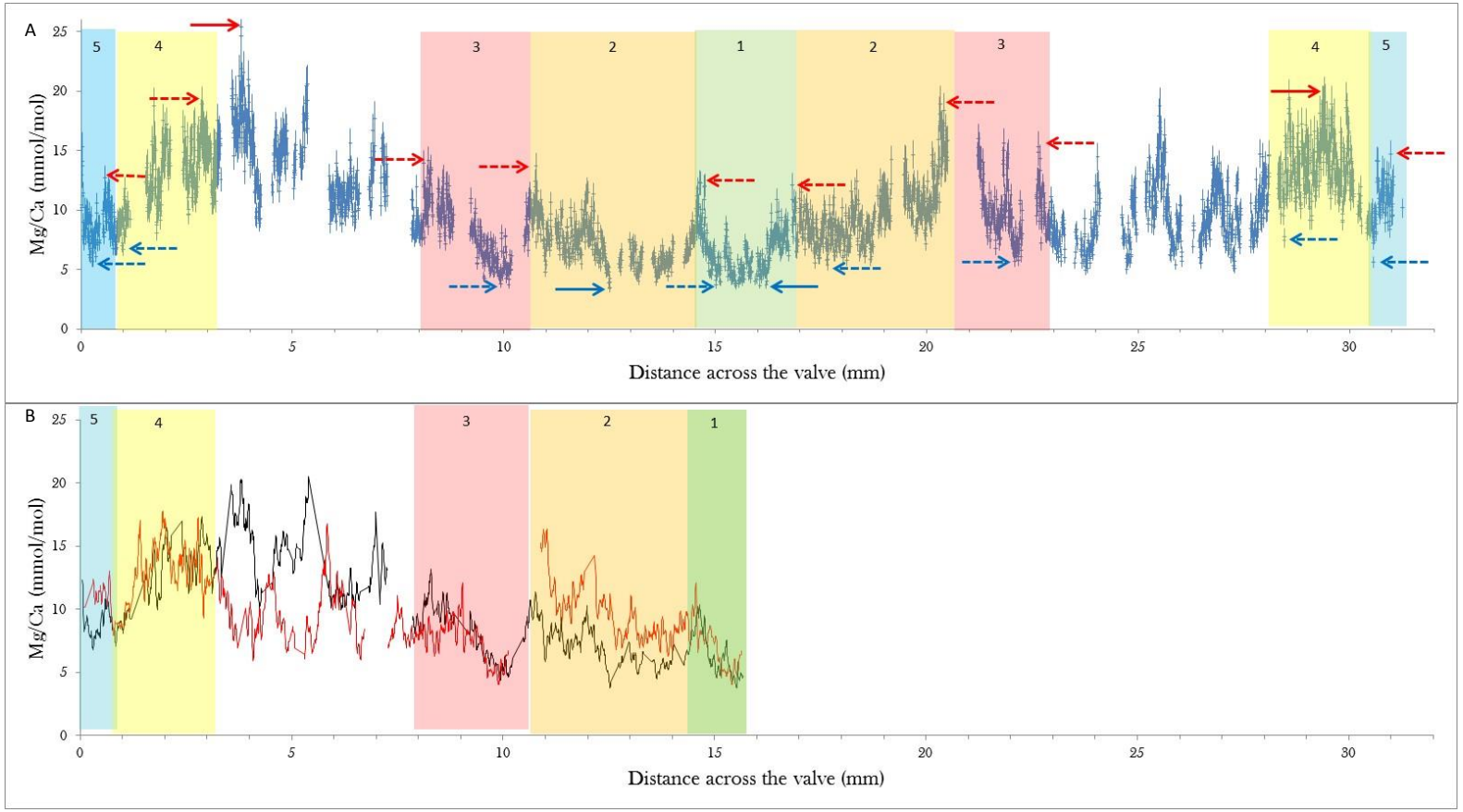

Figure 5.3.1-3. Mg/Ca data from MCLIO4. A shows the laser ablation data with 8 % y-axis error bars and 40 µm x-axis error bars. The solid red and blue arrows indicate the highest Mg/Ca and lowest Mg/Ca respectively on one half of the profile. The dashed red and blue arrows indicate the respective highest and lowest Mg/Ca in each band, bands are identified by the numbered colour boxes. B shows an 8 point moving average of the same data from. The two lines show the left (black) and right (red) halves of the valves starting with the outside of the shell at 0 mm moving towards the centre of the shell.

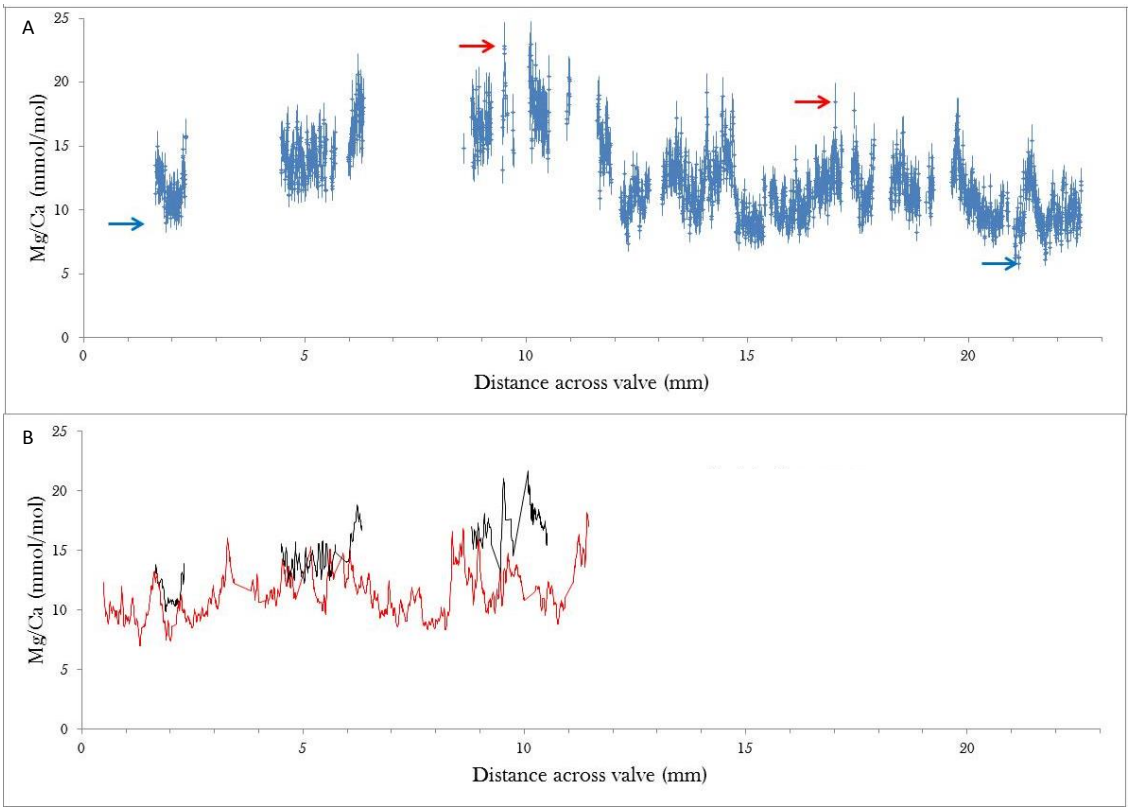

Figure 5.3.1-4. Mg/Ca data from MCLIO5. A shows the laser ablation data with 8 % y-axis error bars and 40 µm x-axis error bars. The solid red and blue arrows indicate the highest Mg/Ca and lowest Mg/Ca respectively on one half of the profile B shows an 8 point moving average of the same data from. The two lines show the left (black) and right (red) halves of the valves starting with the outside of the valve at 0 mm moving towards the centre of the valve. Valve not used in analysis due to large data gaps on the left half of the valve.

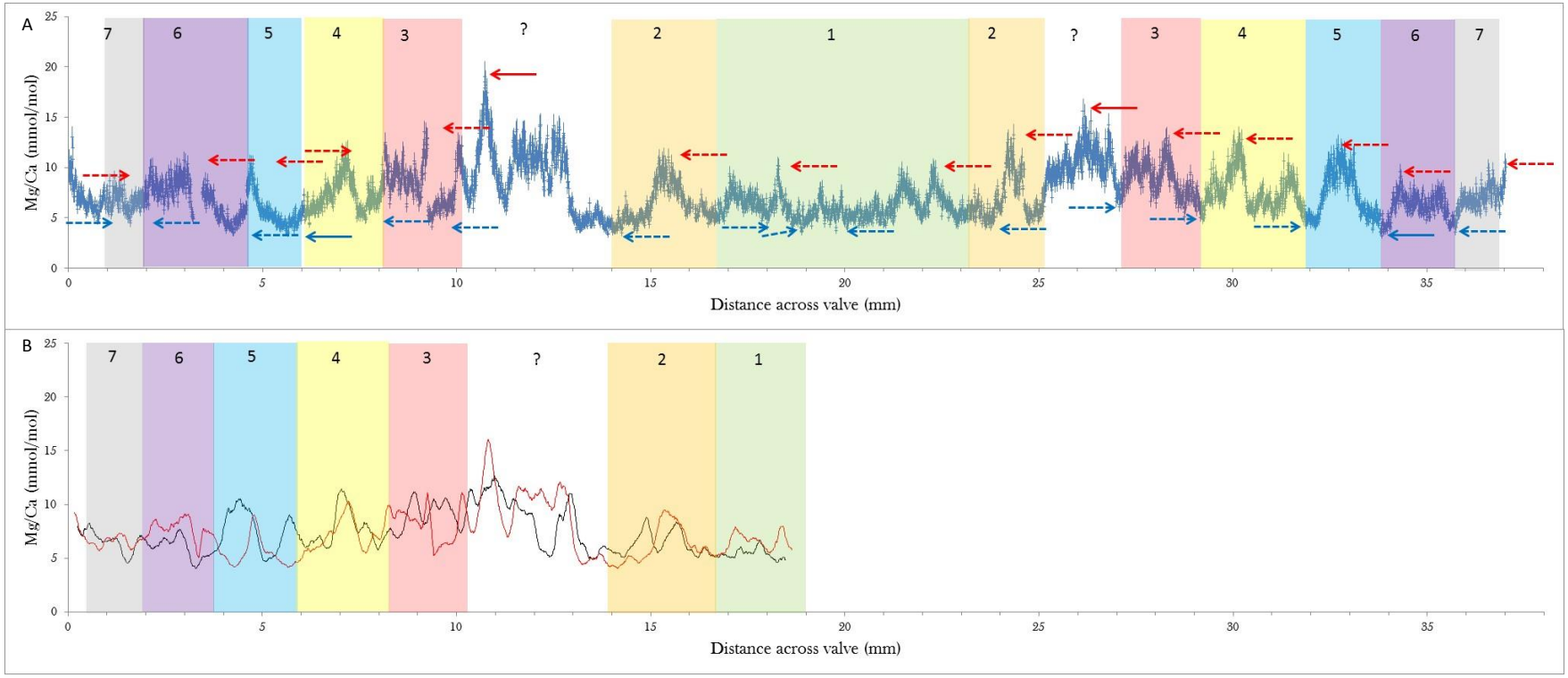

Figure 5.3.1-5. Mg/Ca data from TMLIO1. A shows the laser ablation data with 8 % y-axis error bars and 40 µm x-axis error bars. The solid red and blue arrows indicate the highest Mg/Ca and lowest Mg/Ca respectively on one half of the profile. The dashed red and blue arrows indicate the respective highest and lowest Mg/Ca in each band, bands are identified by the numbered colour boxes. B shows an 8 point moving average of the same data from. The two lines show the left (black) and right (red) halves of the valves starting with the outside of the shell at 0 mm moving towards the centre of the shell.

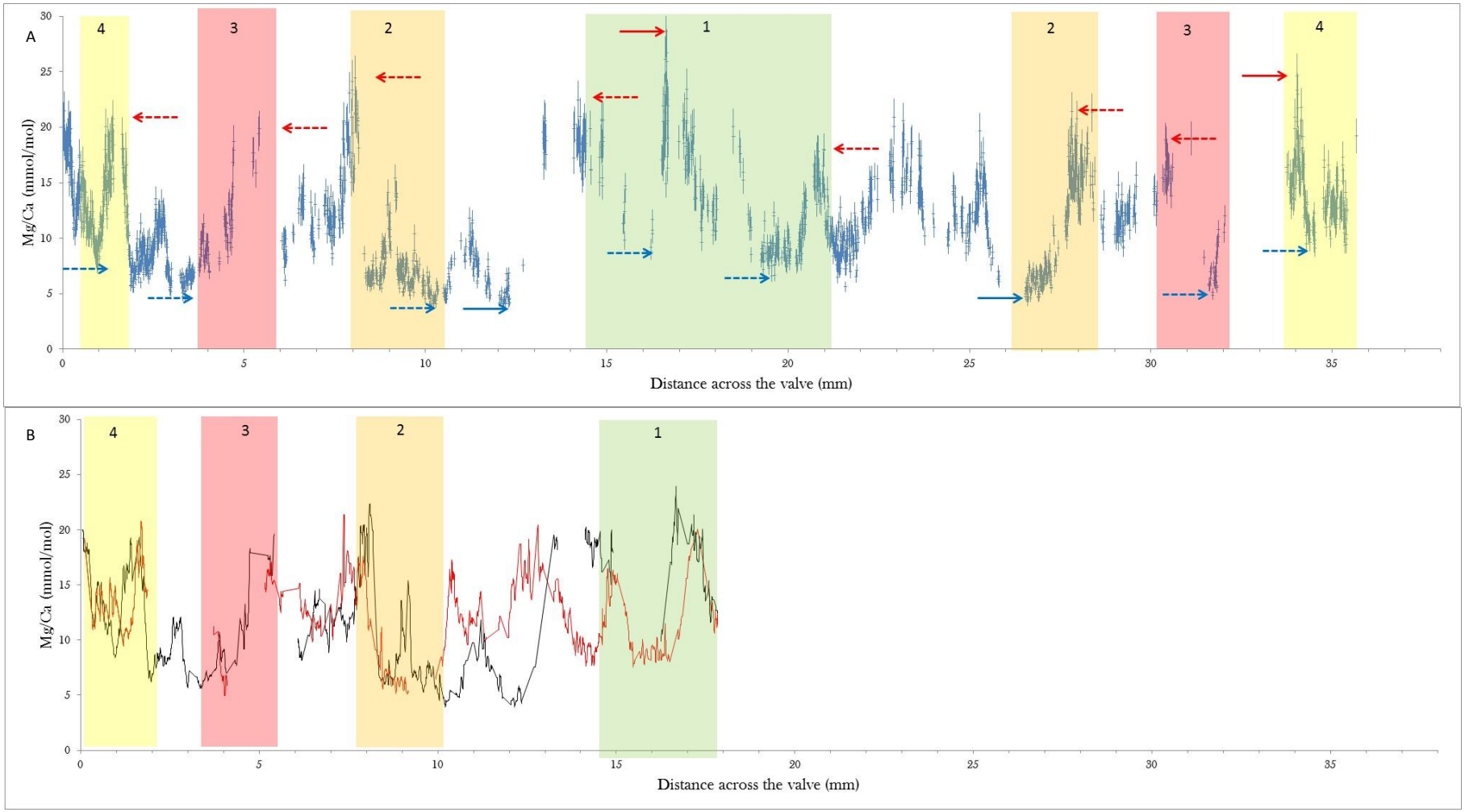

Figure 5.3.1-6. Mg/Ca data from TMLIO2. A shows the laser ablation data with 8 % y-axis error bars and 40 µm x-axis error bars. The solid red and blue arrows indicate the highest Mg/Ca and lowest Mg/Ca respectively on one half of the profile. The dashed red and blue arrows indicate the respective highest and lowest Mg/Ca in each band, bands are identified by the numbered colour boxes. B shows an 8 point moving average of the same data from. The two lines show the left (black) and right (red) halves of the valves starting with the outside of the shell at 0 mm moving towards the centre of the shell.

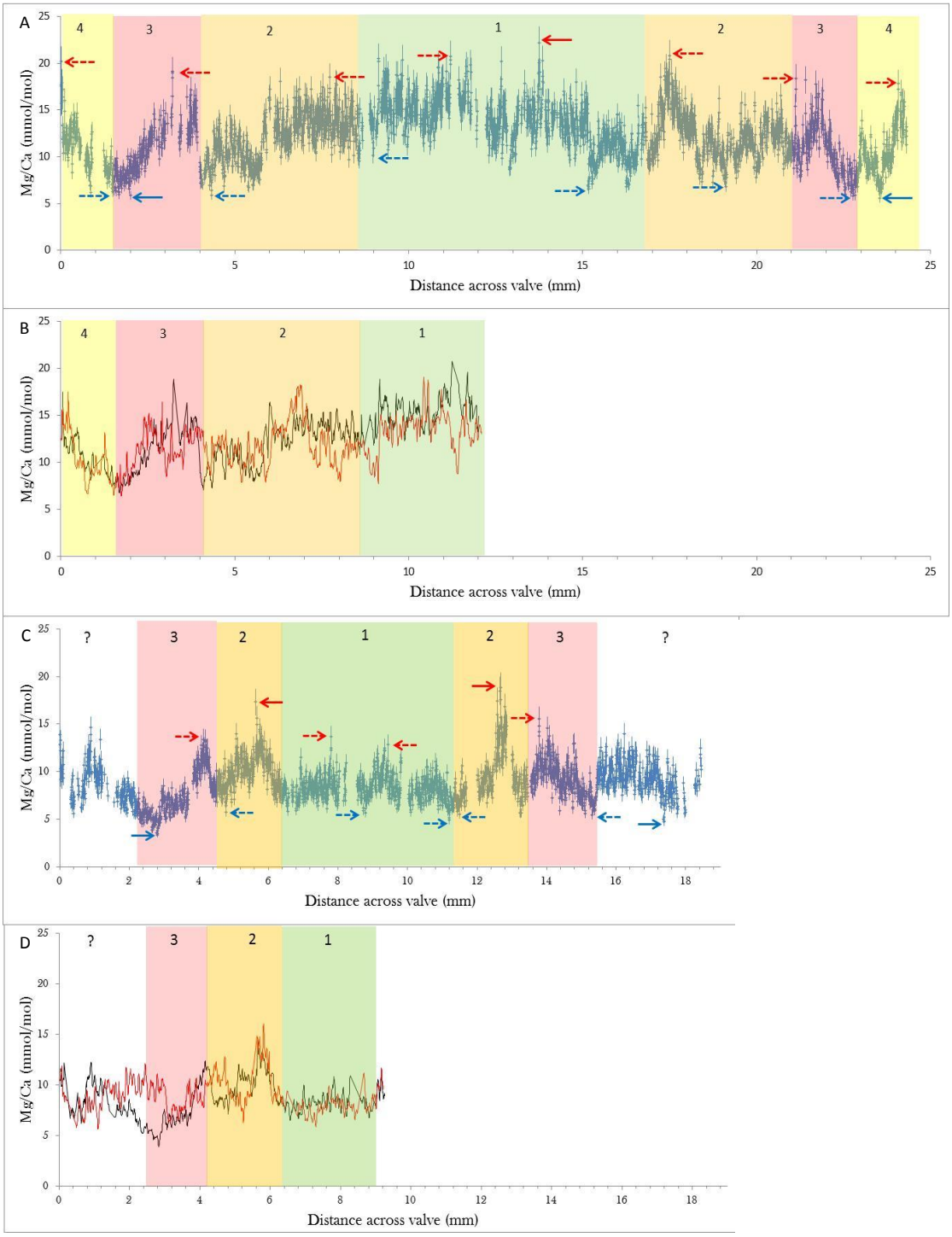

Figure 5.3.1-7. Mg/Ca data from TMLIO3 (A and B) and TMLIO4 (C and D). A and C show the laser ablation data with 8 % y-axis error bars and 40 µm x-axis error bars. The solid red and blue arrows indicate the highest Mg/Ca and lowest Mg/Ca respectively on one half of the profile. The dashed red and blue arrows indicate the respective highest and lowest Mg/Ca in each band, bands are identified by the numbered colour boxes. B and D show an 8 point moving average of the same data from A and C. The two lines show the left (black) and right (red) halves of the valves starting with the outside of the shell at 0 mm moving towards the centre of the shell.

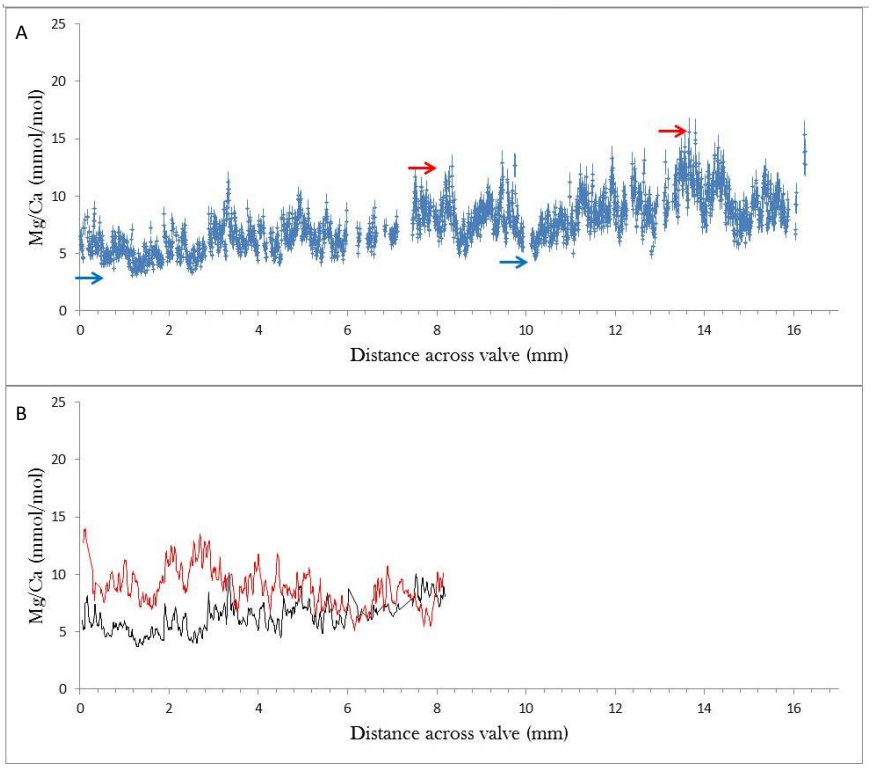

Figure 5.3.1-8. Mg/Ca data from TMLIO5. A shows the laser ablation data with 8 % y-axis error bars and 40 µm x-axis error bars. The solid red and blue arrows indicate the highest Mg/Ca and lowest Mg/Ca respectively on one half of the profile B shows an 8 point moving average of the same data from. The two lines show the left (black) and right (red) halves of the valves starting with the outside of the valve at 0 mm moving towards the centre of the valve. Shells not used in analysis as the profile is asymmetrical.

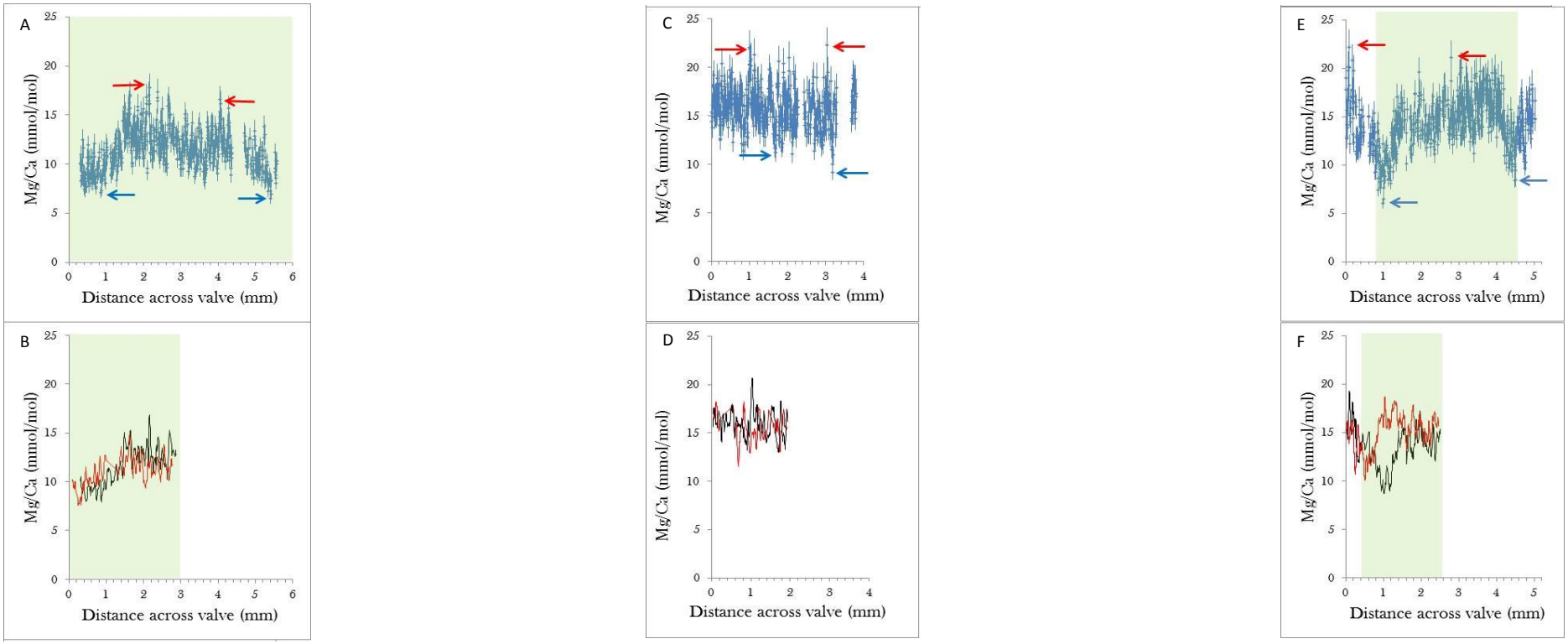

Figure 5.3.1-9. Mg/Ca data from MCTER3 (A and B), MCTER4 (C and D) and MCTER5 (E and F). A, C and E show the laser ablation data with 8 % y-axis error bars and 40 µm x-axis error bars. The solid red and blue arrows indicate the highest Mg/Ca and lowest Mg/Ca respectively on one half of the profile. B, D and F show an 8 point moving average of the same data from A, C and E respectively. The two lines show the left (black) and right (red) halves of the valves starting with the outside of the valve at 0 mm moving towards the centre of the valve.

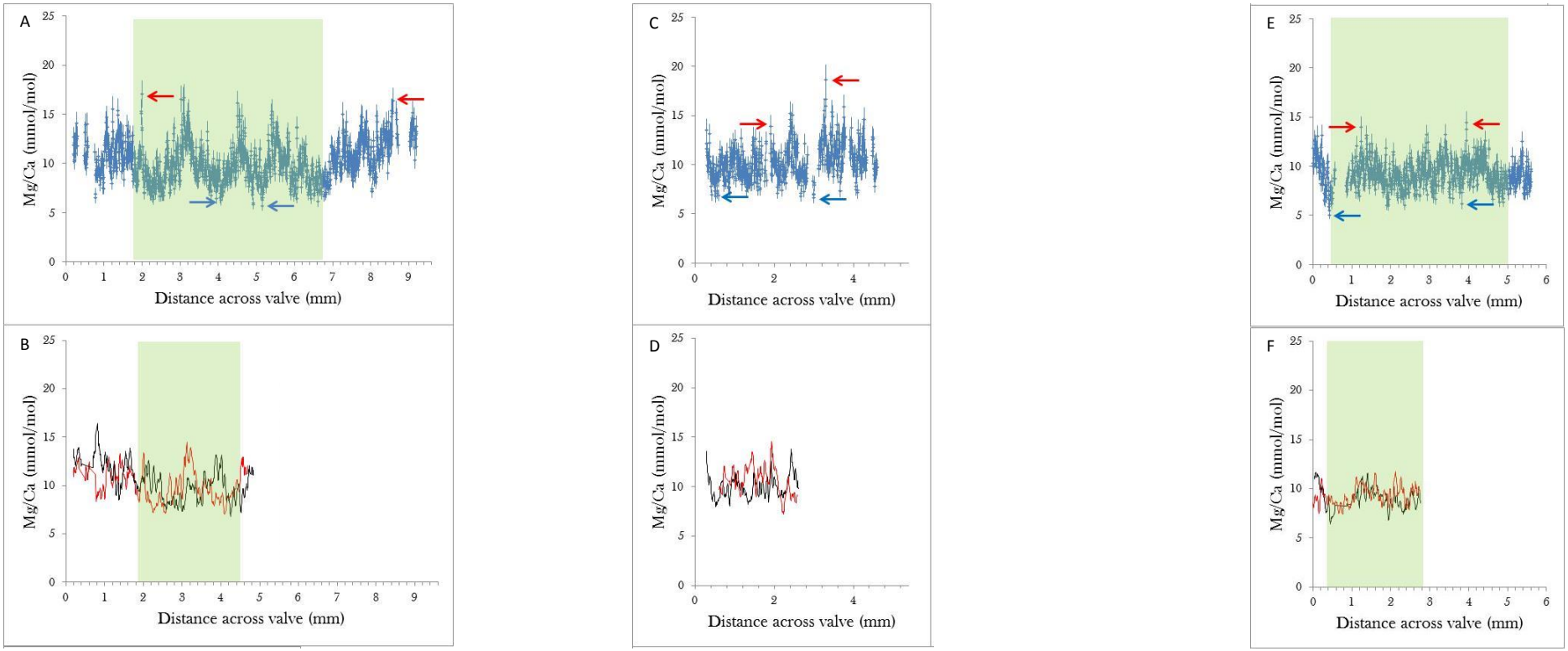

Figure 5.3.1-10. Mg/Ca data from TMTER1 (A and B), TMTER2 (C and D) and TMTER3 (E and F). A, C and E show the laser ablation data with 8 % y-axis error bars and 40 µm x-axis error bars. The solid red and blue arrows indicate the highest Mg/Ca and lowest Mg/Ca respectively on one half of the profile. B, D and F show an 8 point moving average of the same data from A, C and E respectively. The two lines show the left (black) and right (red) halves of the valves starting with the outside of the valve at 0 mm moving towards the centre of the valve.

Terebratulina have not been used in the seasonal analysis from here on because the specimens often display one or no seasonal cycles (Figures 5.3.1-9 and 5.3.1-10). Therefore the data set is not large enough for any robust analysis. In summary, there is no significant difference in any Mg/Ca data between the annual average maxima (Table 5.3.1-5), average annual minima (Table 5.3.1-6) or range of values (Table 5.3.1-7) from the Eocene to Oligocene in *Liothyrella*.

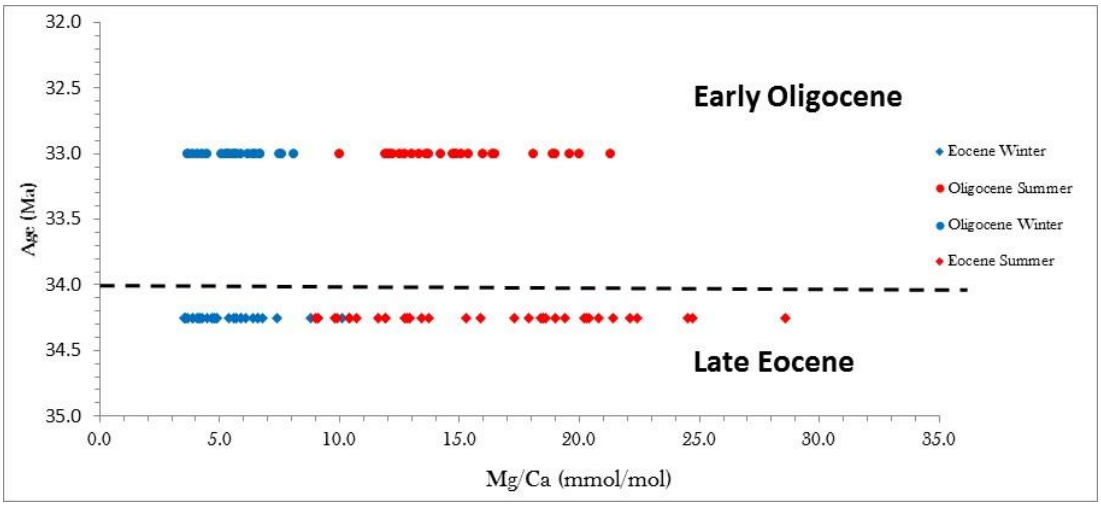

Figure 5.3.2-11. Annual summer maxima and winter minima Mg/Ca values from the Trig M (Late Eocene) and McDonalds Quarry (Early Oligocene)

t-Test: Two-Sample Assuming Unequal Variances	Oligocene Summer Maxima Mg/Ca	Eocene Summer Maxima Mg/Ca
Mean	15.06	16.31
Variance	8.62	25.94
Observations	26	36
Hypothesised Mean Difference	0	
Degrees of Freedom	58	
t Stat	-1.22	
P(T<=t) two-tail	0.23	
t Critical two-tail	2.00	

Table 5.3.2-5. t-Test comparing summer Mg/Ca values from the Oligocene to summer Mg/Ca values from the Eocene.

t-Test: Two-Sample Assuming Unequal Variances	Oligocene Winter Minima Mg/Ca	Eocene Winter Minima Mg/Ca
Mean	5.61	5.32
Variance	1.472	2.69
Observations	24	35
Hypothesised Mean Difference	0	
Degrees of Freedom	57	
t Stat	0.78	
P(T<=t) two-tail	0.44	
t Critical two-tail	2.00	

Table 5.3.2-6. t-Test comparing winter Mg/Ca values from the Oligocene to winter Mg/Ca values from the Eocene.

t-Test: Two-Sample Assuming Unequal Variances	Oligocene Seasonal Variation Mg/Ca	Eocene Seasonal Variation Mg/Ca
Mean	9.23	10.30
Variance	6.51	16.91
Observations	41	56
Hypothesised Mean Difference	0	
df	93	
t Stat	-1.56	
P(T<=t) two-tail	0.12	
t Critical two-tail	1.99	

Table 5.3.2-7. t-Test comparing seasonal variation in Mg/Ca values from the Oligocene to seasonal variation in Mg/Ca values from the Eocene.

5.3.2 Stable isotopes in Liothyrella and Terebratulina across the EOT

Stable isotopes were measured from powders collected from drilled trenches (section 3.3) for both *Liothyrella* and *Terebratulina*; see Table 5.3.2-1 and Figure 5.3.2-1 for individual measurements. A summary of the $\delta^{18}O$ and $\delta^{13}C$ results based on species, age and location can be found in Tables 5.3.2-2 and 5.3.2-3.

Specimen	Species	Age	$\delta^{18}O$ (‰ VPDB)	$\delta^{13}C$ (‰ VPDB)
MCLIO1	Liothyrella oamarutica	Early Oligocene	1.50	3.80
MCLIO2	Liothyrella oamarutica	Early Oligocene	1.60	3.83
MCLIO3	Liothyrella oamarutica	Early Oligocene	1.30	2.26
MCLIO4	Liothyrella oamarutica	Early Oligocene	1.71	4.23
MCLIO5	Liothyrella oamarutica	Early Oligocene	1.50	3.96
TMLIO1	Liothyrella concentrica	Late Eocene	0.15	3.00
TMLIO2	Liothyrella concentrica	Late Eocene	-0.20	0.73
TMLIO3	Liothyrella concentrica	Late Eocene	0.12	2.71
TMLIO4	Liothyrella concentrica	Late Eocene	0.36	3.53
TMLIO5	Liothyrella concentrica	Late Eocene	0.61	3.55
MCTER1	Terebratulinna suessi	Early Oligocene	1.39	2.87
MCTER2	Terebratulinna suessi	Early Oligocene	Altered	Altered
MCTER3	Terebratulinna suessi	Early Oligocene	1.59	2.42
MCTER4	Terebratulinna suessi	Early Oligocene	1.66	2.72
MCTER5	Terebratulinna suessi	Early Oligocene	1.59	2.95
TMTER1	Terebratulinna suessi	Late Eocene	0.49	2.23
TMTER2	Terebratulinna suessi	Late Eocene	-2.49	-5.14
TMTER3	Terebratulinna suessi	Late Eocene	0.49	1.79

Table 5.3.2-1. Individual stable isotope measurements collected from *Liothyrella* and *Terebratulina* from McDonalds Quarry and Trig M. Potentially unreliable readings are in red.

The $\delta^{18}O$ data increase by 1.29 ‰ (VPDB) over the EOT. This increase is from an average of 0.32 ‰ (VPDB) in the Eocene to an average of 1.61 ‰ (VPDB) in the Oligocene (Table 5.3.3-4 and Figure 5.3.3-2). The lowest reliable

measurement in the Eocene is 0.12 ‰ (VPDB) whilst the lowest reading in the Oligocene is 1.5 ‰ (VPDB). The highest reading in the Eocene is 0.49 ‰ (VPDB), the highest in the Oligocene is 1.71 ‰ (VPDB).

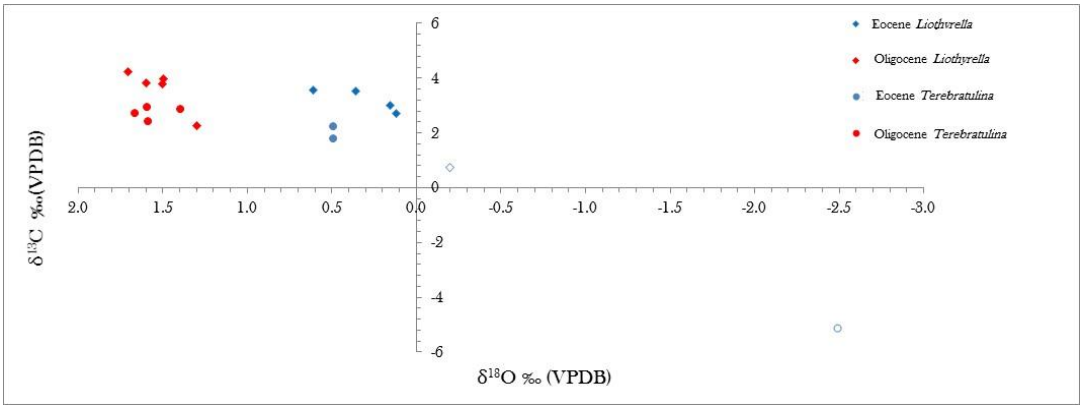

Figure 5.3.2-1. Individual stable isotope measurements collected from *Liothyrella* and *Terebratulina* from McDonalds Quarry and Trig M. Blue markers represent readings from the Eocene, red markers represent readings from the Oligocene, circles represent *Terebratulina* and diamonds *Liothyrella*. Two outliers, that lie more than 2 standard deviations outside the mean are marked as open symbols and are not considered further.

Age	Location	Species	$\delta^{18}O$ Max (‰ VPDB)	$\delta^{18}O$ Min (‰ VPDB)	$\delta^{18}O$ Average (‰ VPDB)	Range (‰ VPDB)
Oligocene	McDonalds Quarry	*Liothyrella oamarutica*	1.71	1.50	1.61	0.21
Oligocene	McDonalds Quarry	*Terebratulina suessi*	1.66	1.59	1.61	0.07
Eocene	Trig M	*Liothyrella concentrica*	0.36	0.12	0.21	0.24
Eocene	Trig M	*Terebratulina suessi*	0.49	0.49	0.49	0.00

Table 5.3.2-2. Summary of the $\delta^{18}O$ data collected from *Liothyrella* and *Terebratulina* from McDonalds Quarry and Trig M.

Age	Location	Species	$\delta^{13}C$ Max (‰ VPDB)	$\delta^{13}C$ Min (‰ VPDB)	$\delta^{13}C$ Average (‰ VPDB)	Range (‰ VPDB)
Oligocene	McDonalds Quarry	*Liothyrella oamarutica*	4.23	3.80	3.95	0.43
Oligocene	McDonalds Quarry	*Terebratulina suessi*	2.95	2.42	2.74	0.53
Eocene	Trig M	*Liothyrella concentrica*	3.53	2.71	3.08	0.82
Eocene	Trig M	*Terebratulina suessi*	2.23	1.79	2.01	0.44

Table 5.3.2-3. Summary of the $\delta^{13}C$ data collected from McDonalds Quarry and Trig M.

Age	Location	Species	$\delta^{18}O$ Max (‰ VPDB)	$\delta^{18}O$ Min (‰ VPDB)	$\delta^{18}O$ Average (‰ VPDB)	$\delta^{18}O$ Range (‰ VPDB)	Number of Specimens
Oligocene	McDonalds Quarry	*Liothyrella oamarutica* and	1.71	1.5	1.61	0.2	6
Eocene	Trig M	*Liothyrella oamarutica* and	0.61	0.12	0.32	0.49	5

Table 5.3.2-3. Summary of the $\delta^{13}C$ data collected from *Liothyrella* and *Terebratulina* from McDonalds Quarry and Trig M.

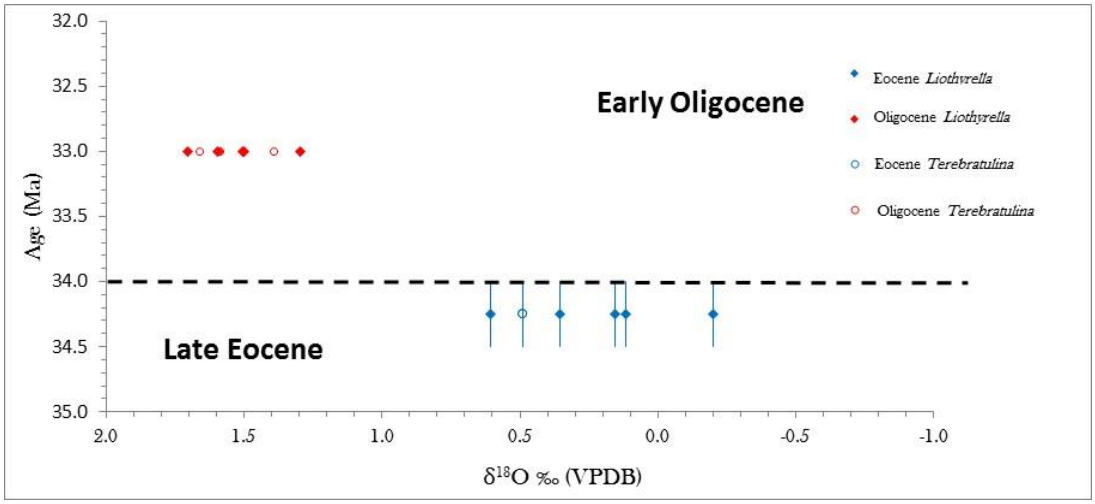

Figure 5.3.2-2. $\delta^{18}O$ measurements collected from *Liothyrella* and *Terebratulina* from McDonalds Quarry and Trig M. Blue markers represent readings from the Eocene, red markers represent readings from the Oligocene, circles represent *Terebratulina* and diamonds *Liothyrella*.. The dashed black line represents the boundary between the Eocene and Oligocene. Error bars represent uncertainty over age of locality.

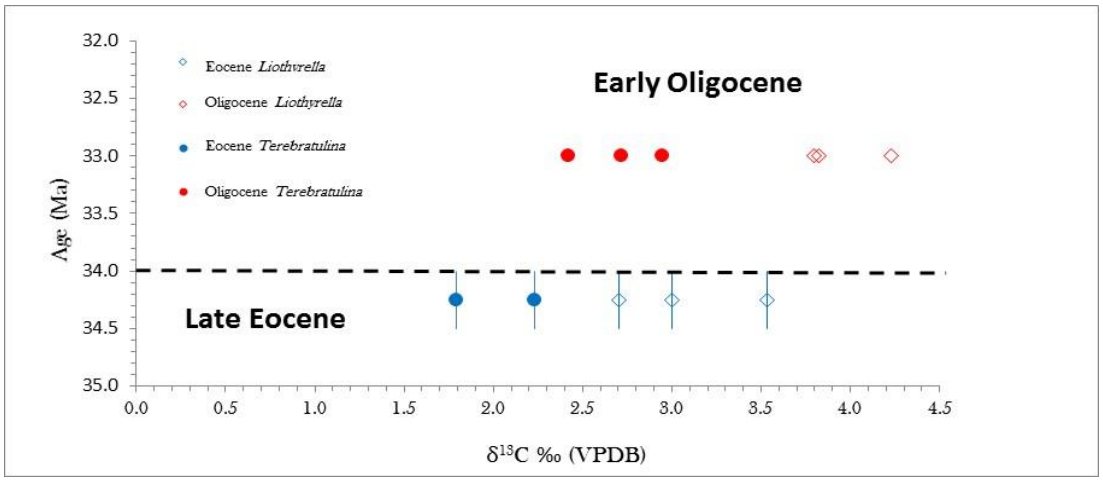

Figure 5.3.2-3. $\delta^{13}C$ measurements collected from *Liothyrella* and *Terebratulina* from McDonalds Quarry and Trig M. Blue markers represent readings from the Eocene, red markers represent readings from the Oligocene, circles represent *Terebratulina* and diamonds *Liothyrella*. The lack of y-axis is due to the slight uncertainty surrounding the exact ages of Trig M and McDonalds Quarry. The dashed black line represents the boundary between the Eocene and

Brachiopod $\delta^{13}C$ increases over the EOT. Due to vital effects influencing $\delta^{13}C$ in different species (e.g. Parkinson et al., 2005) data sets from the two species need to

be separated. The average $\delta^{13}C$ value in *Liothyrella* increases from 3.08 ‰ (VPDB) in the Eocene to 3.95 ‰ (VPDB) in the Oligocene, an increase of 0.87 ‰, Table 5.3.2-3 and Figure 5.2.3-2. In *Terebratulina* there is a similar increase of 0.73 ‰ from Eocene to Oligocene with values rising from 2.01 ‰ to 2.74 ‰ Table 5.3.2-3 and Figure 5.3.2-3.

5.4 Discussion

5.4.1 The EOT in New Zealand – are brachiopods a faithful recorder of environmental change?

McDonalds quarry has been placed ~33 Ma at the base of magnetic chron C12r (Buening et al., 1998), whilst Trig M is known to be Latest Eocene and thought to be contemporaneous to Weston Quarry (Daphne Lee Pers. Comm. March 2012) placed at between 34 and 34.5 Ma (Buening et al., 1998). Minimal bias from sea level fall is assumed as the two sites are both from the Ototara Limestone Formation and are of similar palaeowater depth (45 ±15 m) (Edwards et al., 1991). The shift in brachiopod $\delta^{18}O$ and $\delta^{13}C$ between the two sites can be compared to other records to establish whether the brachiopods can be used to reconstruct environmental change in New Zealand across the EOT. The 0.87 ‰ increase in *Liothyrella* $\delta^{13}C$ from, Eocene to Oligocene, is similar to the 0.73 ‰ increase in *Terebratulina* $\delta^{13}C$, Figure 5.3.2-3. The mean increase from both species is 0.8 ±0.1‰ (2 s.e.). This increase demonstrates that the New Zealand brachiopods capture the global $\delta^{13}C$ increase across the EOT.

When compared to other EOT studies, this shift is slightly larger than a 0.5 ‰ increase in planktic foraminiferal $\delta^{13}C$ from Tanzania, after $\delta^{13}C$ values have

rebounded post-EOGM (Pearson et al., 2008). However the problems with dating the exact age of Trig M, leads to uncertainty in this comparison. If assigning an age of between 34 Ma and 34.5 Ma to Trig M then the uncertainty in this shift in Pearson et al. (2008) is between 0.2 and 0.7 ‰. Other studies from the South Atlantic (Zachos et al., 1996; Liu et al., 2004) and the equatorial eastern Pacific (Coxall et al 2005; Coxall and Wilson, 2011) have a ~1.2 ‰ increase but represent deeper waters. However, this 1.2 ‰ increase is a maximum change associated the EOGM. When comparing the time frame of this study to the Coxall et al. (2005) data at ODP Site 1218 the shift at Site 1218 is between 0.3 and 0.6 ‰.

The reason for this increase in $\delta^{13}C$ is debated. A global increase in export and burial

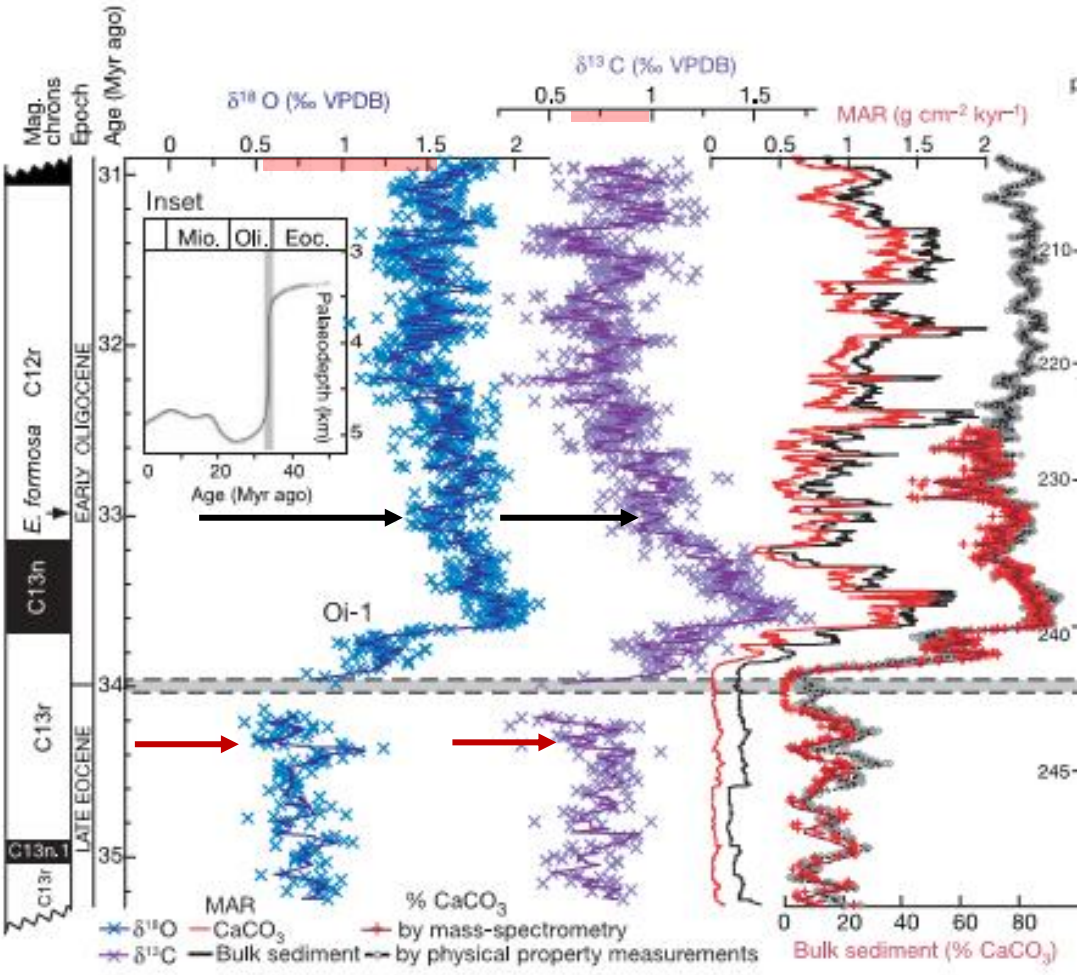

Figure 5.4.1-1. Benthic $\delta^{18}O$ and $\delta^{13}C$ shifts, from ODP Site 1218. Red arrows mark the approximate age of Trig M and the black arrows mark the age of McDonalds Quarry. The highlighted pink boxes on the x axes highlight the magnitude of the $\delta^{18}O$ and $\delta^{13}C$ shifts when considering the age to Trig M compared to McDonalds Quarry, Coxall et al., 2005.

of organic carbon in the deep sea is the most obvious cause for the excursion (Coxall and Wilson, 2011). However, geochemical modelling studies, forced by increased burial of organic carbon, fail to simulate the contemporaneous deepening of the CCD (Merico et al., 2008). Also multi-proxy palaeoproductivity studies from the equatorial Pacific show a decrease in productivity across the EOT (Moore et al., 2014). This suggests that there may be other factors to consider, such as enhanced weathering of newly exposed continent (Zachos and Kump, 2005). This is supported by increased continental weathering of limestones in sea level change led modelling, as this produces a permanent change in the CCD and the excursion in $\delta^{13}C$ (Merico et al., 2008).

Site	Pre –EOGM $\delta^{18}O$ ‰ (VPDB) (34.5-34Ma)	EOGM $\delta^{18}O$ $\delta^{18}O$ ‰ (VPDB)	Post-EOGM $\delta^{18}O$ (33 Ma)	Magnitude of Shift Pre-EOGM to Post EOGM $\delta^{18}O$ ‰ (VPDB)
New Zealand (This Study)	0.32	-	1.61	1.29
ODP Site 1218 (Coxall et al., 2005)	0.6 – 1	2.0	1.6	0.6 – 1.0
ODP Site 744 (Zachos et al., 1994)	0.9 – 1.3	2.4	1.8	0.5 – 0.9
ODP Site 522 (Zachos et al., 1994)	0.8 – 1.5	2.5	2.0	0.5 – 1.2
TDP (Pearson et al., 2008)	-3.2 – -2.7	-1.8	-2.2	0.5 – 1

Table 5.4.1-1. The $\delta^{18}O$ excursion from this sites compared to three deep water ODP Sites and one shallow water TDP sites.

Regardless of the reason for the excursion, this study shows a slightly larger change in shallow water $\delta^{13}C$ to that of Pearson et al. (2008) but also that of deep waters (e.g. Coxall et al., 2005) across the EOT, possibly due to changes in water mass properties (Section 5.4.3).

The stable isotope results show an increase in $\delta^{18}O$ across the transition. They increase from an average of 0.32 ‰ in the Eocene to an average of 1.61 ‰ at 33 Ma in the Oligocene (Figure 5.3.3-2). The magnitude of this shift is slightly larger than other $\delta^{18}O$ increases when comparing other shifts to the time frame used here (34.5-34 Ma to 33 Ma; Table 5.4.1-1, Figure 5.4.1-1)

Based on the $\delta^{13}C$ and $\delta^{18}O$ shifts the brachiopods from the Eocene (Trig M) and Oligocene (McDonalds Quarry) are reliably recording the environmental change across the EOT. However there are many potential reasons to explain the difference in magnitude between this record and other published records (e.g. water depth and water mass properties) these are explored below using Mg/Ca records from the same localities. The $\delta^{13}C$ and $\delta^{18}O$ excursions are global events and it is reasonable to assume that the New Zealand sections do not capture the full extent of the excursion as McDonalds Quarry is dated as post EOGM.

5.4.2 Seasonal seawater temperatures across the EOT

The scope of this project was to assess seasonality over the EOT. The data set collected and the quality of the data allow for investigation of annual cycles in seasonality. The *Liothyrella* specimens are able to resolve relative temperature changes on an annual scale. From here on the maximum values of the annual bands of the shells will be referred to as the summer values and the minimum values will

be referred to as winter values. Mean annual temperatures derived from Mg/Ca in brachiopods for the Late Eocene – Early Oligocene have not been calculated as brachiopods grow at different rates throughout the year. Growth is fastest in summer and autumn and slowest in winter/spring, there may also be brief hiatuses in growth when spawning occurs (Curry, 1982). Therefore any mean value would be skewed towards the summer/autumn values but to what extent is unknown. Modern calibration work (Butler et al., 2015; Chapter 4) suggests that growth continues in brachiopods to temperatures as low as 6 °C. As a result of this continual growth throughout the year, temperature changes over the EOT can best be described using maximum summer and minimum winter temperatures rather than a skewed mean. Relative (Eocene-Oligocene) changes in seawater temperature were calculated using the *Liothyrella* calibration equation derived in Chapter 4, Equation (1) (Table 5.4.1-1).

(1) $Mg/Ca_{Liothyrella} = 0.49 \pm 1.27\ e^{(0.20 \pm 0.11)T}$

Liothyrella shows a decrease over the EOT in the average summer temperature of 0.4 °C and a decrease in maximum summer temperature (the highest reliable Mg/Ca value, converted to temperature, recorded in any of the specimens) of 1.5 °C (Table 5.3.2-1). Whilst a small increase is shown in average winter temperatures of 0.3 °C there is also an increase of 0.3 °C in minimum winter temperature (the lowest reliable Mg/Ca value, converted to temperature, recorded in any of the specimens).

The highest summer value is not found in the same year as the lowest winter value, suggesting that the hottest summers and coolest winters did not follow each other. This is true for both Eocene and Oligocene specimens. In Late Eocene the summer temperatures vary by 5.7 °C whilst winter temperatures vary by 5.2 °C, (range of

summer and winter Mg/Ca in Figure 5.3.2-11 converted to temperature using equation 1). In the Early Oligocene both summer and winter temperature variations are more consistent with variations of 3.8 and 3.7 °C.

The variance is higher in all of the Late Eocene specimens (Tables 5.3.2-5, 5.3.2-6 and 5.3.2-7) possibly suggesting that the Early Oligocene specimens were situated in more stable conditions. This is particularly true for summer values which show a significant difference (Table 5.4.1-2), suggesting that the Eocene might have been prone to a more variable summer temperature. This is also shown by the decrease in 'Maximum Summer Temperature' of 1.5 °C between the two sites.

This study has different findings from that of Ivany et al. (2000) and Wade et al. (2012); both from the Gulf of Mexico and Eldrett et al. (2009) from Greenland. These studies showed a decrease in winter temperatures of around 4 °C across the EOT. In New Zealand assuming no change in water depth between the two sites there are no significant changes in the summer and winter temperatures as well no significant change in seasonality.

	Oligocene	Eocene	Difference from Eocene
Average Summer Mg/Ca (mmol/mol)	**15.1 SD = (2.9)**	**16.5 SD = (5.1)**	**-0.4**
Average Winter Mg/Ca (mmol/mol)	**5.6 SD = (1.21)**	**5.3SD = (1.64)**	**+0.3**
Maximum Summer Mg/Ca (mmol/mol)	**21.3**	**28.6**	**-1.5**
Minimum Summer Mg/Ca (mmol/mol)	**10.0**	**9.0**	**+0.5**
Maximum Winter Mg/Ca (mmol/mol)	**8.1**	**10.1**	**-1.1**
Minimum Winter Mg/Ca (mmol/mol)	**3.7**	**3.5**	**+0.3**
Average Seasonal Difference Mg/Ca (mmol/mol)	**9.2 SD = (2.6)** **Temp** (°C) = ~ 5.0	**10.3 SD = (4.1)** **Temp** (°C) = ~ 5.5	**-0.5**
Maximum Seasonal Difference Mg/Ca (mmol/mol)	**14.8**	**22.0**	**-2.0**
Minimum Seasonal Difference Mg/Ca (mmol/mol)	**4.6**	**4.4**	**+0.3**

Table 5.4.2-1. Combined (values from shell that passed the diagenetic screening test) average, maximum and minimum summer and winter Mg/Ca values from annual bands of Oligocene *Liothyrella oamarutica* and Eocene *Liothyrella concentrica*, along with average, maximum and minimum seasonal differences in Mg/Ca. All are converted to temperature change. Summer temperatures are in red, winter temperatures in blue and differences in black. Average seasonal difference is different to Average Summer Mg/Ca minus Average Winter Mg/Ca as some summer and winter temperatures could not be utilised for this purpose due to data gaps. The temperature calculated for season difference is based on Average Summer Values – Average Winter Values and due to this is a slight overestimation of the temperature difference.

F-Test Two-Sample for Variances

	Eocene Summer Mg/Ca	Oligocene Summer Mg/Ca
Mean	16.31389	15.06231
Variance	25.94133	8.621882
Observations	36	26
df	35	25
F	3.008778	
P(F<=f) two-tail	0.005415	
F Critical one-tail	1.892411	

Table 5.4.2-2. Calculating variance of summer Eocene and summer Oliogcene Mg/Ca values to see if the difference is statistically significant.

In contrast to the findings of Ivany et al. (2000) and Wade et al. (2012), a study by Kobashi et al. (2004) shows no change in temperature over the EOT in the Gulf of Mexico. They find no statistical change in the temperature at the bottom of the seasonal thermocline 19.4 ±2 °C Late Eocene and 19.7 ±2 Early Oligocene. Based on Wade et al. (2012) using a multi-proxy approach their results are taken to be most representative of the change in conditions in the Gulf of Mexico across the EOT.

Water temperatures over the EOT from the Gulf of Mexico and the South Pacific responded in different manners to the glaciation. With the addition of an Antarctic ice sheet to an unglaciated world, models predict an heterogeneous SST response across the EOT, a deep water temperature increase which is delayed by more than 200 thousand years and changes in wind field which may change ocean circulation

(Knorr and Lohmann, 2014; Goldner et al., 2014). The ice sheet on Antarctica could have warmed the oceans in the southern hemisphere (Knorr and Lohmann, 2014; Goldner et al., 2014) negating the known influence of falling atmospheric CO_2 on water temperatures (e.g. Pearson et al., 2009; Zhang et al., 2013). This warming associated with the Antarctic ice sheet would not influence temperatures in the northern hemisphere. As a result the northern hemisphere records (Ivany et al., 2000; Zanazzi et al., 2007; Grimes et al., 2009; Wade et al., 2012) show falling winter temperatures that are probably representative of reduced atmospheric CO_2. Whilst the Southern Pacific temperatures, calculated in this study, remained the same as they represent a combination of the warming associated with the addition of the Antarctic ice sheet and the falling temperatures associated with the reduction of atmospheric CO_2.

5.4.3 Deconvolving $\delta^{18}O$ seawater from temperature across the EOT

The stable isotope results show an increase in $\delta^{18}O$ across the transition. They increase from an average of 0.32 ‰ in the Eocene to an average of 1.61 ‰ at 33 Ma in the Oligocene (Figure 5.3.3-2). Assuming constant oxygen isotopic composition of seawater ($\delta^{18}O_{seawater}$), this shift is equivalent to a 4.5˚C cooling (calculated using equation (2), adapted from Brand et al., 2013; Chapter 4).

$$(2)\quad T\,(°C) = 16.0 - 4.14(\delta^{18}O_{carbonate} - \delta^{18}O_{seawater}) + 0.18(\delta^{18}O_{carbonate} - \delta^{18}O_{seawater})^2$$

The *Liothyrella* Mg/Ca records suggest winter and summer temperatures did not change significantly in this area of New Zealand across the Eocene-Oligocene transition. As explained in section 5.4.2 there are no mean annual temperatures derived directly from the brachiopods due to the varying growth rates and the subsequent skew this may put on the data. However it is possible to make

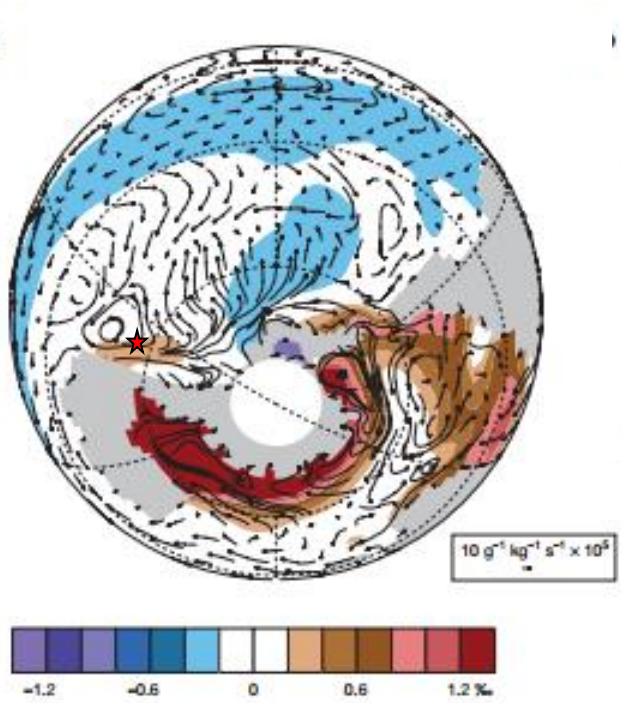

Figure 5.4.3-1. Modelled changes in salinity in terms of $\delta^{18}O$, with the addition of an ice sheet to Antarctica. Taken from Goldner et al., (2014). The star marks the NZ area used in this study.

assumptions about mean annual temperature based on the changes in average summer and average winter temperatures. Because the change in summer and winter temperatures are statistically insignificant, it is reasonable to assume that there was no significant change in mean annual temperature across the climate transition. Unlike deep-water benthic foraminiferal Mg/Ca studies there are no assumed problems associated with the carbonate saturation state changes in shallow waters. The New Zealand brachiopods lived in waters 30-60 m deep, and therefore Mg/Ca can be considered a reliable indicator of temperature. The entire brachiopod $\delta^{18}O$ shift (~1.3 ‰) must therefore be attributed to change in $\delta^{18}O_{seawater}$ across the EOT.

Recent modelling work, in theory, allows for an increase in $\delta^{18}O_{seawater}$ of 1.1 - 1.3 ‰

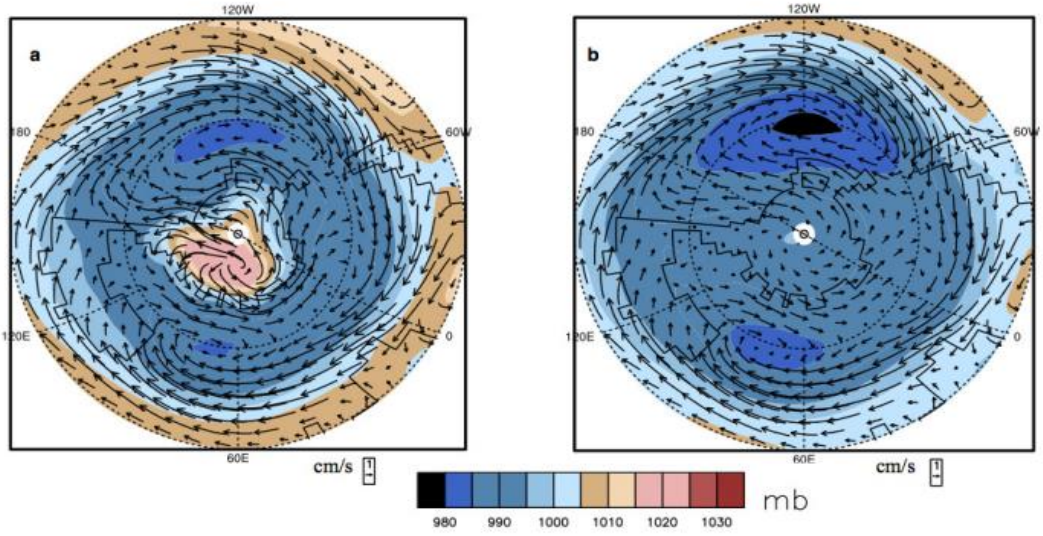

Figure 5.4.3-2. Modelled absolute sea level pressure and surface winds a, after Antarctic glaciation; b prior to glaciation. Taken from Goldner et al., (2014).

to take place due Antarctic glaciation alone as an ice sheet 1.4 times larger than the modern day ice sheet is thought to be possible (Wilson et al., 2013). However attributing the whole of the $\delta^{18}O$ shift shown here to changes in ice volume alone seems unreasonable as there is evidence that the global increase in $\delta^{18}O_{seawater}$ is closer to ~0.6 ‰ (Lear et al., 2008). If Lear et al's., (2008) increase of ~0.6 ‰ is used then the remaining ~ 0.7 ‰ $\delta^{18}O$ increase in the New Zealand brachiopods may reflect increased local salinity. There are three likely causes for an increase in local salinity. The first is a local shoaling event, caused by glacio-eustatic sea level lowering. This is discounted because the two sites are of similar palaeowater depth (Edwards et al., 1991). The second is a change in source of water mass (e.g. from low salinity high latitude to high salinity low latitude). The third possibility is that the increased local salinity reflects a change in the water mass properties, possibly caused by a change in salinity around Antarctica which affected the east coast of South Island New Zealand. This increase in regional salinity also reconciles $\delta^{18}O$

change in this study with ODP Sites 1218, 744 and 522 along with TDP site 12 and 17, as changes at those sites were smaller (Figure 5.4.1-1). A recent community earth system model (CESM), which added an Antarctic ice sheet to a non-glaciated Eocene, suggests that with Antarctic glaciation across the EOT would have led to an increase in regional $\delta^{18}O_{seawater}$ of ~ 0.2 – 0.4 ‰, (Figure 5.4.3-1) in the South Pacific around New Zealand. This is due to oceans around Antarctica having higher salinities partially due to brine rejection from sea ice (Goldner et al., 2014). This is slightly less than the 0.7 ‰ increase shown in this study but is in the right direction. The model also produces increases higher than 0.7 ‰ in other areas suggesting that changes of this magnitude associated with glaciation are possible (Figure 5.4.3-1). This increase in salinity is not associated with a reordering of surface currents; whilst there may be enhanced circulation and stronger surface currents around New Zealand there is no change in the direction (Figure 5.4.3-2). This is consistent with the lack of temperature difference shown over the EOT in New Zealand as a change in circulation constituting a change from a high latitude fresh water mass to a saltier low latitude water mass would most likely be associated with an increase in temperature. However this would be superimposed on the global cooling and may therefore manifest in no difference in temperature. The alternative is that the record is reflecting increasing high latitude temperature and salinity as suggested by Goldner et al. (2014) superimposed on the global cooling. One model suggests there was reorganisation of deeper currents at this time due to the increased salinity leading to surface currents subducting along the Antarctic coast line; along with downwelling of high salinity water at 60 °S this contributed to enhanced deep water formation (Goldner et al., 2014).

5.4.4 Absolute temperature estimates from $\delta^{18}O$ and Mg/Ca

For the $\delta^{18}O$ temperature calculations it is important to know the $\delta^{18}O_{seawater}$. For the Eocene, this study has used the $\delta^{18}O_{seawater}$ calculated by Zachos et al. (1994) of -0.8 ‰ (SMOW). The average temperature calculated for the Late Eocene of New Zealand using the $\delta^{18}O$ calculation in equation (2) is 12.4 °C, which is in agreement with high latitude sea surface temperatures derived from $\delta^{18}O$ of benthic and planktonic foraminifera from deep sea cores (Zachos et al., 1994; Zachos et al., 2001) as well as temperatures calculated from brachiopods of Weston Quarry, eastern New Zealand (Buening et al., 1998) a location of temporal, regional and environmental similarity to Trig M. The Mg/Ca records suggest that the Oligocene temperatures were similar to this Eocene estimate. This is in disagreement with Buening et al. (1998), who had no independent way of assessing temperature as they only used $\delta^{18}O$ and $\delta^{13}C$ isotopes. The excursion in the $\delta^{18}O$ shown here is very similar to that shown in Buening et al. (1998) however they attributed most of the shift to a ~4˚C cooling. They used estimates for $\delta^{18}O_{seawater}$ derived from Zachos et al. (1994) of -0.8 ‰ for the Eocene and -0.5 ‰ for the Oligocene and therefore interpreted most of the 1.3 ‰ shift as being due to a temperature decrease from 12 ˚C to 6-8 °C.

Buening et al. (1998) struggle to reconcile their ~4 °C cooling (which is the average drop in temperature that data here would show if no change in $\delta^{18}O_{seawater}$ is considered) with the palaeontological records of New Zealand. North Island and coastal North Island NZ, have tropical flora and fauna in both the late Eocene and early Oligocene (Lee 1986, Lee and Campbell 1987, Adams et al., 1990, Murray 1991). The lack of significant temperature change on the east coast of the South Island across the EOT suggested by this study supports the idea that no change in the

fauna and flora of the North Island would be expected given the relative close proximity of North and South Island.

When using Mg/Ca to assess absolute palaeotemperatures and palaeoseasonality it is important to consider the Mg/Ca of palaeoseawater. Through proxy data such as Mg/Ca values from ridge flanked vein carbonates (Coggon et al., 2010) fluid inclusions (Lowenstein et al., 2001 and Horita et al., 2001) and echinoderm plates (Dickson, 2004) it is believed that modern day Mg/Ca values of seawater are higher than in the past. The secular changes in Mg/Ca cause inaccuracies in calculations when assessing temperatures over a period numbering in millions of years. As this study is looking at time periods just before and after the Eocene-Oligocene boundary, these secular variations are assumed not to cause a significant problem as the residence time of Mg and Ca are ~10 and ~1 million years respectively. At the time of the EOT it is thought that the Mg/Ca ratio of seawater was between 1.5 and 2.5 mol/mol, whilst today it is ~5.2 mol/mol (Coggon et al., 2010). These proxy data are also in agreement with modelled Mg/Ca seawater values of Stanley and Hardie (1998), Berner (2004) and Demicco et al. (2005), which for the EOT are all within this 1.5 – 2.5 mol/mol range. Here I have used the value modelled by Stanley and Hardie (1998) of ~2.1 mol/mol for the EOT as their model is in best agreement with the proxy data throughout the Cenozoic.

There is another complication when trying to assess absolute palaeotemperatures using Mg/Ca. Inorganic calcite and biogenic calcite from a variety of different organisms including foraminifera, corals and ostracodes do not display a linear uptake of Mg/Ca. This relationship is best explained by a power law and the equation shown below (Hasiuk and Lohmann, 2010).

(3) $Mg/Ca_{calcite} = E(Mg/Ca_{sw})^{H}e^{AT}$

Unfortunately the *H* value is a partition exponent which, for brachiopods, is unknown therefore the most robust findings will come from relative temperatures over the EOT. It is however possible to make some reasonable assumptions about the H value for brachiopods and the subsequent temperatures associated with them.

Here I use two approaches to estimate absolute summer and winter seawater temperature of the Late Eocene and Early Oligocene from eastern New Zealand. The first approach uses the average temperature calculated from stable isotopes in conjunction with the temperature ranges calculated from the Mg/Ca and equation (3) (Table 5.4.2-1). This approach requires an estimate of $\delta^{18}O_{seawater}$ but does not require an estimate of *H*. The second approach uses equation (3) and hence does not require an estimate of $\delta^{18}O_{seawater}$ but does requires an estimate for *H*.

Using the first approach (independent of *H*), the difference in temperature between summer and winter was 5.0 °C in the Oligocene and 5.5 °C in the Eocene (section 5.4.2). The 'average' water temperature calculated from the $\delta^{18}O$ was 12 °C for the Oligocene using a $\delta^{18}O_{seawater}$ of 0.5 ‰ and 12 °C for the Eocene using a $\delta^{18}O_{seawater}$ value of -0.8 ‰ (section 5.4.3). Because most of the brachiopod growth occurs between summer and autumn (Curry, 1982) it is assumed that this temperature represents approximately 75 % of maximum summer water temperature. Therefore I estimate that Oligocene summer and winter water temperatures were 13 °C and 8 °C respectively. The Eocene summers and winter water temperatures were 14 °C and 8 °C respectively.

The second approach to estimating absolute Mg/Ca-palaeotemperatures requires the *H* value for brachiopods to be known (Evans and Müller, 2012) as well as the Mg/Ca of seawater from the period in question. I have used a range of reasonable *H* values, (-0.03 to 1.53) the extremities of which are based on the highest and lowest *H* value determined for a wide range of calcifying organisms in Haisuk and Lohmann (2010), to produce results based on the equation below (Dunkley Jones et al., 2013).

$$T = \frac{1}{A} * \ln\left(\frac{\left(\frac{Mg}{Ca}\right)}{b} * \frac{\left(\left(\frac{Mg}{Ca}\right)sw\right)^{H}}{\left(\left(\frac{Mg}{Ca}\right)sw'\right)^{H}}\right)$$

The temperatures vary with the chosen *H* value up to a maximum of 7 °C, Table 5.4.4-1, however a conclusion can be reached; that these temperatures are higher than the temperatures calculated using $\delta^{18}O$ (Table 5.4.4-1). The possible reasons for this are varied; it could be due to the *H* value of brachiopods not being in the range used, although this is unlikely as the two coccolith species were included in the table because they had the highest and lowest respective *H* values in Haisuk and Lohmann (2010). For brachiopod Mg/Ca to conform to the temperatures calculated from $\delta^{18}O$, brachiopods would require an *H* value of ~ -0.8 (Figure 5.4.4-1), this seems unlikely as this is much lower than the large range of *H* values that have been determined (Haisuk and Lohmann, 2010).

Incorrect assumptions on Mg/Ca of the seawater are unlikely to account for this discrepancy as even using the most favourable H values the Mg/Ca of seawater would need to be >7.5 mol/mol which is unreasonable and not in line with any of the modelled or proxy data for any time in the Cenozoic. Another possible reason is the

Mg/Ca calibration may not work as well at higher temperatures. This seems unlikely as the calibration corroborates other work (Brand et al., 2013) that includes brachiopods from higher temperatures. Diagenesis is excluded as a potential explanation as the shells are well preserved and there is no homogenisation in the elemental profiles. The differences between the two methods are probably due to uncertainties in the proxies, the $\delta^{18}O$ of palaeoseawater, inaccuracies in both the Mg/Ca and $\delta^{18}O$ temperature calibrations and possibly vital effects. Vital effects could account for some of the discrepancy, as different species would have different

Organism or Proxy	*H* value	Oligocene Average Summer Temperature (°C)	Oligocene Average Winter Temperature (°C)	Eocene Average Summer Temperature (°C)	Eocene Average Winter Temperature (°C)
Abiotic Cement	0.68	20.2	15.2	20.6	15.0
Coccolith (*O.neopolitanan*)	1.53	24.0	19.1	24.4	18.8
Coccolith (*C.neohelis*)	-0.03	17.0	12.1	17.4	11.8
Shrimp (*P. pugio*)	1.22	22.6	17.7	23.0	17.4
Crab carapace (*P. gibbesi*)	0.94	21.3	16.4	21.8	16.1
$\delta^{18}O$	N/A	13.0	8.0	14.0	8.0

Table 5.4.4-1 Changes in temperature over the Eocene-Oligocene Boundary based on Mg/Ca data with H values derived from a range of organism, from Haisuk and Lohmann, 2010, and $\delta^{18}O$ dervied temperatures.

"E" in equation 5.4.4-1 although *L. concentrica*, *L. neozelanica* and *L. oamarutica* may all be the same species (Jeffrey Robinson Pers. Comm. March 2012).

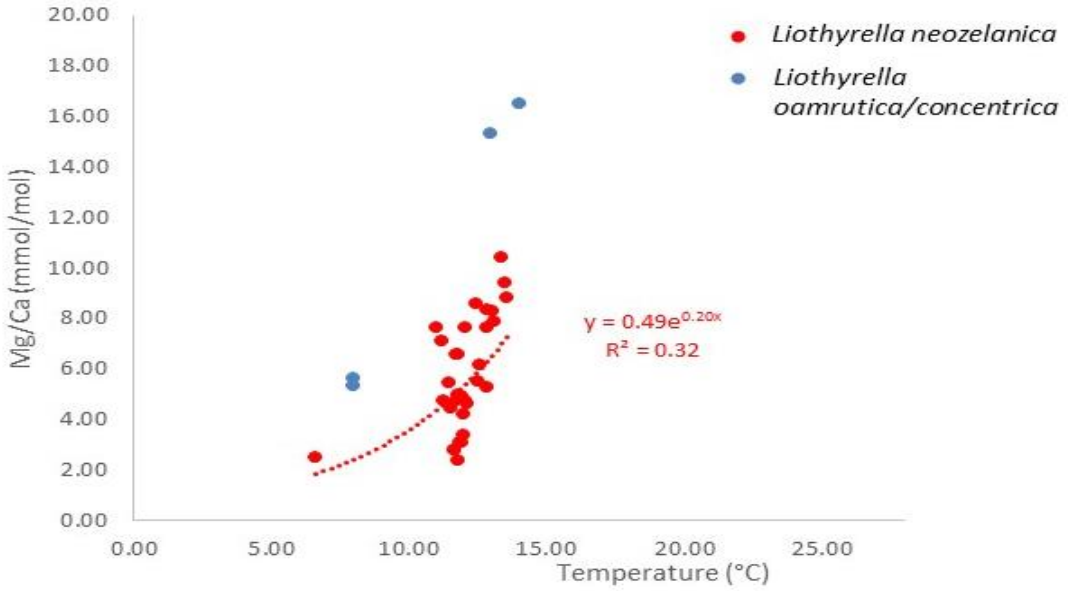

Figure 5.4.4-1 Modern *Liothyrella neozelanica* calibration with Summer and Winter Mg/Ca from the Eocene and Oligocene plotted against calculated $\delta^{18}O$ temperatures for comparison, The offset between the two can be reconciled with a *H* value of -0.8 with seems unlikely to be correct.

The absolute summer temperatures outlined in Table 5.4.4-1 (*H* estimates of *P. pugio* and *P. gibbesi*) are very similar to SSTs calculated using TEX_{86} at ODP Site 1172 in the South Pacific. ODP Site 1172 (Figure 5.4.4-2) is of similar latitude to Trig M in eastern New Zealand and both are thought to have been fed by Antarctic currents (Huber et al., 2004; Bijl et al., 2009). TEX_{86} data from the early to middle Eocene of New Zealand (Burgess et al., 2008; Hollis et al., 2009) are shown to have temperatures that closely match that of ODP Site 1172 (Bijl et al., 2009), making a direct comparison between eastern New Zealand and ODP Site 1172 possible.

TEX_{86} data from ODP Site 1172 show temperatures decreased to ~21 °C in the late Eocene (Bijl et al., 2009). This temperature falls within the range of summer temperatures (~17 – 24 °C), calculated using equation (3), for the late Eocene from Trig M, (Table 5.4.4-1). Furthermore, the temperatures calculated using estimates of

H that are based on multicellular animals, (potentially the most suitable analogues) are ~ 21 – 23 °C (Table 5.4.4-1). Bijl et al. (2009) suggest that their TEX_{86} values may be skewed towards summer temperatures. This agreement between the summer Mg/Ca temperatures and TEX_{86} suggest that the temperatures calculated using Mg/Ca could potentially be more reliable than temperatures calculated using $\delta^{18}O$ in this area. To reconcile $\delta^{18}O$ temperatures with these Mg/Ca and TEX_{86} derived temperatures $\delta^{18}O_{seawater}$ would need to be at least 1.2 ‰ in the Late Eocene, assuming that $\delta^{18}O$ in these brachiopods represent 75% of the summer temperature. This seems unlikely as modelling of $\delta^{18}O_{seawater}$ in the Eocene suggests values were ~ -1 ‰ in surface waters (Tindall et al., 2010). This comparison supports the suggestion that TEX_{86} may be representative of summer temperatures rather than a mean annual temperature. Caution is therefore urged when comparing TEX_{86} data to mean annual temperature data (e.g. Liu et al., 2009).

The discrepancy between $\delta^{18}O$ values and temperatures derived from other proxies such as Mg/Ca, TEX_{86}, $U^{K'}_{37}$ is not just isolated to the South Pacific. There are discrepancies at mid-high latitude and high latitude sites in both hemispheres, which are attributed in part, to seasonal differences (Liu et al., 2009). These discrepancies have previously been explained by TEX_{86} and $U^{K'}_{37}$ being representative of Autumn/Spring temperatures and by deep water $\delta^{18}O$ forming in winter (Liu et al., 2009). Whilst this is reasonable the Mg/Ca data in this study are not from deep waters and even the winter Mg/Ca temperatures are higher than the 'average' $\delta^{18}O$ temperatures. The $\delta^{18}O$ temperatures calculated in this study are probably skewed towards summer temperatures, due to brachiopod growth, there must be another reason for this discrepancy. The theory that deep water $\delta^{18}O$ formation occurs in winter and the TEX_{86} and $U^{K'}_{37}$ are representative of Autumn/Spring temperatures as

suggested by Liu et al. (2009) is not a good enough explanation for the offset between these proxies as this does not explain the $\delta^{18}O$ temperatures in shallow waters being lower than calculated Mg/Ca winter temperatures. As there is agreement between Mg/Ca, TEX_{86}, $U^{K'}_{37}$ it is suggested that a multi-proxy approach be used to investigate temperatures derived from $\delta^{18}O$ data wherever possible.

5.4.5 Mechanisms for cooling of the South Pacific

This study shows little or no cooling across the EOT in Eastern New Zealand. However, there is evidence that a considerable amount of cooling occurred in the South Pacific between Early and Late Eocene. Earliest Eocene sea surface temperatures of ~30 °C are recorded in the South Pacific at ODP Site 1172 (Bijl et

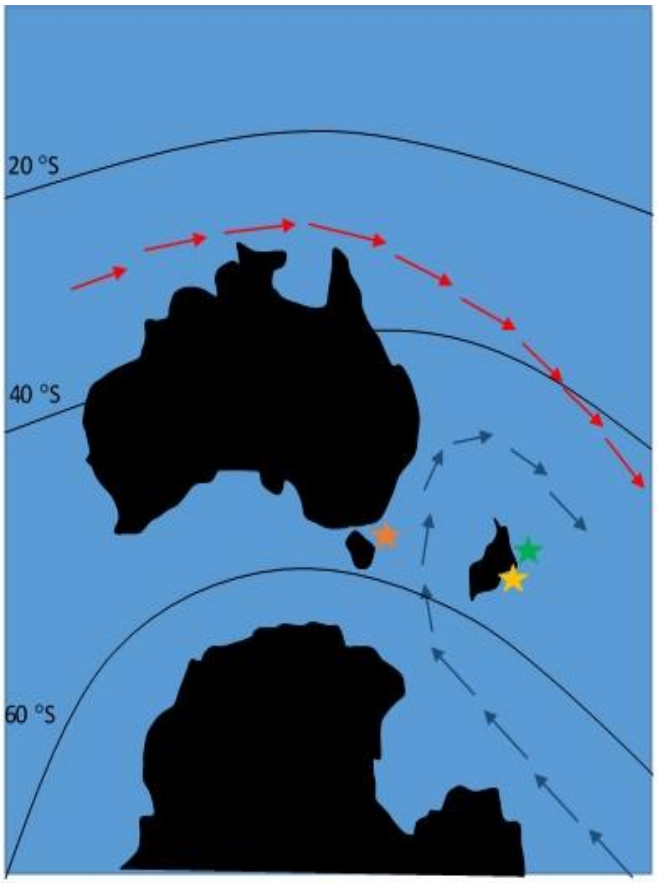

Figure 5.4.5-1. Palaeogeographic map of 33 Ma adapted from Buening et al (1998). With Middle Eocene surface currents after Bijl et al., (2009). Blue arrows represent Tasman Current and the red arrows represent the East Australia Current. These currents are consistent with modelled surface winds of the Late Eocene (Goldner et al. 2014). Orange, yellow and green stars mark Sites 1172, sites used in this study and the Canterbury Basin respectively.

al., 2009; Bijl et al., 2013), and in the Canterbury Basin, eastern New Zealand (Hollis et al., 2009; Figure 5.4.5-1). Whilst there is support from paleontological evidence for such high temperatures at this time, modelling has struggled to replicate these temperatures even under the most favourable greenhouse conditions (Hollis et al., 2009). In the Middle Eocene there are calculated sea surface temperatures of 23-25 °C and bottom water temperatures of 11-13 °C at paleolatitudes the equivalent of 55 degrees South in the Pacific from South Island New Zealand (Burgess et al., 2008).

This substantial cooling throughout the Eocene is concordant with decreasing CO_2 values, however there is little cooling at low latitudes (Pearson, 2010). This is hard to reconcile with decreasing temperatures in the southern Pacific and Southern Ocean if decreasing CO_2 is considered as the sole driving mechanism (Bijl et al., 2013). A plausible mechanism for cooling the southern high latitudes is an earlier opening of the Tasmanian Gateway ~ 49-50 Ma (Bijl et al., 2013). One possibility is that whilst declining CO_2 was likely the main cause of cooling over the EOT the cooling in the Eocene is a combination of opening oceanic gateways and associated changes in ocean circulation and falling CO_2.

The decline in temperatures over the Eocene followed by the lack of temperature change over the EOT, shown here, may suggest that changes in surface currents off the coast of NZ occurred throughout the Eocene but were relatively stable by the Late Eocene and across the EOT (Figure 5.4.5-1). Whether this decrease in water temperatures over the Eocene and subsequently stable temperatures over the EOT off eastern NZ is due to a drawdown of atmospheric CO_2 (e.g. Huber and Nof, 2006) or

whether it is due to an earlier opening of the Drake Passage (e.g. Livermore et al., 2007) is beyond the scope of this project.

5.5 CONCLUSIONS

- *Liothyrella* is more statistically significant than *Terebratulina* for reconstructing palaeoseasonality. In a transversely sectioned *Liothyrella* there are up to eight seasonal cycles whilst in transversely sectioned Terebratulina there is at most one seasonal cycle.
- The $\delta^{18}O$ excursion over the EOT has no temperature component and reflects a combined change in global and regional $\delta^{18}O_{seawater}$ of 1.3 ‰; 0.6 ‰ from the global signal and 0.7 ‰ from the regional signal. Most of the regional change could be due to the glaciation on Antarctica and changes in water mass salinity partially associated with brine rejection. The $\delta^{13}C$ data highlights a 0.8 ‰ excursion over the EOT, this is slightly larger than other studies and may be due to changes in water mass property associated with the Antarctic ice sheet.
- Brachiopod Mg/Ca profiles suggest there is no change in mean summer or winter temperature over the EOT in the South West Pacific, off the eastern coast of modern day New Zealand. Therefore there was no change in seasonality. This is in contrast to the winter cooling shown in the northern hemisphere.
- Summer and winter temperatures have similar ranges (maximum to minimum summer temperatures and maximum to minimum winter

temperatures) in the Oligocene, they vary by 3.7 °C and 3.8 °C respectively. The Eocene summer temperatures show larger variation than the winter temperatures, they vary by 5.7 °C and 5.2 °C respectively. A significant difference between summer Eocene and summer Oligocene temperatures may suggest that summer temperatures were more stable in the Oligocene. However this may be a product of vital effects or slightly poorer preservation in the Eocene.

- The highest summer and lowest winter temperatures recorded in a shell are never found in the same annual band, suggesting hot summers do not follow cold winters and vice versa, in both the Late Eocene and Early Oligocene.
- Absolute temperature estimates from Mg/Ca are in conflict with temperatures calculated by $\delta^{18}O$. Mg/Ca derived summer temperatures were ~17 - 24.4 °C, winter temperatures were ~12.1 - 19.1 °C. Mean $\delta^{18}O$ derived temperatures were 11.8 - 12.4 °C, mean $\delta^{18}O$ temperatures should be skewed towards summer temperatures due to decreased brachiopod growth in the winter (Curry, 1982) but show temperatures lower than the coldest Mg/Ca winter estimate. This discrepancy could be due to uncertainties in the proxies, the $\delta^{18}O$ of palaeoseawater, inaccuracies in both the Mg/Ca and $\delta^{18}O$ temperature calibrations and possibly vital effects. However, summer Mg/Ca data from New Zealand are in agreement with TEX_{86} data from ODP Site 1172 and as such the absolute Mg/Ca temperatures may be more representative of the true temperatures than temperatures calculated using $\delta^{18}O$.

- There was no change in surface currents around New Zealand. The change in regional salinity is partially associated with brine rejection from the newly formed Antarctic ice sheet. Modelling shows a regional $\delta^{18}O_{seawater}$ increase of up to 0.4 ‰ whilst this study shows an increase of 0.7 ‰

CHAPTER 6: USING Mg/Ca RATIOS TO ASSESS SEAWATER TEMPERATURES ACROSS THE SILURIAN 'IREVIKEN EXCURSION' ON GOTLAND, SWEDEN

6.1 Introduction

It is not known whether or not Mg/Ca ratios in brachiopods could be used to assess ocean temperature changes as far back in geological time as the Silurian, this chapter sets out to study the possibility. The first challenge was to find fossils from this time that have little or no diagenetic alteration. Secondly, was the Earth system similar to today at this time, and were Mg/Ca ratios of the ocean similar to today or fundamentally different? Thirdly, do brachiopods from the Palaeozoic incorporate Mg/Ca into their shells in the same way as their modern counterparts?

The early Silurian was long considered a relatively stable period of Earth's history with greenhouse conditions and relatively high sea levels (Johnson et al., 1991), wide ranging faunas and lacking significant effects of orogeny. Shallow epicontinental seas were widely distributed around continents without vast relief. However, the Silurian of Gotland has been the focus of many detailed studies of sea level cycles, conodont bioevents and their relationships to palaeoclimates and stable isotope excursions that have shown a more dynamic environment than originally envisaged. This study intends to build on data from studies of sequence stratigraphy (e.g. McLaughlin et al., 2012), $\delta^{18}O$ of brachiopod carbonate (e.g. Munnecke et al., 2003; Brand et al., 2006), $\delta^{18}O$ of conodont apatite (e.g. Lehnert et al., 2010), $\delta^{13}C$ of carbonates (e.g. Cramer and Saltzman, 2005) and clumped isotopes (Cummins et al., 2014) to try and understand the early Silurian Ireviken Excursion not only on Gotland but globally. Mg/Ca ratios in brachiopods are controlled at shallow depths

by a mixture of ontogeny and temperature. As temperatures can be assessed without the added complications of salinity or $\delta^{18}O_{seawater}$, this proxy will be most useful in helping to deconvolve the $\delta^{18}O$ record for the Ireviken Excursion.

6.1.1 Geology of Gotland

Gotland is a Swedish island in the Baltic Sea, ~75 km off the east coast of the mainland. The classic Silurian succession on Gotland, (500-750 m; Jeppsson et al., 2006) dips gently southeast and is exposed extensively around the coast. It represents a stable carbonate platform setting in the Baltic Basin, an intra- to pericratonic basin

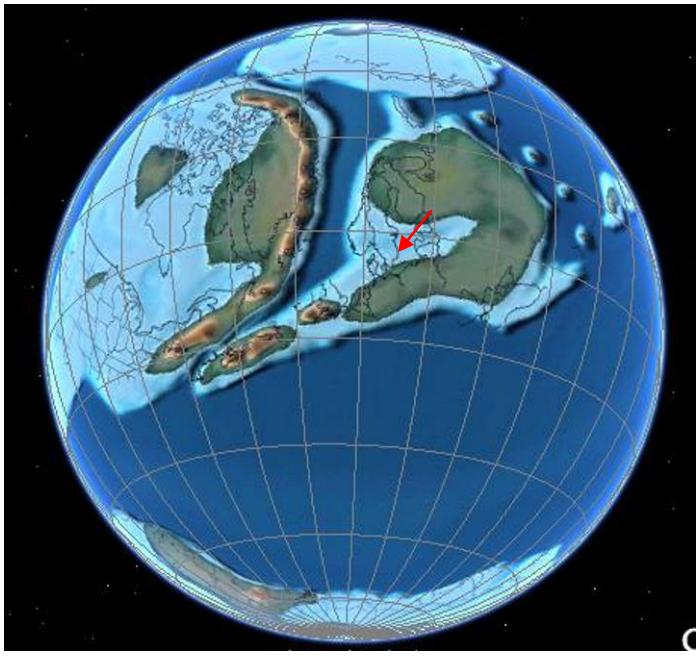

Figure 6.1.1-1 Early Silurian Palaeogeography . The red arrow marks the position of Gotland at this time, light blue and dark blue colours represent shallow epicontinental seas and deep ocean respectively (Scotese Paleomap Project 2013 www.globalgeology.com)

that developed on the southern margin of the Baltic Shield and East European platform (Calner et al., 2004; Figure 6.1.1-1). The bedrock strata range in age from late Llandovery through to late Ludlow, spanning ~11 million years (ICS 2013) of

Earth history. The strata show little tectonic disturbance and have never been deeply buried, as indicated by the very low conodont alteration index (Jeppsson, 1983).

Early research of Gotland focused on the very well preserved fossils, and their use to resolve the stratigraphy (e.g. Lindstrom 1884; summary in Hede, 1960). Many systematic studies have been based on the fossils from Gotland (e.g. Martinsson, 1967; Laufeld, 1974; Basssett and Cocks, 1974; Larsson, 1979; Munnecke et al., 2000).

6.1.2 Stratigraphy

The Lower Visby (LVF) and Upper Visby (UVF) formations are the oldest units on Gotland, with outcrop areas fringing the NW coastline; representing a prograding sequence of limestone-marl alterations (Calner et al., 2004). The LVF is dominated by marls with thin limestones that increase in thickness and frequency up into the UVF. A shallowing in the depositional facies continues into limestones of the overlying Högklint Formation, which post-dates the Ireviken event, Figure 6.1.2-1, and will therefore not be discussed further.

6.1.2.1 Lower Visby Formation

(latest Llandovery - early Wenlock; *C. cf murchisoni* graptolite biozone; Lower and Upper *Ps.bicornis*, and Lower *P. procerus* conodont biozones; Figure 6.1.2-1)

The exposed formation comprises 12 m of fossil-poor alternations of 10 cm marl beds and very thin, 2-5 cm wavy-bedded to nodular argillaceous limestones. Thin layers of small brachiopods and bryozoan debris are found at irregular intervals. There are three distinct bentonite horizons (Batchelor and Jeppsson 1994). A bed rich in corals, the *Phaulactis* layer, marks the base of the overlying UVF (Samtleben

et al., 1996; Fig. 6.1.5). The sequence was deposited in a distal shelf setting beneath both the storm wave base and photic zone (Calner et al., 2004).

6.1.2.2 Upper Visby Formation

(Lower Wenlock**;** *M. firmus*-lower *M. riccartonensis* graptolite biozones; Upper *P. procerus* - Lower *K. ranuliformis* conodont biozones; Figure. 6.2-1)

This formation of marls and nodular argillaceous limestones is up to 12 m thick with less regular bedding than the Lower Visby formation; the limestone-marl ratio increases upwards. Calcareous algae, ripple marks and erosional surfaces suggest that the energy of the depositional environment has increased to within the photic zone (Calner et al., 2004). This is supported by increased abundance of shelly fossils such as crinoids, tabulate corals, brachiopods, bryozoans and stromatoporoids (Jaanusson et al., 1979).

Silurian Epoch	**Conodont Zone**	**Conodont Datum Points**	**Stratigraphic Unit on Gotland**	**Event Stratigraphy (Jeppsson, 1990)**	**The $\delta^{13}C$ excursion from Gotland (Munnecke et al., 2003)**
WENLOCK	Upper *K. ranuliformis* Zone	8	Högklint Formation	Vattenfallet Secundo Episode	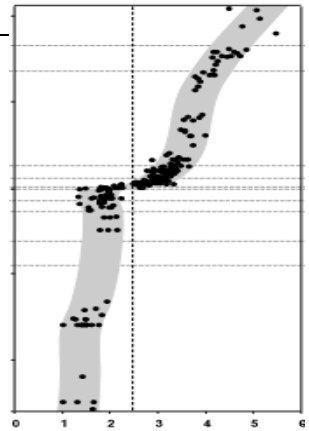
	Lower *K. ranuliformis* Zone	7	Upper Visby Formation		
	Upper *P. procerus* Zone	6			
		5			
	Lower *P. procerus* Zone	4	Lower Visby Formation	Ireviken Event	
	Upper *Ps. bicornis* Zone	3			
LLANDOVERY	Lower *Ps. bicornis* Zone	2			
		1			

Figure 6.1.2-1 Latest Llandovery–early Wenlock stratigraphy of Gotland showing conodont biozonation and datum points (Aldridge et al., 1993) and event stratigraphy (Jeppsson 1990).

6.1.3 Ireviken Bio-Event/ Ireviken Event (conodont extinction)

There is potential confusion with the nomenclature for the Ireviken Event. The 'Ireviken Event' was originally used in reference to a conodont biotic event spanning the Lower *P. bicornis* zone through to the top of the Lower *K. ranuliformis* zone on Gotland (Jeppsson, 1998). It has more recently been used for the chemostratigraphic $\delta^{13}C$ positive excursion (Munnecke et al., 2003; Cramer and Saltzman, 2007) that occurs around this time. However, since two conodont biozones separate the start of the conodont extinction (datum 2) and the start of the $\delta^{13}C$ excursions (datum 4; Figure 6.1.2-1), these two events may not be associated with the same environmental changes (Loydell, 2007). In this study the biotic extinctions will be referred to as the Ireviken Event and the isotope excursions will be referred to as the Ireviken Excursion.

There are four conodont extinction events recognised on Gotland between the late Llandovery and the late Ludlow, namely the Ireviken, Mulde, Linde and Lau. During the Ireviken event 80% of conodont species (Aldridge et al., 1993; Jeppsson, 1997a) and 50% of trilobite species (Ramsköld, 1985) became extinct, acritarchs, grapotolites, chitinozoans and corals were also affected.

Jeppsson (1997b) analysed conodont biodiversity and distribution across the Ireviken Event. At datum 2; where the largest decrease in diversity of conodont faunas is seen, conodont species that were previously widespread became extinct (Munnecke et al., 2003). It has been suggested that an unconformity on Gotland at this datum point may exaggerate the severity of extinction (Loydell, 2007). A second major extinction level at datum 4 (Jeppsson, 1997b) may also be exaggerated by a hiatus (Nestor et al., 2002; Munnecke et al., 2003).

6.1.4 Early Silurian glaciations

Grahn and Caputo (1992) recorded four glaciation events within the Early Silurian of South America, part of Gondwana. These are dated as latest Ashgill and/or earliest Llandovery, early middle Llandovery , late middle – early late Llandovery and the one coincident with the Ireviken Event late Llandovery-early Wenlock, also known as the Sheinwoodian glaciation. The most widespread tillite is associated with the late Llandovery- early Wenlock glaciation. Glacigenic sediments, structures and geomorphology provide direct evidence for glaciations at this time, (see reviews in Page et al. 2007; Cherns and Wheeley, 2007, Cherns and Wheeley, 2009; Cherns et al., 2013).

6.1.5 Carbon isotope excursions and the Ireviken Excursion

The Ireviken Excursion (also referred to as the Early Sheinwoodian Carbon Isotope Excursion (ESCIE)), takes place shortly after the Llandovery-Wenlock boundary, 433 Ma at conodont datum 4 of the Ireviken event (Figure 6.1.2-1). There is little doubt from conodont, brachiopod and whole rock isotope studies that the Ireviken Excursion is a global event (e.g. Lehnert et al., 2010; Brand et al., 2006; Kaljo et al., 2004, 2007). In contrast, the younger Mulde isotope excursion on Gotland, although greater in magnitude, is known only from Gotland. At the time of the Ireviken Excursion localities from around the world show a positive $\delta^{13}C$ excursion of 6.6 ‰ from Norway (Kaljo et al., 2004), 4.5 ‰ (Cramer and Saltzman, 2005) and 3 ‰ (Brand et al., 2006) from North America, up to 4.5 ‰ from Gotland, Sweden (Figure 6.1.5-1) and 3 ‰ from Tunisia (Munnecke et al., 2003).

Stratification of the water column has been discounted as a possible cause of the positive $\delta^{13}C$ excursion. The depositional environment shallowed overall from the base of the LVF to the top of the UVF and throughout this time the relatively shallow water column was well mixed (Vandenbroucke et al., 2013), which would rule out declining $\delta^{13}C$ depth gradient through the water column (Kroopnick et al., 1972). Changes in carbonate facies are also excluded as a possibility for $\delta^{13}C$ excursions as contemporaneous deposits of different facies show almost identical

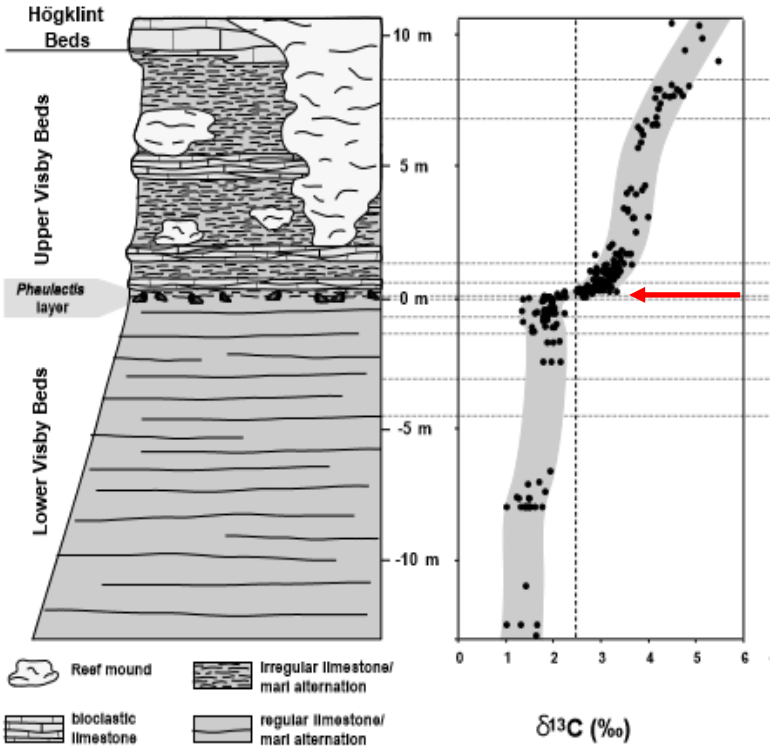

Figure 6.1.5-1 $\delta^{13}C$ excursion shown against the stratigraphy of Gotland. The red arrow marks the onset of the Ireviken Excursion. Adapted from Munnecke et al. (2003).

$\delta^{13}C$ values regardless of depositional environment (Samtleben et al., 2000).

A decrease in primary productivity shown by reduced absolute and relative abundances of acritarchs, sphaeromorphs and prasinophytes had the potential to trigger the Llandovery-Wenlock $\delta^{13}C_{carb}$ excursions, including the early Ireviken

excursion (Cramer and Saltzman, 2007a). However, there is a stratigraphical offset of a few metres between the start of the conodont bioevent (between datum 2 and 3) and the onset of the $\delta^{13}C_{carb}$ excursion (at datum 4) (Vandenbroucke et al., 2013). As well as this there is also an offset between the $\delta^{13}C_{carb}$ excursion and the $\delta^{13}C_{org}$ data as an earlier 1 ‰ increase in $\delta^{13}C_{org}$ at the start of the Ireviken Event is shown (Vandenbroucke et al., 2013). This offset suggested that $\delta^{13}C$ and the burial of $\delta^{13}C_{org}$ material may not always be directly linked and that the mechanisms behind the excursion are not fully understood.

Another explanation for positive $\delta^{13}C$ excursions is increased continental weathering and probably also enhanced burial of organic carbon (Kump et al., 1999; Cramer and Saltzman, 2007a and 2007b). The $\delta^{13}C$ excursions in the Llandovery to Wenlock are thought to be coincident with sea level fall as a result of ice sheet growth on the South American part of Gondwana (Loydell, 2007). This fits with decline in magnitude of the excursion further away from the palaeoshoreline, but not with both maxima and minima in the carbon isotope record being more pronounced in the shallow water sections (Kaljo, 1997). The precise cause and effect of the Ireviken Excursion remain debatable.

Interpretation of the $\delta^{13}C$ values from brachiopods also needs to consider that upper Wenlock brachiopods show different values depending on location, either through local effects or potentially different habitats (Brand et al., 2006). This study aims to show whether or not a change in temperature over the Ireviken Excursion is a contributory factor to the positive $\delta^{13}C$ shift.

6.1.6 Silurian climate states

Jeppsson (1990) proposed a model of alternating oceanic states for the Silurian, Primo (P) and Secundo (S) states (Figure 6.1.6-1). S states are characterised by polar warming, low nutrient availability in epeiric seas, weakened thermohaline circulation and occasionally episodes of salinity-driven halothermal circulation. P states are characterised by icehouse conditions, polar cooling, high nutrient availability in

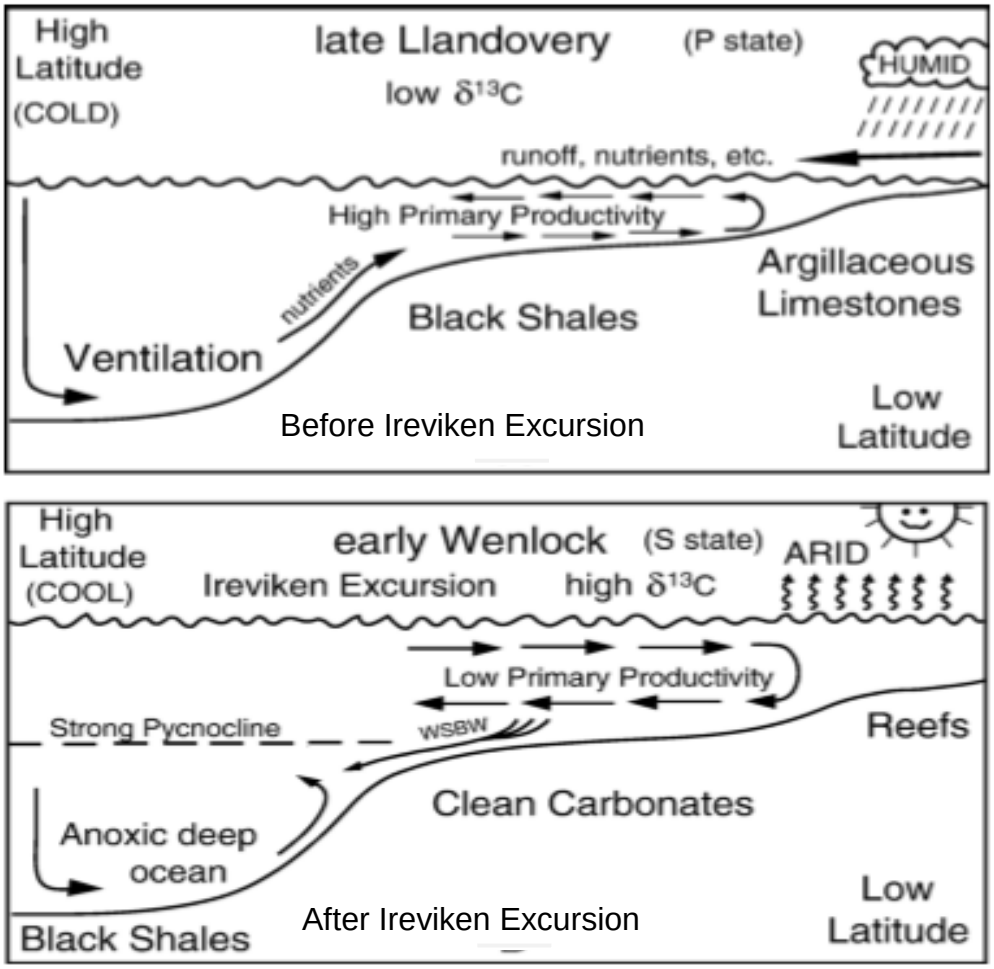

Figure 6.1.6. Climate states for the Silurian first proposed by Jeppsson (1990) and adapted by Cramer and Saltzman (2007). Adapted from Cramer and Saltzman (2007).

epeiric seas and strong thermohaline circulation. Among 20 alternations of these states within the Silurian the Ireviken excursion lies at the transition between two oceanic states (Fig. 6.1.2-1). (Calner et al., 2004; Cramer and Saltzman 2007a). It is proposed that these two states could potentially explain the difference in $\delta^{13}C$ values within the Silurian with S states having higher $\delta^{13}C$ than P states. The reasons for

this are not entirely understood but are potentially a mixture of the factors outlined in section 6.1.5.

This study will add another proxy, one that is temperature dependent, to this area of research. It will help to identify whether or not there is a change in temperature at low latitudes between these two climate states.

6.1.7 Ireviken oxygen isotope excursion and Sheinwoodian glaciations

Brachiopod $\delta^{18}O$ data from Niagara Gorge, Anticosti Island, Britain, Gotland and Estonia clearly reflect a warm climate interval during the latest Llandovery; associated with the Silurian sea level highstand (Brand et al., 2006). In the early Wenlock a fall in sea level is associated with the onset of the Cancańiri glaciation in the southern hemisphere. This is shown by a large $\delta^{18}O$ excursion at paleolatitudes higher than 23.5 °, such as ~2.5 ‰ at Niagara Gorge, while at low latitude sites positive excursions are much less pronounced, for palaeomap see Figure 4.1.7-1 , such as Gotland ~0.4 ‰ (Munnecke et al., 2003). Notably, a recent study into $\delta^{18}O$ across the Ireviken excursion on Gotland failed to show any positive excursion in $\delta^{18}O$ data (Cummins et al., 2014).

Silurian brachiopods appear to be depleted in $\delta^{18}O$ by ~ 3 ‰ when compared to their modern shallow water, low latitude counterparts (Brand et al., 2006). If modern seawater chemistry is assumed for the Silurian and the $\delta^{18}O$ range from brachiopod calcite over the Ireviken excursion (-3.2 to -6.2 ‰) is used to calculate palaeoseawater temperature this produces unrealistic temperatures up to 52 °C (Brand et al., 2006). One way to obtain more realistic temperatures based on any of the brachiopod $\delta^{18}O$ is to assume that $\delta^{18}O_{seawater}$ has changed, which could indicate

secular evolution of seawater over time (Veizer et al., 1999). This is a longstanding and controversial hypothesis but such changes are theoretically possible due to

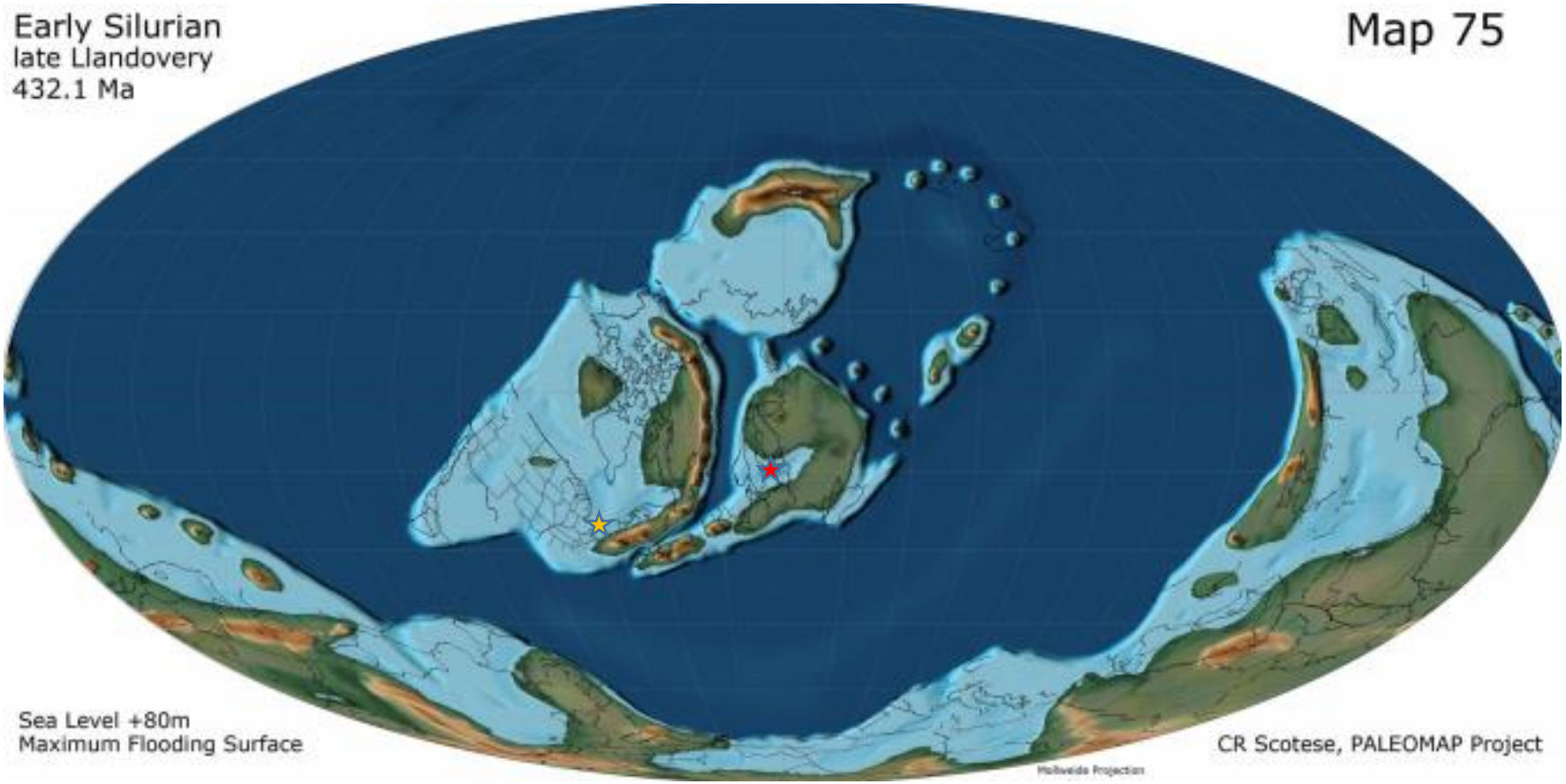

Figure 6.1.7-1 Early Silurian Palaeogeography . The red star marks the position of Gotland at this time and yellow that of Niagara Gorge, light blue and dark blue colours represent shallow epicontinental seas and deep ocean respectively (Scotese Paleomap Project 2013 www.globalgeology.com)

changing rates over time of continental weathering and sea floor alteration through hydrothermal processes. However, evidence is lacking for a large change in $\delta^{18}O_{seawater}$ over time other than the depletion in $\delta^{18}O$ of carbonates and it is possible that this depletion could be caused by diagenetic alteration (Knauth and Kennedy, 2009).

The alternative hypothesis is that $\delta^{18}O_{seawater}$ has remained relatively constant throughout time and that the interactions between ocean water and rock through hydrothermal processes have remained constant over at least the Phanerozoic. This theory suggests that chemical weathering of continental material has little or no influence on the oxygen composition of the ocean because the amount of material weathered is insignificant compared to the amount of seafloor that is altered through hydrothermal processes (Muehlenbachs, 1998). Several studies based on $\delta^{18}O$ measurements of materials other than biogenic carbonates support this hypothesis. Ophiolites and eclogites from the Ordovician of Norway (Muehlenbachs et al., 2003) as well as ophiolites from the Cambrian, Ordovician and Cretaceous (Turchyn et al., 2013) show no secular change in $\delta^{18}O_{seawater}$. However, Turchyn et al. (2013) argue that $\delta^{18}O$ values from the Cambrian are different from the younger, Ordovician and Cretaceous rocks sampled and to model that requires significantly different fluid rock interactions in Cambrian systems (not difference in $\delta^{18}O_{seawater}$). Conodont apatite $\delta^{18}O$ values from the Devonian convert to temperatures ~8 °C lower than that calculated from brachiopod calcite, possibly due to diagenetic alteration of brachiopods (Joachimski et al., 2004). Assumption of a completely ice free world to account for the difference in $\delta^{18}O$ (Lecuyer and Allemand, 1999) can be disregarded as the Ireviken Excursion correlates approximately with Gondwanan glacigenic deposits (Calner et al., 2004).

Even in a completely ice free world $\delta^{18}O_{seawater}$ would still need to be lower than values for the ice free world of the early Eocene of ~-1.2 ‰.

The Cummins et al. (2014) study into $\delta^{18}O$ over the Ireviken excursion based on clumped isotopes (Figure 6.1.7-1), shows that the surrounding micrite is depleted in $\delta^{18}O$ compared to the calcitic brachiopods. They question whether even samples that

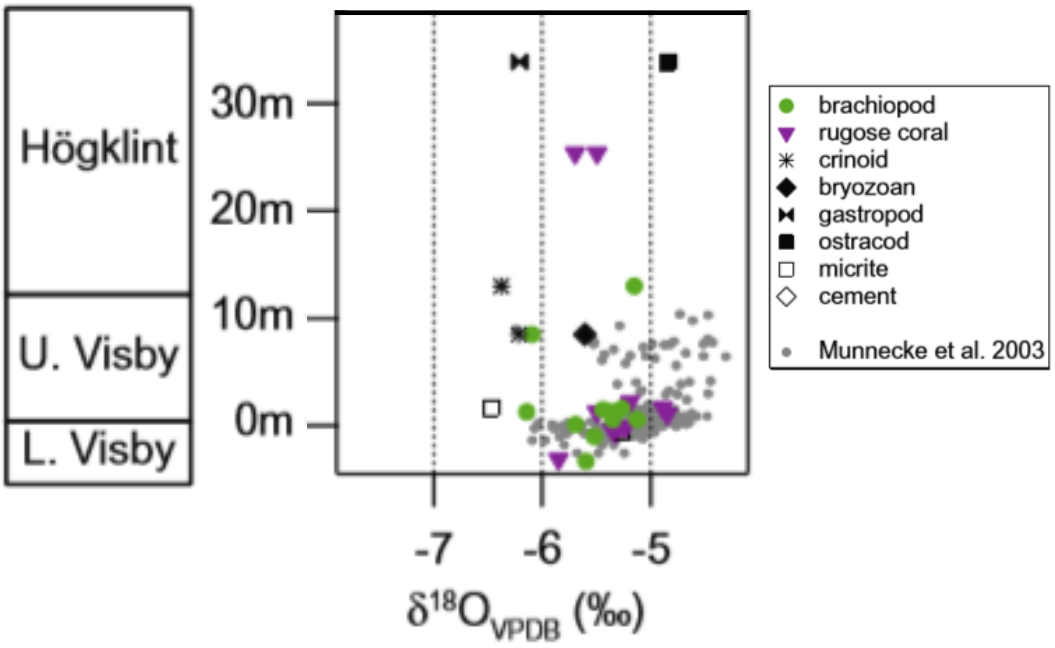

Figure 6.1.7-1. $\delta^{18}O$ Ireviken Excursion of 0.5 ‰ shown in the Munnecke et al. (2003) data, whilst no positive excursion is shown in the remaining data from Cummins et al. (2014). Adapted from Cummins et al. (2014).

have very carefully been screened for diagenesis may be altered, suggesting that in a closed diagenetic system high Mn, Fe and corresponding low Sr may not be as indicative of alteration as they are in an open diagenetic system; SEM and microstructure analysis are their preferred method for determining the quality of preservation. Using the specimen with the highest $\delta^{18}O$ value Cummins et al. (2014) calculate ocean temperatures just after the Ireviken excursion to be 35 °C ± 7 °C, with $\delta^{18}O_{seawater}$ of ~ -1.2 ‰. This agrees with another clumped isotope study by Finnegan et al. (2011) giving weight to the argument that previous brachiopod $\delta^{18}O$

studies (Brand et al., 2006; Munnecke et al., 2003) produced temperatures that are too high.

The $\delta^{18}O$ and Mg/Ca data from this study will help to decipher whether or not there is a change in $\delta^{18}O$ over the Ireviken Excursion as suggested by Munnecke et al. (2003) and Brand et al. (2006) or whether there is no change as suggested by Cummins et al. (2014). The trace metal screening carried out in my study is of a much higher resolution than in previous studies, enabling identification of diagenetically altered specimens and even altered areas of an individual shell and is therefore not solely reliant on microstructure analysis. The Mg/Ca data will not be able to help in terms of absolute temperatures however it will give an independent analysis on temperature change over the Ireviken Excursion.

6.1.8 Ireviken Excursion in a Wider Context

The Ireviken Excursion correlates approximately with Gondwanan glacigenic deposits. On Gotland it is associated with a facies change, follows biotic extinctions mainly in conodont species and precedes early Sheinwoodian glacio-eustatic lowstand (Calner et al. 2004).

The Ireviken Excursion, which in terms of glacioeustacy falls within the Sheinwoodian glaciation, is one of 32 events from the Mid-Late Cambrian to end Silurian interpreted as global cooling events, based on a range of facies indicators and geochemical proxies. The mean frequency of c. 2.6 myr for these events demonstrates a high probability of correlation with long term eccentricity time series, and of orbital climate forcing (Cherns et al., 2013). Continental ice may have been present through the early Paleozoic, with repeated episodes of cooling indicating rapid climate switches, even within 'greenhouse' intervals (Cherns et al., 2013).

There have been no previous Mg/Ca studies of the Ireviken Excursion. The data collected in this study cannot resolve the cause of the positive $\delta^{13}C$ excursion but can help to resolve whether or not there was any change in seawater temperature over the Ireviken Excursion. The potential problems, outlined in section 6.1 have been addressed. Firstly, well preserved brachiopods from the island of Gotland, Sweden have been used. This island is renowned for extremely well preserved shallow shelly faunas. Secondly, it is likely that Mg/Ca ratios are different from that of the modern day. However, relative changes in temperature can still be assessed using the brachiopod Mg/Ca calibrations (Butler et al., 2015; Chapter 4). Studying $\delta^{18}O$ values allows an attempt to be made at quantifying temperatures, facilitating direct comparison with previous studies. In addition to this, an attempt is made at constraining the Mg/Ca of seawater from the early Silurian, and at comparing annual variations in water temperature to modern day tropical environments.

6.2 Methodology

6.2.1 Summary of methodology

For full materials and methodology, see Chapters 2 and 3 respectively. However a brief summary of analytical methods used to assess diagenesis, shell symmetry and palaeoseasonality is given here.

6.2.2 Screening for influences of diagenesis and instrument performance

Brachiopods from the four sites, Nyhamn and North Nyhamn from the Lower Visby and Ygne and Ireviken from the Upper Visby Formation were screened for diagenetic alteration in the same way as the Eocene/Oligocene specimens; see Section 5.2.2 for a full description.

Locality	Samples	Al/Ca Screened Level (mmol/mol)	Mn/Ca Screened Level (mmol/mol)
Ygne	YGNE1	0.5	-
	YGNE2	0.5	-
	YGNE3	0.5	-
Ireviken	IREVIKEN1	1.0	-
	IREVIKEN2	1.0	-
	IREVIKEN3	1.0	-
Nyhamn	NYH1	0.5	1.2
	NYH2	0.5	1.2
	NYH3	0.5	-
North Nyhamn	NNYH1	0.5	-
	NNYH2	0.5	-
	NNYH3	0.5	-

Table 6.2.2-1 Levels of Al and Mn/Ca used for diagenetic screening.

Ygne samples were screened to 0.5 mmol/mol Al/Ca as YGNE2 had a positive correlation with Mg/Ca: R^2= 0.28 above and R^2= 0.02 below 0.5 mmol/mol Al/Ca respectively. Ygne samples were not screened for Mn/Ca as there was no strong diagenetic correlation between Mn/Ca and Mg/Ca (Figure 6.2.2-1; Table 6.2.2-1). Ireviken was screened to an Al/Ca ratio of 1 mmol/mol, (Figure 6.2.2-2; Table 6.2.2-1) as IRE 2 showed a strong correlation between Mg/Ca and Al/Ca; R^2= 0.9 above and R^2< 0.01 below this threshold. Ireviken was not screened to any level for Mn/Ca as no diagenetic correlation between Mn/Ca and Mg/Ca was shown.

Nyhamn was screened to 0.5 mmol/mol for Al/Ca, (Figure 6.2.2-3) and 1.2 mmol/mol for Mn/Ca (Table 6.2.2-1); in NHY1 R^2= 0.84 above and R^2= 0.04 below the threshold. Two of the specimens from Nyhamn, NYH1 and NYH2 show a strong correlation between Mn/Ca and Mg/Ca, interpreted as a diagenetic signal and neither are considered further for trace metal analysis. NYH3 shows no correlation between Mg/Ca and Mn/Ca suggesting that the main influence on Mg/Ca in this shell is temperature. North Nyhamn was screened to an Al/Ca ratio of 0.5 mmol/mol (Figure

6.2.2-4; Table 6.2.2-1); in NNY1 R^2= 0.67 above and R^2< 0.01 below this threshold.

North Nyham was not screened for Mn/Ca (Figure 6.2.2-4).

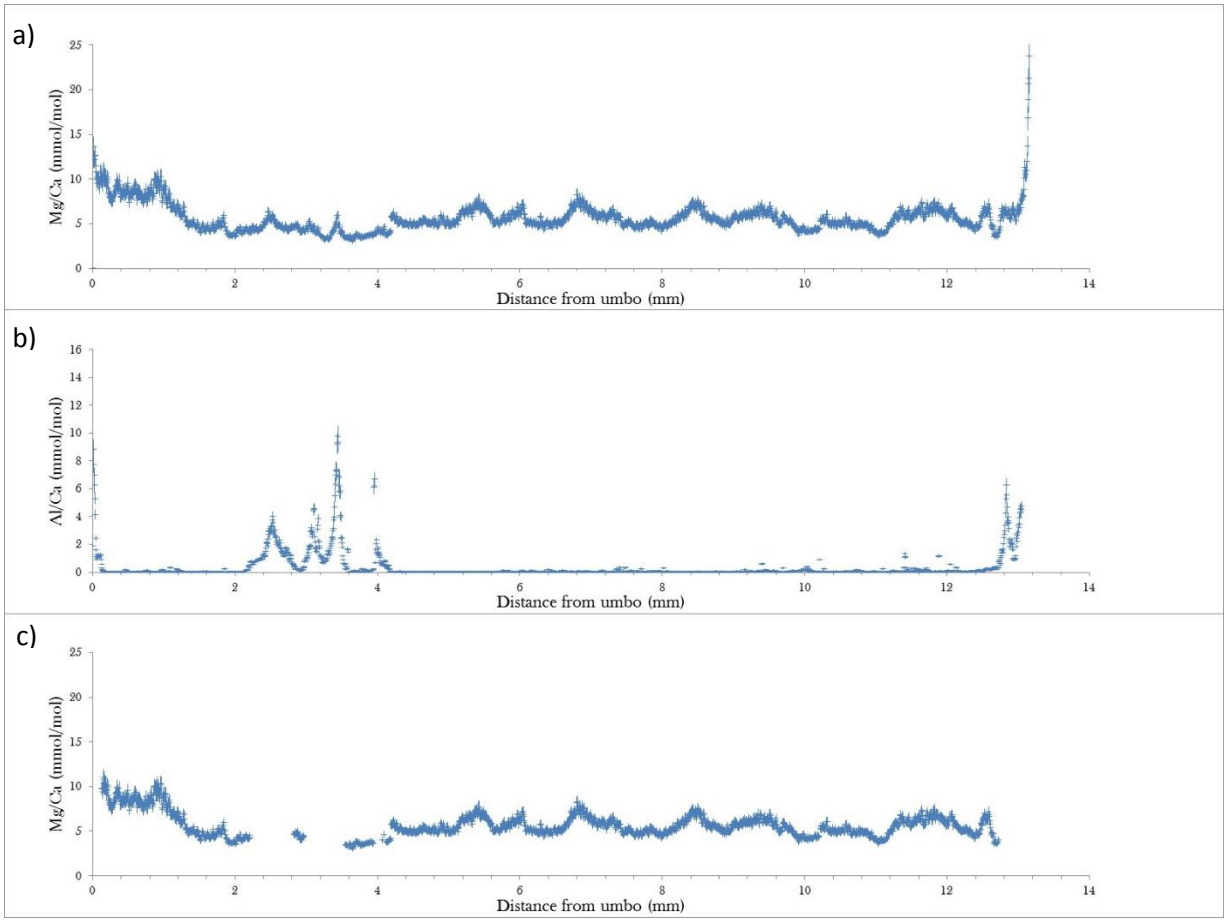

Figure 6.2.2-1 Ygne (YGNE1) a) Mg/Ca pre-screening b) Al/Ca showing correlation between Al/Ca and Mg/Ca c) Mg/Ca post screening.

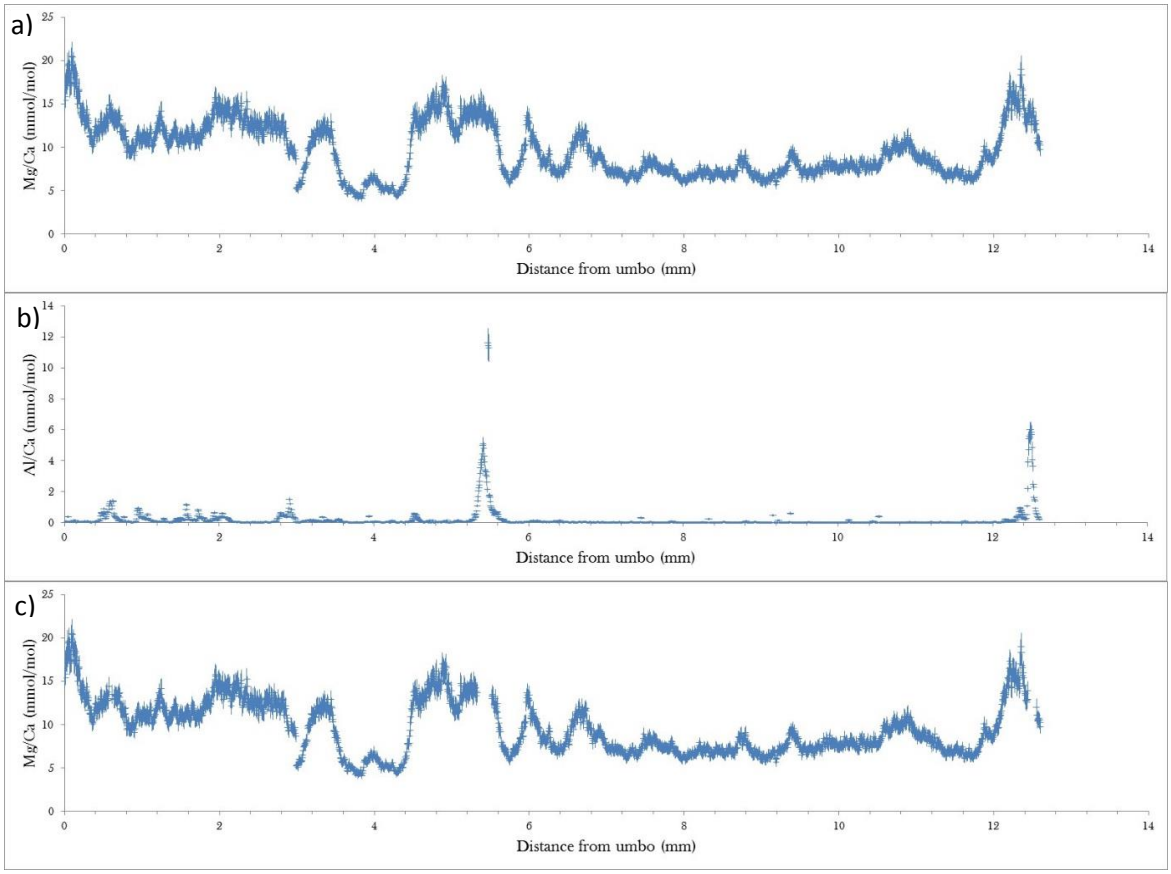

Figure 6.2.2-2 Ireviken (IRE1) a) Mg/Ca pre-screening b) Al/Ca showing correlation between Al/Ca and Mg/Ca c) Mg/Ca post screening.

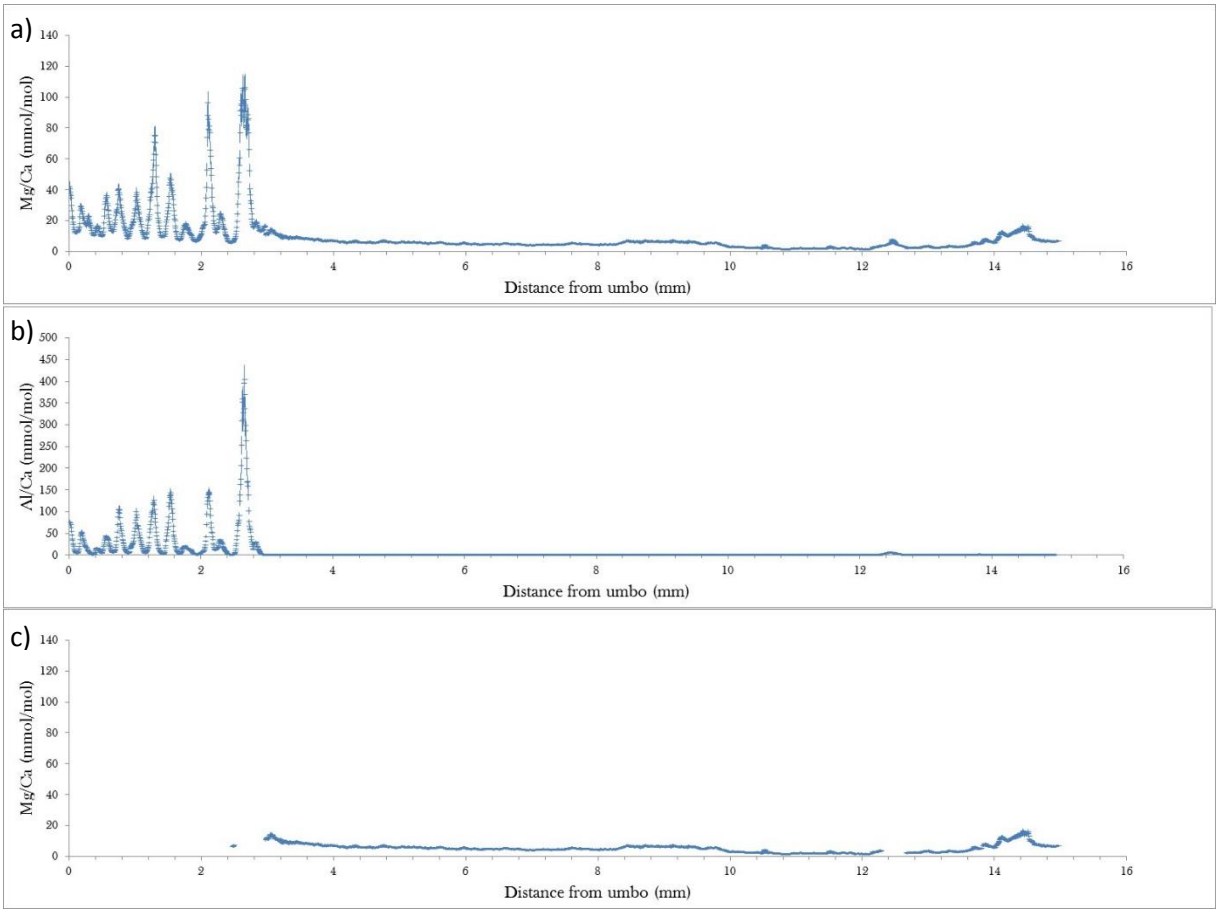

Figure 6.2.2-3 Nyhamn (NHY1) a) Mg/Ca pre-screening b) Al/Ca showing correlation between Al/Ca and Mg/Ca c) Mg/Ca post screening.

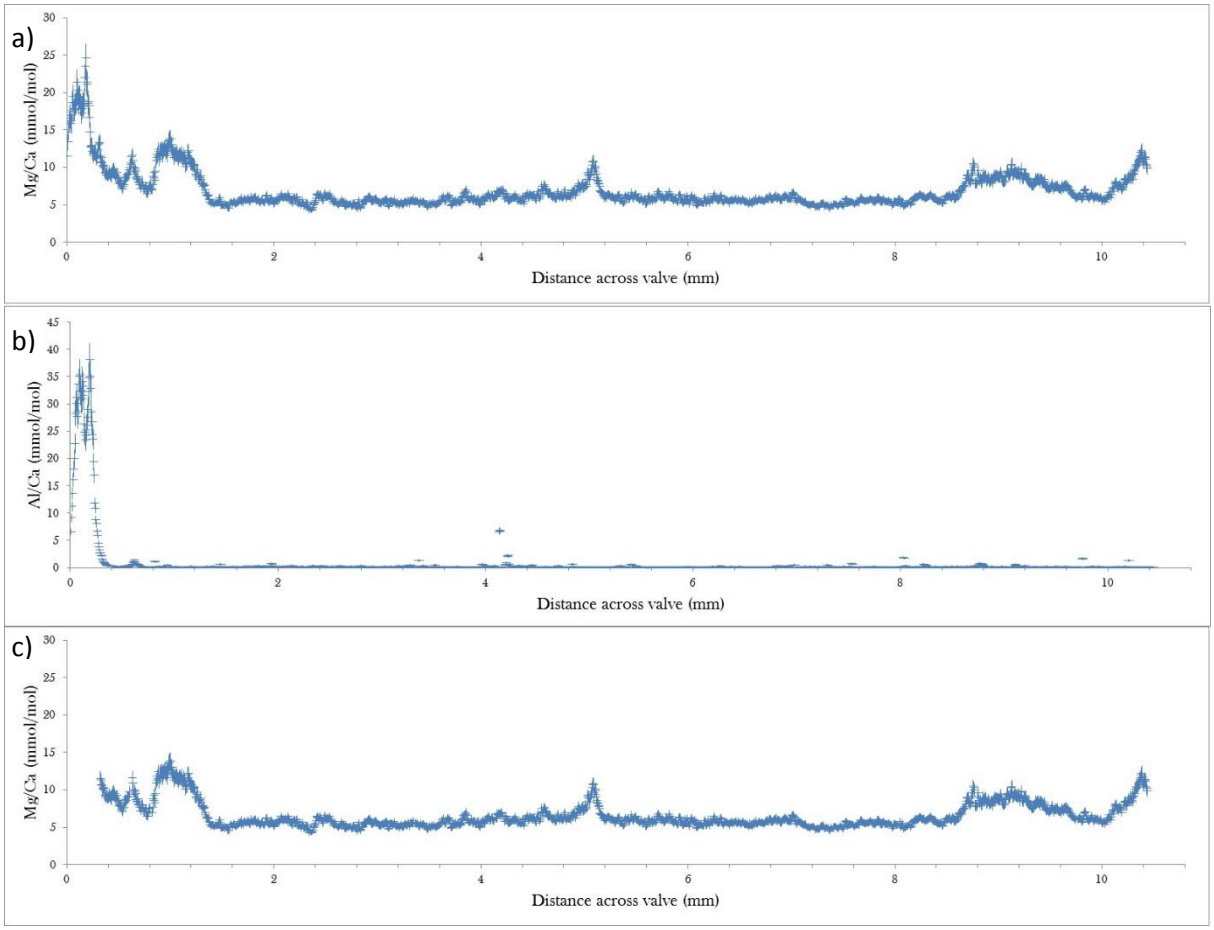

Figure 6.2.2-4 North Nyhamn (NNY3) a) Mg/Ca pre-screening b) Al/Ca showing correlation between Al/Ca and Mg/Ca c) Mg/Ca post screening.

6.2.3 Screening for low values of Sr/Ca

In the modern and EOT shells, Sr/Ca has mainly been constant at 1-2.5 with only a few specimens outside this range. This is also the case for most specimens from the Silurian. However, the shells from Ireviken display values outside of this range. IRE1 and IRE2 have Sr/Ca ratios as low as 0.54 mmol/mol and 0.74 mmol/mol

respectively. IRE3 has extremely low Sr/Ca consistently < 0.1 mmol/mol, strongly correlated with Mg/Ca (Appendix 4), and is therefore considered to be diagenetically altered, and hence will not be considered any further. One specimen from Ygne, YGNE2, also has low Sr/Ca values in the umbo region of the shell, in an area with limited data after heavy screening due to high levels of Al/Ca (Appendix 4).

6.2.4 Assessing shell symmetry as an internal check on the brachiopod Mg/Ca palaeothermometer

The same method was carried out as explained in Section 5.2.3. The symmetry cross plots for the three well preserved shells sectioned transversely are shown in Figure 6.2.4-1. All three shells, YGNE3, NYH3 and NNY3 passed the symmetry test.

6.2.5 Estimating palaeoseasonality from intra-shell Mg/Ca profiles

All three transversely sectioned shells were assessed for palaeoseasonality using the method explained in Section 5.2.4

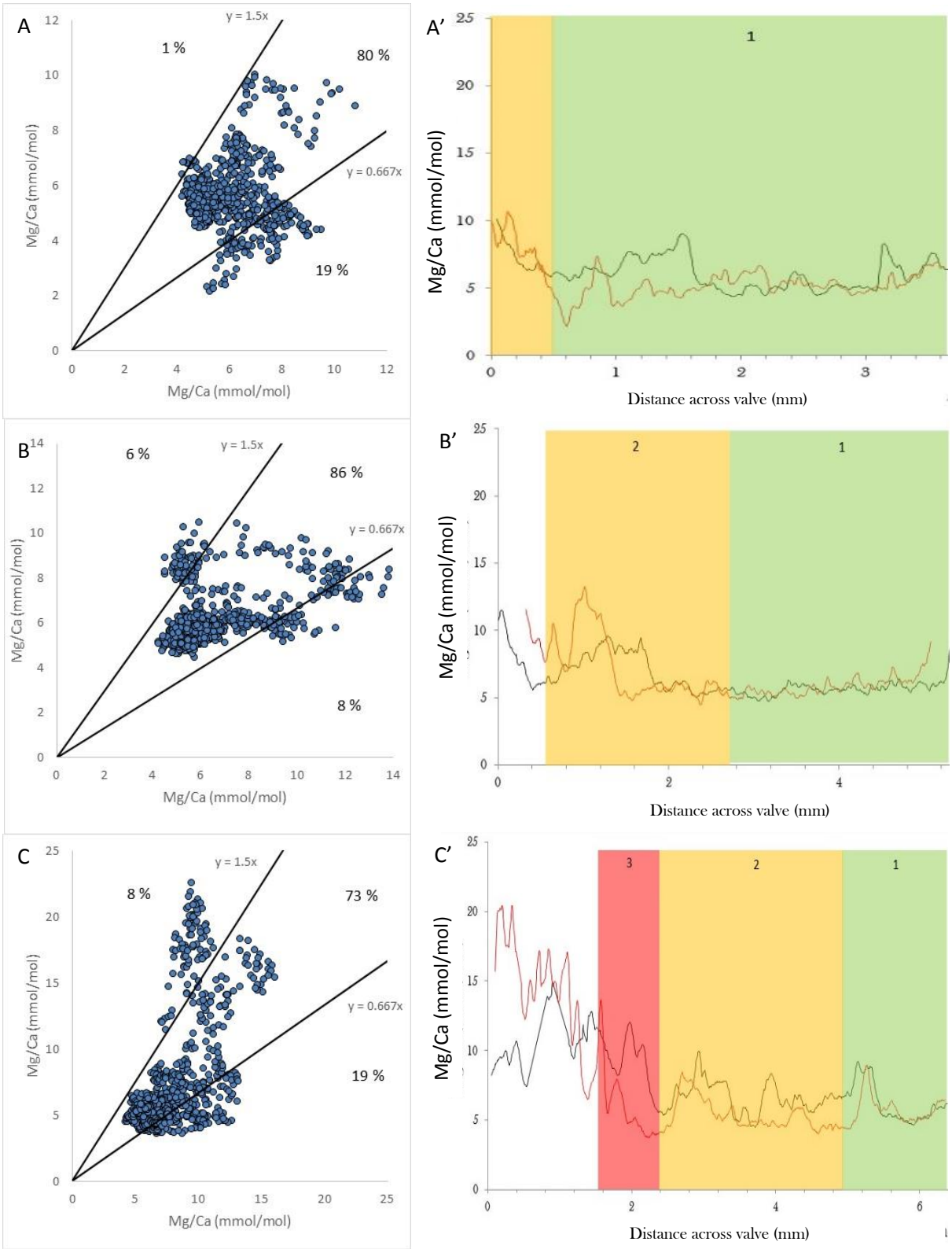

Figure 6.2.4-1 Right half of the transverse geochemical profile plotted against the left half of the transverse geochemical profile for A YGNE3, B NNY3 and C NYH3. Black lines display error envelope of y=1.5x and y=0.667x. Percentages mark data that plot above y=1.5, below y=0.667x and in between y=1.5x and y=0.667x. A', B' and C' corresponding 8 point moving average data plotted with right half of the shell as a red line and left half as a black line, outside edge of the shell starts at 0 mm. All three shells passed the symmetry test.

6.3 Results

6.3.1 Mg/Ca data from transverse geochemical profiles

One shell from each location was sampled transversely. The shell from Ireviken has

YGNE 3 Maximum and Minimum Mg/Ca (mmol/mol) from the Green Zone	YGNE 3 Difference between Maximum and Minimum Mg/Ca (mmol/mol) from the Green Zone	NYH3 Maximum and Minimum Mg/Ca (mmol/mol) from the Green Zone	NYH3 Difference between Maximum and Minimum Mg/Ca (mmol/mol) from the Green Zone	NNY3 Maximum and Minimum Mg/Ca (mmol/mol) from the Green Zone	NNY 3 Difference between Maximum and Minimum Mg/Ca (mmol/mol) from the Green Zone
10.78	-	7.74	-	6.73	-
5.39	5.39	11.86	4.12	13.55	6.82
9.48	4.09	5.17	6.69	4.25	9.3
4.34	5.14	10.21	5.04	10.74	6.49
8.33	3.99	4.24	5.97	4.99	5.75
3.64	4.69	9.17	4.93	10.51	5.52
7.74	4.1	4.43	4.74	5.36	5.15
2.15	5.59	-	-		
9.64	7.49	4.54	-		
		9	4.46		
		3.9	5.1		
		8.88	4.98		
		3.74	4.14		
		11.19	7.45		
		6.08	5.11		

Table 6.3.1-1. Mg/Ca data from YGNE3, NYH3 and NNY3 and. Red values mark summer Mg/Ca values and correspond to the dashed red arrows in Figures 6.3.1-1 and 6.3.1-2, blue values indicate winter temperatures and correspond to dashed blue arrows in the Figures 6.3.1-1 and 6.3.1-2. Black values show the difference between connected summer and winter values.

low levels of Sr/Ca which correlate with Mg/Ca suggesting that this shell is diagenetically altered. The three shells from Ygne, North Nyhamn and Nyhamn are all well preserved.

The three specimens show a generally good correlation between the left and right halves of the valve (Figures, 6.2.4-1 6.3.1-1 and 6.3.1-2), which suggests that a true temperature signal is displayed in the data. The Mg/Ca values from the LVF sites, Nyhamn and North Nyhamn, differ in that on average Nyhamn has higher Mg/Ca values than North Nyhamn. Both of these sites have higher Mg/Ca than Ygne (Table 6.3.1-1 and 6.3.1-2). The sample numbers are too small to indicate whether there is a significant difference between Upper and Lower Visby formations. However, even if

Specimen	Age	Average Summer Maximum Mg/Ca (mmol/mol)	Average Winter Minimum Mg/Ca (mmol/mol)	Average difference between Maximum and Minimum (mmol/mol)
YGNE3	Upper Visby	9.2	3.9	5.1
NNY3	Lower Visby	11.6	5.3	6.5
NYH3	Lower Visby	10.1	5	5.2

Table 6.3.1-2. Average summer and winter Mg/Ca data from YGNE3, NNY3 and NHY3 along with average difference in connected summer and winter Mg/Ca values.

there is a difference in Mg/Ca between the Lower and Upper Visby Formations this is likely to be due to chance. As the difference between Lower and Upper Visby cannot be distinguished from local effects within one horizon. The difference between summer and winter temperatures is similar for Nyhamn and Ygne.

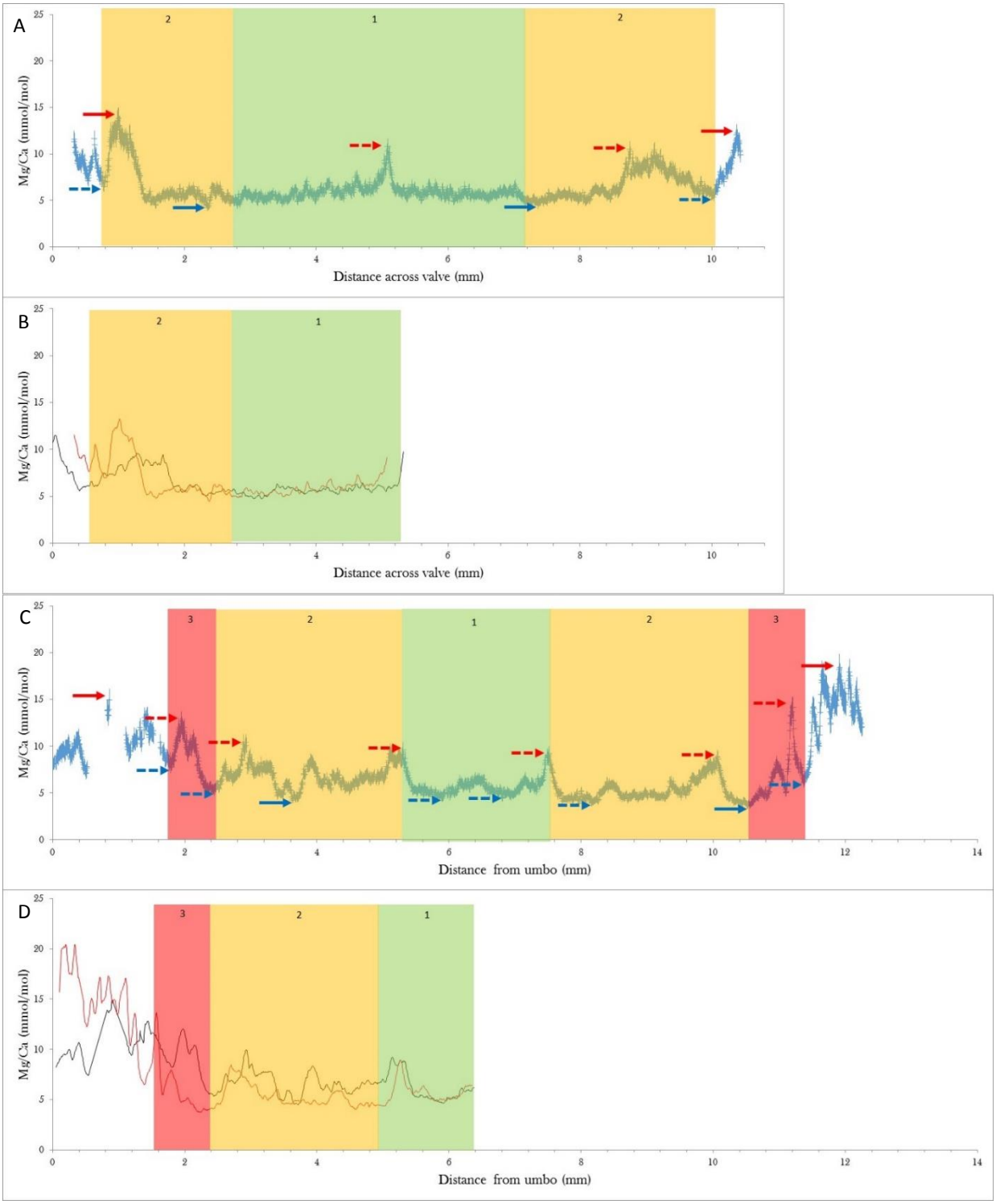

Figure 6.3.1-1. Mg/Ca data from NNY3 (A and B) and NHY3 (C and D). A and C show the laser ablation data with 8 % y-axis error bars and 40 µm x-axis error bars. The solid red and blue arrows indicate the highest Mg/Ca and lowest Mg/Ca respectively on one half of the profile. The dashed red and blue arrows indicate the respective highest and lowest Mg/Ca in each band, bands are identified by the numbered colour boxes. B and D show an 8 point rolling average of the same data from. The two lines show the left (black) and right (red) halves of the valves starting with the outside of the shell at 0 mm moving towards the centre of the shell.

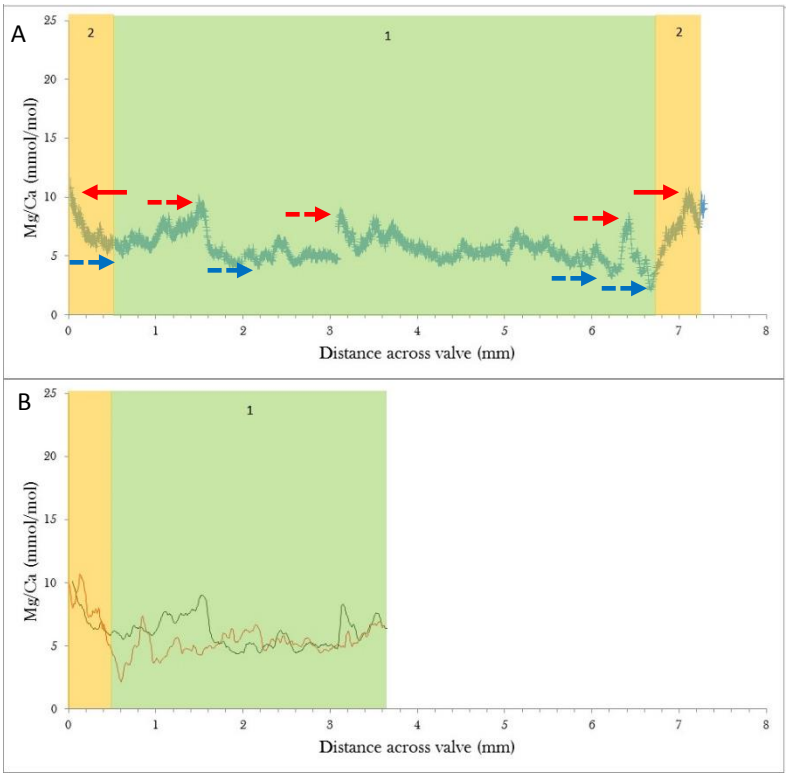

Figure 6.3.1-2. Mg/Ca data from YGNE3. A shows the laser ablation data with 8 % y-axis error bars and 40 µm x-axis error bars. The solid red and blue arrows indicate the highest Mg/Ca and lowest Mg/Ca respectively on one half of the profile. The dashed red and blue arrows indicate the respective highest and lowest Mg/Ca in each band, bands are identified by the numbered colour boxes. B shows an 8 point rolling average of the same data from. The two lines show the left (black) and right (red) halves of the valves starting with the outside of the shell at 0 mm moving towards the centre of the shell.

6.3.2 Mg/Ca from longitudinal geochemical profiles

The longitudinal profiles have been split into four different sections. The umbo section, representing the juvenile stage of life, 1, is marked in red on the graphs. This section, usually 2-3 mm in length, is the posterior-most in the shell, and is noted by high Mg/Ca ratios which steadily decline and eventually plateau.

Section 2, adolescent stage of life, is the part of the shell where biological influences overwrite any temperature signal. Mg/Ca will vary throughout this section but the diagnostic point is that Sr/Ca and Mn/Ca co-vary. This area is shaded amber on the graphs and should not be used for trace metal palaeoclimate studies.

Section 3, adult stage of life, is marked by stable Sr/Ca values generally in the region of 1.5 - 2 mmol/mol, any variations will be lower than those in section 2. Mn/Ca and Sr/Ca do not co vary and changes in Mg/Ca are more gradual than in the previous two sections. This section, marked green on the graphs, is the ideal portion of the shell for assessing palaeoclimate through trace metals and is here on referred to as the 'sweet spot'.

Section 4, death phase, marked blue on the graphs, is denoted by either a large spike in Mg/Ca or Sr/Ca. It can equally be marked by a rapid decrease in Mg/Ca or Sr/Ca. This area should not be used for any palaeoclimatic interpretation using trace metals. Section 4 is not present in all of the shells.

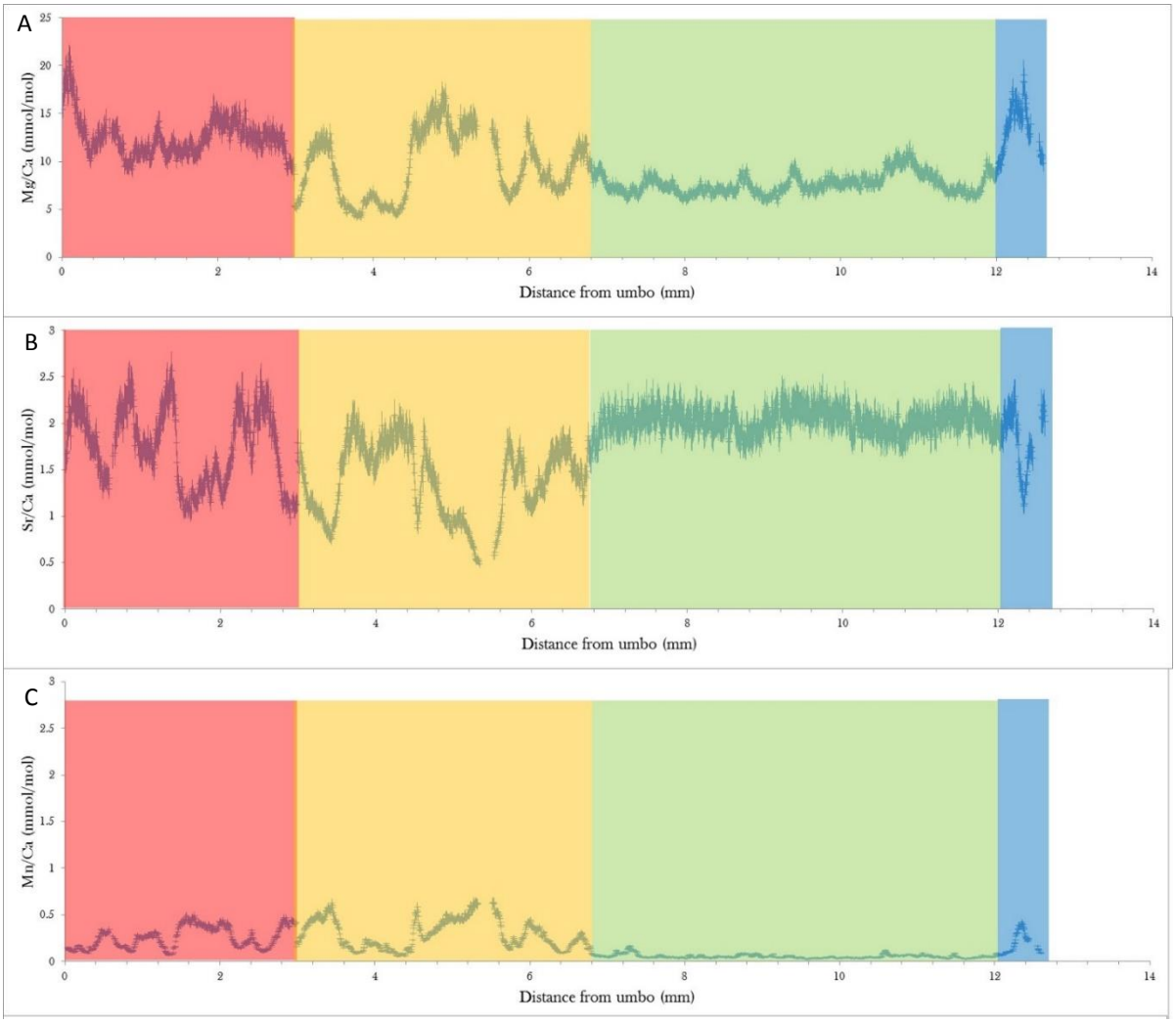

Figure 6.3.2-1. Mg/Ca data, Sr/Ca and Mn/Ca data from IRE1. Laser ablation Mg/Ca data with 8 % y-axis error bars and 40 µm x-axis error bars; A) Mg/Ca data, B) Sr/Ca data and C) Mn/Ca data. The red band indicates the umbo area of the shell, the amber band indicates the area mainly influenced by ontogenetic effects, the green band indicates the area most directly influenced by seawater temperature changes and the blue band indicates the dying area of the shell.

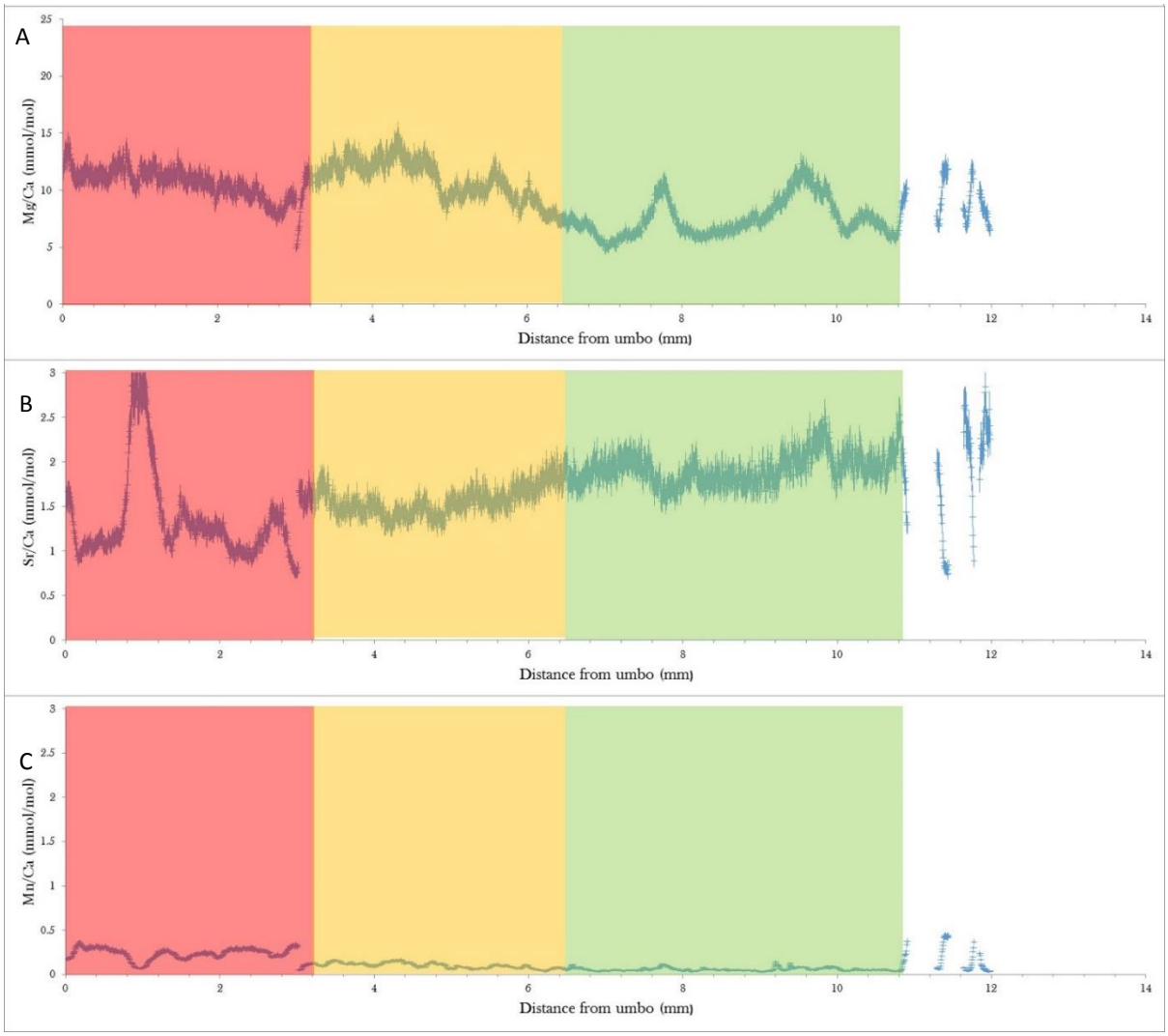

Figure 6.3.3-2. Mg/Ca data, Sr/Ca and Mn/Ca data from IRE2. Laser ablation Mg/Ca data with 8 % y-axis error bars and 40 µm x-axis error bars; A) Mg/Ca data, B) Sr/Ca data and C) Mn/Ca data. The red band indicates the umbo area of the shell, the amber band indicates the area mainly influenced by ontogenetic effects and the green band indicates the area influenced by seawater temperature changes.

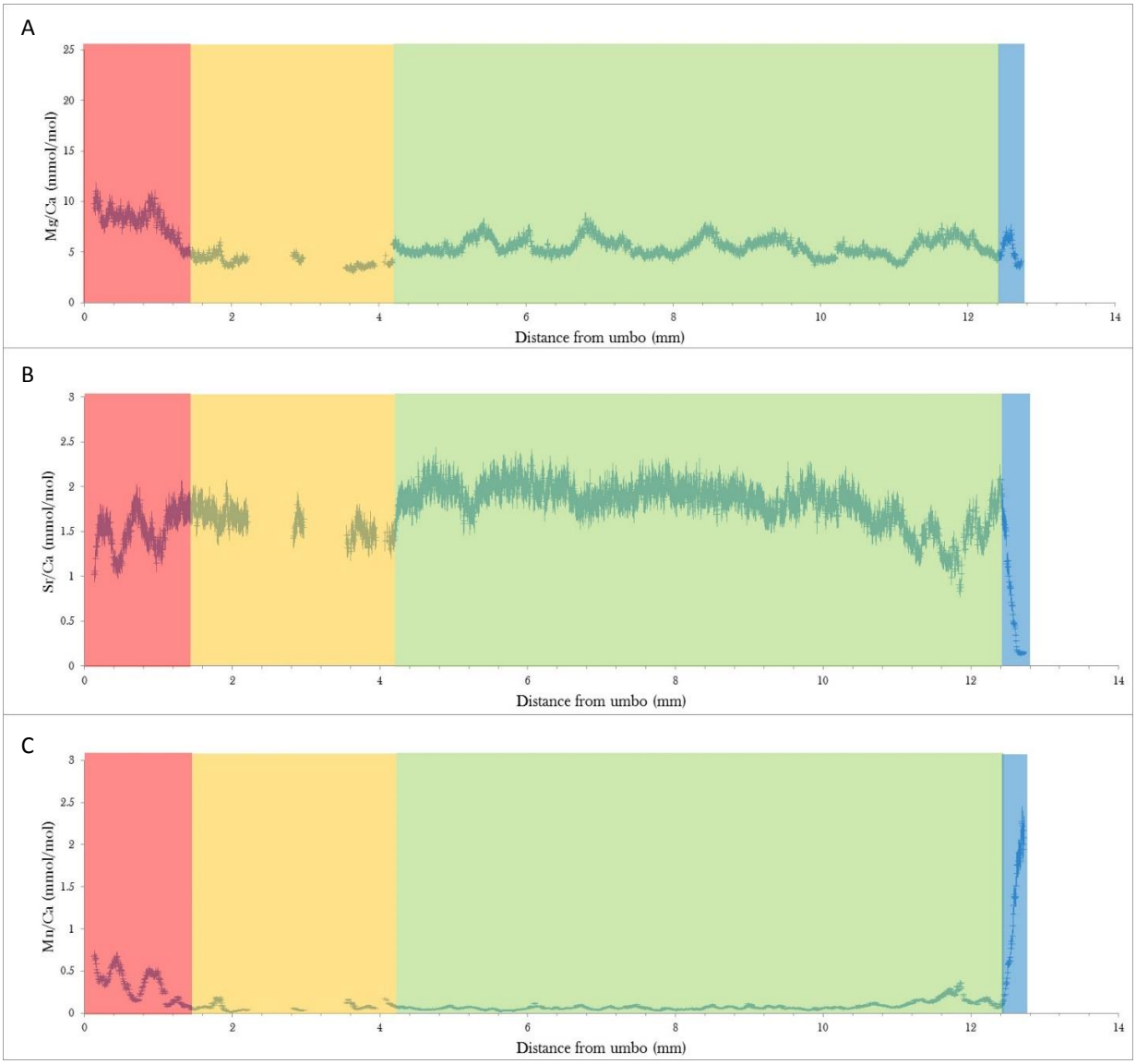

Figure 6.3.2-3. Mg/Ca data, Sr/Ca and Mn/Ca data from YGNE1. Laser ablation Mg/Ca data with 8 % y-axis error bars and 40 µm x-axis error bars; A) Mg/Ca data, B) Sr/Ca data and C) Mn/Ca data. The red band indicates the umbo area of the shell, the amber band indicates the area mainly influenced by ontogenetic effects, the green band indicates the area most directly influenced by seawater temperature changes and the blue band indicates the dying area of the shell.

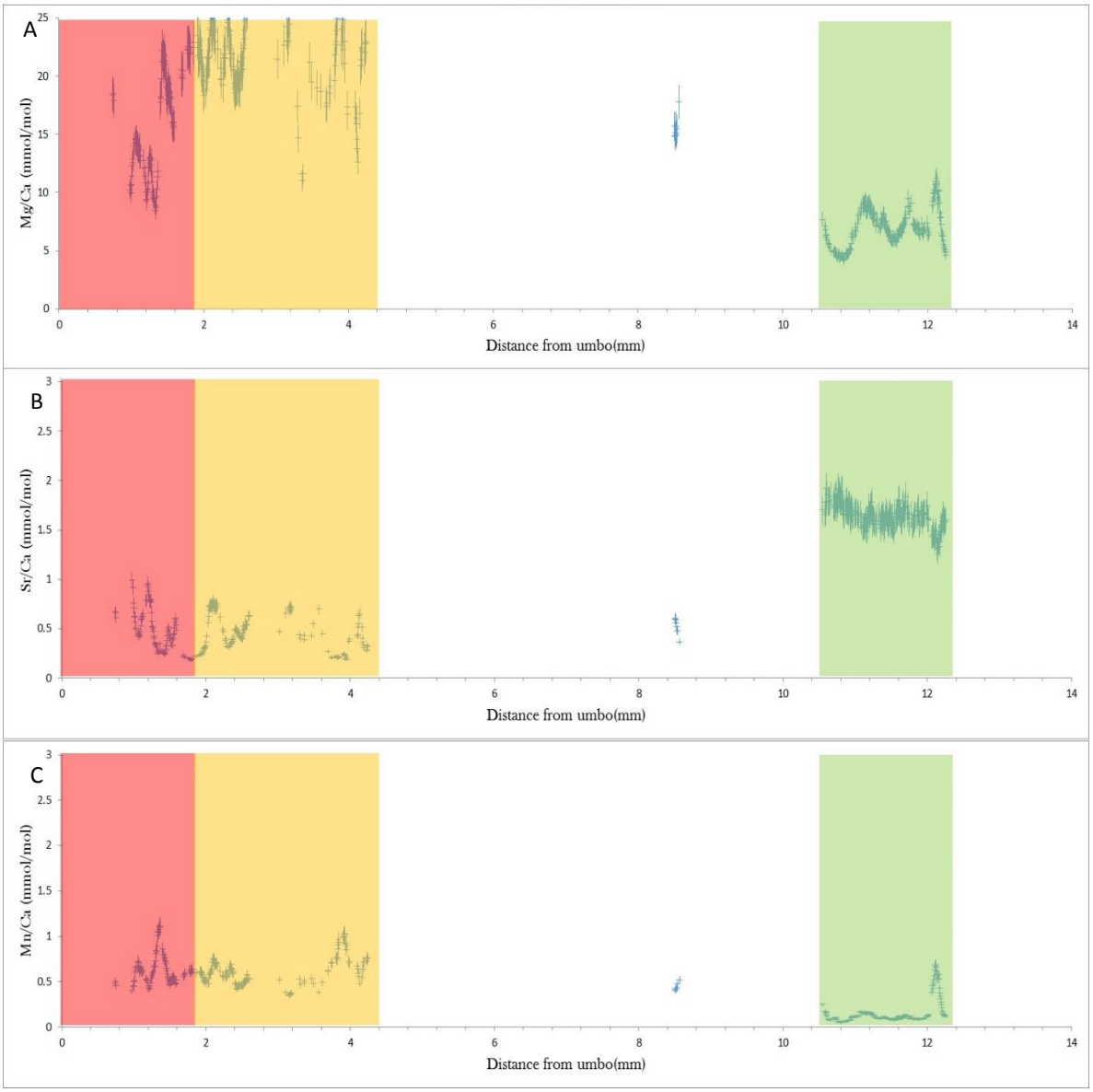

Figure 6.3.2-4. Mg/Ca data, Sr/Ca and Mn/Ca data from YGNE2. Laser ablation Mg/Ca data with 8 % y-axis error bars and 40 µm x-axis error bars; A) Mg/Ca data, B) Sr/Ca data and C) Mn/Ca data. The red band indicates the umbo area of the shell, the amber band indicates the area mainly influenced by ontogenetic effects and the green band indicates the area most directly influenced by seawater temperature changes.

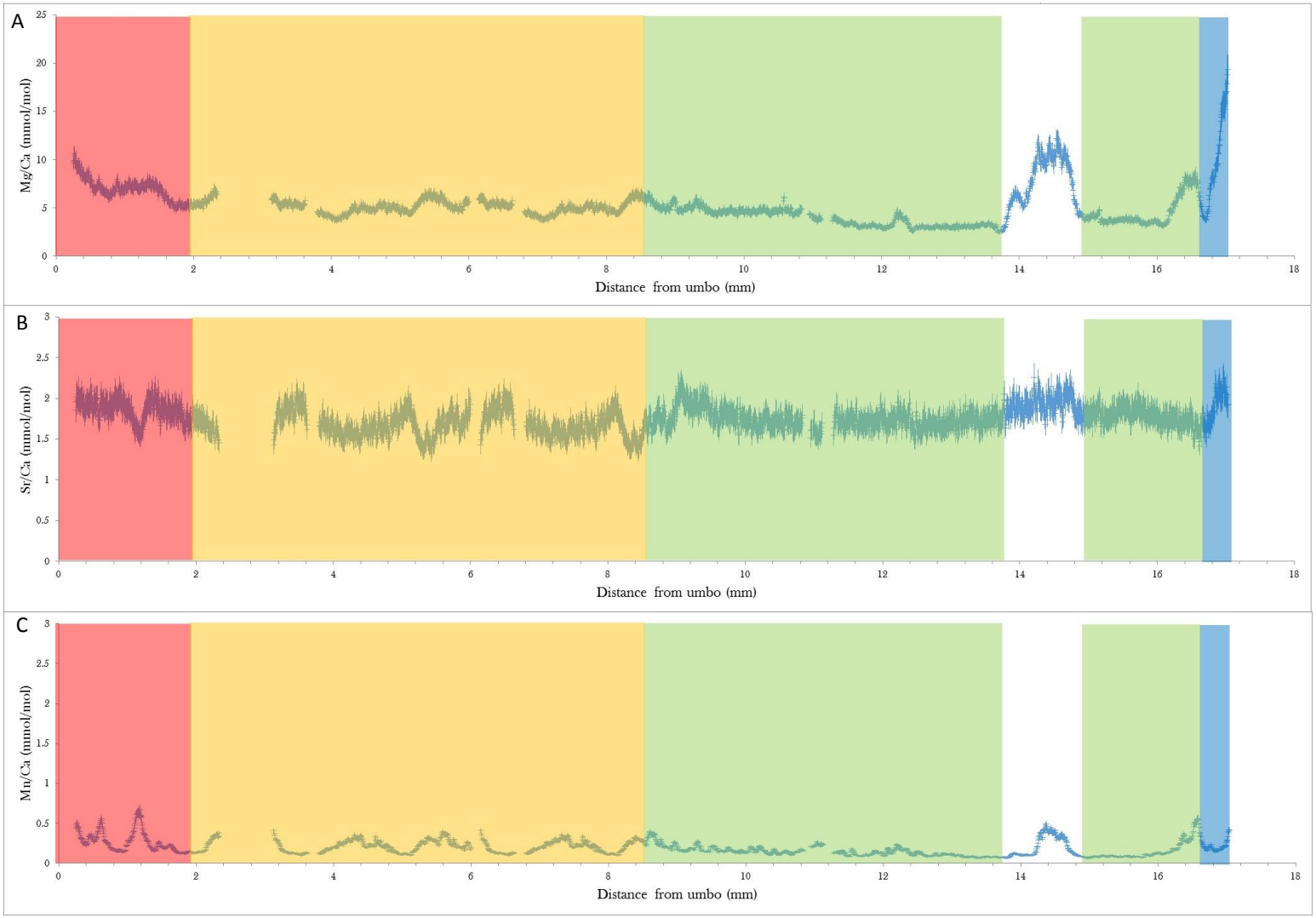

Figure 6.3.2-5. Mg/Ca data, Sr/Ca and Mn/Ca data from NNY1. Laser ablation Mg/Ca data with 8 % y-axis error bars and 40 µm x-axis error bars; A) Mg/Ca data, B) Sr/Ca data and C) Mn/Ca data. The red band indicates the umbo area of the shell, the amber band indicates the area mainly influenced by ontogenetic effects, the green band indicates the area most directly influenced by seawater temperature changes and the blue band indicates the dying area of the shell.

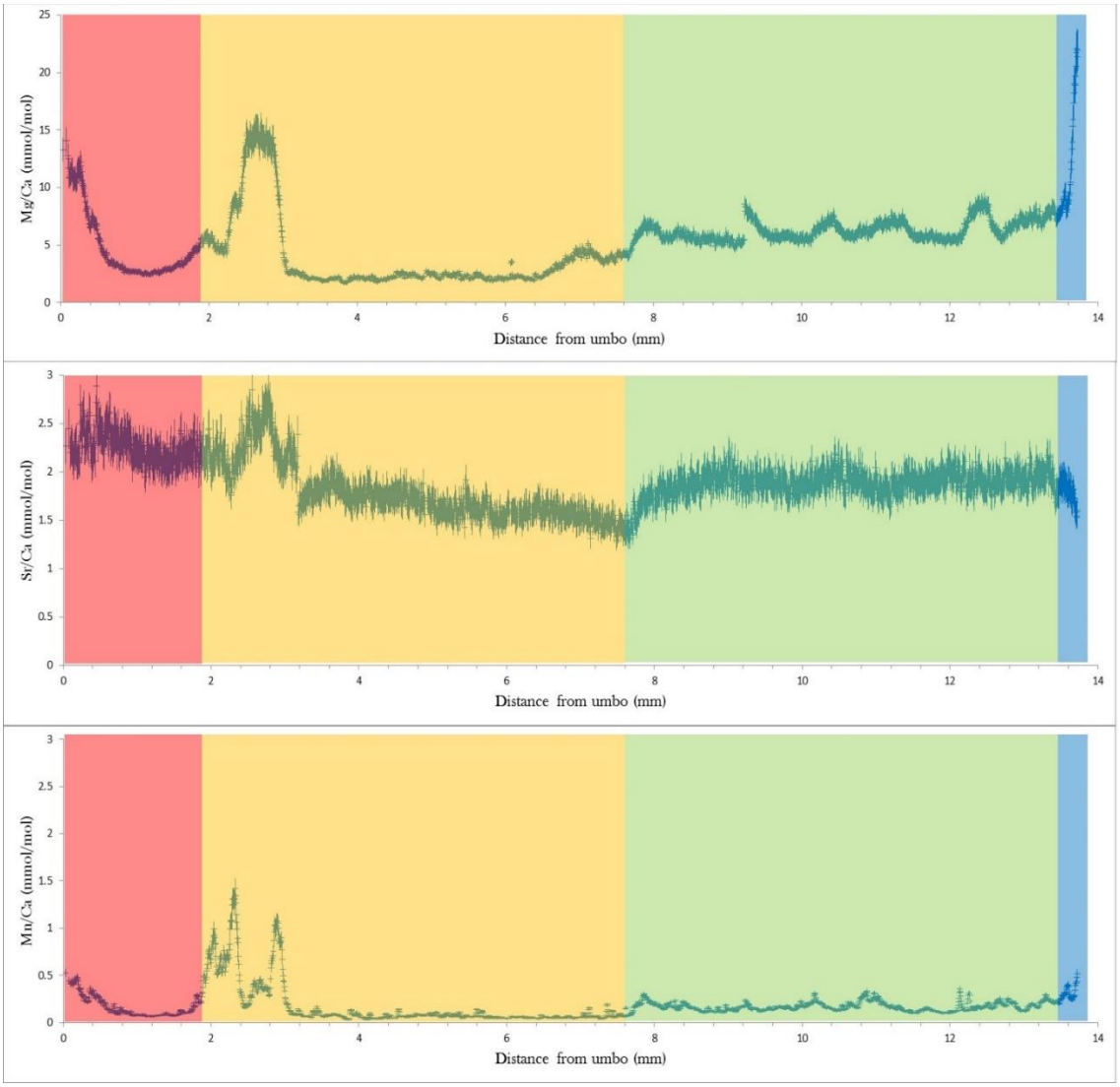

Figure 6.3.2-6. Mg/Ca data, Sr/Ca and Mn/Ca data from NNY2. Laser ablation Mg/Ca data with 8 % y-axis error bars and 40 µm x-axis error bars; A) Mg/Ca data, B) Sr/Ca data and C) Mn/Ca data. The red band indicates the umbo area of the shell, the amber band indicates the area mainly influenced by ontogenetic effects, the green band indicates the area most directly influenced by seawater temperature changes and the blue band indicates the dying area of the shell.

The Mg/Ca values from the 'sweet spot' should be representative of the seawater temperatures that the brachiopods lived in. For the longitudinal profiles the 'sweet spot' is denoted by the green band on the graphs as explained at the start of section 6.3.2, and for the transverse sections the whole profile is considered to be within the 'sweet spot', due to the way it was sampled. The average maximum and minimum values (Table 6.3.2-1, Figure 6.3.2-1) show a slight increase over the Ireviken Event. The average Mg/Ca values from the LVF and UVF are 6.1 and 6.6 mmol/mol, respectively. The average maxima (calculated by averaging the maximum value from each specimen and horizon for the LVF and UVF are 10.5 and 10.8 mmol/mol, respectively. The average minima (calculated by averaging the minimum value from each specimen and horizon) for the LVF and UVF are 3.6 and 4.1 mmol/mol, respectively.

Specimen	Age	Average Mg/Ca (mmol/mol) from the Sweet Spot	Maximum Mg/Ca (mmol/mol) from the Sweet Spot	Minimum Mg/Ca (mmol/mol) from the Sweet Spot
IRE1	Upper Visby	7.6	11.4	5.7
IRE2	Upper Visby	7.5	12.3	4.7
IRE3	Upper Visby		Altered	
YGNE1	Upper Visby	5.3	8.3	3.6
YGNE2	Upper Visby	6.9	11.3	4.2
YGNE3	Upper Visby	5.9	10.8	2.2
NNY1	Lower Visby	4.2	8.6	2.5
NNY2	Lower Visby	6.3	8.9	3.9
NNY3	Lower Visby	6.5	13.9	4.2
NYH1	Lower Visby		Altered	
NYH2	Lower Visby		Altered	
NYH3	Lower Visby	7.4	21.4	3.6

Table 6.3.2-1. Average, maximum and minimum Mg/Ca values from the sweet spot of individual specimens from Ygne, Ireviken, North Nyhamn and Nyhamn.

Location	Age	Average Mg/Ca (mmol/mol) from the Green Zone	Maximum Mg/Ca (mmol/mol) from the Green Zone	Minimum Mg/Ca (mmol/mol) from the Green Zone
IREVIKEN	Upper Visby	7.6	11.9	5.2
YGNE	Upper Visby	6	10.1	3.3
NORTH NYHAMNN	Lower Visby	5.7	11.1	3.5
NYHAMNN	Lower Visby	7.4	21.4	3.6

Table 6.3.2-2. Average, maximum and minimum Mg/Ca values from the sweet spots all specimens from Ygne, Ireviken, North Nyhamn and Nyhamn.

Formation	Average Mg/Ca (mmol/mol) from the Green Zone	Maximum Mg/Ca (mmol/mol) from the Green Zone	Minimum Mg/Ca (mmol/mol) from the Green Zone
Upper Visby	6.6	10.8	5.1
Lower Visby	6.1	10.5	3.6

Table 6.3.2-3. Average, maximum and minimum Mg/Ca values from the 'sweet spots' of all specimens from Upper and Lower Visby Formations.

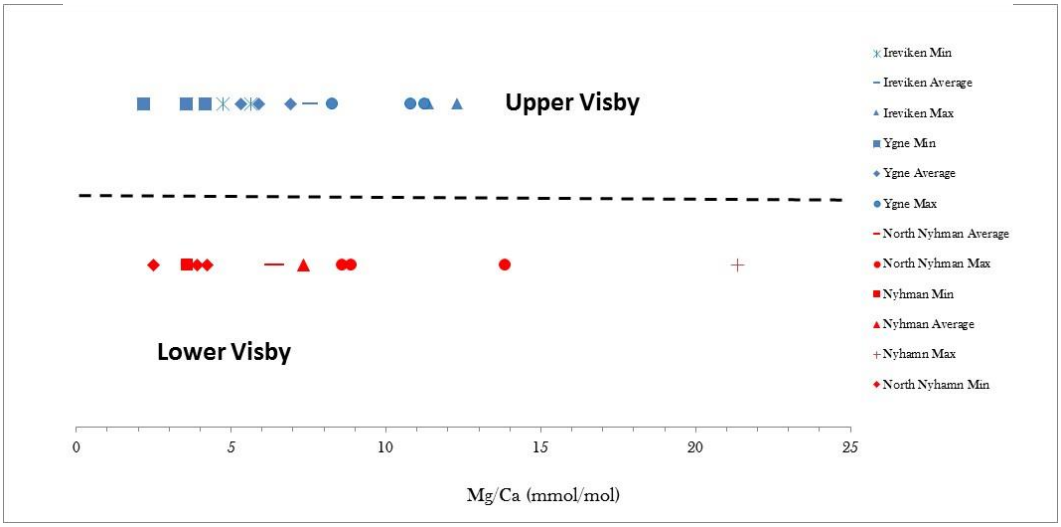

Figure 6.3.2-1. Average, maximum and minimum Mg/Ca values from the 'sweet spots' of all individual specimens from Ygne, Ireviken, Nyhamn and North Nyhamn.

6.3.3 Stable Isotopes

Stable isotopes, $\delta^{18}O$ and $\delta^{13}C$ were measured from all specimens from the four locations (Table 6.3.3-1, Figure 6.3.3-1). In the longitudinal se`ctions the shells were

Specimen	Area of Shell	Age	$\delta^{18}O$ (‰ VPDB)	$\delta^{13}C$ (‰ VPDB)
IRE1	Umbo	Upper Visby	-4.69	2.68
IRE1	Anterior	Upper Visby	-4.7	3.99
IRE2	Umbo	Upper Visby	-5.5	4.07
IRE2	Anterior	Upper Visby	-4.23	4.74
IRE3	Anterior	Upper Visby	-5.3	4.68
YGNE1	Umbo	Upper Visby	-5.53	3.6
YGNE1	Anterior	Upper Visby	-6.49	3.56
YGNE2	Umbo	Upper Visby	-5.36	2.96
YGNE2	Anterior	Upper Visby	-5.44	3.12
YGNE3	Anterior	Upper Visby	-4.8	3.4
NNY1	Umbo	Lower Visby	-5.46	1.12
NNY1	Anterior	Lower Visby	-4.93	1
NNY2	Umbo	Lower Visby	-5.14	1.33
NNY2	Anterior	Lower Visby	-5.19	1.58
NNY3	Anterior	Lower Visby	-4.26	1.59
NYH1	Umbo	Lower Visby	-5.38	1.25
NYH1	Anterior	Lower Visby	-5.51	1.68
NYH2	Anterior	Lower Visby	-5.73	1.37

Table 6.3.3-1. Individual stable isotope measurements collected from *Atrypa* from Ygne and Ireviken, Upper Visby and North Nyhamn and Nyhamn, Lower Visby.

sampled in two places, one in the umbo and one in the anterior part of the shell. This was to detect any regular offset between the two areas. No regular offset was identified in either $\delta^{18}O$ or $\delta^{13}C$ (Table 6.3.3-2). The two sites from the Upper Visby, Ygne and Ireviken, have average $\delta^{18}O$ values of -5.5 ‰ and -4.9 ‰ respectively (Table 6.3.3-3), whilst the two sites from the Lower Visby, North Nyhamn and Nyhamn have averages of -5 ‰ and -5.5 ‰ respectively. There is no overall change in the average of $\delta^{18}O$ from the Lower Visby Formation

Specimen	Age	Difference from umbo to anterior $\delta^{18}O$ (‰ VPDB)	Difference from umbo to anterior $\delta^{13}C$ (‰ VPDB)
IRE1	Upper Visby	0.01	1.31
IRE2	Upper Visby	1.27	0.67
YGNE1	Upper Visby	-0.96	-0.04
YGNE2	Upper Visby	-0.08	0.16
NNY1	Lower Visby	0.57	-0.12
NNY2	Lower Visby	-0.05	0.33
NYH1	Lower Visby	-0.13	0.43

Table 6.3.3-2. Difference between stable isotope measurements from the umbo and anterior regions in specimens of *Atrypa* from Ygne and Ireviken, Upper Visby: North Nyhamn and Nyhamn, Lower Visby.

to the Upper Visby Formation. The average of all measurements from the Lower Visby is -5.2 ‰ and the Upper Visby is -5.2 ‰ (Table 6.3.3-4), indicating no change in $\delta^{18}O$ values over the Ireviken Event.

The $\delta^{13}C$ values for the two Upper Visby sites, Ygne and Ireviken are 4.0 ‰ and and 3.3 ‰ respectively (Table 6.3.3-4). The $\delta^{13}C$ values from the two Lower Visby sites, North Nyhamnn and Nyhamnn are 1.33 ‰ and 1.43 ‰ respectively (Table

6.3.3-4). There is a positive shift of 2.3 ‰. in average $\delta^{13}C$ values, from 1.4 ‰ in the Lower Visby to 3.7 ‰ in the Upper Visby.

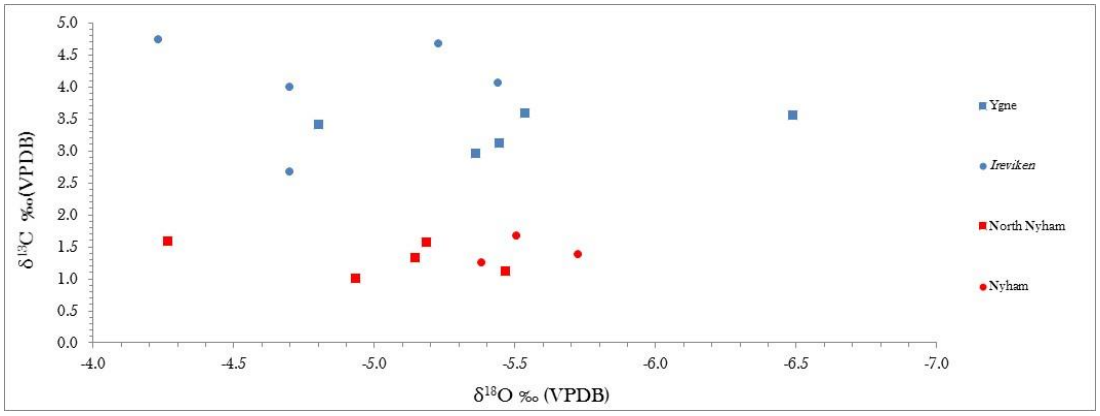

Figure 6.3.3-1. Individual stable isotope measurements from the umbo and anterior regions in specimens of *Atrypa* from Ygne and Ireviken, Upper Visby: North Nyhamn and Nyhamn, Lower Visby.

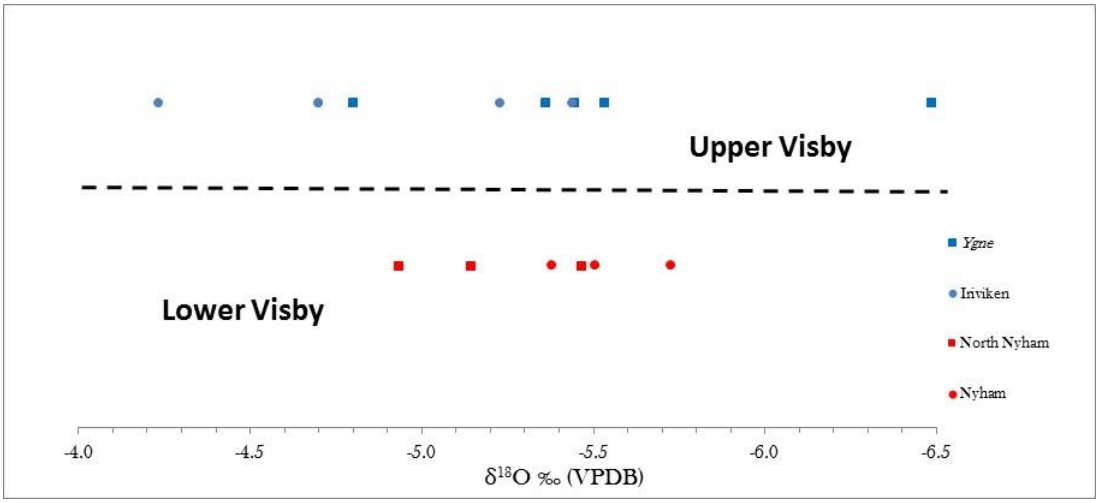

Figure 6.3.3-2 $\delta^{18}O$ measurements from specimens of *Atrypa* from Ygne and Ireviken, Upper Visby: North Nyhamn and Nyhamn, Lower Visby.

Formation	Location	Species	$\delta^{18}O$ Max (‰ VPDB)	$\delta^{18}O$ Min (‰ VPDB)	$\delta^{18}O$ Average (‰ VPDB)	Range (‰ VPDB)
Upper Visby	Ygne	*Atrypa*	-4.8	-6.48	-5.53	1.69
Upper Visby	Iriviken	*Atrypa*	-4.23	-5.44	-4.86	1.21
Lower Visby	North Nyhamn	*Atrypa*	-4.26	-5.46	-5	1.2
Lower Visby	Nyhamn	*Atrypa*	-5.38	-5.73	-5.54	0.35

Table 6.3.3-3. Average, maximum, minimum and range of $\delta^{18}O$ measurements from the four locations used in this study. Ygne and Ireviken, Upper Visby: North Nyhamn and Nyhamn, Lower Visby.

Formation	Species	$\delta^{18}O$ Max (‰ VPDB)	$\delta^{18}O$ Min (‰ VPDB)	$\delta^{18}O$ Average (‰ VPDB)	Range (‰ VPDB)
Upper Visby	*Atrypa*	-4.23	-6.48	-5.2	2.25
Lower Visby	*Atrypa*	-4.26	-5.73	-5.2	1.47

Table 6.3.3-4. Average, maximum, minimum and range of $\delta^{18}O$ measurements from the two different formations used in this study.

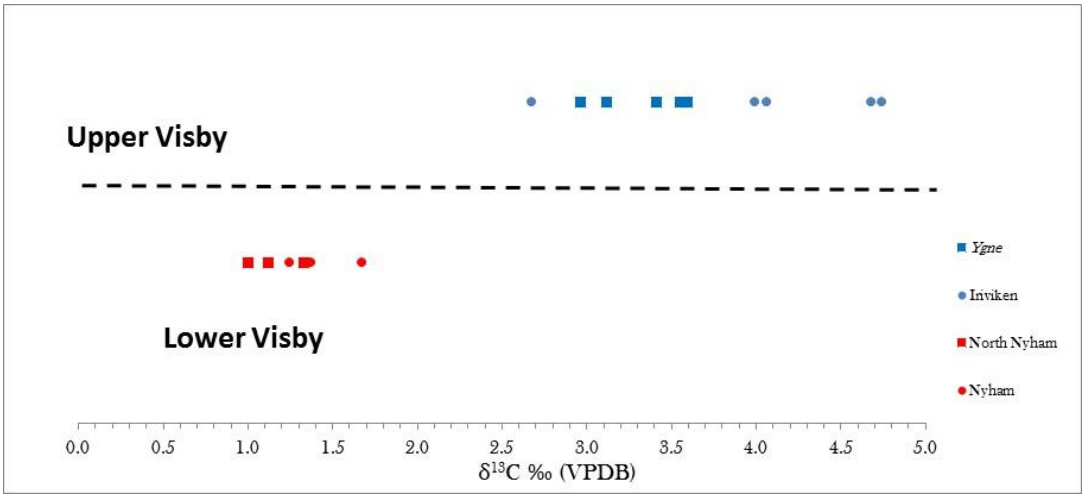

Figure 6.3.3-3 $\delta^{13}C$ isotope measurements from specimens of *Atrypa* from Ygne and Ireviken, Upper Visby: North Nyhamn and Nyhamn, Lower Visby.

Formation	Location	Species	$\delta^{13}C$ Max (‰ VPDB)	$\delta^{13}C$ Min (‰ VPDB)	$\delta^{13}C$ Average (‰ VPDB)	Range (‰ VPDB)
Upper Visby	Ygne	*Atrypa*	3.6	2.96	4.03	0.64
Upper Visby	Iriviken	*Atrypa*	4.74	2.68	3.32	2.06
Lower Visby	North Nyhamn	*Atrypa*	1.59	1	1.33	0.59
Lower Visby	Nyhamn	*Atrypa*	1.68	1.25	1.43	0.43

Table 6.3.3-6. Average, maximum, minimum and range of $\delta^{18}O$ measurements from the two formations used in this study.

Formation	Species	$\delta^{13}C$ Max (‰ VPDB)	$\delta^{13}C$ Min (‰ VPDB)	$\delta^{13}C$ Average (‰ VPDB)	Range (‰ VPDB)
Upper Visby	*Atrypa*	4.74	2.68	3.68	2.06
Lower Visby	*Atrypa*	1.68	1	1.37	0.68

Table 6.3.3-5. Average, maximum, minimum and range of $\delta^{13}C$ measurements from the from the four locations used in this study. Ygne and Ireviken, Upper Visby: North Nyhamn and Nyhamn, Lower Visby.

6.4 Discussion

6.4.1 Mg/Ca in Silurian brachiopods compared with Modern and Eocene-Oligocene brachiopods

The way brachiopods uptake Mg/Ca and distribute it across the shell has varied little over time. Brachiopods from the Silurian have the same shape of geochemical profile to the modern brachiopods, the different absolute values are species, temperature and seawater chemistry dependent (Figure 6.4.1-1). The distribution of Mg/Ca across an ontogenetic section is typified by an enrichment of Mg/Ca in the umbo area of the shell, followed by an area where ontogeny and associated vital effects are the main influence on Mg/Ca, Sr/Ca and Mn/Ca, and then a 'sweet spot' or area where palaeoclimatic signals are the most prevalent. The final section, not always present, is shell where there is a sharp change in the trace metal ratios, for reasons that seem to be associated with the senility of the brachiopod or possible contamination from the resin that the brachiopod was set in (Figures 6.3.2-1, 6.3.2-2, 6.3.2-3, 6.3.2-4, 6.3.2-5 and 6.3.2-6).

Some of the modern shells, show a correlation between Mn/Ca and Mg/Ca. This is more common in the Silurian samples, so it is probable that the level of Mn/Ca uptake is species specific. The cause of this correlation is difficult to interpret because in some shells the Mn/Ca:Mg/Ca correlation is one that is controlled in parts of the shell by diagenesis, in others ontogeny and in other areas by water temperature. I believe it to be a combination of all three. Spikes in Mn/Ca in some areas can also be associated with spikes in Al/Ca and a coincident spike in Mg/Ca, this I would consider to be a diagenetic signal. In the second area of the shell, highlighted amber on longitudinal profiles, Sr/Ca and Mn/Ca co-vary. This

covariance takes place in the same part of the shell, and the values of Mg/Ca are generally but not always higher than in the more adult third of the shell, marked green. This covariance is not diagenetic because it is regularly in the same place within the shell, in the centre of an ontogenetic profile. Finally in the 'sweet spot' section the Mn/Ca and Mg/Ca can follow each other fairly closely but Sr/Ca remains stable. I am confident this area of the shell produces a temperature signal even in the Silurian shells as the transverse sections are symmetrical and have stable Sr/Ca values, a principle that underpins the way the modern shells were assessed.

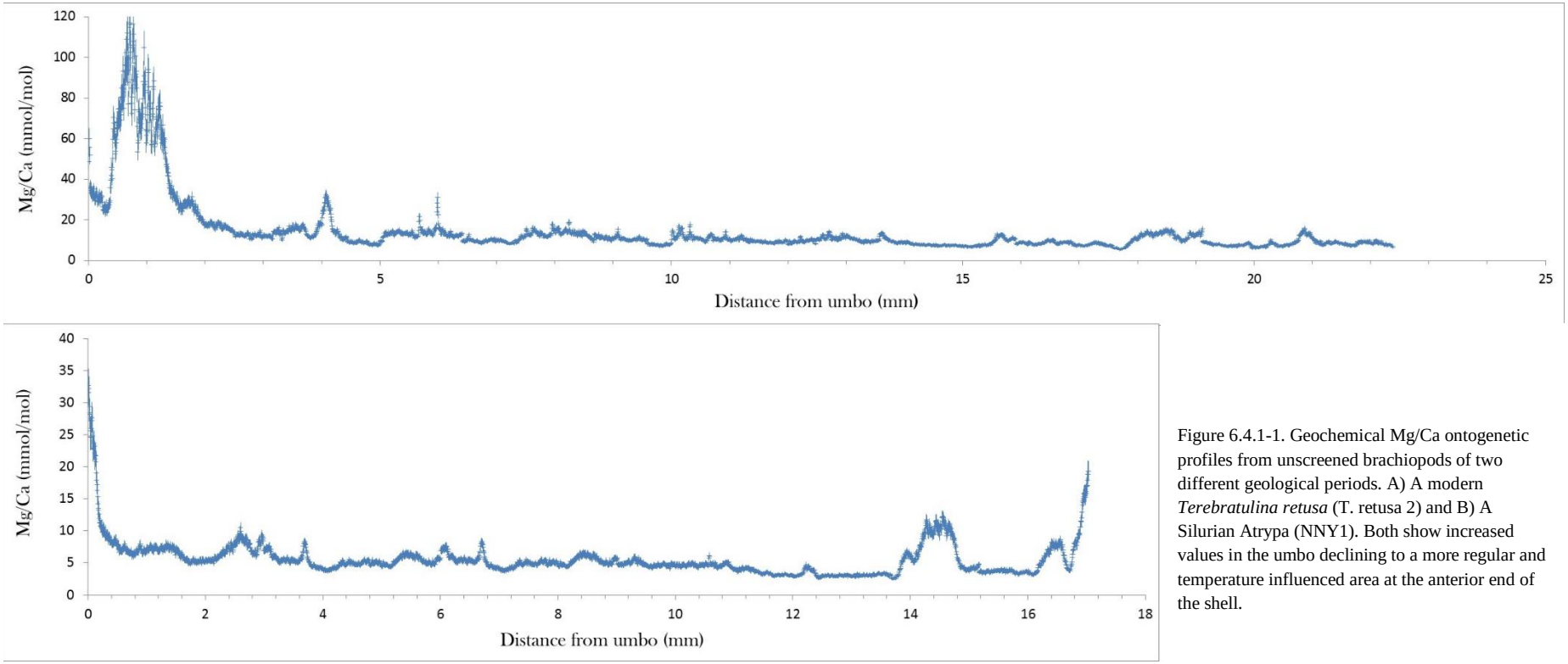

Figure 6.4.1-1. Geochemical Mg/Ca ontogenetic profiles from unscreened brachiopods of two different geological periods. A) A modern *Terebratulina retusa* (T. retusa 2) and B) A Silurian Atrypa (NNY1). Both show increased values in the umbo declining to a more regular and temperature influenced area at the anterior end of the shell.

6.4.2 Mg/Ca and changes in temperature across the Ireviken Excursion

Longitudinal profiles cannot be used in quite the same way as the transverse profiles to assess seasonality as there is no internal check on the data via the mirror image produced in the transverse sections due to the shell symmetry. Once the parts of the longitudinal profile where the Mg/Ca ratio is influenced mainly by ontogenetic, diagenetic and vital effects have been identified and discounted the remaining area of the shell can be looked at for average, maximum and minimum Mg/Ca.

The Mg/Ca data support the $\delta^{18}O$ data (section 6.4.5) and add weight to the idea there is no or little change in temperature over the Ireviken Excursion. The datasets from the Upper and Lower Visby Formations show that there is a slight warming of 0.4 °C in average temperatures over the Ireviken Excursion, this may be due to a slight warming of equatorial waters. However at the Llandovery-Wenlock boundary it is thought to be unlikely because the Ireviken Excursion marks the transition between P and S states (Cramer and Saltzman, 2007a) and also a transition into a glacial period as marked by the glacinogenic sediments of Brazil (Grahn and Caputo, 1992). This apparent warming is most likely associated with the shallowing of the water column that occurs gradually from the LVF to the UVF (Calner et al., 2004).

Changes in temperature can be assessed with a degree of certainty between the summer and winter temperatures for each locality. The relative seasonal changes can be calculated regardless of the *H* value of the brachiopod or the $Mg/Ca_{seawater}$. As it is uncertain which of the modern calibrations would best represent *Atrypa*, relative temperature changes have been produced using both *Liothyrella* and *Terebratulina* calibrations. Temperature changes are shown in Table 6.4.2-1.

The changes in temperature from winter to summer are approximately 3.5 – 5.4 °C. This is in keeping with modern day equatorial water temperatures off the coast of Brazil which show a temperature change of 4 °C annually (Wienders et al., 2000). This shows that there was nothing necessarily unusual or fundamentally different

Specimen	Age	Difference between summer and winter temperatures using *Liothyrella* calibration °C	Difference between summer and winter temperatures using *Terebratulina* calibration °C
YGNE3	Upper Visby	4.3	5.4
NNY3	Lower Visby	3.5	4.4
NYH3	Lower Visby	3.9	4.9

Table 6.4.2-1. Average Summer-Winter seasonal variations in temperature shown by three brachiopods across the Ireviken Event.

between seasonality of the Silurian and the modern day sub-equatorial regions. It is also pleasing to note that this seasonality of 3.5 – 5.4 °C is lower than the seasonality calculated for the mid-latitude sites of New Zealand (4.9 -5.6 °C) that were used for the seasonality study across the EOT. No attempts have been made to reconstruct absolute temperatures using Mg/Ca from the Silurian due to the complexities of ocean chemistry.

6.4.3 Mg/Ca of Silurian seawater

During the Llandovery-Wenlock transition, Gotland lay 19° ±5.1° South of the equator (Torsvik et al., 1992) and was bathed in tropical waters with temperatures that are thought to be similar to, or slightly warmer, than those of modern-day equatorial regions; clumped isotope studies indicate an average temperature of approximately 35 °C ±7 °C (Cummins et al., 2014; Finnegan et al., 2011). That said,

some $\delta^{18}O$ temperature data suggest temperatures were much warmer; up to 52 °C (Brand et al., 2006). Such high temperatures are thought unreasonable because at temperatures over 43 °C biological molecules, principally proteins, begin to denature (Bond et al., 1988; Parag et al., 1987), making life for most multicellular organisms (except for extremophiles) unviable for more than a few hours. Abundant brachiopod, conodont and trilobite faunas show that life was prevalent and flourishing in these tropical waters at this time.

It is problematic to use Mg/Ca ratios directly to investigate seawater temperatures: temporal differences in $Mg/Ca_{seawater}$ are well documented throughout the Cenozoic (Coggan et al., 2010, Dickson 2002, Ries 2010, Lowenstien et al., 2005), from ~5.2 mol/mol in the modern ocean to lower values of ~2.5 mol/mol at the Eocene-Oligocene boundary. It is likely that this trend of changing Mg/Ca ratios affected the whole Phanerozoic as the residence times of Mg and Ca are ~10 Ma and ~1 Ma respectively. If the average Mg/Ca values for the UVF and LVF are converted to temperature assuming modern levels for $Mg/Ca_{seawater}$ and using the *Liothyrella* calibration the temperatures are 13 °C and 12.6 °C respectively. These temperatures are far too low for equatorial regions and in complete contrast to the high temperatures which are calculated from the $\delta^{18}O$ data. This shows that the $Mg/Ca_{seawater}$ must have been significantly different from the modern day.

As explained in Chapter 5 the uptake of Mg/Ca into biogenic calcite with varying $Mg/Ca_{seawater}$ is not a linear relationships and is best explained by a power law function. Using a variety of *H* values for Mg/Ca in brachiopods and both Mg/Ca temperature calibrations for *Terebratulina* and *Liothyrella*, here I calculate and attempt to constrain $Mg/Ca_{seawater}$ for the Llandovery/Wenlock boundary in the Silurian. This is assuming that tropical water temperature is on average

approximately 35 °C ± 7°C (Cummins et al., 2014; Finnegan et al., 2011), the way brachiopods uptake Mg/Ca into their shells has not changed over time and that brachiopods have *H* values similar to that of the more complex animals such as the crabs and shrimps that were documented by Haisuk and Lohmann (2010).

I have used *H* values of 0.94 from a crab carapace, *P.gibbesi* and 1.22 from the shrimp, *P.pugio* (Haisuk and Lohmann 2010). With the highest value reported of 1.53 from the coccolith *O.neopolitanan* and a lower value of 0.68 from abiotic calcite (Haisuk and Lohmann 2010), this gives a reasonable range of potential brachiopod H values.

Organism	***H* value**	**$Mg/Ca_{seawater}$ of Silurian Ocean Water Using *Liothyrella* Calibration (mol/mol)**	**$Mg/Ca_{seawater}$ of Silurian Ocean Water Using *Terebratulina* Calibration (mol/mol)**
Coccolith (*O.neopolitanan*)	1.53	0.3	0.3
Shrimp (*P.pugio*)	1.22	0.2	0.2
Crab Carapace (*P. gibbesi*)	0.94	0.05	0.05
Abotic Calcite	0.68	0.008	0.008

Table 6.4.3-1. Potential Mg/Ca seawater values for the Silurian based on H values from Haisuk and Lohman (2010) and temperature studies from Cummins et al. (2014) and this study.

Regardless of calibration or *H* value the Silurian $Mg/Ca_{seawater}$ is much lower than that of the modern day. This is corroborated by Holt et al. (2014) who indicate a period from the Late Cambrian to the Mid Devonian where $Mg/Ca_{seawater}$ values were low < 2 mol/mol. These values are associated with 'calcite seas' (Holt et al., 2014). A model by Demicco et al. (2005) also shows Silurian $Mg/Ca_{seawater}$ values lower still at ~0.7-0.8 mol/mol, and predicts Cambrian $Mg/Ca_{seawater}$ values as low as 0.3 mol/mol. The assumptions I have used here are relatively large, however the low values are in keeping with modelled values and 'calcitic sea' intervals.

6.4.4 Comparison of stable isotopes from the umbo (juvenile) and anterior (adult) secondary layer calcite

The reason behind sampling for $\delta^{18}O$ both from the umbo and anterior sections of the shell was to see if there was a fundamental difference and common offset between stable isotope values in these two areas. It is widely accepted that $\delta^{18}O$ stable isotope values from Silurian brachiopods have produced temperatures which would be problematic for multicellular organisms. Several studies (Brand et al., 2006; Munnecke et al., 2003; Azmy et al., 1998) have used brachiopod $\delta^{18}O$ to assess temperatures and it is not always clear which part of the shell the powders were drilled or 'flaked' from. The umbo is the easiest section of the shell to drill, purely because it is often the thickest area and it is also the area of the brachiopod shell with the highest preservation potential. It is less likely to be broken into smaller pieces post mortem making it a likely target for sampling. From my study in Chapter 3 and other studies (Perez-Huerta et al., 2008, Perez-Huerta et al., 2011) the umbo is an unreliable region for assessing trace metals in brachiopods. If taken as being indicative of temperature the Mg/Ca values from this area of the shell would produce much higher temperatures than were actually correct. Investigating whether or not

the umbo region would produce erroneous values in the $\delta^{18}O$ and the $\delta^{13}C$ data was important.

The data show that there is no difference between the umbo and the adult areas of the shell, suggesting that unlike the trace metals, the stable isotopes are less easily influenced by ontogeny and vital effects in the juvenile area of the inside of the secondary layer. This shows that studies which sample the umbo would not produce the high ocean temperatures associated with brachiopod $\delta^{18}O$ values, however if primary layer calcite was included in the analysed material then this may decrease the $\delta^{18}O$ values and subsequently increase the temperatures calculated from $\delta^{18}O$ (Parkinson et al., 2005).

6.4.5 Absolute temperatures across the Ireviken Excursion

Munnecke et al. (2003) show a ~0.4 ‰ positive increase in $\delta^{18}O$ over the Ireviken excursion which is not replicated in this study. The findings here support that of Cummins et al. (2014) who used clumped isotopes to look at the potential change across this time period and also found no excursion. As Cummins et al. (2014) state, the reason that their study and subsequently this study do not show the ~0.4 ‰ positive excursion could be because of the lower sample numbers in both studies compared with the number used by Munnecke et al. (2003). Another reason suggested by Cummins et al. (2014) was the preservation quality of their samples was poorer than initially though, although they followed the most rigorous of manual sampling techniques to ensure that only pure unaltered secondary layer calcite was included. The diagenetic trace metal analysis on the fossils used in my study was also rigorous because of the resolution of the laser ablation sampling. I therefore believe that inconsistencies in diagenetic screening in Cummins et al. (2104) and

here do not explain the lack of detection of the ~0.4 ‰ excursion, identified but poorly resolved by Munnecke et al. (2003). The possibility remains that there is no change in $\delta^{18}O$ in equatorial regions such as Gotland over the Ireviken Excursion. The excursion in $\delta^{18}O$ values is much more pronounced in higher latitude sites (Brand et al., 2006), which change from P to S climate states.

Cummins et al. (2014) show average values of $\delta^{18}O$ over the Ireviken excursion of -5.5 ‰, compared with my study average of -5.2 ‰. The absolute difference in these values could be due to a number of factors. Different analytical techniques, clumped isotopes in Cummins et al. (2014) and stable isotopes in this study, may produce slightly different results. The shells were also taken from different localities which could lead to local variations in $\delta^{18}O$ being reflected in the differing values.

Using the $\delta^{18}O$ calculation adapted from Brand et al., (2013) and using the assumption of an ice free world for the early Silurian of ~ -1.1 ‰, seawater temperatures are calculated as being 37.1 °C. This is much lower than $\delta^{18}O$ stable isotope studies have shown in the past (Azmy et al., 1998, Munnecke et al., 2003 and Brand et al., 2006). Temperature studies based on clumped isotopes have achieved similar results (Finnegan et al., 2011; Cummins at al., 2014). The reason the temperatures in this study seem much more realistic could be due to the way the shells are sampled. Here the upmost care was taken not to include any of the primary layer which is known to have a lower $\delta^{18}O$ value than the secondary and tertiary layers of the brachiopod shells (Parkinson et al., 2005). The method used here involved use of a microdrill to obtain the powder and target only the thickest areas of shell, therefore drilling in an area of shell where the inclusion of primary layer material was reduced almost to zero.

Cummins et al. (2014), when converting their $\delta^{18}O$ values to temperature used their highest $\delta^{18}O$ value as they state this most likely represents their best preserved sample. Whilst the merit of doing this is obvious, it gives lower more reasonable temperatures and excludes the possibility of micrite being incorporated into the analysis, I believe their use of the lowest value is correct but may have been done for the wrong reason. Their study flaked off pieces of the secondary layer. Whilst that is currently a valid technique, I would caution against anyone using a similar method in future for the following reasons. Parkinson et al. (2005), in a detailed study of $\delta^{18}O$ in modern brachiopods, clearly state that their study "provides tantalising evidence that $\delta^{18}O$ determinations from the inner part of the secondary/tertiary shell layer of most modern articulated brachiopods accurately record ambient seawater temperatures". This is a phenomenon not just specific to $\delta^{18}O$; Perez-Huerta et al. (2008; 2011) show that towards the outer part of the secondary layer, i.e. closer to the primary layer, Mg/Ca ratios are increasingly out of equilibrium with the ambient seawater. Hence, not just anywhere within the secondary layer can be used for $\delta^{18}O$ or Mg/Ca analysis. The flaking technique cannot guarantee that the material collected is only from the inner part of the secondary layer. The lowest values shown in Cummins et al. (2014) are likely where their flaking technique has obtained material from the very inside of the secondary layer.

The data here show no change in $\delta^{18}O$ values over the Ireviken Excursion. However the data do agree with past work which has shown a positive excursion in $\delta^{13}C$ over this event (Munnecke et al., 2003; Brand et al., 2006; Azmy et al., 1998). This change in $\delta^{13}C$ cannot be interpreted as relating to changes in temperature because the $\delta^{18}O$ values do not change over the Ireviken Excursion and the small change in Mg/Ca values is most likely due to a shallowing of the water column.

The $\delta^{13}C$ excursion is a global event with slightly different levels of positive excursion being recorded at different locations around the world (Munnecke et al., 2003; Azmy et al., 1998; Brand et al., 2006; Cummins et al., 2014). This shows that the whole ocean chemistry must have changed during this time. It is beyond the scope of this work to try to assess the mechanisms for this change other than to rule out or include a change in temperature.

6.5 Conclusions

- There is little or no change in temperature on Gotland over the Ireviken Excursion. This is supported by both $\delta^{18}O$ and Mg/Ca data. A slight warming shown by the Mg/Ca data is probably due to a shallowing of the water column.
- Average temperatures for the Silurian have been calculated at 37.1 °C in keeping with clumped isotope work and much lower than any previous stable isotope study.
- Only carbonate material from the very inside of the secondary layer or tertiary layer should be used for trace metal and stable isotope analysis. Wherever possible the use of a microdrill is much preferred to any attempt at flaking off pieces of secondary layer as the inside of the shell can be directly targeted.
- There is no common offset between inside of the secondary layer in the umbo and the inside of the secondary layer in the anterior region of the shell in terms of stable isotopes.
- Annual temperature changes in sub-equatorial regions in the early Silurian (3.5 – 5.4 °C) are very similar to modern day sub-equatorial regions (4 °C).
- The positive excursion in the $\delta^{13}C$ data is still recognisable in this study and cannot be associated with a change in temperature.
- $Mg/Ca_{seawater}$ for the Silurian may be very low < 0.3 mol/mol which would be consistent with 'calcite seas'.

Chapter 7: SYNTHESIS

7.1 Wider Implications of this study

This study extended the application of the well-established Mg/Ca palaeotemperature proxy, previously used in Cenozoic foraminifera (e.g. Lear et al., 2000; Lear et al., 2004; Lear et al., 2008; Hollis et al., 2009), to brachiopods to investigate seasonal temperature changes. It aimed to use evidence from these macrobenthos to further investigate environmental change over the EOT, with particular emphasis on seasonality in the southern Pacific. The long fossil record of brachiopods (Cambrian-Recent), extends the potential for application of this technique back into the Palaeozoic, and this study set out to verify this by investigating Mg/Ca across a marked Silurian $\delta^{13}C$ and $\delta^{18}O$ isotope excursion (Ireviken Excursion).

Rhynchonelliformean brachiopods have a shell of low-Mg calcite. The potential of using brachiopod Mg/Ca as a palaeothermometer was clear after Cusack et al. (2008) had shown that Mg in brachiopods lies within the calcite crystal lattice. In addition some promising results were obtained with regards to the hypothesis of brachiopod calcite Mg/Ca being dependent on water temperature (Lee et al., 2004; Perez-Huerta et al., 2008; Yammamoto et al., 2010). Laser ablation was selected as the sampling method because it allowed specific targeting of the shell ultrastructure. As Perez-Huerta et al. (2008) had shown that the outer half of the secondary layer produced unreliable Mg/Ca values and Parkinson et al. (2005) had shown that the outer half of the secondary layer was out of oxygen isotopic equilibrium with ambient sea water, a method where the inside of the secondary layer/tertiary layer could be reliably targeted was imperative. Laser ablation allows very good accuracy and with ablation

tracks able to be drawn in any shape the curvature of the brachiopod shell was not a problem for this method.

The laser ablation methodology used in construction of temperature calibration curves for modern brachiopods is described in Chapter 3 and Butler et al. (2015). The brachiopod shell is sectioned longitudinally or transversely according to the information required. The advantages of sampling the brachiopod transversely in the anterior third of the shell are twofold. This area of the shell displays no vital effects (Perez-Hueta et al., 2008 Butler et al., 2015), except in some samples at the edges of the shell when the brachiopod was dying or senescent, therefore all values in this part of the shell can be deemed reliable after diagenetic screening (see discussion below) has taken place. In addition to this; because the line of section is perpendicular to the symmetry of the shell an internal check on the data is possible as a shell showing a truly temperature dependent Mg/Ca relationship would be expected to be symmetrical (Lee et al., 2004). The main disadvantage with sampling the shell transversely is that the full range of seasonal cycles will not be captured because not all the growth rings are sampled. Ontogenetic – longitudinal - sectioning allows data to be collected through the entirety of the brachiopod's life, and vital effects in the umbo and more juvenile areas of the shell can be assessed.

For the temperature calibration curve, the laser ablation method was applied to two modern brachiopod species, *Terebratulina retusa* from the Firth of Lorne, Scotland and *Liothyrella neozelanica* from a depth transect north of North Island, New Zealand. *Terebratulina* has a geological range from Upper Jurassic to Recent (Lee et al., 2006) and any calibration produced for this species would have great potential for reliable future fossil record use. *Liothyrella neozelanica* was selected because it lives in depths 100 m – 1500 m, and as a result tolerates a wide range of

temperatures. *Liothyrella* is also present through much of the Cenozoic on New Zealand, therefore also allowing any future calibration to be applied to the fossil record.

Diagenesis was recognised by investigating correlations between Mg/Ca and Al/Ca, Mg/Ca and Mn/C and finally Mg/Ca and Sr/Ca. Since any strong positive correlation noted for Al/Ca suggests that clays may be present (Barker et al., 2003), then all shells from that particular location were screened to a value where this strong positive correlation was no longer present. Mn/Ca was screened for on a shell by shell basis. Silurian *Atrypa* are among species of brachiopod that incorporate Mn/Ca into the crystal lattice of the shell in life, so that it is not always a product of diagenesis. Others, such as *Liothyrella*, do not, and a positive correlation in this species led to the shells being screened to values where the Mg/Ca and Mn/Ca no longer correlated.

Comparison was made of the trace metal laser ablation data against stable isotope data obtained by microdrilling. The limitations of this were that the very high spatial resolution Mg/Ca profiles, ~40 µm, had to be compared to low resolution ~ 1 mm stable isotope profiles. Hence the full range of temperatures shown in the Mg/Ca profiles was not seen in the $\delta^{18}O$ profiles as the peaks in Mg/Ca were between 100 and 400 µm wide. This could be improved on by using laser ablation analysis for stable isotopes as the Mg/Ca and stable isotope results would be easier to compare against each other. However, whilst this was a limitation of this study it did not detract from producing two reliable calibrations. The quality of the data produced here is higher than in in previous studies using laser ablation in brachiopods. Perez-Huerta et al. (2008 and 2011) used spots to produce their results rather than tracks; as such the spatial resolution was much lower than that in this study. It is recommended

that brachiopod shells are sampled using tracks rather than spots. This work highlights the benefits of using brachiopods for palaeoclimate studies. Whilst the two calibrations in this study are only the start of using Mg/Ca to assess seawater temperatures and palaeoseawater temperatures, they provide a real step forward in this field. Some previous brachiopod Mg/Ca studies (e.g. Powell et al., 2009) have used a bivalve (*Mytilus edulis*) Mg/Ca calibration (Vander Putten et al., 2000). The brachiopod Mg/Ca calibrations have a higher sensitivity than this bivalve linear calibration (Butler et al., 2015) and are strongly recommended for use in any future work.

7.2 Applying modern calibrations to the fossil record

The EOT was chosen as a potential time period for study because it is the first time in the Cenozoic that the presence of semi-permanent ice sheets on Antarctica is widely accepted (Zachos et al., 1996) and Late Eocene to Early Oligocene brachiopods from New Zealand allow study (Chapter 5). In addition, all previous seasonality studies for the EOT which span the transition itself are from the northern hemisphere (e.g. Ivany et al., 2000; Grimes et al., 2009; Wade et al., 2012). The seasonality study from the southern hemisphere, from Seymour island Antarctica (Dutton et al. 2002), does not have any data post the EOGM. This meant that the New Zealand brachiopods provided a unique opportunity to assess southern hemisphere seasonality across the EOT. Shell symmetry was used to identify reliable annual bands in transverse geochemical profiles (Chapter 5). The brachiopods were assessed for seasonality by using highest and lowest Mg/Ca in identified annual bands. This method provided more representative summer and winter temperatures as there was more than one seasonal cycle present in the *Liothyrella* shells. Taking the highest and lowest value from each shell would have artificially increased annual

seasonality. The Mg/Ca data from this study show that there is no change in seasonality over the EOT in New Zealand. However, there may have been a change in seasonality during the EOGM as this part of the geological record was not sampled; this study has a snapshot before at 34 – 34.5 Ma and after at 33 Ma. The surface ocean currents did not change over this time and the 1.3 ‰ change in the $\delta^{18}O$ data are a product of a 0.6 ‰ increase in global $\delta^{18}O_{seawater}$ (Lear et al., 2008) and a 0.7 ‰ increase in regional $\delta^{18}O_{seawater}$ partially due to increased brine rejection from sea ice around Antarctica (Goldner et al., 2014). Absolute sea water temperatures in the South Pacific are most likely represented by Mg/Ca derived temperatures as they are in good agreement with TEX_{86} derived temperatures (Bijl et al., 2009 and Hollis et al., 2009). The Mg/Ca and $\delta^{18}O$ data are not reconcilable with $\delta^{18}O$ derived temperature showing average temperatures lower than the winter Mg/Ca derived temperatures. This work could be expanded by more precise dating of sites in New Zealand: once that age model were in place then it would be possible to assess the changes in seasonality over a longer time period.

This study also highlights the usefulness of brachiopods in assessing seasonality. Unlike other organisms, such as bivalves or fish otoliths, which appear to cease growing in winter (Dutton et al., 2002; Ivany et al., 2000) brachiopods continue growing at temperatures as low as 6 °C if not lower (Butler et al., 2015). It is therefore recommended that brachiopods be used for future seasonality studies following the sampling method outlined in Chapter 3 and the seasonality method described in Chapter 5. The method allows the whole of a season to be taken into consideration and by taking the maximum and minimum values from an annual band there is no bias towards either summer or winter temperatures. This is important as

organisms where growth ceases will have data that are skewed and not representative of a full season.

The early Silurian Ireviken Excursion was chosen for investigation of using the methodology back in the mid Palaeozoic because there is a globally recognised $\delta^{13}C$ and $\delta^{18}O$ excursion at this time ~428 Ma (e.g. Azmy et al., 1998, Munnecke et al., 2003 and Brand et al., 2006). Brachiopods from Gotland are notably well preserved (Bassett and Cox, 1974) and provide an ideal opportunity to apply the brachiopod Mg/Ca calibrations to this event in the Silurian. The Mg/Ca proxy has not been applied to this event before. With a potential glaciation event at this time (Grahn and Caputo, 1992) it was problematic to establish whether the ~0.4 ‰ increase in $\delta^{18}O$ at low latitudes (Munnecke et al., 2003) or the ~2.5 ‰ increase at higher latitudes (Brand et al., 2006) are due to changes in temperature or changes in ice volume. The Mg/Ca data here identify no change in temperaure over the Ireviken Excursion, this is supported by $\delta^{18}O$ data which also show no change and agree with similar results obtained in a recent clumped isotope study (Cummins et al., 2014). This implies that there is no change in $\delta^{18}O$ or temperature over the Ireviken Excursion at low latitudes, casting doubt on the poorly defined ~0.4 ‰ excursion previously noted (Munnecke et al., 2003). Seasonal differences in Mg/Ca show that equatorial waters ~428 Ma have a similar temperature range 3.5 – 5.4 °C to the modern day equatorial temperature range of 4 °C (Wienders et al., 2000). $\delta^{18}O$ derived temperatures of ~37 °C are much lower and more realistic than previous studies (e.g. Azmy et al., 1998, Munnecke et al., 2003 and Brand et al., 2006).

This study has established that Mg/Ca in brachiopod shells can be used as a temperature proxy in the early Palaeozoic, which represents a step forward in palaeoclimate studies. The specifically targeted sampling in this study is much more

reliable than the method which required 'flaking off' secondary layer material which has been used in previous studies (e.g. Cummins et al., 2014). This along with the Mg/Ca brachiopod calibrations (Chapter 4) produce a more realistic estimate for early Palaeozoic ocean temperatures. Brand et al. (2006) produced temperature calibrations for the Ireviken Excursion that at ~52 °C were far too high. The more reasonable temperatures obtained here may be explained by the targeting of the inner part of the secondary layer, rather than throughout this layer. Parkinson et al., (2005) showed that the outer part of the secondary layer was out of oxygen isotopic equilibrium with the ambient sea water.

The Silurian Ireviken Excursion results show that Mg/Ca temperature records can add an independent temperature proxy to the Palaeozoic. It has been well documented that $\delta^{18}O$ temperatures from this far back may be unreliable, with many studies questioning whether diagenesis or micrite incorporation have reduced the $\delta^{18}O$ in brachiopod calcite and artificially increased the apparent water temperature (e.g. Cummins et al., 2014). With the correct sampling of Palaeozoic brachiopod shells, following sampling procedures outlined in Chapter 3 and discussed in Chapter 6, it has been possible not only to assess relative temperature changes in Mg/Ca but also to produce reasonable $\delta^{18}O$ temperatures (37 °C). While these temperatures are ~8 °C warmer than modern day equatorial water temperatures, they allow diverse benthic faunal communities and populations to exist.

7.3 Future work

More work needs to be carried out on improving the Mg/Ca temperature calibration especially at the higher and lower ends of the temperature range. Brachiopods from tropical sea mounds should be targeted for sampling for the upper end of this

temperature range. *Liothyrella uva* from Antarctica would be ideal for studying temperatures at the lower end providing their differing metabolism does not have an overriding vital effect influence on the Mg/Ca data (Peck, 1996).

With the ubiquity of *Liothyrella* in Eocene-Miocene sediments of North Otago, New Zealand a record of seasonal temperature change could be acquired from Eocene right through to the Pliocene. In one location, Old Rifle Butts, from the Miocene (Fordyce, 1981), *Liothyrella* are so abundant and dominant that it is possible to sample brachiopods from the stratigraphical succession at intervals < 10 cm, producing a very high resolution record that would allow a continuous assessment of seasonality. This would add to the understanding of temperatures in New Zealand throughout the Cenozoic and also how seasonality changed over the short term (hundreds to thousands of years) and long term (millions of years).

This research has opened up the exciting possibility of using Mg/Ca palaeothermometry on almost the whole of the Phanerozoic. With the excellent preservation shown by the brachiopods from Gotland, and questions raised over repeated climatic changes and stable isotope excursions through the Silurian (e.g. Calner et al., 2004; Cherns et al., 2013) , this methodology has obvious applications. Initial results suggest that the Ireviken Excursion, at least at low latitudes, was probably not associated with a change in seawater temperature across the stable isotope excursion, but it would be instructive to extend study to other $\delta^{13}C$ excursions (Mulde, Linde and Lau) to investigate any changes in temperature and seasonality; the Lau $\delta^{13}C$ isotope excursion is larger than the Ireviken one (Calner et al., 2004). If there is no change in seawater temperature over those other events, it would support the findings of this study and show that seawater temperature did not contribute to the $\delta^{13}C$ excursions of the Silurian.

Further work could also be carried out on seasonality across the Ireviken Excursion. As shown in Chapter 6 low latitude seasonal temperature differences were ~ 3.5 – 5.4 °C, but it would be beneficial to assess seasonality at higher latitudes. Specimens are available from high latitude sites such as Niagara Gorge and Anticosti Island, which show a much larger $\delta^{18}O$ excursion over the Ireviken Excursion, ~ 2.5 ‰ (Brand et al., 2006). The palaeotemperatures calculated for these sites seem extremely high at ~52 °C (Brand et al., 2006). Use of the laser ablation method for Mg/Ca and more targeted and reliable sampling of the brachiopods for $\delta^{18}O$ would enable estimates of palaeoseasonality to be made, confirm changes in the $\delta^{18}O$ and recalculate palaeotemperatures.

8. BIBLIOGRAPHY

Adams, C. G., D. E. Lee and B. R. Rosen (1990). "Conflicting isotopic and biotic evidence for tropical sea-surface temperatures during the Tertiary." Palaeogeography Palaeoclimatology Palaeoecology **77**(3-4): 289-313.

Aldridge, R. J., L. Jeppsson and K. J. Dorning (1993). "Early Silurian oceanic episodes and events." Journal of the Geological Society **150**: 501-513.

Allan, R. S. (1932). "The genus Liothyrella (Brachiopoda) in New Zealand." Trans and Proc New Zealand Inst **63**((1)): 1-10.

Anand, P., H. Elderfield and M. H. Conte (2003). "Calibration of Mg/Ca thermometry in planktonic foraminifera from a sediment trap time series." Paleoceanography **18**(2): 15.

Azmy, K., J. Veizer, M. G. Bassett and P. Copper (1998). "Oxygen and carbon isotopic composition of Silurian brachiopods: Implications for coeval seawater and glaciations." Geological Society of America Bulletin **110**(11): 1499-1512.

Barker, S., M. Greaves and H. Elderfield (2003). "A study of cleaning procedures used for foraminiferal Mg/Ca paleothermometry." Geochemistry, Geophysics, Geosystems **4**(9).

Basak, C. and E. E. Martin (2013). "Antarctic weathering and carbonate compensation at the Eocene-Oligocene transition." Nature Geoscience **6**(2): 121-124.

Bassett, M. G. and L. R. M. Cocks (1974). "A review of Silurian brachiopods from Gotland Sweden." Fossils and Strata(3): 1-56.

Batchelor, R. A. and L. Jeppsson (1994). "Late Llandovery bentonites from Gotland, Sweden, as chemostratigraphic Markers." Journal of the Geological Society **151**: 741-746.

Berggren, W. A., D. V. Kent, J. J. Flynn and J. A. Vancouvering (1985). "Cenozoic geochronology." Geological Society of America Bulletin **96**(11): 1407-1418.

Berner, R. A. (2004). "A model for calcium, magnesium and sulfate in seawater over Phanerozoic time." American Journal of Science **304**(5): 438-453.

Bijl, P. K., S. Schouten, A. Sluijs, G. J. Reichart, J. C. Zachos and H. Brinkhuis (2009). "Early Palaeogene temperature evolution of the southwest Pacific Ocean." Nature **461**(7265): 776-779.

Bijl, P. K., A. Sluijs and H. Brinkhuis (2013). "A magneto- and chemostratigraphically calibrated dinoflagellate cyst zonation of the early Palaeogene South Pacific Ocean." Earth-Science Reviews **124**: 1-31.

Brand, U. (2004). "Carbon, oxygen and strontium isotopes in Paleozoic carbonate components: an evaluation of original seawater-chemistry proxies." Chemical Geology **204**(1-2): 23-44.

Brand, U., K. Amy and J. Veizer (2006). "Evaluation of the Salinic I tectonic, Cancaniri glacial and Ireviken biotic events: Biochemostratigraphy of the lower Silurian succession in the Niagara Gorge area, Canada and USA." Palaeogeography Palaeoclimatology Palaeoecology **241**(2): 192-213.

Brand, U., K. Azmy, M. A. Bitner, A. Logan, M. Zuschin, R. Came and E. Ruggiero (2013). "Oxygen isotopes and MgCO3 in brachiopod calcite and a new paleotemperature equation." Chemical Geology **359**: 23-31.

Brand, U., R. E. Came, H. Affek, K. Azmy, R. Mooi and K. Layton (2014). "Climate-forced change in Hudson Bay seawater composition and temperature, Arctic Canada." Chemical Geology **388**: 78-86.

Brand, U., A. Logan, N. Hiller and J. Richardson (2003). "Geochemistry of modern brachiopods: applications and implications for oceanography and paleoceanography." Chemical Geology **198**(3-4): 305-334.

Brand, U. and J. Veizer (1980). "Chemical diagenesis of a multicomponent carbonate system .1. Trace-elements." Journal of Sedimentary Petrology **50**(4): 1219-1236.

Buening, N. and S. J. Carlson (1992). "Geochemical inevestigation of growth in selected Recent articulate brachiopods." Lethaia **25**(3): 331-345.

Buening, N., S. J. Carlson, H. J. Spero and D. E. Lee (1998). "Evidence for the Early Oligocene formation of a proto-Subtropical Convergence from oxygen isotope records of New Zealand Paleogene brachiopods." Palaeogeography Palaeoclimatology Palaeoecology **138**(1-4): 43-68.

Burgess, C. E., P. N. Pearson, C. H. Lear, H. E. G. Morgans, L. Handley, R. D. Pancost and S. Schouten (2008). "Middle Eocene climate cyclicity in the southern Pacific: Implications for global ice volume." Geology **36**(8): 651-654.

Butler, S., T. R. Bailey, C. H. Lear, G. B. Curry, L. Cherns and I. McDonald (2015). "The Mg/Ca–temperature relationship in brachiopod shells: Calibrating a potential palaeoseasonality proxy." Chemical Geology **397**(0): 106-117.

Calner, M., L. Jeppsson and A. Munnecke (2004). "The Silurian of Gotland " Erlanger Geologische Abhandlungen **Sonderband 5**.

Campbell, D. C. a. C., M. R. (2003). Biotic patterns in Eocene-Oligocene mollusks of the Atlantic Coastal Plain, U.S.A. From Greenhouse to Icehouse. D. R. Prothero, Ivany, L. C. and Nesbitt, E.A. New York, Columbia University Press.

Carpenter, S. J. and K. C. Lohmann (1995). "Delta-O-18 and Delta-C-13 Values of modern brachiopod shells." Geochimica Et Cosmochimica Acta **59**(18): 3749-3764.

Carroll, M. L., B. J. Johnson, G. A. Henkes, K. W. McMahon, A. Voronkov, W. G. Ambrose Jr and S. G. Denisenko (2009). "Bivalves as indicators of environmental variation and potential anthropogenic impacts in the southern Barents Sea." Marine Pollution Bulletin **59**(4–7): 193-206.

Chen, L., Y. S. Liu, Z. C. Hu, S. Gao, K. Q. Zong and H. H. Chen (2011). "Accurate determinations of fifty-four major and trace elements in carbonate by LA-ICP-MS using normalization strategy of bulk components as 100%." Chemical Geology **284**(3-4): 283-295.

Cherns, L. and J. R. Wheeley (2007). "A pre-Himantian (Late Ordovician) interval of global cooling - The Boda event re-assessed." Palaeogeography Palaeoclimatology Palaeoecology **251**(3-4): 449-460.

Cherns, L. and J. R. Wheeley (2009). "Early Palaeozoic cooling events: Peri-gondwana and beyond." Geological Society Special Publication **325**(1): 257-278.

Cherns, L., J. R. Wheeley, L. E. Popov, M. G. Pour, R. M. Owens and A. R. Hemsley (2013). "Long-period orbital climate forcing in the early Palaeozoic?" Journal of the Geological Society **170**(5): 707-710.

Chivas, A. R., P. Dedeckker and J. M. G. Shelley (1986). "Magnesium content of nonmarine ostracod shells - a new paleosalinometer and paleothermometer." Palaeogeography Palaeoclimatology Palaeoecology **54**(1-4): 43-61.

Clarkson, E. N. K. (1998). Invertebrate palaeontology and evolution. Cambridge, Blackwell Science.

Coggon, R. M., D. A. H. Teagle, C. E. Smith-Duque, J. C. Alt and M. J. Cooper (2010). "Reconstructing past seawater Mg/Ca and Sr/Ca from mid-ocean ridge flank calcium carbonate veins." Science **327**(5969): 1114-1117.

Committee, W. D. P. (2002). 2. World ocean circulation experiment global data, Version 3.0. Southampton, UK. , WOCE International Project Office. **WOCE Report No. 180/02**.

Cotton, L. J., P. N. Pearson and W. Renema (2014). "Stable isotope stratigraphy and larger benthic foraminiferal extinctions in the Melinau Limestone, Sarawak." Journal of Asian Earth Sciences **79**: 65-71.

Coxall, H. K. and P. N. Pearson (2007). "The Eocene-Oligocene Transition." Deep-Time Perspectives on Climate Change: Marrying the Signal from Computer Models and Biological Proxies: 351-387.

Coxall, H. K. and P. A. Wilson (2011). "Early Oligocene glaciation and productivity in the eastern equatorial Pacific: Insights into global carbon cycling." Paleoceanography **26**: 18.

Coxall, H. K., P. A. Wilson, H. Palike, C. H. Lear and J. Backman (2005). "Rapid stepwise onset of Antarctic glaciation and deeper calcite compensation in the Pacific Ocean." Nature **433**(7021): 53-57.

Cramer, B. D. and M. R. Saltzman (2005). "Sequestration of C-12 in the deep ocean during the early Wenlock (Silurian) positive carbon isotope excursion." Palaeogeography Palaeoclimatology Palaeoecology **219**(3-4): 333-349.

Cramer, B. D. and M. R. Saltzman (2007a). "Early Silurian paired delta C-13(carb) and delta C-13(org) analyses from the Midcontinent of North America: Implications for paleoceanography and paleoclimate." Palaeogeography Palaeoclimatology Palaeoecology **256**(3-4): 195-203.

Cramer, B. D. and M. R. Saltzman (2007b). "Fluctuations in epeiric sea carbonate production during Silurian positive carbon isotope excursions: A review of proposed paleoceanographic models." Palaeogeography Palaeoclimatology Palaeoecology **245**(1-2): 37-45.

Cummins, R. C., S. Finnegan, D. A. Fike, J. M. Eiler and W. W. Fischer (2014). "Carbonate clumped isotope constraints on Silurian ocean temperature and seawater delta O-18." Geochimica Et Cosmochimica Acta **140**: 241-258.

Curry, G. B. (1982). "Ecology and population-strucutre of the Recent brachiopod Terebratulina from Scotland." Palaeontology **25**(APR): 227-246.

Cusack, M., Y. Dauphin, P. Chung, A. Perez-Huerta and J. P. Cuif (2008b). "Multiscale structure of calcite fibres of the shell of the brachiopod Terebratulina retusa." Journal of Structural Biology **164**(1): 96-100.

Cusack, M., D. Parkinson, A. Perez-Huerta, J. England, G. B. Curry and A. E. Fallick (2008a). "Relationship between delta O-18 and minor element composition of Terebratalia transversa." Earth and Environmental Science Transactions of the Royal Society of Edinburgh **98**: 443-449.

Cusack, M., A. Perez-Huerta, M. Janousch and A. A. Finch (2008c). "Magnesium in the lattice of calcite-shelled brachiopods." Chemical Geology **257**(1-2): 59-64.

Dalman, J. W. (1828). " Uppställning och Beskrifning af de i Sverige funne Terebratuliter." Kongliga Svenska Vetenskapsakademien Handlingar for År **1827**: 85-155.

DeConto, R. M. and D. Pollard (2003a). "A coupled climate-ice sheet modeling approach to the Early Cenozoic history of the Antarctic ice sheet." Palaeogeography Palaeoclimatology Palaeoecology **198**(1-2): 39-52.

DeConto, R. M. and D. Pollard (2003b). "Rapid Cenozoic glaciation of Antarctica induced by declining atmospheric CO2." Nature **421**(6920): 245-249.

DeConto, R. M., D. Pollard, P. A. Wilson, H. Palike, C. H. Lear and M. Pagani (2008). "Thresholds for Cenozoic bipolar glaciation." Nature **455**(7213): 652-U652.

Demicco, R. V., T. K. Lowenstein, L. A. Hardie and R. J. Spencer (2005). "Model of seawater composition for the Phanerozoic." Geology **33**(11): 877-880.

Dickson, J. A. D. (2004). "Echinoderm skeletal preservation: Calcite-aragonite seas and the Mg/Ca ratio of phanerozoic oceans." Journal of Sedimentary Research **74**(3): 355-365.

Dockery, D. T. a. L., P. (2003). Molluscan faunas across the Eocene-Oligocene boundary in the North American Gulf Coastal Plain, with comparisons to those of the Eocene and Oligocene of France. From Greenhouse to Ice House. D. R. Prothero, Ivany, L. C. and Nesbitt, E.A. New York, Columbia University Press.

Dunkley Jones, T., D. J. Lunt, D. N. Schmidt, A. Ridgwell, A. Sluijs, P. J. Valdes and M. Maslin (2013). "Climate model and proxy data constraints on ocean warming across the Paleocene–Eocene Thermal Maximum." Earth-Science Reviews **125**(0): 123-145.

Dutton, A. L., K. C. Lohmann and W. J. Zinsmeister (2002). "Stable isotope and minor element proxies for Eocene climate of Seymour Island, Antarctica." Paleoceanography **17**(2): 13.

Dwyer, G. S., T. M. Cronin, P. A. Baker, M. E. Raymo, J. S. Buzas and T. Correge (1995). "North-Atlantic deep-water temperature-change during Late Pliocene and Late Quaternary climatic cycles." Science **270**(5240): 1347-1351.

Edwards, A. R. (1991). "The Oamaru Diatomite." New Zealand Geological Survey Paleontological Bulletin(64): 1-260.

Egan, K. E., R. E. M. Rickaby, K. R. Hendry and A. N. Halliday (2013). "Opening the gateways for diatoms primes Earth for Antarctic glaciation." Earth and Planetary Science Letters **375**: 34-43.

Elderfield, H., J. Yu, P. Anand, T. Kiefer and B. Nyland (2006). "Calibrations for benthic foraminiferal Mg/Ca paleothermometry and the carbonate ion hypothesis." Earth and Planetary Science Letters **250**(3–4): 633-649.

Eldrett, J. S., D. R. Greenwood, I. C. Harding and M. Huber (2009). "Increased seasonality through the Eocene to Oligocene transition in northern high latitudes." Nature **459**(7249): 969-U991.

England, J., M. Cusack and M. R. Lee (2007). "Magnesium and sulphur in the calcite shells of two brachiopods, Terebratulina retusa and Novocrania anomala." Lethaia **40**(1): 2-10.

Evans, D. and W. Muller (2012). "Deep time foraminifera Mg/Ca paleothermometry: Nonlinear correction for secular change in seawater Mg/Ca." Paleoceanography **27**: 11.

Farkas, J., F. Bohm, K. Wallmann, J. Blenkinsop, A. Eisenhauer, R. van Geldern, A. Munnecke, S. Voigt and J. Veizer (2007). "Calcium isotope record of Phanerozoic oceans: Implications for chemical evolution of seawater and its causative mechanisms." Geochimica Et Cosmochimica Acta **71**(21): 5117-5134.

Finnegan, S., K. Bergmann, J. M. Eiler, D. S. Jones, D. A. Fike, I. Eisenman, N. C. Hughes, A. K. Tripati and W. W. Fischer (2011). "The magnitude and duration of Late Ordovician-Early Silurian glaciation." Science **331**(6019): 903-906.

Fordyce, R. E. (1981). "Redescription of Early Miocene dolphin Phocaenopsis mantelli Huxley, 1859 (Odontoceti incertae sedis)." New Zealand Journal of Geology and Geophysics **24**(4): 563-568.

Foster, G. L. (2008). "Seawater pH, PCO2 and CO32- variations in the Caribbean Sea over the last 130 kyr: A boron isotope and B/Ca study of planktic forminifera." Earth and Planetary Science Letters **271**(1-4): 254-266.

Gage, M. (1957). "The Geology of Waitaki Subdivision " N.Z Geological Survery Bulletin **55**.

Gallagher, T. M. and N. D. Sheldon (2013). "A new paleothermometer for forest paleosols and its implications for Cenozoic climate." Geology **41**(6): 647-650.

Gasson, E., D. J. Lunt, R. DeConto, A. Goldner, M. Heinemann, M. Huber, A. N. LeGrande, D. Pollard, N. Sagoo, M. Siddall, A. Winguth and P. J. Valdes (2014). "Uncertainties in the modelled CO2 threshold for Antarctic glaciation." Climate of the Past **10**(2): 451-466.

Goldner, A., N. Herold and M. Huber (2014). "Antarctic glaciation caused ocean circulation changes at the Eocene-Oligocene transition." Nature **511**(7511): 574-+.

Grahn, Y. and M. V. Caputo (1992). "Early Silurian glaciations in Brazil." Palaeogeography Palaeoclimatology Palaeoecology **99**(1-2): 9-15.

Grantham, B. (1983). Firth of Lorne Study, Reports 1 and 2. Oban.

Grantham, B., D. Boyd, R. Gowen, J. Lewis and A. Weeks (1983a). Firth of Lorne Study. Report 3. Oban.

Grantham, B., A. Chadwick and J. Shaw (1983b). Firth of Lorne Study. Report 4. Oban.

Grimes, S. T., J. J. Hooker, M. E. Collinson and D. P. Mattey (2005). "Summer temperatures of late Eocene to early Oligocene freshwaters." Geology **33**(3): 189-192.

Grossman, E. L., H. S. Mii and T. E. Yancey (1993). "Stable isotopes in Late Pennsylvanian brachiopods from the United-States - implications for Carboniferous paleoceanography." Geological Society of America Bulletin **105**(10): 1284-1296.

Grossman, E. L., H. S. Mii, C. L. Zhang and T. E. Yancey (1996). "Chemical variation in Pennsylvanian brachiopod shells - Diagenetic, taxonomic, microstructural, and seasonal effects." Journal of Sedimentary Research **66**(5): 1011-1022.

Grossman, E. L., T. E. Yancey, T. E. Jones, P. Bruckschen, B. Chuvashov, S. J. Mazzullo and H. S. Mii (2008). "Glaciation, aridification, and carbon sequestration in the Permo-Carboniferous: The isotopic record from low latitudes." Palaeogeography Palaeoclimatology Palaeoecology **268**(3-4): 222-233.

Hansen, J. (2008). "Target atmospheric CO2: Where should humanity aim?" Open Atmospheric Science Journal **2**: 217-231.

Hasiuk, F. J. and K. C. Lohmann (2010). "Application of calcite Mg partitioning functions to the reconstruction of paleocean Mg/Ca." Geochimica Et Cosmochimica Acta **74**(23): 6751-6763.

Hede, J. (1960). The Silurian of Gotland. The Lower Palaeozoic of Scania, 44-89. Guide to Excursions A22 and C17, 21st International Geological Congress, Norden 1960. G. Regnell and J. E. Hede**:** 44-89.

Hemming, N. G. and G. N. Hanson (1992). "Boron isotopic composition and concentration in modern marine carbonates." Geochimica Et Cosmochimica Acta **56**(1): 537-543.

Hill, D. J., A. M. Haywood, P. J. Valdes, J. E. Francis, D. J. Lunt, B. S. Wade and V. C. Bowman (2013). "Paleogeographic controls on the onset of the Antarctic circumpolar current." Geophysical Research Letters **40**(19): 5199-5204.

Hollis, C. J., L. Handley, E. M. Crouch, H. E. G. Morgans, J. A. Baker, J. Creech, K. S. Collins, S. J. Gibbs, M. Huber, S. Schouten, J. C. Zachos and R. D. Pancost (2009). "Tropical sea temperatures in the high-latitude South Pacific during the Eocene." Geology **37**(2): 99-102.

Hollis, C. J., K. W. R. Taylor, L. Handley, R. D. Pancost, M. Huber, J. B. Creech, B. R. Hines, E. M. Crouch, H. E. G. Morgans, J. S. Crampton, S. Gibbs, P. N. Pearson and J. C. Zachos (2012). "Early Paleogene temperature history of the Southwest Pacific Ocean: Reconciling proxies and models." Earth and Planetary Science Letters **349**: 53-66.

Holt, N. M., J. Garcia-Veigas, T. K. Lowenstein, P. S. Giles and S. Williams-Stroud (2014). "The major-ion composition of Carboniferous seawater." Geochimica Et Cosmochimica Acta **134**: 317-334.

Horita, J., H. Zimmermann and H. D. Holland (2002). "Chemical evolution of seawater during the Phanerozoic: Implications from the record of marine evaporites." Geochimica et Cosmochimica Acta **66**(21): 3733-3756.

Hren, M. T., N. D. Sheldon, S. T. Grimes, M. E. Collinson, J. J. Hooker, M. Bugler and K. C. Lohmann (2013). "Terrestrial cooling in Northern Europe during the

Eocene-Oligocene transition." Proceedings of the National Academy of Sciences of the United States of America **110**(19): 7562-7567.

Huber, M., H. Brinkhuis, C. E. Stickley, K. Doos, A. Sluijs, J. Warnaar, S. A. Schellenberg and G. L. Williams (2004). "Eocene circulation of the Southern Ocean: Was Antarctica kept warm by subtropical waters?" Paleoceanography **19**(4).

Huber, M. and D. Nof (2006). "The ocean circulation in the southern hemisphere and its climatic impacts in the Eocene." Palaeogeography Palaeoclimatology Palaeoecology **231**(1-2): 9-28.

Hughes, J. M., D. J. Schmidt, J. I. Macdonald, J. A. Huey and D. A. Crook (2014). "Low interbasin connectivity in a facultatively diadromous fish: evidence from genetics and otolith chemistry." Molecular Ecology **23**(5): 1000-1013.

Hughes, W. W., G. D. Rosenberg and R. D. Tkachuck (1988). "Growth increments in the shell of the living Brachiopod Terebratalia-Transversa." Marine Biology **98**(4): 511-518.

Huxley, T. H. (1869). An introduction to the classification of animals. London, John Churchill & Sons.

Ivany, L. C., W. P. Patterson and K. C. Lohmann (2000). "Cooler winters as a possible cause of mass extinctions at the eocene/oligocene boundary." Nature **407**(6806): 887-890.

Jaanusson, V. (1979). Introduction. Lower Wenlock Faunal and Floral Dynamics - Vattenfallet Section, Gotland. V. Jaanusson, S. Laufeld and R. Skoglund, Sveriges Geologiska Undersokning. **C762:** 7-38.

Jaramillo-Vogel, D., A. Strasser, G. Frijia and S. Spezzaferri (2013). "Neritic isotope and sedimentary records of the Eocene-Oligocene greenhouse-icehouse transition: The Calcare di Nago Formation (northern Italy) in a global context." Palaeogeography Palaeoclimatology Palaeoecology **369**: 361-376.

Jeppsson, L. (1983). "Silurian conodont faunas from Gotland." Fossils and Strata **15**: 121-144.

Jeppsson, L. (1990). "An oceanic model for lithological and faunal changes, tested on the Silurian record." Journal of the Geological Society **147**: 663-674.

Jeppsson, L. (1996). "Recognition of a probable secundo-primo event in the Early Silurian." Lethaia **29**(4): 311-315.

Jeppsson, L. (1997a). "A new latest Telychian, Sheinwoodian and Early Homerian (Early Silurian) standard conodont zonation." Transactions of the Royal Society of Edinburgh-Earth Sciences **88**: 91-114.

Jeppsson, L. (1997b). The anatomy of the mid-Early Silurian Ireviken Event. Paleontological Events: Stratigraphic, Ecological, and Evolutionary Implications,. C.

E. Brett and G. C. Baird. New York, Paleontological Events: Stratigraphic, Ecological, and Evolutionary Implications,**:** 451-492.

Jeppsson, L., M. E. Eriksson and M. Calner (2006). "A latest Llandovery to latest Ludlow high-resolution biostratigraphy based on the Silurian of Gotland - a summary." Gff **128**: 109-114.

Jimenez-Lopez, C., C. S. Romanek, F. J. Huertas, H. Ohmoto and E. Caballero (2004). "Oxygen isotope fractionation in synthetic magnesian calcite." Geochimica Et Cosmochimica Acta **68**(16): 3367-3377.

Joachimski, M. M., R. van Geldern, S. Breisig, W. Buggisch and J. Day (2004). "Oxygen isotope evolution of biogenic calcite and apatite during the Middle and Late Devonian." International Journal of Earth Sciences **93**(4): 542-553.

Johnson, M. E., B. G. Baarli, H. Nestor, M. Rubel and D. Worsley (1991). "Eustatic sea-level patterns from the Lower Silurian (Llandovery Series) of southern Norway and Estonia." Geological Society of America Bulletin **103**(3): 315-335.

Kaljo, D., V. Grytsenko, T. Martma and M. A. Motus (2007). "Three global carbon isotope shifts in the Silurian of Podolia (Ukraine): stratigraphical implications." Estonian Journal of Earth Sciences **56**(4): 205-220.

Kaljo, D., T. Kiipli and T. Martma (1997). "Carbon isotope event markers through the Wenlock-Pridoli sequence at Ohesaare (Estonia) and Priekule (Latvia)." Palaeogeography Palaeoclimatology Palaeoecology **132**(1-4): 211-223.

Katz, A. (1973). "Interaction of magnesium with calcite during crystal-growth at 25-90 degrees C and one atmosphere." Geochimica Et Cosmochimica Acta **37**(6)

Katz, M. E., K. G. Miller, J. D. Wright, B. S. Wade, J. V. Browning, B. S. Cramer and Y. Rosenthal (2008). "Stepwise transition from the Eocene greenhouse to the Oligocene icehouse." Nature Geoscience **1**(5): 329-334.

Klein, R. T., K. C. Lohmann and C. W. Thayer (1996). "Bivalve skeletons record sea-surface temperature and delta O-18 via Mg/Ca and O-18/O-16 ratios." Geology **24**(5): 415-418.

Knauth, L. P. and M. J. Kennedy (2009). "The late Precambrian greening of the Earth." Nature **460**(7256): 728-732.

Knorr, G. and G. Lohmann (2014). "Climate warming during Antarctic ice sheet expansion at the Middle Miocene transition." Nature Geoscience **7**(5): 376-381.
Kroopnick, P. M., R. F. Weiss and H. Craig (1972). "Total CO2, 13C, and Dissolved Oxygen-18 at GEOSECS II in the North Atlantic." Earth and Planetary Science Letters **16**: 103-110.

Kump, L. R., M. A. Arthur, M. E. Patzkowsky, M. T. Gibbs, D. S. Pinkus and P. M. Sheehan (1999). "A weathering hypothesis for glaciation at high atmospheric

pCO(2) during the Late Ordovician." Palaeogeography Palaeoclimatology Palaeoecology **152**(1-2): 173-187.

Larsson, K. (1979). "Silurian Tentaculitids from Gotland and Scania." Fossils and Strata **11**: 1-180.

Laufeld, S. (1974). "Silurian Chitinozoa from Gotland Sweden." Fossils and Strata(5): 1-130.

Lear, C. H. (2007). Mg/Ca palaeothermometry: A new window into Cenozoic climate change. Deep time perspectives on climate change: marrying the signal from computer models and biological proxies. M. Williams, Hayward, A. M., Gregory, F. J. and Schmidt, D. N. . London.

Lear, C. H., Bailey, T., Pearson, P.N., Coxall, H.K. and Rosenthal, Y. (2008). "Cooling and ice growth across the Eocene-Oligocene Transition." Geology **36**(3): 251-254.

Lear, C. H., H. Elderfield and P. A. Wilson (2000). "Cenozoic deep-sea temperatures and global ice volumes from Mg/Ca in benthic foraminiferal calcite." Science **287**(5451): 269-272.

Lear, C. H., E. M. Mawbey and Y. Rosenthal (2010). "Cenozoic benthic foraminiferal Mg/Ca and Li/Ca records: Toward unlocking temperatures and saturation states." Paleoceanography **25**.

Lear, C. H. and Y. Rosenthal (2006). "Benthic foraminiferal Li/Ca: Insights into Cenozoic seawater carbonate saturation state." Geology **34**(11): 985-988.

Lear, C. H., Y. Rosenthal and N. Slowey (2002). "Benthic foraminiferal Mg/Ca-paleothermometry: a revised core-top calibration." Geochimica Et Cosmochimica Acta **66**(19): 3375-3387.

Lear, C. H., Rosenthal, Y., Coxall, H. K. and Wilson, P.A. (2004). "Late Eocene to Early Miocene ice sheet dynamics and the global carbon cycle." Paleoceanography **19**.

Lecuyer, C. and P. Allemand (1999). "Modelling of the oxygen isotope evolution of seawater: Implications for the climate interpretation of the delta O-18 of marine sediments." Geochimica Et Cosmochimica Acta **63**(3-4): 351-361.

Lee, D. E. (1986). Paleoecology and biogeogrpahy of the New Zealand paleogene brachiopod fauna. Les Brachiopod Fossiles et Actuels. P. R. Racheboeuf and C. C. Emig**:** 477-483.

Lee, D. E. and J. D. Campbell (1987). "Cenozoic records of the genus Lingula." Brachiopoda: Inarticulata in New Zealand. Journal of the Royal Society of New Zealand **17**: 17-30.

Lee, D. E., D. I. Mackinnon, T. N. Smirnova, P. G. Baker, J. Yu-Gan and S. Dong-LI (2006). Terebratulida. Treatise on Invertebrate Paleontology Brachiopoda (Part H) Revised. R. L. Kaesler, Geological Society of America. **5**.

Lee, X. Q., R. Z. Hu, U. Brand, H. Zhou, X. M. Liu, H. L. Yuan, C. L. Yan and H. G. Cheng (2004). "Ontogenetic trace element distribution in brachiopod shells: an indicator of original seawater chemistry." Chemical Geology **209**(1-2): 49-65.

LeGrande, A. N. and G. A. Schmidt (2006). "Global gridded data set of the oxygen isotopic composition in seawater." Geophysical Research Letters **33**(12): 5.

Lehnert, O., P. Mannik, M. M. Joachimski, M. Calner and J. Fryda (2010). "Palaeoclimate perturbations before the Sheinwoodian glaciation: A trigger for extinctions during the 'Ireviken Event'." Palaeogeography Palaeoclimatology Palaeoecology **296**(3-4): 320-331.

Lindstrom, G. (1884). On the Silurian gastropoda and pteropoda of Gotland. Stockholm, P.A. Norstedt.

Linnaeus [Linné], C. (1758). Systema Naturae. 10th ed. sive Regna tria Naturae systematicae proposita per Classes, Ordines. Stockholm, Holmiae.

Liu, Z. F., S. T. Tuo, Q. H. Zhao, X. R. Cheng and W. Huang (2004). "Deep-water earliest oligocene glacial maximum (EOGM) in South Atlantic." Chinese Science Bulletin **49**(20): 2190-2197.

Livermore, R., C. D. Hillenbrand, M. Meredith and G. Eagles (2007). "Drake Passage and Cenozoic climate: An open and shut case?" Geochemistry Geophysics Geosystems **8**: 11.

Logan, A. (2007). Geographic distribution of extant articulated brachiopods. Treatise on Invertebrate Paleontology Brachiopoda (Part H6) Revised. P. Selden, Geological Society of America.

Lowenstam, H. A. (1961). "Mineralogy, O-18/O-16 Ratios, and Strontium AND Magnesium Contents of Recent and Fossil Brachiopods and Their Bearing on the History of the Oceans." Journal of Geology **69**(3): 241-260.

Lowenstein, T. K., M. N. Timofeeff, S. T. Brennan, L. A. Hardie and R. V. Demicco (2001). "Oscillations in Phanerozoic seawater chemistry: Evidence from fluid inclusions." Science **294**(5544): 1086-1088.

Loydell, D. K. (2007). Graptolites from the Upper Ordovician and Lower Silurian of Jordan. Graptolites from the Upper Ordovician and Lower Silurian of Jordan, Palaeontological Assoc, C/O Dr Tim Palmer, I G E S , Univ Uk, Aberystwyth Sy23 3db, Uk.

Martinsson, A. (1967). "The succession and correlation of Ostracode faunas in the Silurian of Gotland." Geol Foren Stockholm Forh **89**((3)): 350-386.

McLaughlin, P. I., P. Emsbo and C. E. Brett (2012). "Beyond black shales: The sedimentary and stable isotope records of oceanic anoxic events in a dominantly oxic basin (Silurian; Appalachian Basin, USA)." Palaeogeography Palaeoclimatology Palaeoecology **367**: 153-177.

Merico, A., T. Tyrrell and P. A. Wilson (2008). "Eocene/Oligocene ocean de-acidification linked to Antarctic glaciation by sea-level fall." Nature **452**(7190): 979-U976.

Mii, H. S. and E. L. Grossman (1994). "Late Pennsylvanian seasonality reflected in the O-18 and elemental composition of a brachiopod shell." Geology **22**(7): 661-664.

Mii, H. S., E. L. Grossman and T. E. Yancey (1999). "Carboniferous isotope stratigraphies of North America: Implications for Carboniferous paleoceanography and Mississippian glaciation." Geological Society of America Bulletin **111**(7): 960-973.

Miller, K. G., J. D. Wright and R. G. Fairbanks (1991). "Unlocking the ice house - Oligocene-Miocene oxygen isotopes, eustacy, and margain erosion." Journal of Geophysical Research-Solid Earth and Planets **96**(B4): 6829-6848.

Mitsuguchi, T., P. X. Dang, H. Kitagawa, T. Uchida and Y. Shibata (2008). "Coral Sr/Ca and Mg/Ca records in Con Dao Island off the Mekong Delta: Assessment of their potential for monitoring ENSO and East Asian monsoon." Global and Planetary Change **63**(4): 341-352.

Montagna, P., M. McCulloch, C. Mazzoli, S. Silenzi and R. Odorico (2007). "The non-tropical coral Cladocora caespitosa as the new climate archive for the Mediterranean: high-resolution (~weekly) trace element systematics." Quaternary Science Reviews **26**(3–4): 441-462.

Moore, T. C., B. S. Wade, T. Westerhold, A. M. Erhardt, H. K. Coxall, J. Baldauf and M. Wagner (2014). "Equatorial Pacific productivity changes near the Eocene-Oligocene boundary." Paleoceanography **29**(9): 825-844.

Mouchi, V., M. de Rafélis, F. Lartaud, M. Fialin and E. Verrecchia (2013). "Chemical labelling of oyster shells used for time-calibrated high-resolution Mg/Ca ratios: A tool for estimation of past seasonal temperature variations." Palaeogeography, Palaeoclimatology, Palaeoecology **373**(0): 66-74.

Muehlenbachs, K. (1998). "The oxygen isotopic composition of the oceans, sediments and the seafloor." Chemical Geology **145**(3-4): 263-273.

Muehlenbachs, K., H. Furnes, H. C. Fonneland and B. Hellevang (2003). Ophiolites as faithful records of the oxygen isotope ratio of ancient seawater: The Solund-Stavfjord Ophiolite Complex as a Late Ordovician example. Ophiolites in Earth History. Y. Dilek and P. T. Robinson. Bath, Geological Soc Publishing House. **218:** 401-414.

Munnecke, A., C. Samtleben and T. Bickert (2003). "The ireviken event in the lower Silurian of Gotland, Sweden relation to similar palaeozoic and proterozoic events." Palaeogeography Palaeoclimatology Palaeoecology **195**(1-2): 99-124.

Munnecke, A., T. Servais and D. Vachard (2000). "A new family of calcareous microfossils from the Silurian of Gotland, Sweden." Palaeontology **43**: 1153-1172.

Murray, J. W. (1991). Ecology and palaeoecology of benthic formainifera. New York, Longman.

Nestor, V., R. Einasto and D. K. Loydell (2002). "Chitinozoan biostratigraphy and lithological characteristics of the Lower and Upper Visby boundary beds in the Ireviken 3 Section, northwest Gotland." Proceedings of the Estonian Academy of Sciences, Geology **51**: 215-226.

Nurnberg, D., J. Bijma and C. Hemleben (1996). "Assessing the reliability of magnesium in foraminiferal calcite as a proxy for water mass temperatures (vol 60, pg 803, 1995)." Geochimica Et Cosmochimica Acta **60**(13): 2483-2483.

Pagani, M., J. C. Zachos, K. H. Freeman, B. Tipple and S. Bohaty (2005). "Marked decline in atmospheric carbon dioxide concentrations during the Paleogene." Science **309**(5734): 600-603.

Page, A. A., J. A. Zalasiewicz, M. Williams and L. E. Popov (2007). Were transgressive black shales a negative feedback modulating glacioeustasy in the Early Palaeozoic Icehouse?, Geological Soc Publishing House, Unit 7, Brassmill Enterprise Ctr, Brassmill Lane, Bath Ba1 3jn, Avon, Uk.

Palike, H., J. Frazier and J. C. Zachos (2006). "Extended orbitally forced palaeoclimatic records from the equatorial Atlantic Ceara Rise." Quaternary Science Reviews **25**(23-24): 3138-3149.

Parag, H. A. (1987). "Effect of heat shock on protein degredation in mammalian cells." EMBO Journal **6**: 55-61.

Parkinson, D., G. B. Curry, M. Cusack and A. E. Fallick (2005). "Shell structure, patterns and trends of oxygen and carbon stable isotopes in modern brachiopod shells." Chemical Geology **219**(1-4): 193-235.

Pawlowski, J., M. Holzmann, C. Berney, J. Fahrni, A. J. Gooday, T. Cedhagen, A. Habura and S. S. Bowser (2003). "The evolution of early Foraminifera." Proceedings of the National Academy of Sciences of the United States of America **100**(20): 11494-11498.

Pearson, P. N. (2010). "Increased atmospheric CO2 During the Middle Eocene." Science **330**(6005): 763-764.

Pearson, P. N., G. L. Foster and B. S. Wade (2009). "Atmospheric carbon dioxide through the Eocene–Oligocene climate transition." Nature **461**(7267): 1110-1113.

Pearson, P. N., I. K. McMillan, B. S. Wade, T. Dunkley Jones, H. K. Coxall, P. R. Bown and C. H. Lear (2008). "Extinction and environmental change across the Eocene-Oligocene boundary in Tanzania." Geology **36**(2): 179-182.

Perez-Huerta, A., A. E. Aldridge, K. Endo and T. E. Jeffries (2014). "Brachiopod shell spiral deviations (SSD): Implications for trace element proxies." Chemical Geology **374**: 13-24.

Perez-Huerta, A., M. Cusack and P. Dalbeck (2011). "Crystallographic contribution to the vital effect in biogenic carbonates Mg/Ca thermometry." Earth and Environmental Science Transactions of the Royal Society of Edinburgh **102**: 35-41.

Perez-Huerta, A., M. Cusack, T. E. Jeffries and C. T. Williams (2008). "High resolution distribution of magnesium and strontium and the evaluation of Mg/Ca thermometry in Recent brachiopod shells." Chemical Geology **247**(1-2): 229-241.

Popp, B. N., T. F. Anderson and P. A. Sandberg (1986). "Brachiopods as indicators of original isotopic compositions in some palaeozoic limestones." Geological Society of America Bulletin **97**(10): 1262-1269.

Powell, M. G., B. R. Schone and D. E. Jacob (2009). "Tropical marine climate during the late Paleozoic ice age using trace element analyses of brachiopods." Palaeogeography Palaeoclimatology Palaeoecology **280**(1-2): 143-149.

Prentice, M. L. and R. K. Matthews (1991). "Tertiary ice-sheet dyanamics - the snow gun hypothesis." Journal of Geophysical Research-Solid Earth and Planets **96**(B4): 6811-6827.

Pusz, A. E., R. C. Thunell and K. G. Miller (2011). "Deep water temperature, carbonate ion, and ice volume changes across the Eocene-Oligocene climate transition." Paleoceanography **26**: 15.

Ramskold, L. (1985). "Silurian Phacopid and Dalmanitid Trilobites from Gotland " Stockholm Contributions in Geology **40**: 1-62.

Richardson, J. R. (1981). "Distribution and orientation of 6 atriculate brachiopod species from New-Zealand." New Zealand Journal of Zoology **8**(2): 189-196.

Ries, J. B. (2010). "Review: geological and experimental evidence for secular variation in seawater Mg/Ca (calcite-aragonite seas) and its effects on marine biological calcification." Biogeosciences **7**(9): 2795-2849.

Rosenberg, G. D., W. W. Hughes and R. D. Tkachuck (1988). "Intermediary metabolism and shell growth in the brachiopod Terebratalia-Transversa." Lethaia **21**(3): 219-230.

Rosenthal, Y., E. A. Boyle and N. Slowey (1997). "Temperature control on the incorporation of magnesium, strontium, fluorine, and cadmium into benthic foraminiferal shells from Little Bahama Bank: Prospects for thermocline paleoceanography." Geochimica Et Cosmochimica Acta **61**(17): 3633-3643.

Rowell A.J. and Grant, R. E. (1987). Phylum Brachiopoda. Fossil Invertebrates. R. S. Boardman, Cheetham, A.H. and Rowell A.J.,. Oxford, Blackwell Scientific.

Samtleben, C., A. Munnecke and T. Bickert (2000). "Development of facies and C/O-isotopes in transects through the Ludlow of Gotland: Evidence for global and local influences on a shallow-marine environment." Facies **43**: 1-38.

Samtleben, C., A. Munnecke, T. Bickert and J. Patzold (1996). "The Silurian of Gotland (Sweden). Facies interpretation based on stable isotopes in brachiopod shells." Geologische Rundschau **85**(278-292).

Sarkar, A., S. Sarangi, S. K. Bhattacharya and A. K. Ray (2003). "Carbon isotopes across the Eocene-Oligocene boundary sequence of Kutch, western India: Implications to oceanic productivity and pCO(2) change." Geophysical Research Letters **30**(11): 4.

Schmahl, W. W., E. Griesshaber, R. Neuser, A. Lenze, R. Job and U. Brand (2004). "The microstructure of the fibrous layer of terebratulide brachiopod shell calcite." European Journal of Mineralogy **16**(4): 693-697.

Sosdian, S., D. K. Gentry, C. H. Lear, E. L. Grossman, D. Hicks and Y. Rosenthal (2006). "Strontium to calcium ratios in the marine gastropod Conus ermineus: Growth rate effects and temperature calibration." Geochemistry Geophysics Geosystems **7**.

Sosdian, S. M., C. H. Lear, K. Tao, E. L. Grossman, A. O'Dea and Y. Rosenthal (2012). "Cenozoic seawater Sr/Ca evolution." Geochemistry Geophysics Geosystems **13**: 23.

Stanley, S. M. and L. A. Hardie (1998). "Secular oscillations in the carbonate mineralogy of reef-building and sediment-producing organisms driven by tectonically forced shifts in seawater chemistry." Palaeogeography Palaeoclimatology Palaeoecology **144**(1-2): 3-19.

Takesue, R. K. and A. van Geen (2004). "Mg/Ca, Sr/Ca, and stable isotopes in modern and Holocene Protothaca staminea shells from a northern California coastal upwelling region." Geochimica et Cosmochimica Acta **68**(19): 3845-3861.

Thomson (1918). "Brachiopoda. Australian Antarctic Expedition 1911–1914. Scientific Reports, Series C vol IV, part 3 (75 pp. 4 pls).".

Tigchelaar, M., von der Heydt, A.S. and Dijkstra, H.A. (2010). "A new interpretation of the two-step δ18O signal at the Eocene-Oligocene boundary." Climate of the Past Discussions **6**: 1391-1419.

Torsvik, T. H., M. A. Smethurst, R. Van der Voo, A. Trench, N. Abrahamsen and E. Halvorsen (1992). "Baltica - A Synopsis of Vendian-Permian palaeomagnetic data and their palaeotectonic implications." Earth Science Reviews **33**: 133-152.

Tripati, A. and H. Elderfield (2005). "Deep-sea temperature and circulation changes at the Paleocene-Eocene thermal maximum." Science **308**(5730): 1894-1898.

Turchyn, A. V., J. C. Alt, S. T. Brown, D. J. DePaolo, R. M. Coggon, G. X. Chi, J. H. Bedard and T. Skulski (2013). "Reconstructing the oxygen isotope composition of late Cambrian and Cretaceous hydrothermal vent fluid." Geochimica Et Cosmochimica Acta **123**: 440-458.

Vandenbroucke, T. R. A., A. Munnecke, M. J. Leng, T. Bickert, O. Hints, D. Gelsthorpe, G. Maier and T. Servais (2013). "Reconstructing the environmental conditions around the Silurian Ireviken Event using the carbon isotope composition of bulk and palynomorph organic matter." Geochemistry Geophysics Geosystems **14**(1): 86-101.

Vander Putten, E., F. Dehairs, E. Keppens and W. Baeyens (2000). "High resolution distribution of trace elements in the calcite shell layer of modern Mytilus edulis: Environmental and biological controls." Geochimica Et Cosmochimica Acta **64**(6): 997-1011.

Veizer, J., D. Ala, K. Azmy, P. Bruckschen, D. Buhl, F. Bruhn, G. A. F. Carden, A. Diener, S. Ebneth, Y. Godderis, T. Jasper, C. Korte, F. Pawellek, O. G. Podlaha and H. Strauss (1999). "Sr-87/Sr-86, delta C-13 and delta O-18 evolution of Phanerozoic seawater." Chemical Geology **161**(1-3): 59-88.

Veizer, J., P. Fritz and B. Jones (1986). "Geochemistry of brachiopods: Oxygen and carbon isotopic records of Paleozoic oceans." Geochimica Et Cosmochimica Acta **50**(8): 1679-1696.

Wade, B. S., A. J. P. Houben, W. Quaijtaal, S. Schouten, Y. Rosenthal, K. G. Miller, M. E. Katz, J. D. Wright and H. Brinkhuis (2012). "Multiproxy record of abrupt sea-surface cooling across the Eocene-Oligocene transition in the Gulf of Mexico." Geology **40**(2): 159-162.

Wade, B. S. and P. N. Pearson (2008). "Planktonic foraminiferal turnover, diversity fluctuations and geochemical signals across the Eocene/Oligocene boundary in Tanzania." Marine Micropaleontology **68**(3-4): 244-255.

Westerhold, T., U. Rohl, H. Palike, R. Wilkens, P. A. Wilson and G. Acton (2014). "Orbitally tuned timescale and astronomical forcing in the middle Eocene to early Oligocene." Climate of the Past **10**(3): 955-973.

Wienders, N., M. Arhan and H. Mercier (2000). "Circulation at the western boundary of the South and Equatorial Atlantic: Exchanges with the ocean interior." Journal of Marine Research **58**(6): 1007-1039.

Wilkinson, B. H. and T. J. Alego (1989). "Sedimentary carbonate record of calcium-magnesium cycling." American Journal of Science **289**(10): 1158-1194.

Williams, A. (1956). "The calcareous shell of the Brachiopoda and its importance to their classification." Biological Reviews of the Cambridge Philosophical Society **31**(3): 243-287.
Williams, A., S. J. Carlson, C. H. C. Brunton, L. E. Holmer and L. Popov (1996). "A supra-ordinal classification of the Brachiopoda." Philosophical Transactions of the Royal Society B-Biological Sciences **351**(1344): 1171-1193.

Williams, A. and M. Cusack (2007). Chemicostructural diversity of the Brachiopod shell Treatise on Invertebrate Paleontology Brachiopoda (Part H6) Revised. P. Selden, Geological Society of America.

Williams, A. a. R., A.J., Ed. (1965). Morphology. Treatise on invertebrate paleontology. Part H, Brachiopoda. The Geological Society of America & The University of Kansas Press, New York & Lawrence.

Williams, C., B. P. Flower, D. W. Hastings, T. P. Guilderson, K. A. Quinn and E. A. Goddard (2010). "Deglacial abrupt climate change in the Atlantic Warm Pool: A Gulf of Mexico perspective." Paleoceanography **25**: 12.

Wilson, D. S., D. Pollard, R. M. DeConto, S. S. R. Jamieson and B. P. Luyendyk (2013). "Initiation of the West Antarctic Ice Sheet and estimates of total Antarctic ice volume in the earliest Oligocene." Geophysical Research Letters **40**(16): 4305-4309.

Yamaguchi, T., R. D. Norris and D. T. Dockery (2014). "Shallow-marine ostracode turnover during the Eocene-Oligocene transition in Mississippi, the Gulf Coast Plain, USA." Marine Micropaleontology **106**: 10-21.

Yamamoto, K., R. Asami and Y. Iryu (2010a). "Carbon and oxygen isotopic compositions of modern brachiopod shells from a warm-temperate shelf environment, Sagami Bay, central Japan." Palaeogeography Palaeoclimatology Palaeoecology **291**(3-4): 348-359.

Yamamoto, K., R. Asami and Y. Iryu (2010b). "Within-shell variations in carbon and oxygen isotope compositions of two modern brachiopods from a subtropical shelf environment off Amami-o-shima, southwestern Japan." Geochemistry Geophysics Geosystems **11**.

Yamamoto, K., R. Asami and Y. Iryu (2011). "Brachiopod taxa and shell portions reliably recording past ocean environments: Toward establishing a robust paleoceanographic proxy." Geophysical Research Letters **38**: 5.

Yang, S., E. Galbraith and J. Palter (2014). "Coupled climate impacts of the Drake Passage and the Panama Seaway." Climate Dynamics **43**(1-2): 37-52.

Zachos, J., M. Pagani, L. Sloan, E. Thomas and K. Billups (2001). "Trends, rhythms, and aberrations in global climate 65 Ma to present." Science **292**(5517): 686-693.

Zachos, J. C. and L. R. Kump (2005). "Carbon cycle feedbacks and the initiation of Antarctic glaciation in the earliest Oligocene." Global and Planetary Change **47**(1): 51-66.

Zachos, J. C., T. M. Quinn and K. A. Salamy (1996). "High-resolution (10(4) years) deep-sea foraminiferal stable isotope records of the Eocene-Oligocene climate transition." Paleoceanography **11**(3): 251-266.

Zachos, J. C., S. Schouten, S. Bohaty, T. Quattlebaum, A. Sluijs, H. Brinkhuis, S. J. Gibbs and T. J. Bralower (2006). "Extreme warming of mid-latitude coastal ocean during the Paleocene-Eocene Thermal Maximum: Inferences from TEX86 and isotope data." Geology **34**(9): 737-740.

Zachos, J. C., L. D. Stott and K. C. Lohmann (1994). "Evolution of Early Cenozoic marine temperatures." Paleoceanography **9**(2): 353-387.

Zachos, J. C., M. W. Wara, S. Bohaty, M. L. Delaney, M. R. Petrizzo, A. Brill, T. J. Bralower and I. Premoli-Silva (2003). "A transient rise in tropical sea surface temperature during the Paleocene-Eocene Thermal Maximum." Science **302**(5650): 1551-1554.

Zanazzi, A., M. J. Kohn, B. J. MacFadden and D. O. Terry (2007). "Large temperature drop across the Eocene-Oligocene transition in central North America." Nature **445**(7128): 639-642.

Zhang, Y. G., M. Pagani, Z. H. Liu, S. M. Bohaty and R. DeConto (2013). "A 40-million-year history of atmospheric CO2." Philosophical Transactions of the Royal Society a-Mathematical Physical and Engineering Sciences **371**(2001): 20.

Zhang, Z., S. P. Robson, C. C. Emig and D. Shu (2008). "Early Cambrian radiation of brachiopods: A perspective from South China." Gondwana Research **14**(1–2): 241-254.

CHAPTER 9: APPENDICES

Appendix 1

Specimen	Valve	Colour	Translucency	Proportions (mm)
C777	Pedicle	Cream-brown	Nearly opaque	Length 7 Width 5 Thickness 0.5
C797	Pedicle	Orange-brown	Opaque	Length 17 Width 19 Thickness 1.5
J691	?	Cream-white	Semi-translucent	Length ? Width ? Thickness 0.5
E720	Pedicle	White	Semi-translucent	Length 31 Width 25 Thickness 0.75

X128	Brachial	Cream-white	Semi-Translucent	Length 21 Width 25 Thickness 0.5
E840	Pedicle	Cream-brown	Opaque	Length 38 Width 35 Thickness 1
X193	Pedicle	Cream-white	Semi-translucent	Length 13 Width 11 Thickness 1
E870	Pedicle	White	Semi-translucent	Length 7 mm Width 7 mm Thickness 0.5 mm

Hand Specimen Observations

C777

Under the hand lens a very small network of 'vein' like structures can be seen on the outside of the shell. There seems to be no obvious sign of diagenesis or encrusting organisms however the colour may suggest that the calcite is impure.

C797

Cracked and broken towards the anterior end. Orange-brown colour throughout the shell with the colour intensifying towards the cracked anterior margin. The outside of the shell has a dull appearance in comparison to other specimens and may suggest that diagenesis had already begun to take place on the sea floor.

J691

Anterior end of unknown valve as broken towards the posterior end. A white 'dendritic' pattern is found in places on the outside of the shell, looks to be in very good condition with little alteration. Growth lines towards the anterior margin are very closely spaced suggesting that this specimen is a very mature adult.

E720

Minor creamy brown discolouration in places. One possible boring hole towards the umbo of the shell but boring is not prevalent. The growth bands are very close together in all areas of the valve with the exception of the umbo where the spacing is slightly larger.

X128

Complete except for one small fleck on the edge of the shell that is less than 1 mm wide. On the outside of the shell there are over 20 circular markings that are lighter in colour than the rest of the shell, these areas look as if they are where encrusting organisms have been manually removed from the shell. These markings do not all appear on the inside of the shell.

E840

Cream-brown colour, boring looks to have taken place in places on the outside of the shell, encrusting organisms can be found on the outside of the shell as well as

sediment. An Fe oxide coloured vein can be seen towards the anterior end of the valve. Inside of the valve, towards the umbo, there is an area of Fe oxide discolouration. This shell does not look pristine and may be less than half of the original size.

X193

Sediment was still in place in the umbo end of the valve. This was manually removed. Broken towards the anterior end of the shell. Minor amounts of discolouration.

E870

There is no evidence of boring or predation. The specimen is only fragmented slightly towards the anterior end and has no discolouration.

SEM Observations

C777

The primary layer is not present.

The distinction between the secondary and tertiary layers of ultrastructure is difficult to make out in this specimen.

The alteration seems to penetrate right through to the centre of the shell.

Some borings penetrate 100 μm into the shell (Figure C777-1A)

Secondary layers looks much less fibrous than other specimens, it looks more granular and less uniform (C777-1B), it has potentially been replaced which could in part be due to the deep borings facilitating diagenesis deeper within the shell.

The borings on the inside and outside of the shell suggest that the brachiopod was dead at the time the valve was collected (C777-1C).

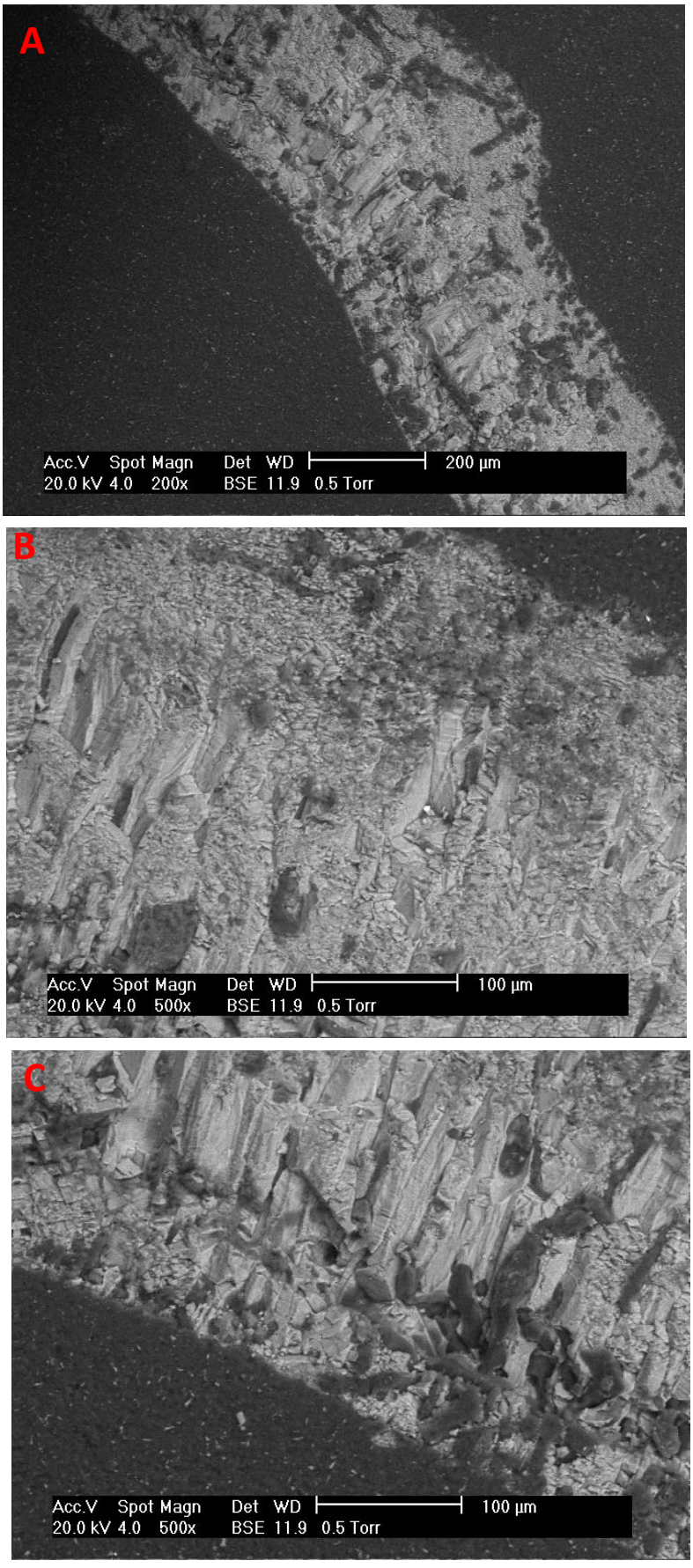

Figure C777-1, SEM images, A) Borings and showing the difficulty to pick out different levels of the ultrastructure, B) Granular secondary layer C) Borings on the inside of the shell.

C797

The primary layer has been removed by a combination of boring and abrasion (Figure C797-2A)

Fibrous secondary layer is between 50 and 100 μm thick.

The tertiary layer has more blocky prisms than the other shells (Figure C797-A and C), the prisms could be growing in a slightly different orientation as this is very close to the umbo, in different brachiopod species Perez-Huerta et al. (2011) have found that the secondary layer in this part of the shell grows with a different crystallographic orientation.

The blocky prisms could also be due to diagenetic alteration.

The borings on the inside and the outside of the shell suggest that the brachiopod was dead and the associated valve had been on the sea floor long enough for the early stages of diagenesis to take place

Parts of this shell are very poorly preserved (Figure C797-2B)

The punctae are infilled with a material that is not resin, there is a contrast between the tone of the resin and the tone of the material infilling the punctae (Figure C797-2C).

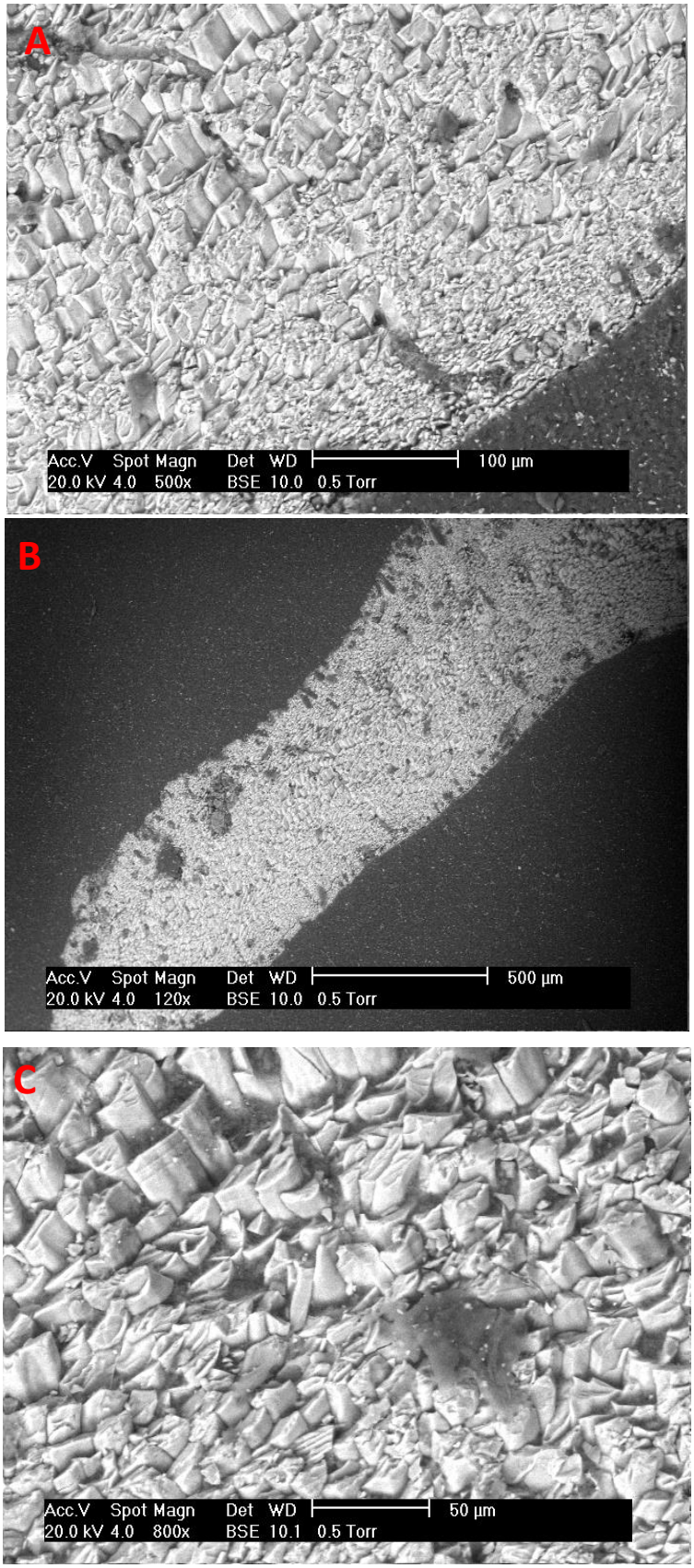

Figure C797-1, SEM images, A) Granular texture of tertiary layer, B) Borings on the inside and outside edges of the shell, C) Close up of more granular texture

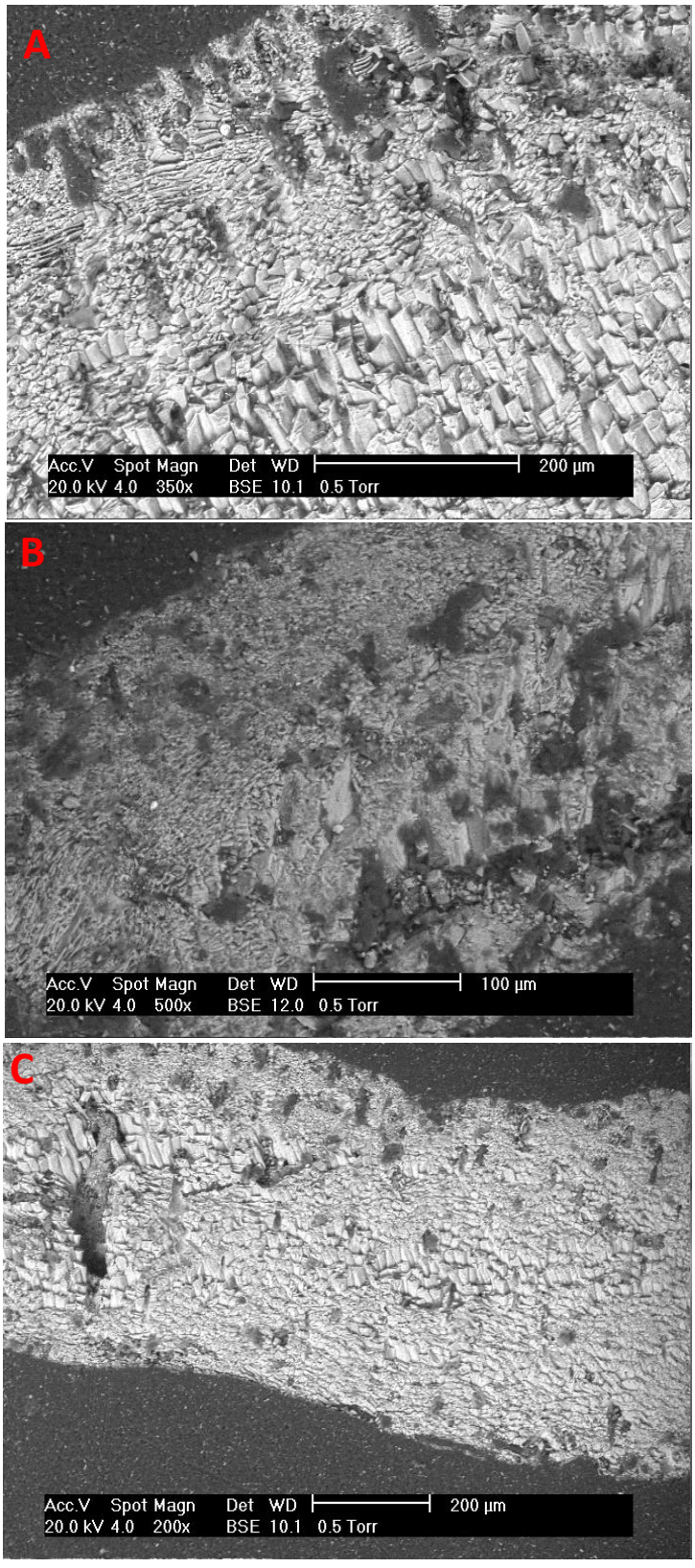

Figure C797-2, SEM images, A) Boring and abrasion leading to removal of the primary layer, B) Showing an area of very poor preservation, C) Punctae with lack of resin in fill.

J691

All three layers of the ultrastructure present (Figure J691-1A).

Thickest primary layer of all the specimens, possibly due to much larger size than other specimens.

Secondary layer ~ 200 μm thick. (Figure J691-1B)

Tertiary layer 100 – 150 μm thick.

Preservation is generally very good; both outer and inner edges of the shell are very sharp and show very few signs of alteration except for one area (Figure J691-1C).

Tertiary layer remains unaffected by alteration; this is the area sampled by laser ablation and therefore is not a problem.

Borings are shown in the area of alteration and could be the reason for the alteration.

Very few punctae (Figure J691-2A and B).

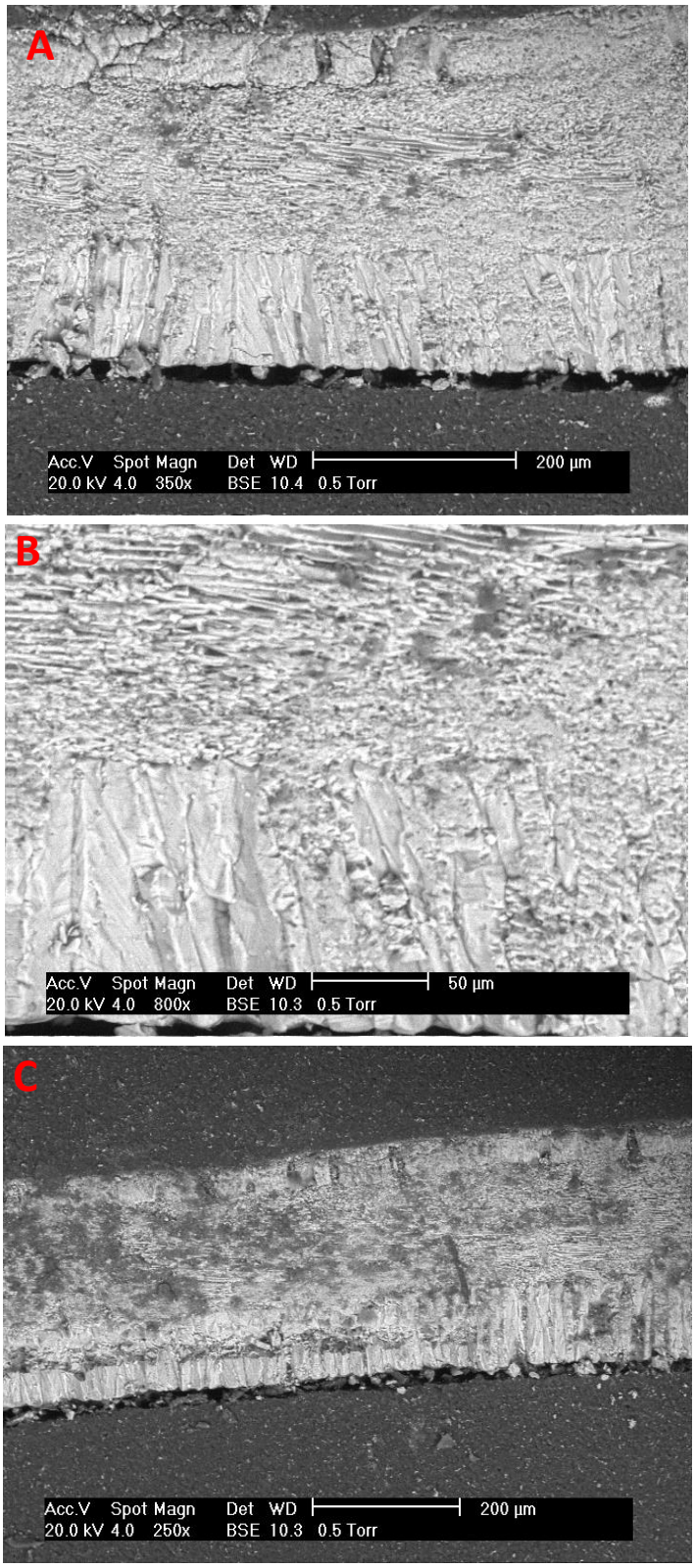

Plate J691-1, SEM images, A) Three layers of the ultrastructure, B) Boundary between the secondary and tertiary layers, C) Poor preservation of secondary layer in one part of the shell

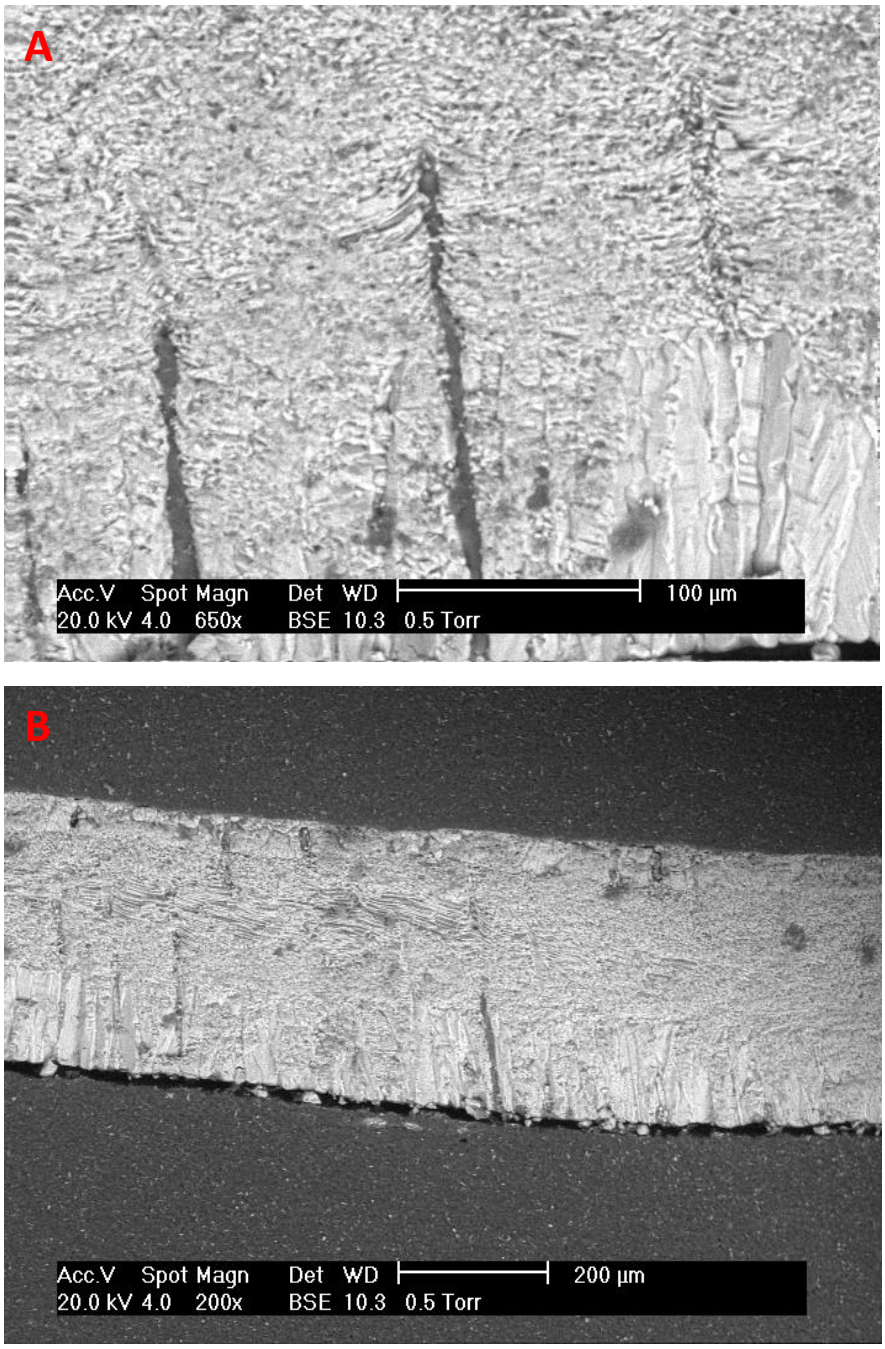

Figure J691-2, SEM images, A) Punctae and features associated with inward growth, B) Punctae at a lower magnification.

E720

Very well preserved, with all three layers of the ultrastructure present. (Figure E720-A-C)

Granular primary layer, 50 μm thick (Figure E720-2A)

Fibrous secondary layer, ~150 μm thick (Figure E720-2B)

Prismatic tertiary layer, ~200 μm thick (Figure E720-2C)

Outside edge of the shell shows very few signs of boring

Primary layer has been abraded away from one area of the shell (Figure E720-3C)

No borings or alterations found on the inside of the valve, which suggests the specimen was collected before or just after the death of the brachiopod.

Punctae are oval shaped, ~10 μm by μm ~20 – 30 μm, they appear to be infilled with resin (Figure C720-3A and B).

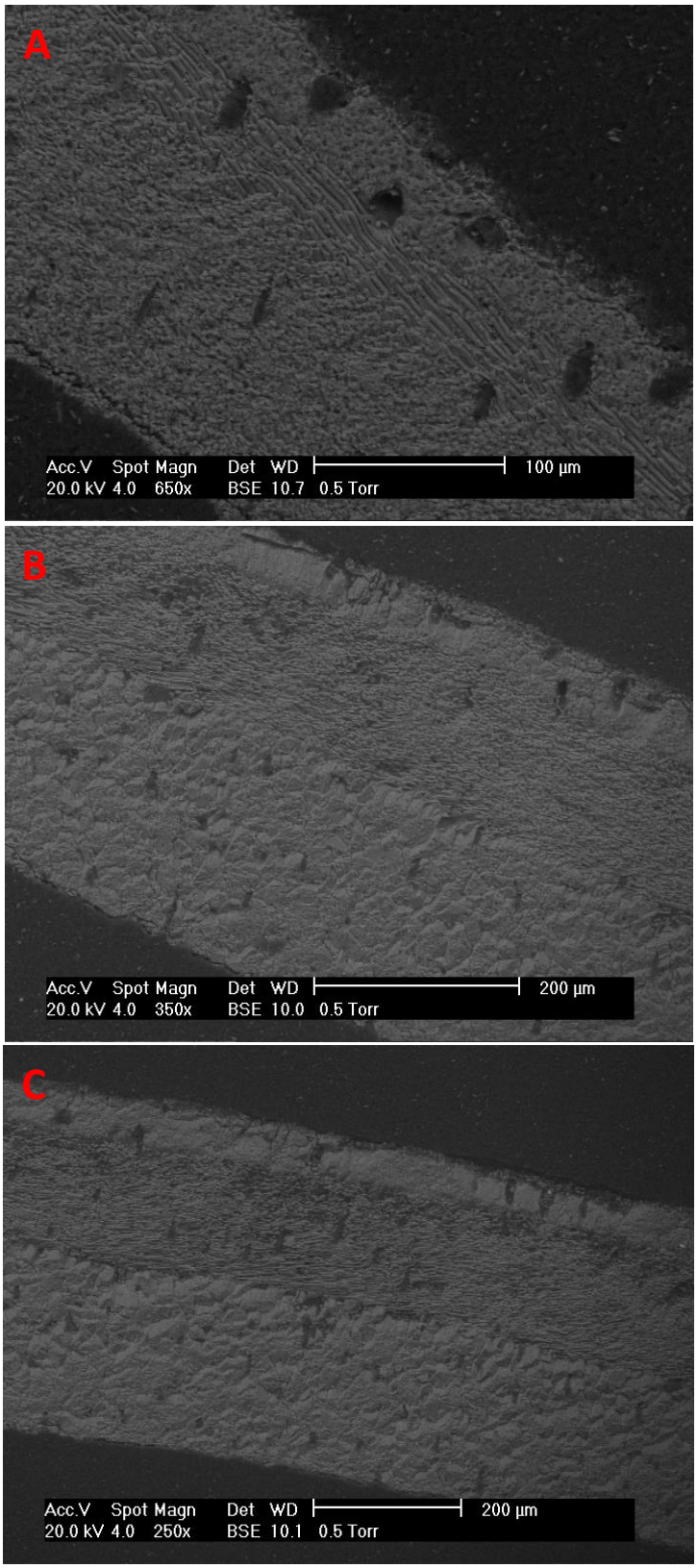

Figure E720-1, SEM images, A) Punctae with no in fill, B and C) Thicknesses of the ultrastructure across the shell.

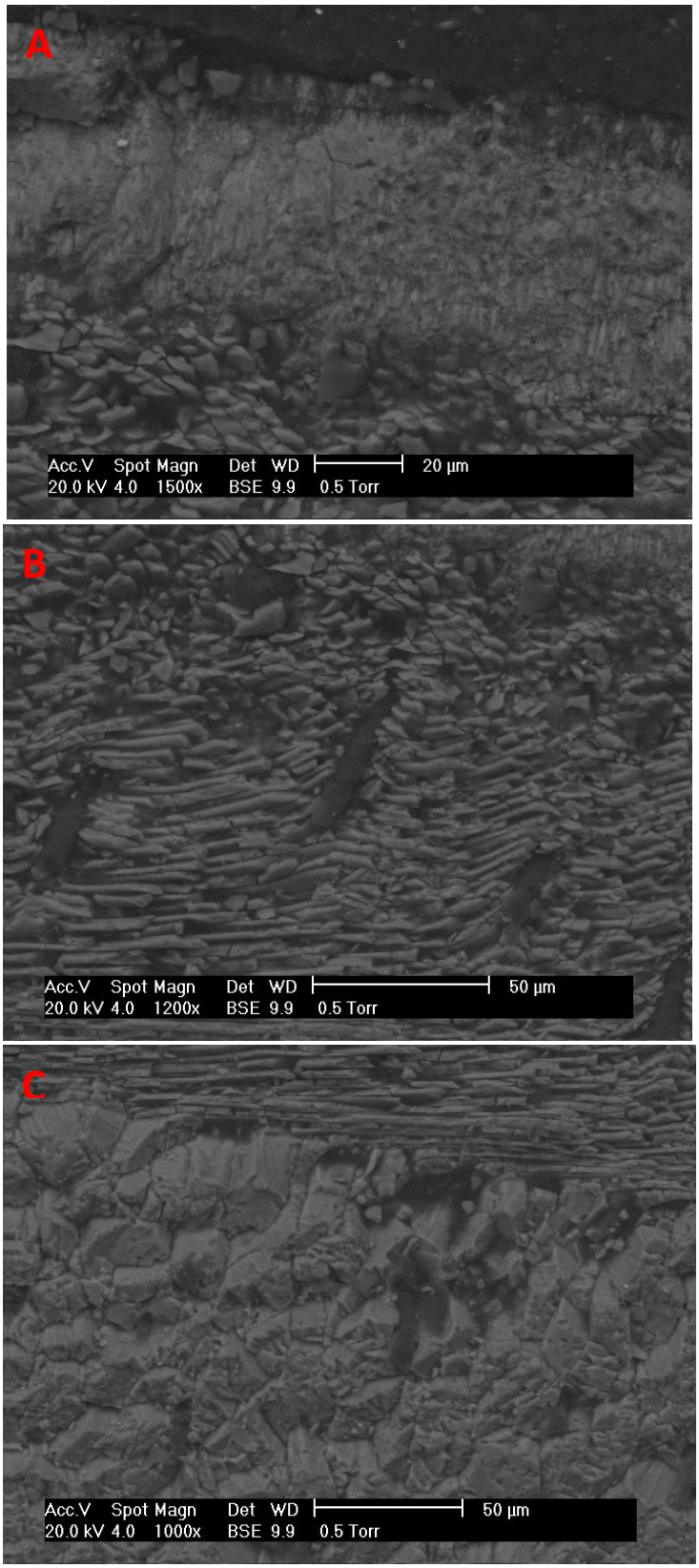

Figure E720-2, SEM images, A) Close up of primary layer, B) Close up of secondary layer, C) Close up of tertiary layer.

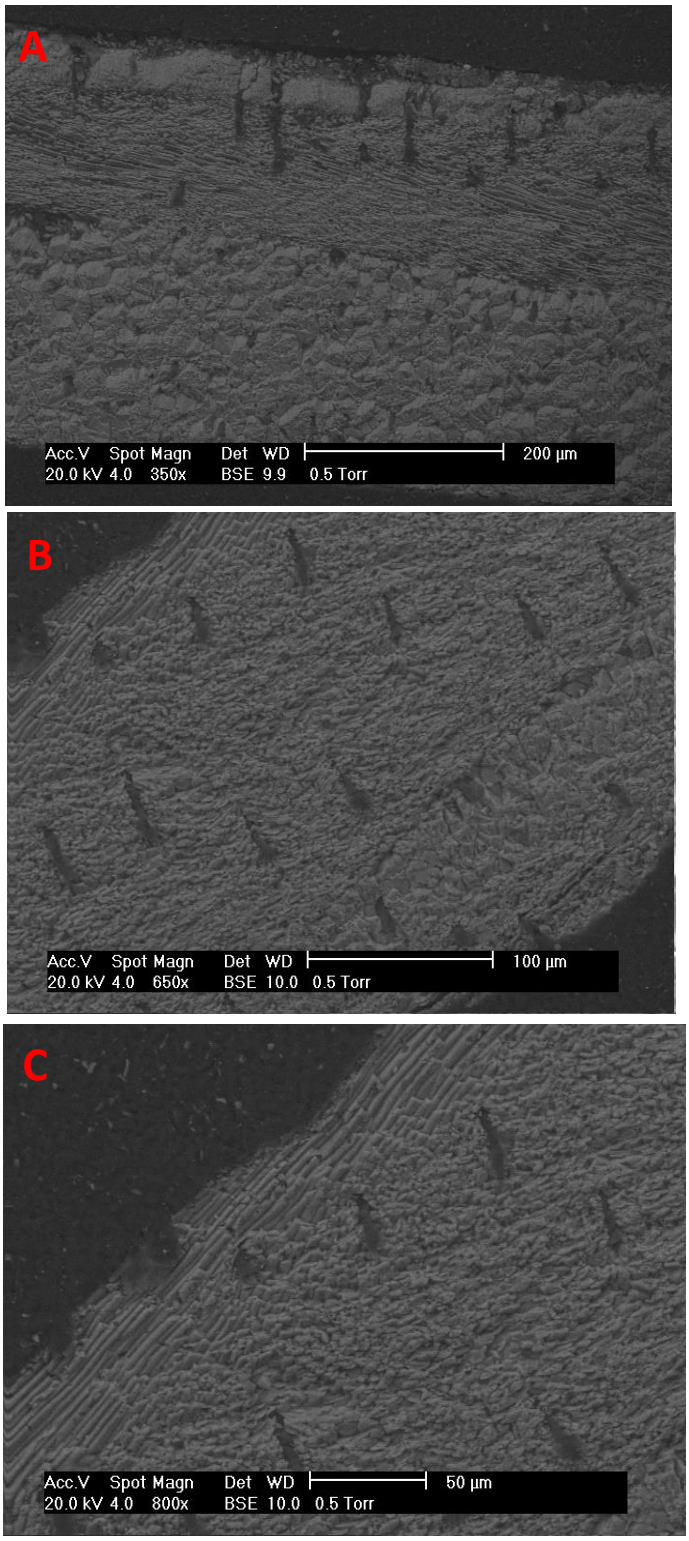

Figure E720-3, SEM images, A) Borings in one place on the outside of the shell, B) Regular punctae with no in fill, C) Abrasion of the primary layer

X128

Large borings associated with this shell (Figure X128-1A)

The borings along with the encrusting organisms on the outside of the valve suggest that the valve spent a long time on the sea floor after the death of the brachiopod.

All three layers of the ultrastructure are present but due to the large nature of the borings means that are area of unaffected calcite is hard to find (Figure X128-1B and C)

Small borings on the inside of the shell.

This valve shows the value of checking specimens under SEM as it looked relatively unaltered in hand specimen.

E840

Primary layer not present.

Only small amounts of secondary layer suggesting large amounts of abrasion.

The valve is comprised mostly of the tertiary layer (Figure E840-1B)

Borings on the inside of the shell show the brachiopod was dead at the time the specimen was collected (Figure E840-1C)

Large crack ~200 μm wide running diagonally through the shell (Figure E840-1A), crack developed during the sectioning process

The shell seems to have been mostly altered and abraded towards the centre of the valve (Figure E840-2A - C), the edges show a more pristine pattern (Figure E840-3A – C), they have sharper inner and outer edges to the valves and a secondary layer that is more prominent albeit it ~50 μm thick.

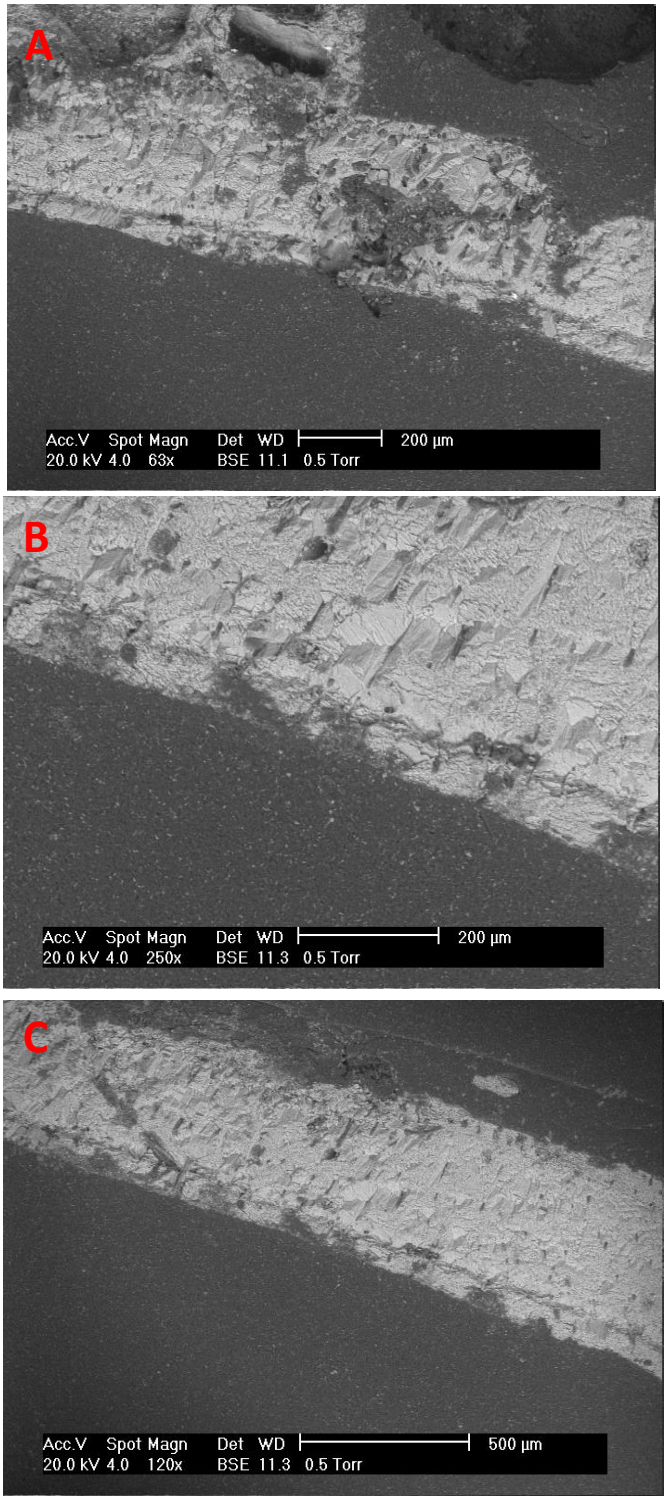

Figure E840-1, SEM images, A) Large diagonal crack running through the thickness of the shell, B) Prismatic tertiary layer, C) Area of abrasion on the outside of the shell

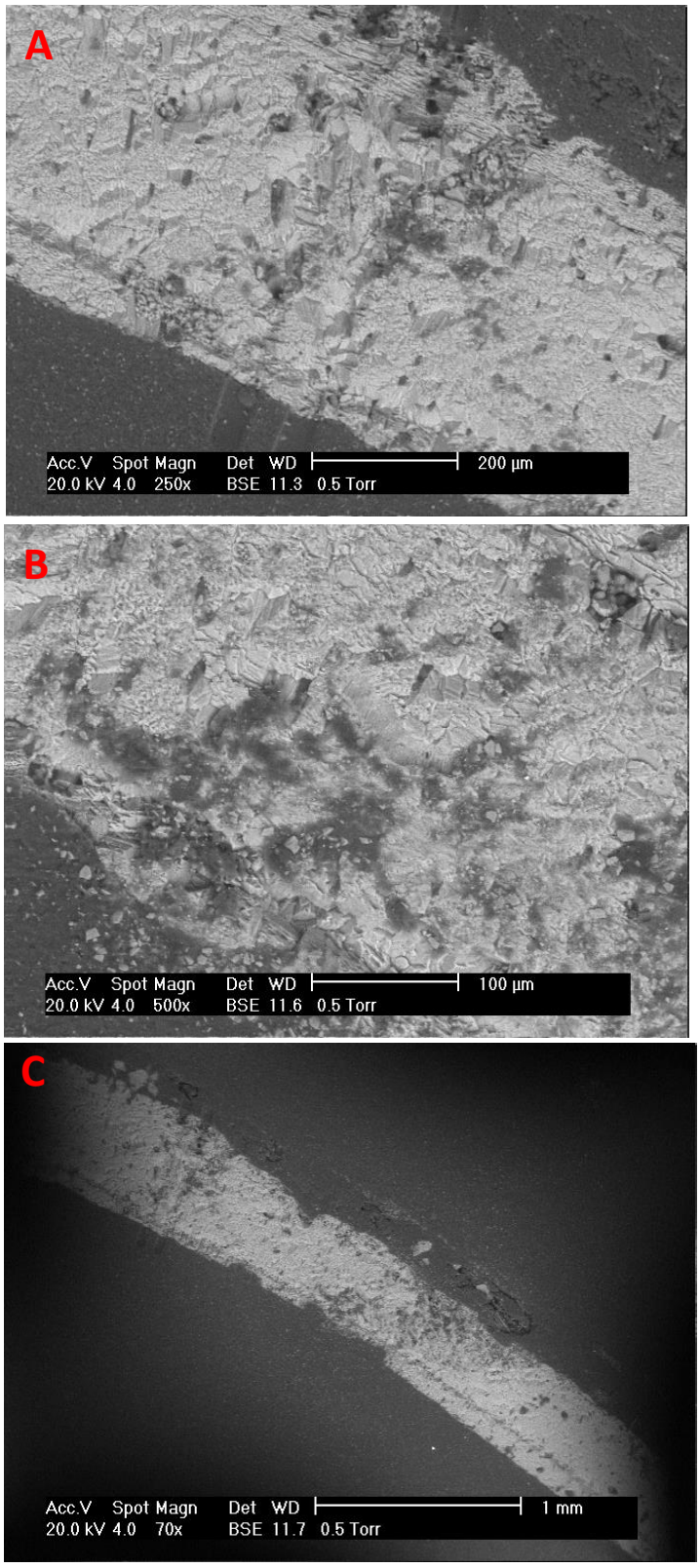

Figure E840-2 SEM images A-C) Showing poor preservation in central part of the shell section.

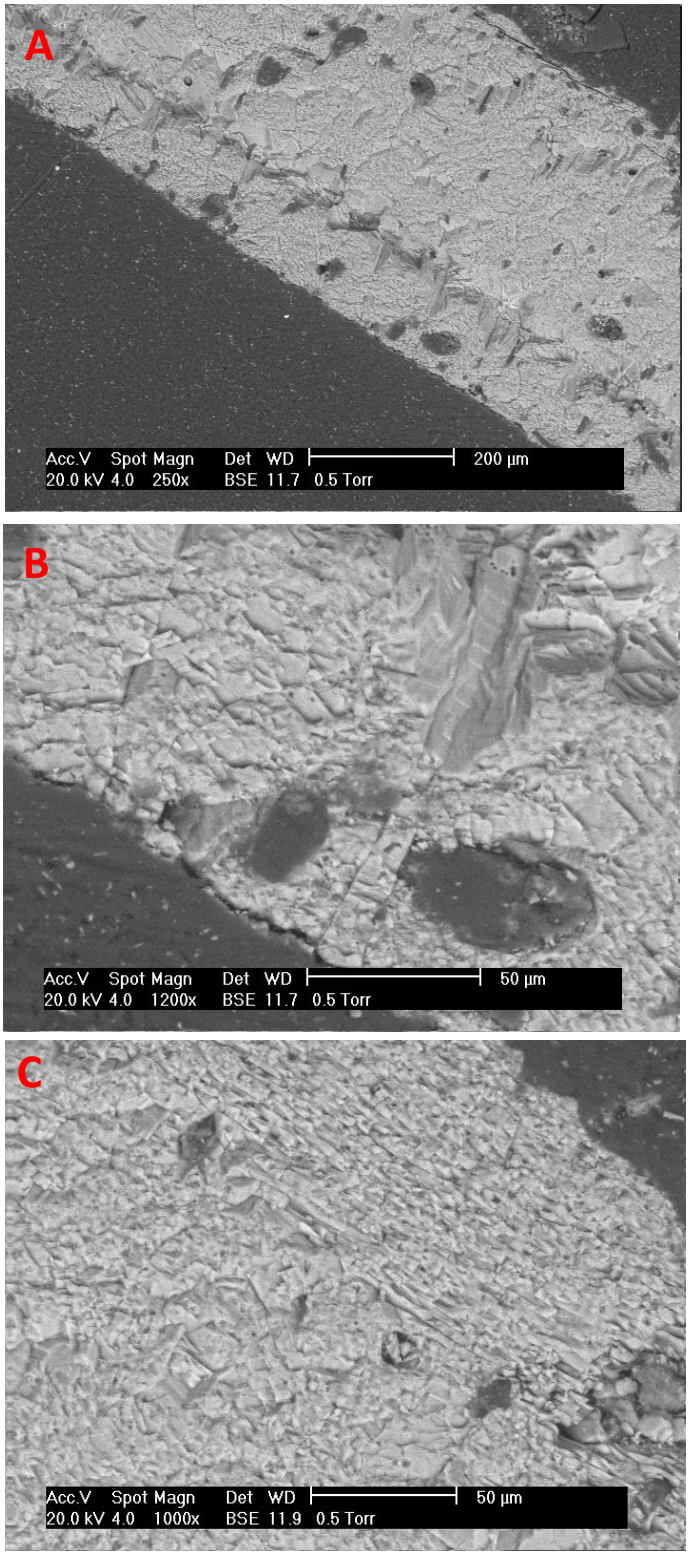

Figure E840-3, SEM images A-C) Showing the pristine preservation of the calctie towards the edge of the shell.

E870

All three layers of the ultrastructure present (Figure E870-1A and B).

Prismatic Tertiary layer, 100 μm thick.

Fibrous secondary layer, ~30 μm thick.

Prismatic tertiary layer, ~ 10 μm thick (Figure E870-1C).

Edges of the shell both very regular and very sharp.

Small areas of abrasion on the outside of the shell where the primary layer has been worn away.

No alteration or abrasion on the inside of the shell, suggesting that the shell was collected alive or shortly after the death of the brachiopod.

Prominent crack between the secondary and tertiary layers, probably an artefact of the sampling procedure as the sectioning is likely to have accentuated the natural weakness between the two layers (Figure E870-2B).

A similar crack is seen in one place between the primary and secondary layers.

The calcite in general looks very clean.

Punctae increase in number towards the centre of the shell, appear in all three layers and do not appear to be infilled with resin or any other material.

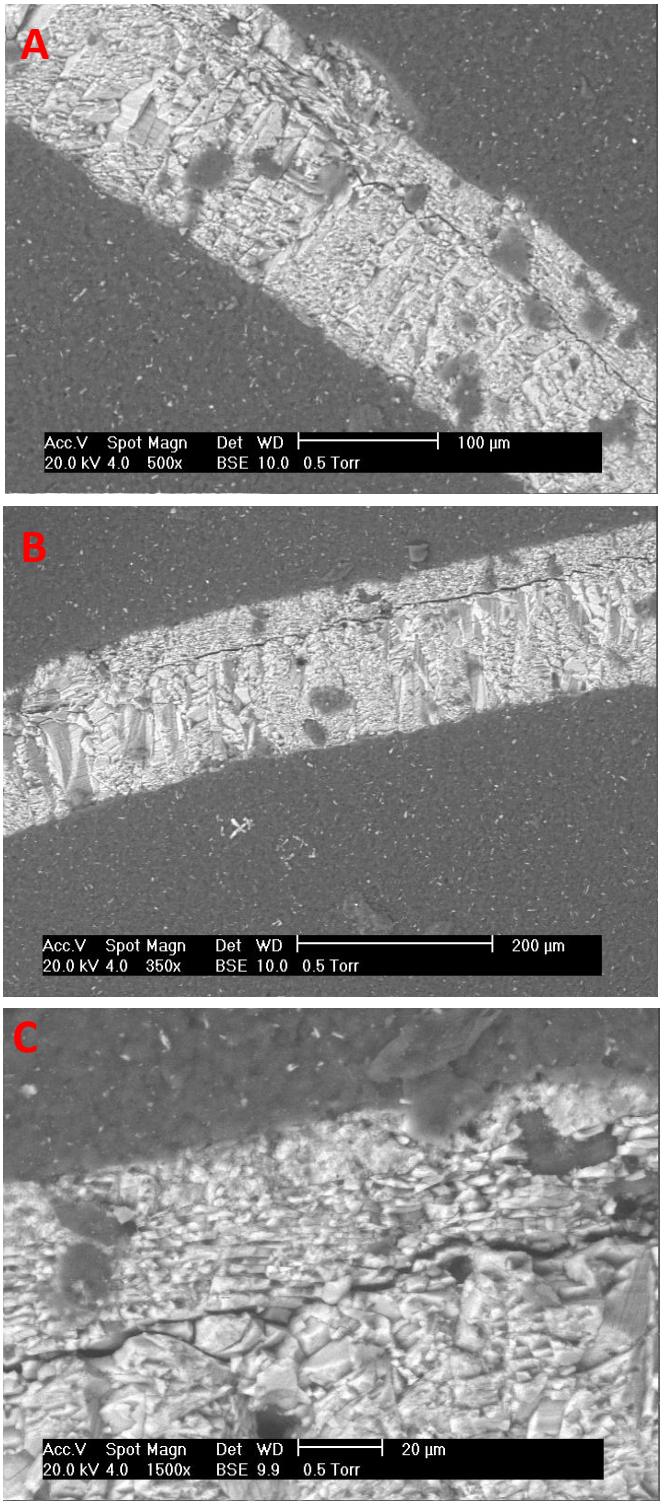

Figure E870-1, SEM images A and B) All three layers of the shell ultrastructure C) Close up of the granular primary layer.

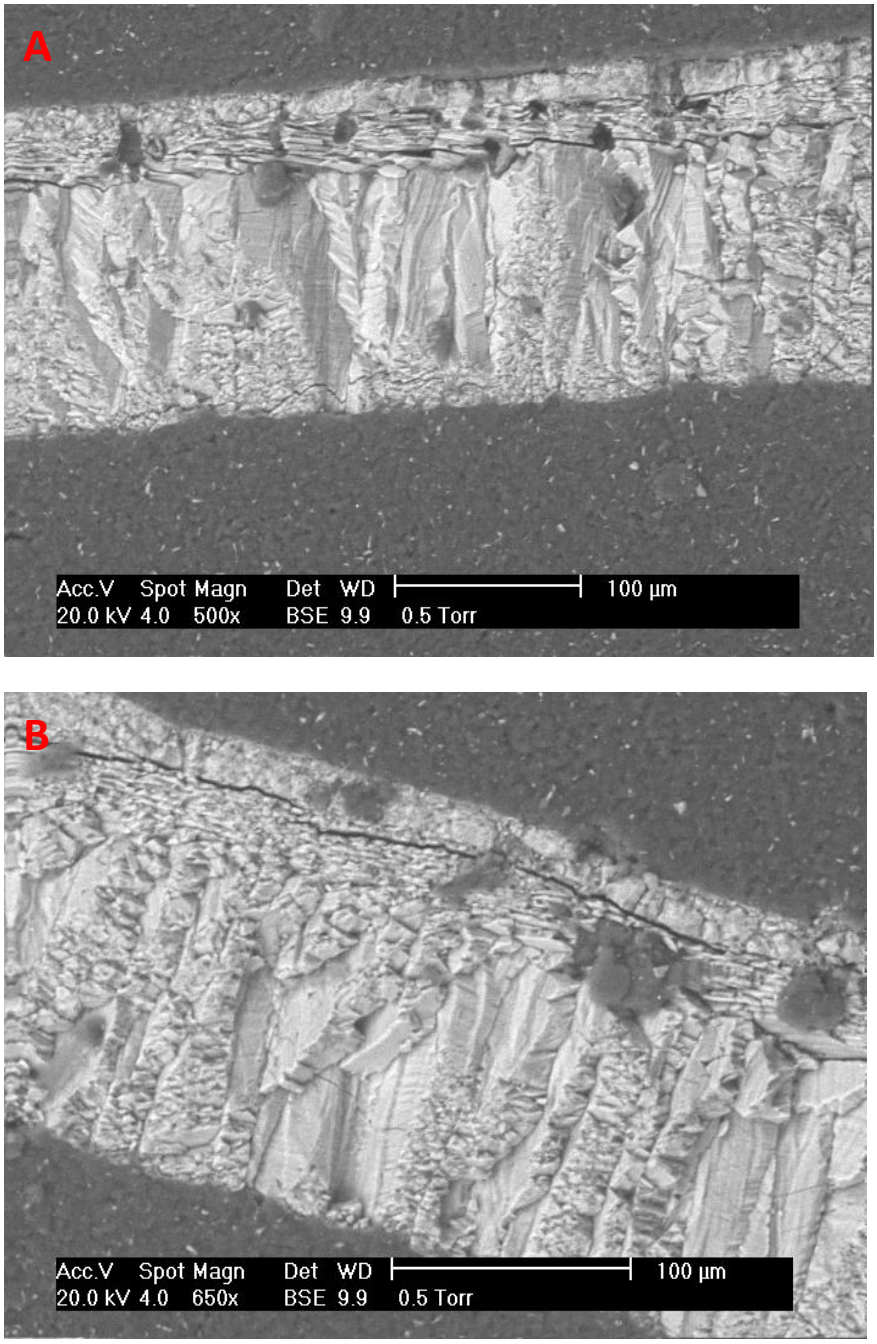

Plate E870-2, SEM images A) all three layers of the shell ultrastructure, B) highlighting the crack that probably occurred during preparation of the sample.

Appendix 2

The following graphs are all from specimens of *Liothyrella neozelanica* from offshore of North Island, New Zealand. In all specimens each graph represents the following:

A) Mg/Ca across a transverse section.

B) Al/Ca across a transverse section.

C) Ca^{43}/Ca^{48} across a transverse section.

D) Mn/Ca across a transverse section.

E) Sr/Ca across a transverse section.

.

.

C777

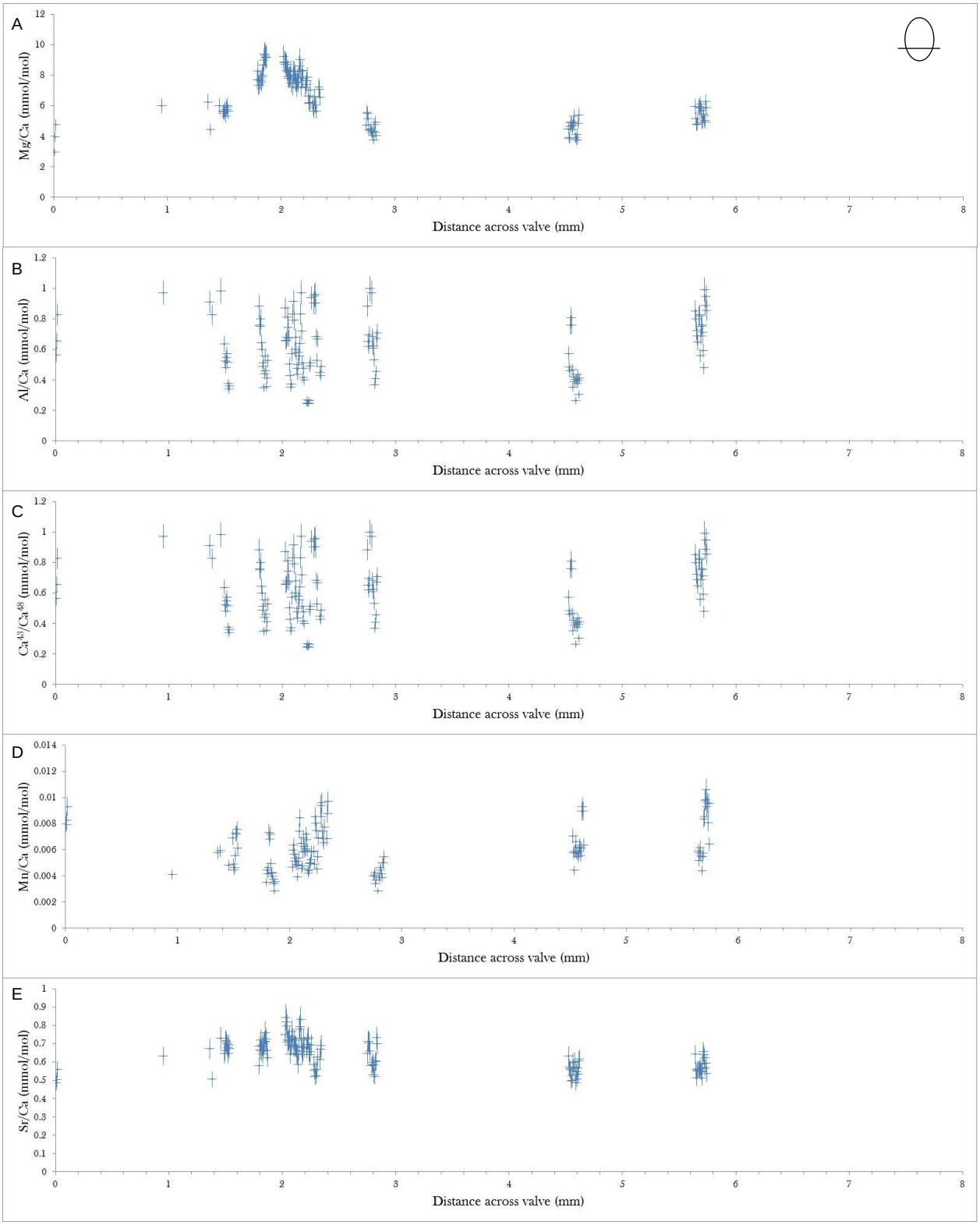
A
Mg/Ca (mmol/mol)
Distance across valve (mm)
B
Al/Ca (mmol/mol)
Distance across valve (mm)
C
Ca43/Ca48 (mmol/mol)
Distance across valve (mm)
D
Mn/Ca (mmol/mol)
Distance across valve (mm)
E
Sr/Ca (mmol/mol)
Distance across valve (mm)

C797

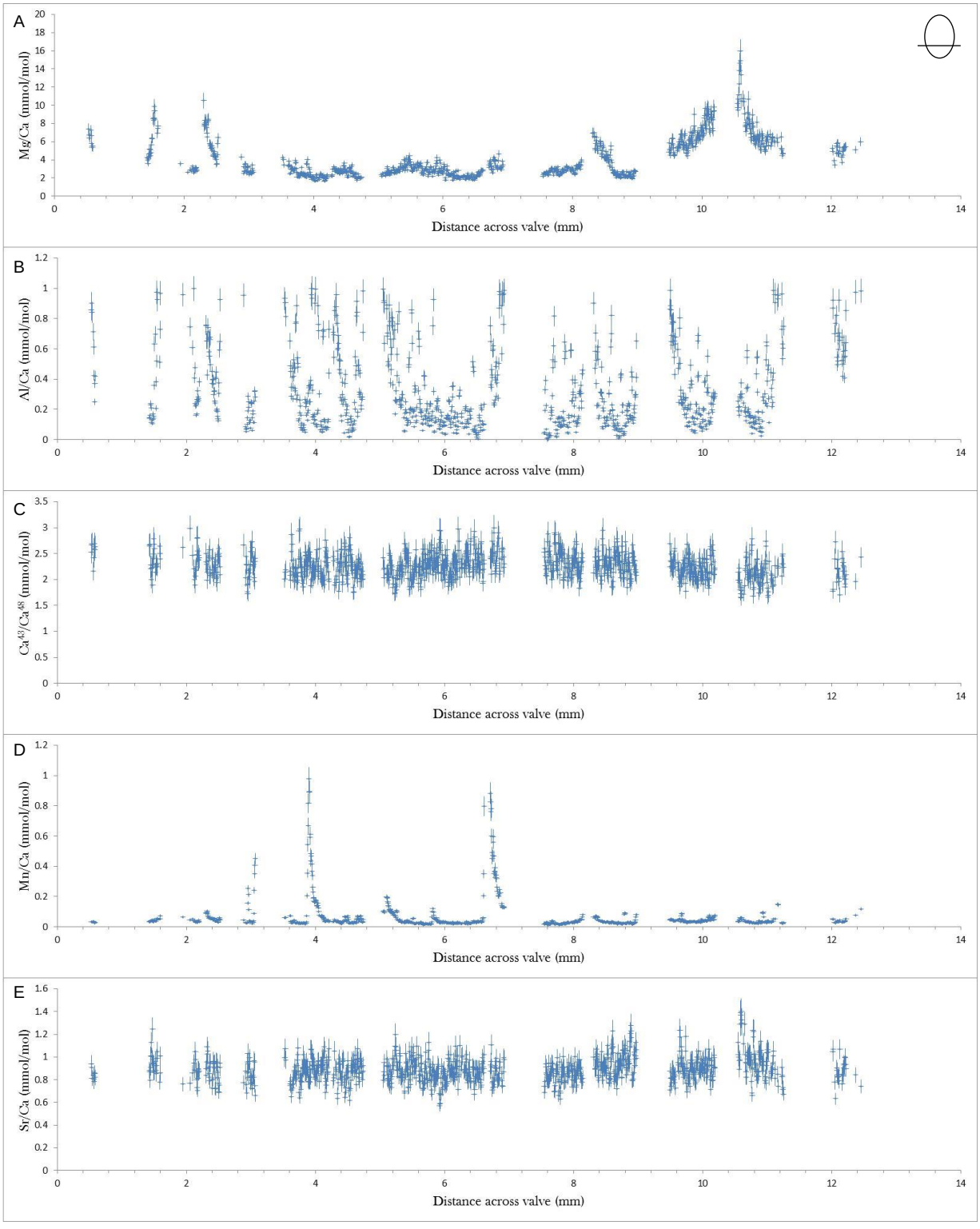
A
Mg/Ca (mmol/mol)
Distance across valve (mm)
B
Al/Ca (mmol/mol)
Distance across valve (mm)
C
Ca43/Ca48 (mmol/mol)
Distance across valve (mm)
D
Mn/Ca (mmol/mol)
Distance across valve (mm)
E
Sr/Ca (mmol/mol)
Distance across valve (mm)

J691

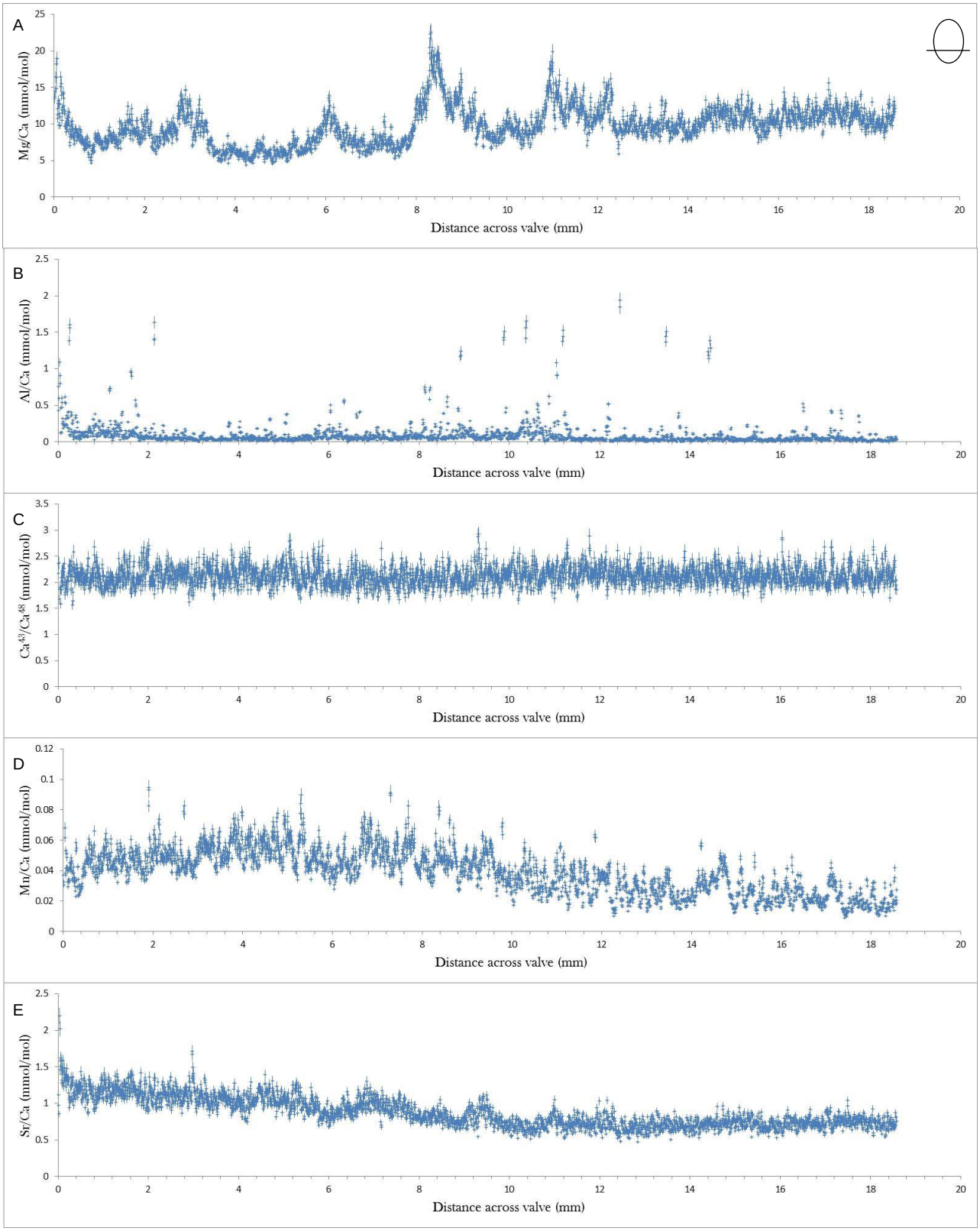
A
Mg/Ca (mmol/mol)
Distance across valve (mm)
B
Al/Ca (mmol/mol)
Distance across valve (mm)
C
Ca^{43}/Ca^{48} (mmol/mol)
Distance across valve (mm)
D
Mn/Ca (mmol/mol)
Distance across valve (mm)
E
Sr/Ca (mmol/mol)
Distance across valve (mm)

E720

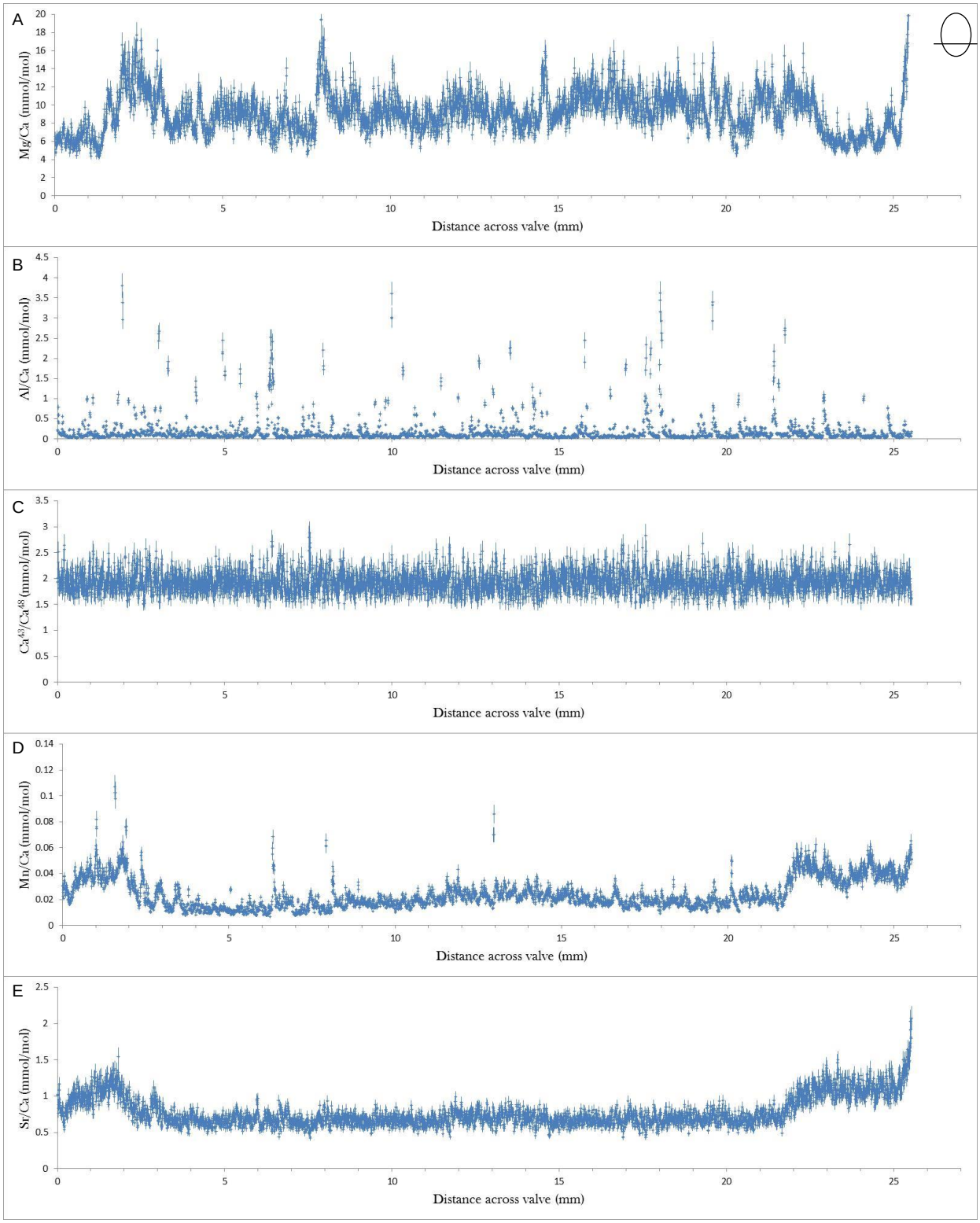
A
Mg/Ca (mmol/mol)
Distance across valve (mm)
B
Al/Ca (mmol/mol)
Distance across valve (mm)
C
Ca43/Ca48 (mmol/mol)
Distance across valve (mm)
D
Mn/Ca (mmol/mol)
Distance across valve (mm)
E
Sr/Ca (mmol/mol)
Distance across valve (mm)

X128

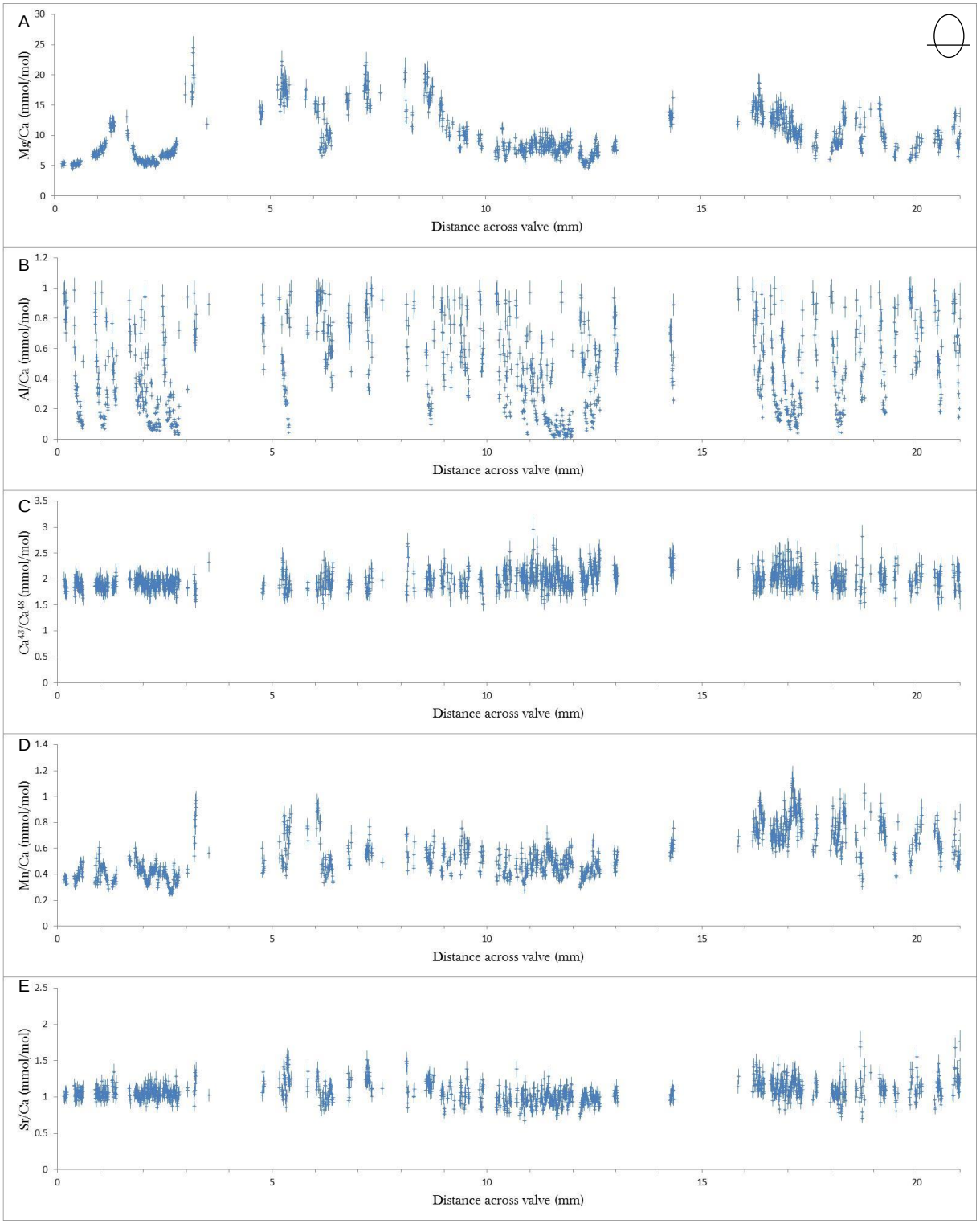
A
Mg/Ca (mmol/mol)
Distance across valve (mm)
B
Al/Ca (mmol/mol)
Distance across valve (mm)
C
Ca^{43}/Ca^{48} (mmol/mol)
Distance across valve (mm)
D
Mn/Ca (mmol/mol)
Distance across valve (mm)
E
Sr/Ca (mmol/mol)
Distance across valve (mm)

E840

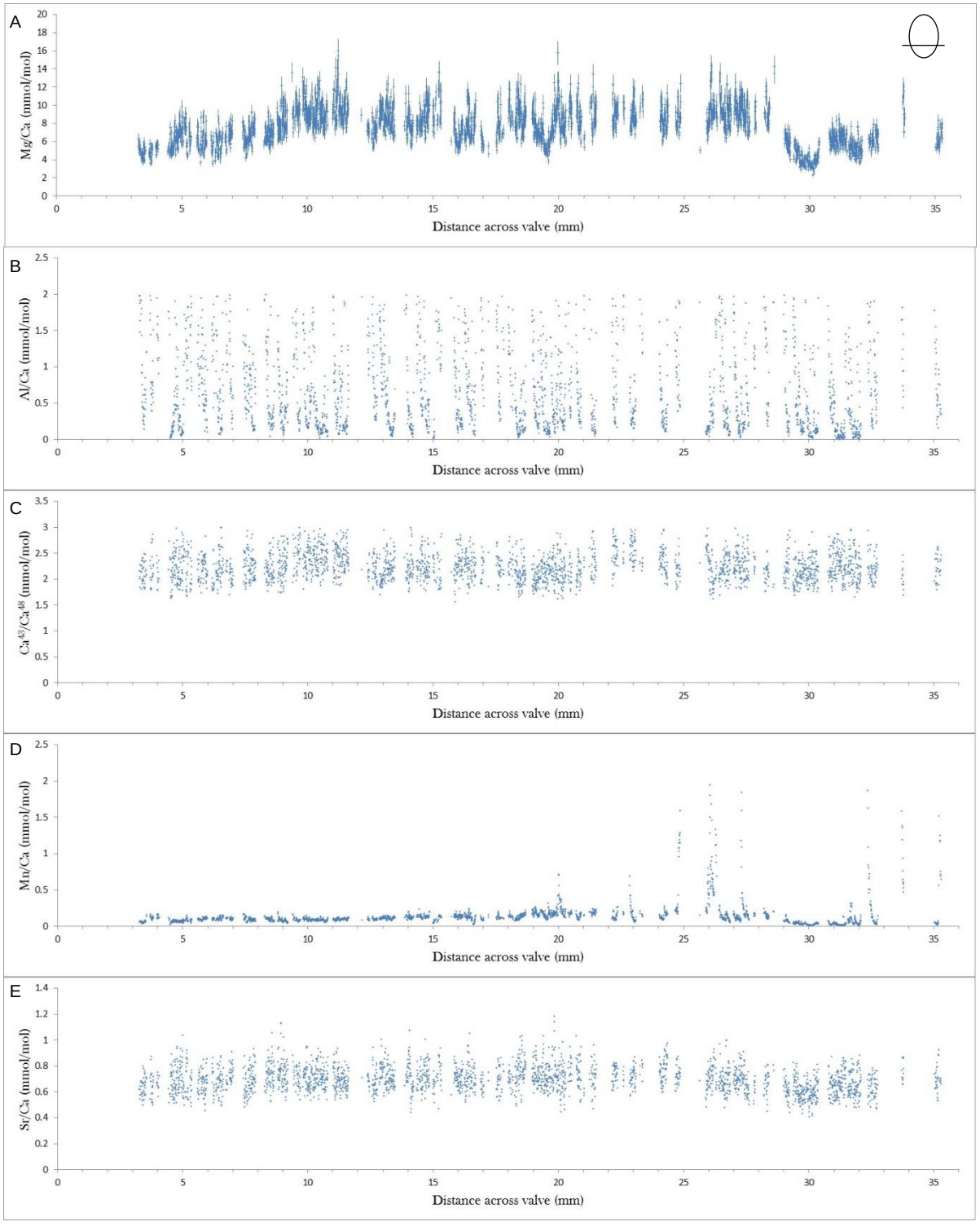
A
Mg/Ca (mmol/mol)
Distance across valve (mm)
B
Al/Ca (mmol/mol)
Distance across valve (mm)
C
Ca43/Ca48 (mmol/mol)
Distance across valve (mm)
D
Mn/Ca (mmol/mol)
Distance across valve (mm)
E
Si/Ca (mmol/mol)
Distance across valve (mm)

E870

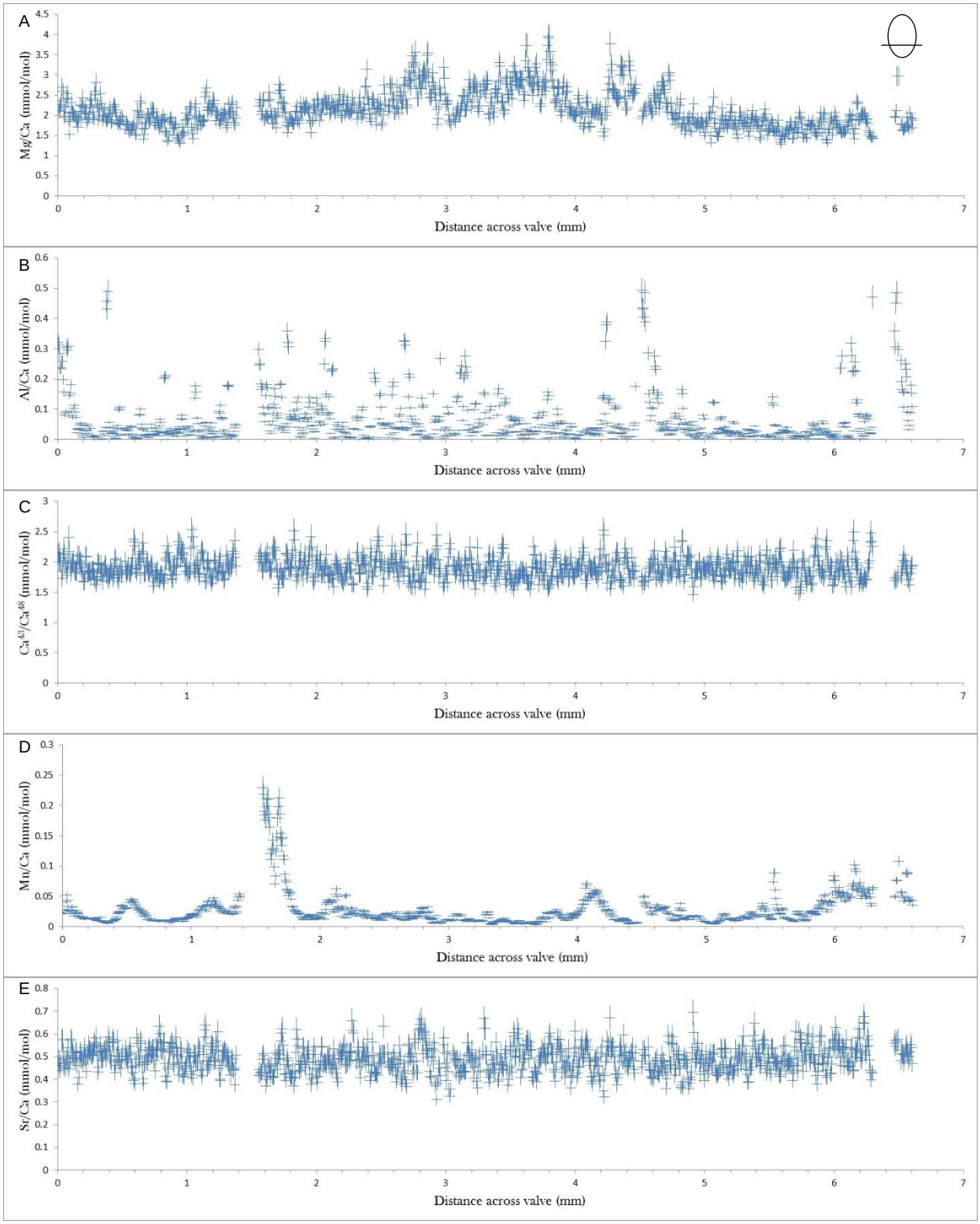
A
Mg/Ca (mmol/mol)
Distance across valve (mm)
B
Al/Ca (mmol/mol)
Distance across valve (mm)
C
Ca43/Ca48 (mmol/mol)
Distance across valve (mm)
D
Mn/Ca (mmol/mol)
Distance across valve (mm)
E
Sr/Ca (mmol/mol)
Distance across valve (mm)

X193

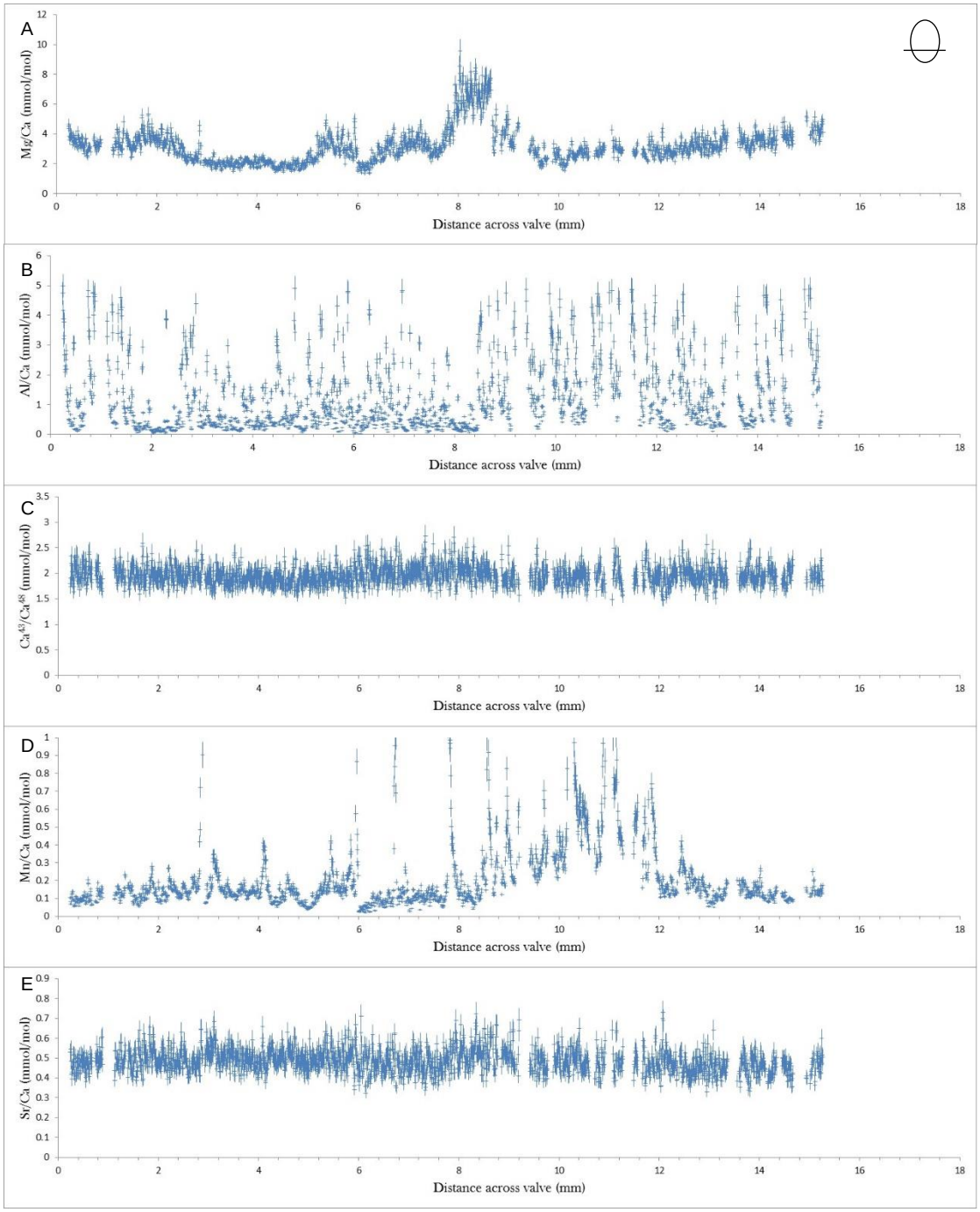
A
Mg/Ca (mmol/mol)
Distance across valve (mm)
B
Al/Ca (mmol/mol)
Distance across valve (mm)
C
Ca^{43}/Ca^{48} (mmol/mol)
Distance across valve (mm)
D
Mn/Ca (mmol/mol)
Distance across valve (mm)
E
Sr/Ca (mmol/mol)
Distance across valve (mm)

Appendix 3

The following graphs are all from specimens of *Liothyrella oamarutica* from McDonalds Quarry, Oligocene of North Otago, New Zealand. In MCLIO1, MCLIO2, MCLIO3, MCLIO4 and MCLIO5 each graph represents the following:

A) Mg/Ca across a transverse section.

B) Al/Ca across a transverse section.

C) Ca/Ca across a transverse section.

D) Mn/Ca across a transverse section.

E) Sr/Ca across a transverse section.

MCLIO1

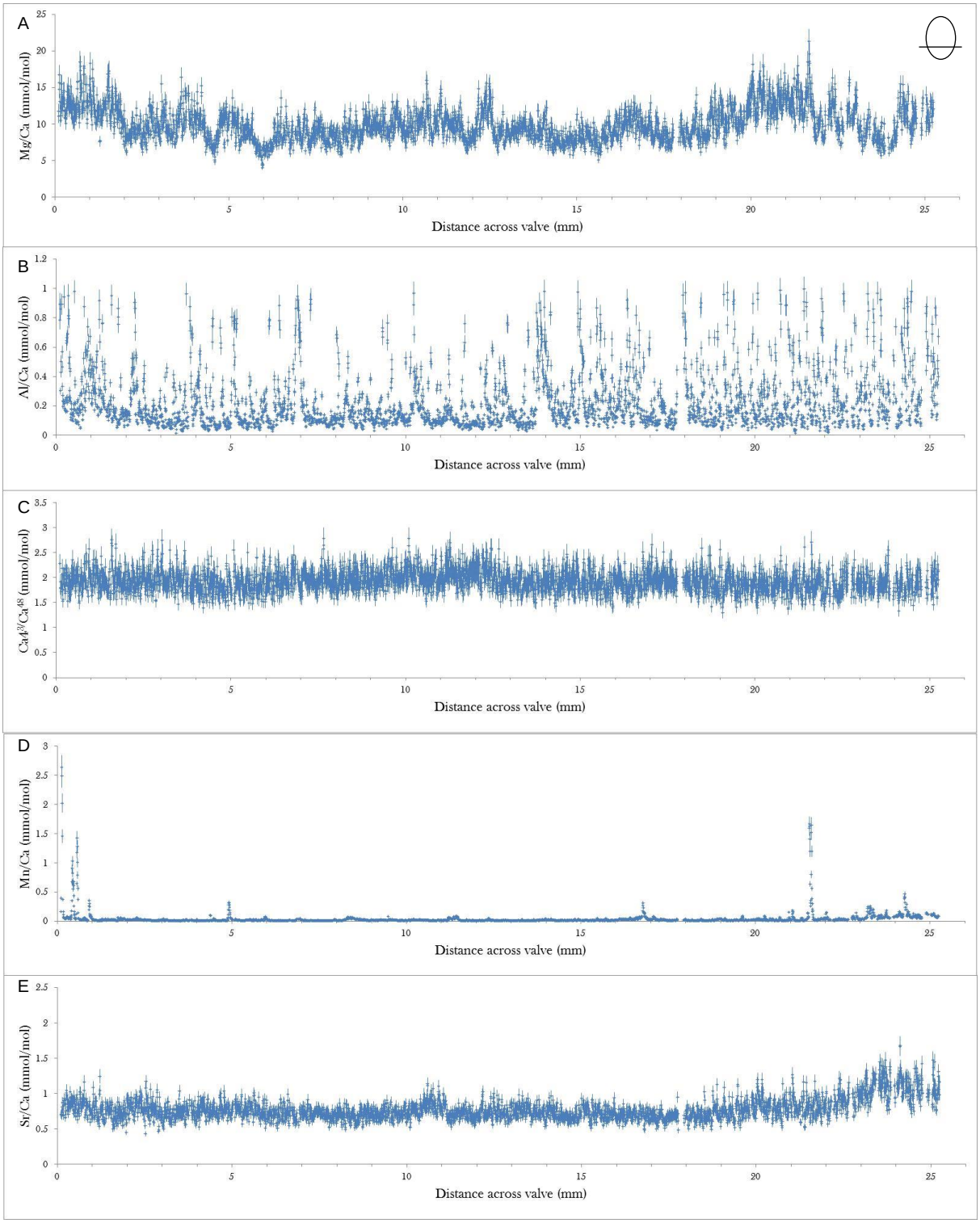
A
Mg/Ca (mmol/mol)
Distance across valve (mm)
B
Al/Ca (mmol/mol)
Distance across valve (mm)
C
Distance across valve (mm)
D
Mn/Ca (mmol/mol)
Distance across valve (mm)
E
Sr/Ca (mmol/mol)
Distance across valve (mm)

MCLIO2

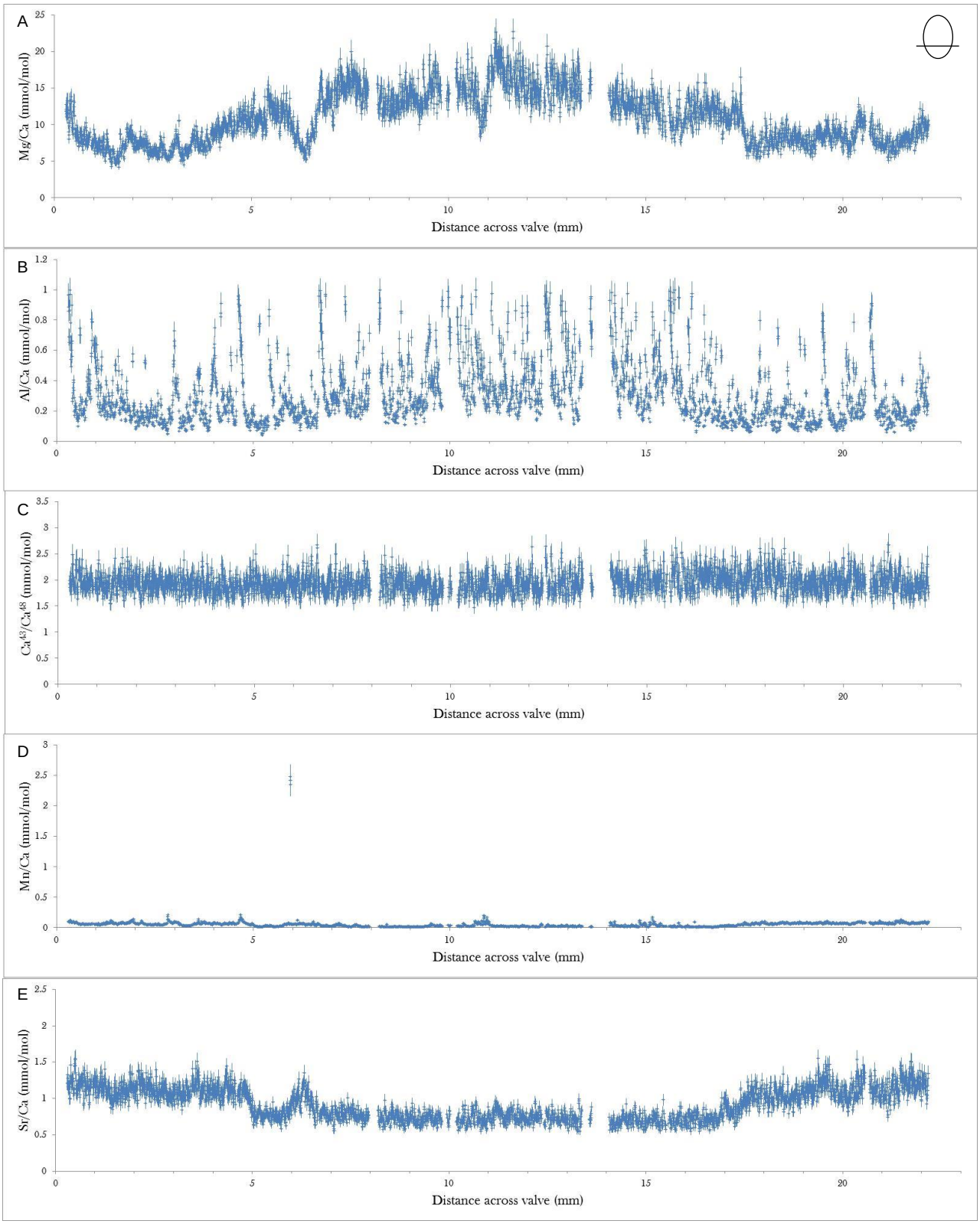
A
Mg/Ca (mmol/mol)
Distance across valve (mm)
B
Al/Ca (mmol/mol)
Distance across valve (mm)
C
Ca43/Ca48 (mmol/mol)
Distance across valve (mm)
D
Mn/Ca (mmol/mol)
Distance across valve (mm)
E
Sr/Ca (mmol/mol)
Distance across valve (mm)

MCLIO3

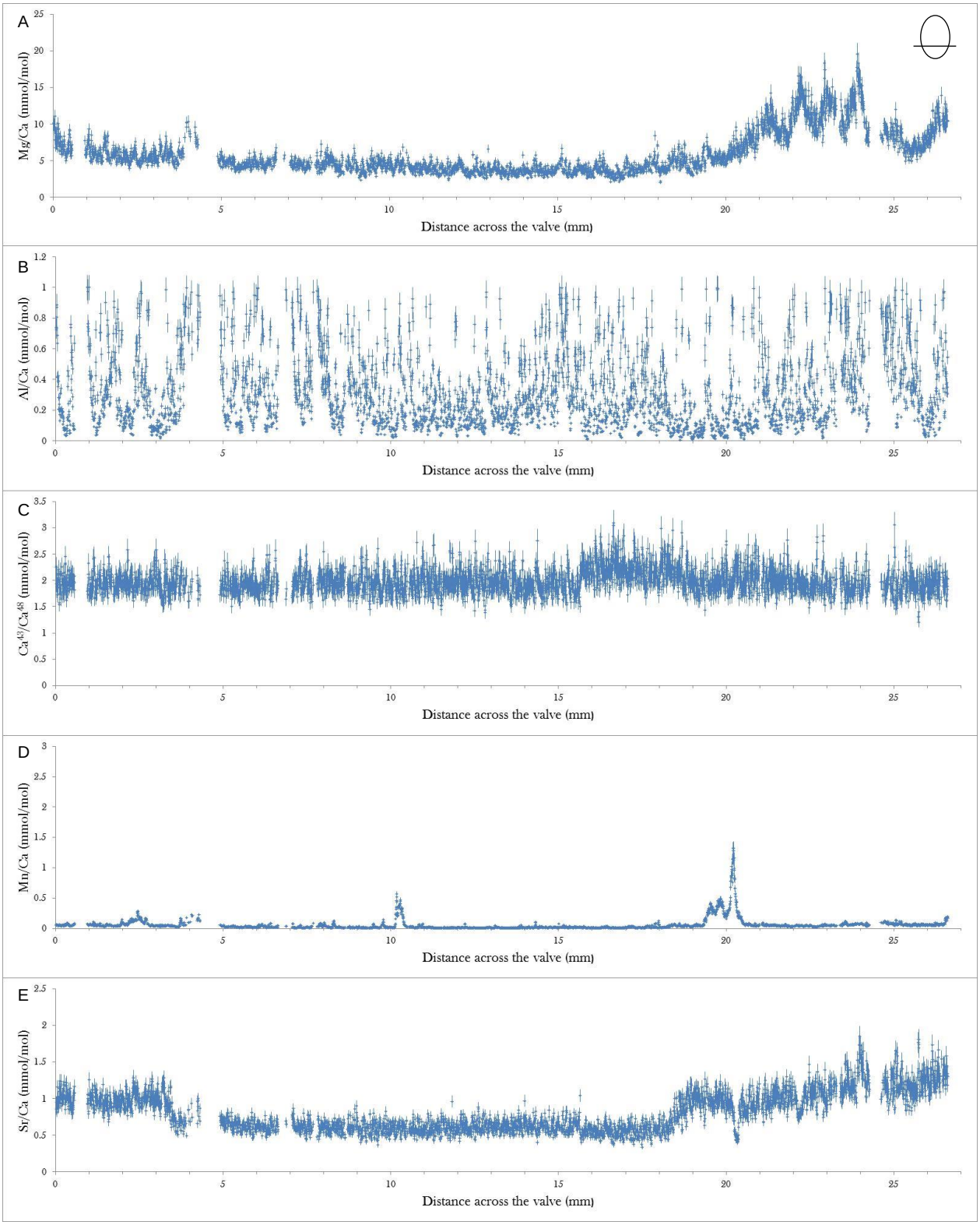
A
Mg/Ca (mmol/mol)
Distance across the valve (mm)
B
Al/Ca (mmol/mol)
Distance across the valve (mm)
C
Ca43/Ca48 (mmol/mol)
Distance across the valve (mm)
D
Mn/Ca (mmol/mol)
Distance across the valve (mm)
E
Sr/Ca (mmol/mol)
Distance across the valve (mm)

MCLIO4

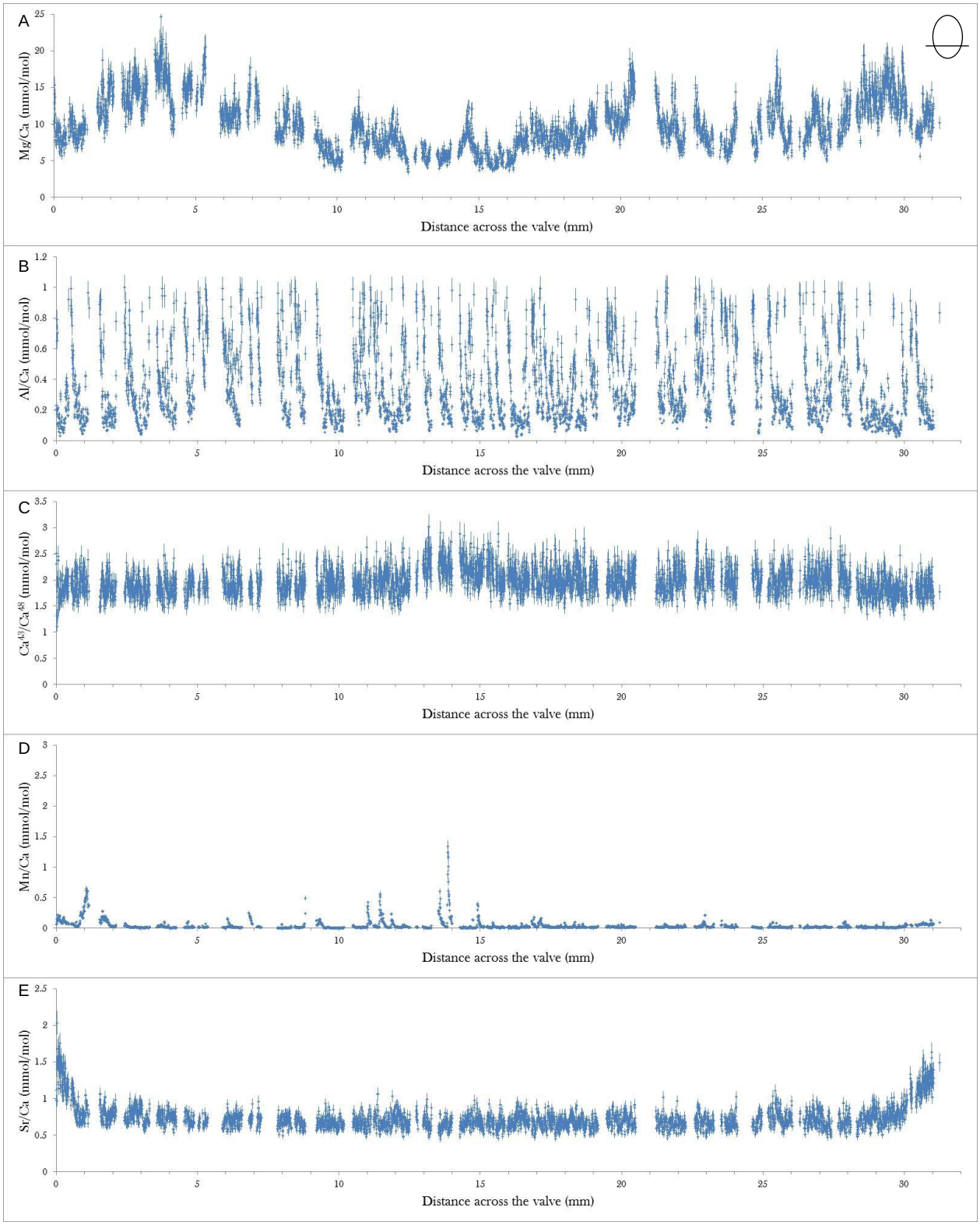
A
Mg/Ca (mmol/mol)
Distance across the valve (mm)
B
Al/Ca (mmol/mol)
Distance across the valve (mm)
C
Ca43/Ca48 (mmol/mol)
Distance across the valve (mm)
D
Mn/Ca (mmol/mol)
Distance across the valve (mm)
E
Sr/Ca (mmol/mol)
Distance across the valve (mm)

MCLIO5

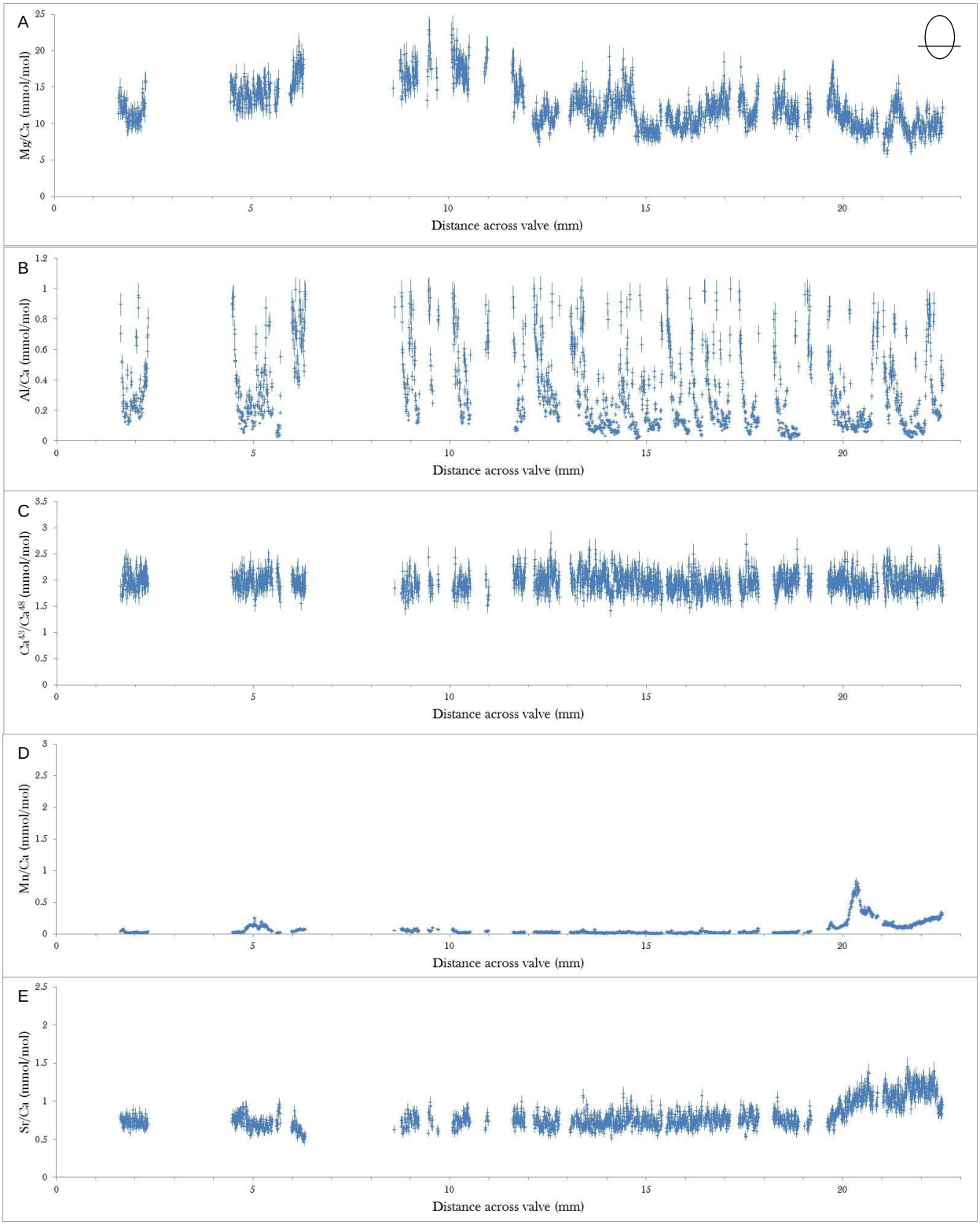
A
Mg/Ca (mmol/mol)
Distance across valve (mm)
B
Al/Ca (mmol/mol)
Distance across valve (mm)
C
Ca43/Ca48 (mmol/mol)
Distance across valve (mm)
D
Mn/Ca (mmol/mol)
Distance across valve (mm)
E
Sr/Ca (mmol/mol)
Distance across valve (mm)

The following graphs are all from specimens of *Terebratulina suessi* from McDonalds Quarry, Oligocene of North Otago, New Zealand. In MCTER1, MCTER2, MCTER3, MCTER4 and MCTER5 each graph represents the following:

A) Mg/Ca across a transverse section.

B) Al/Ca across a transverse section.

C) Ca/Ca across a transverse section.

D) Mn/Ca across a transverse section.

E) Sr/Ca across a transverse section.

MCTER1

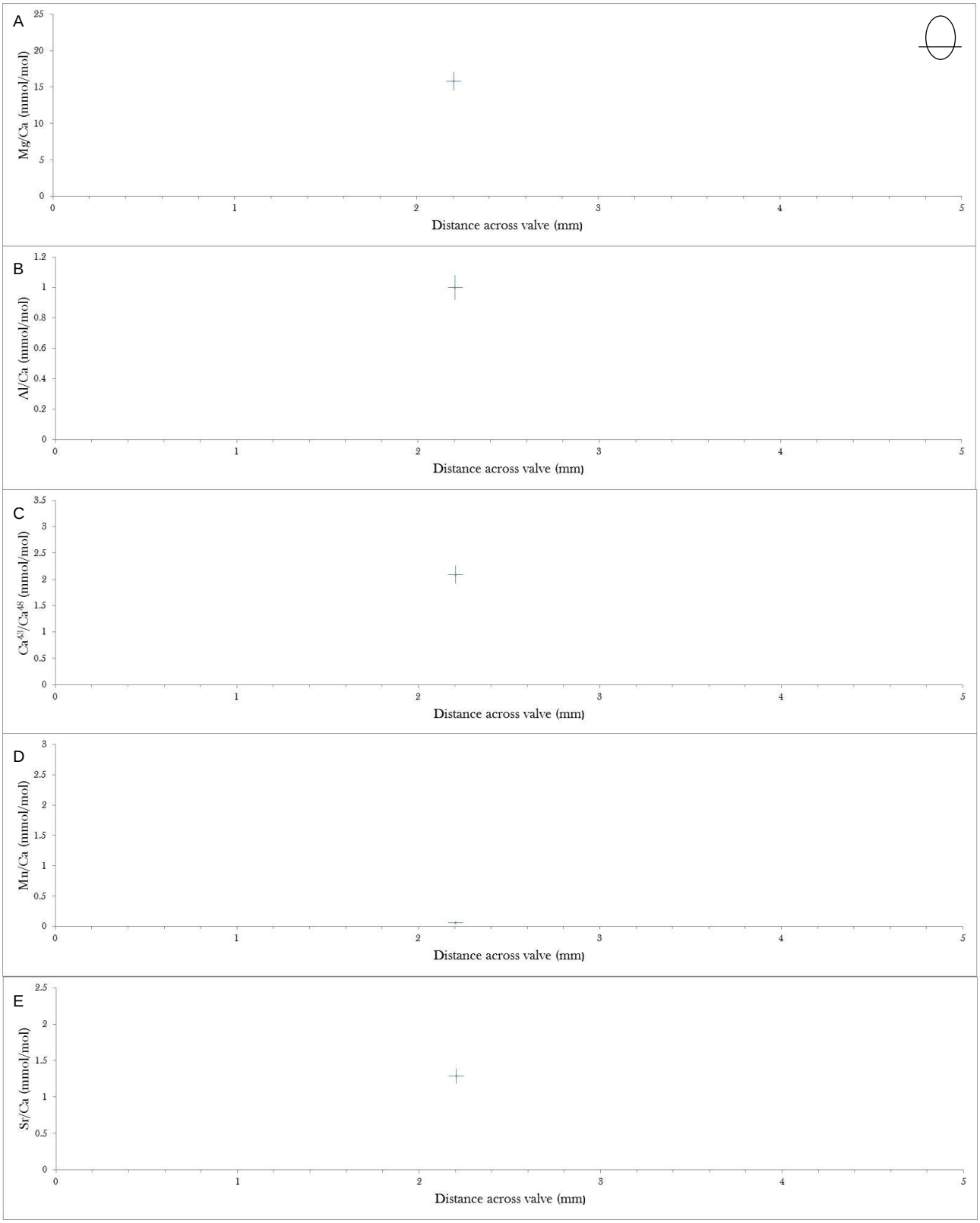
A
Mg/Ca (mmol/mol)
Distance across valve (mm)
B
Al/Ca (mmol/mol)
Distance across valve (mm)
C
Ca43/Ca48 (mmol/mol)
Distance across valve (mm)
D
Mn/Ca (mmol/mol)
Distance across valve (mm)
E
Sr/Ca (mmol/mol)
Distance across valve (mm)

MCTER2

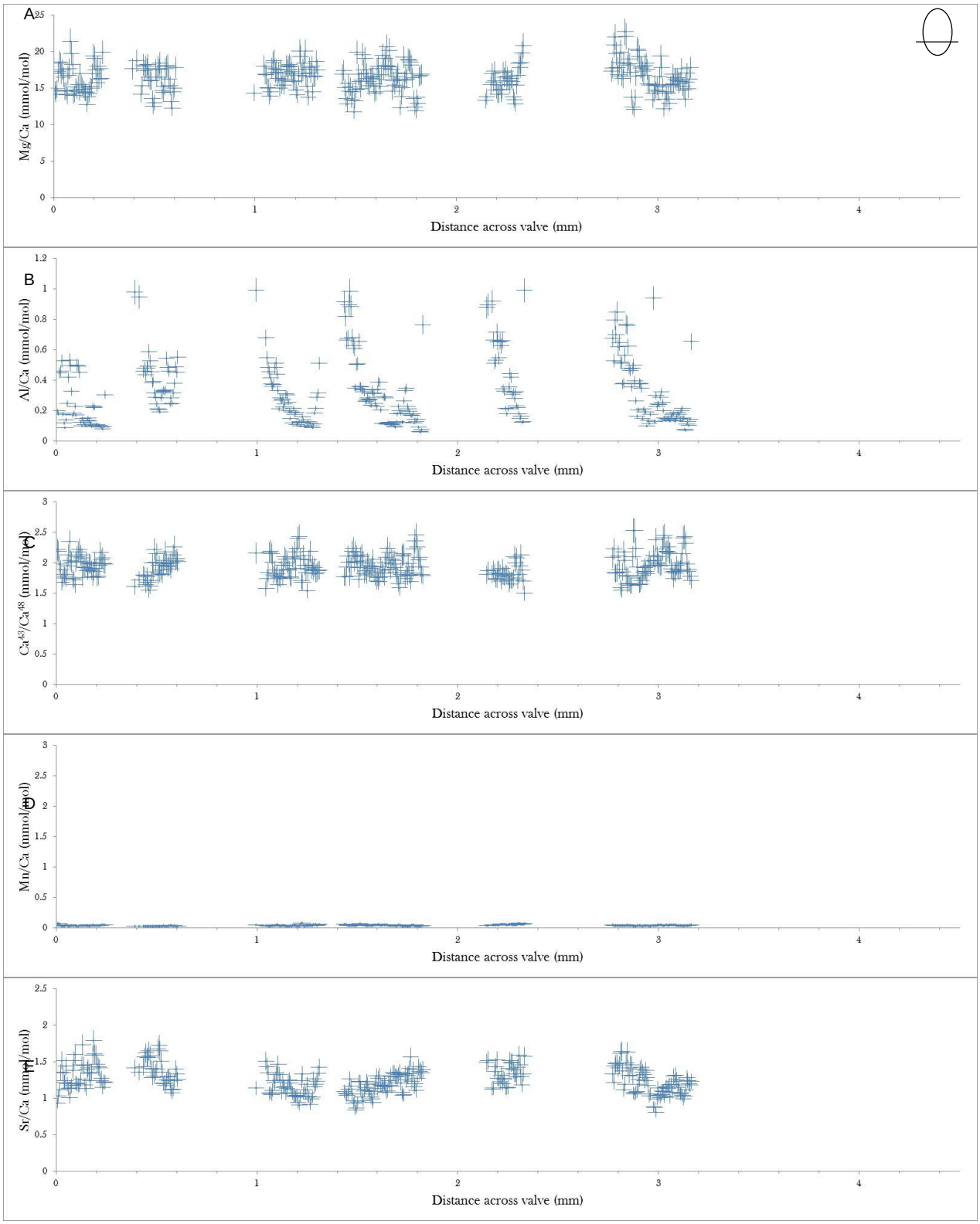
A
Mg/Ca (mmol/mol)
Distance across valve (mm)
B
Al/Ca (mmol/mol)
Distance across valve (mm)
C
Ca43/Ca48 (mmol/mol)
Distance across valve (mm)
D
Mn/Ca (mmol/mol)
Distance across valve (mm)
E
Sr/Ca (mmol/mol)
Distance across valve (mm)

MCTER3

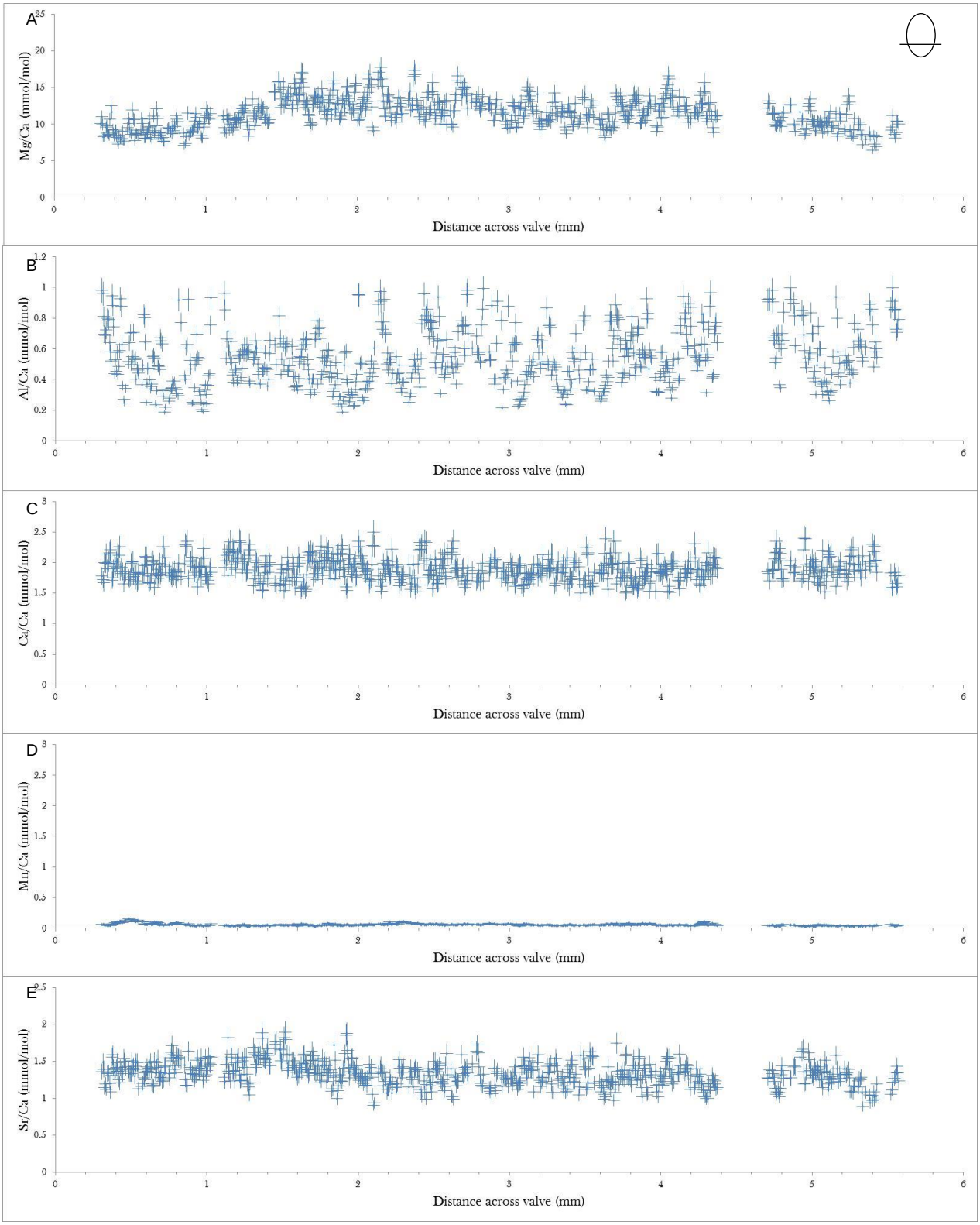
A
Mg/Ca (mmol/mol)
Distance across valve (mm)
B
Al/Ca (mmol/mol)
Distance across valve (mm)
C
Ca/Ca (mmol/mol)
Distance across valve (mm)
D
Mn/Ca (mmol/mol)
Distance across valve (mm)
E
Sr/Ca (mmol/mol)
Distance across valve (mm)

MCTER4

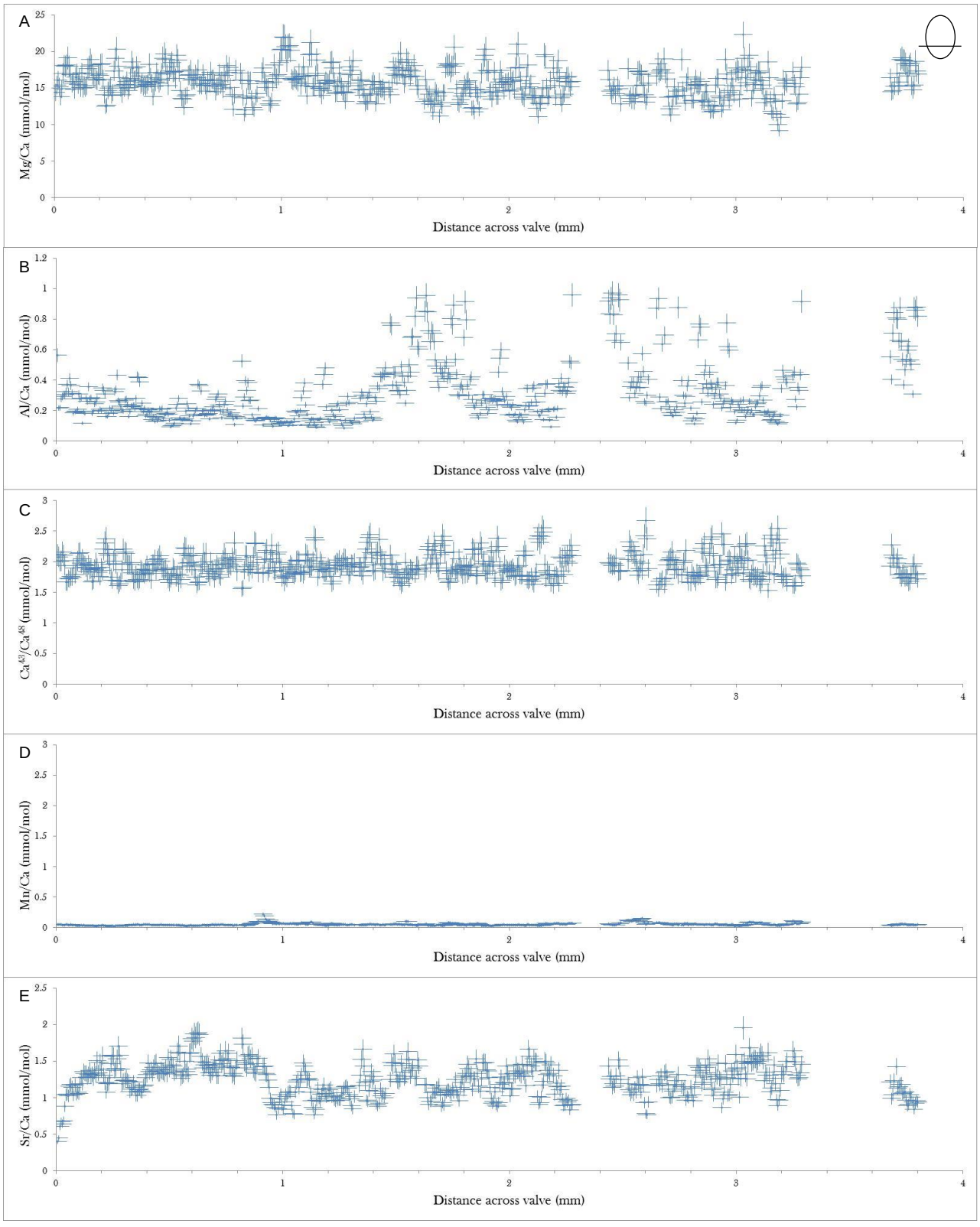
A
Mg/Ca (mmol/mol)
Distance across valve (mm)
B
Al/Ca (mmol/mol)
Distance across valve (mm)
C
Ca^{43}/Ca^{48} (mmol/mol)
Distance across valve (mm)
D
Mn/Ca (mmol/mol)
Distance across valve (mm)
E
Sr/Ca (mmol/mol)
Distance across valve (mm)

MCTER5

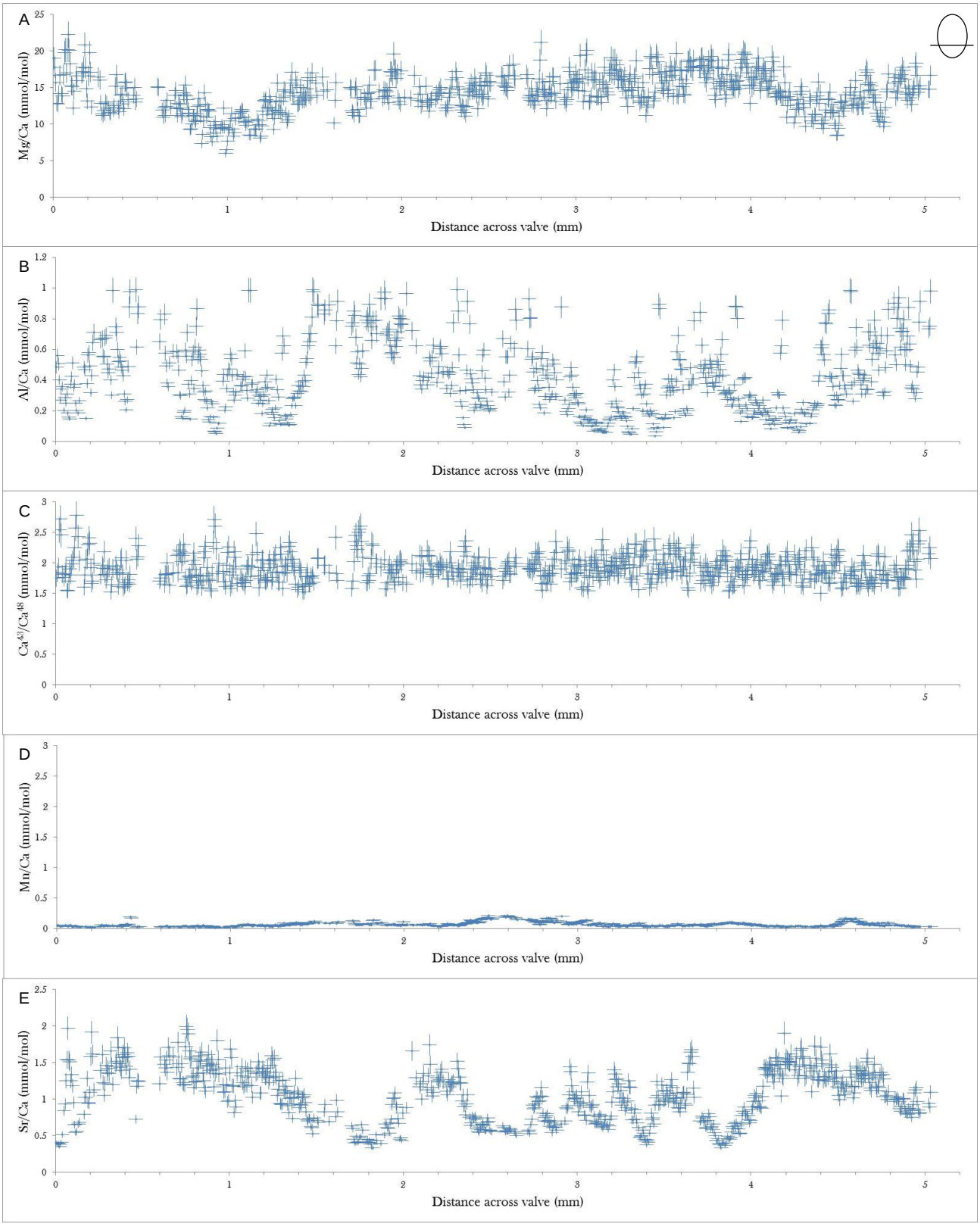
A
Mg/Ca (mmol/mol)
Distance across valve (mm)
B
Al/Ca (mmol/mol)
Distance across valve (mm)
C
Ca43/Ca48 (mmol/mol)
Distance across valve (mm)
D
Mn/Ca (mmol/mol)
Distance across valve (mm)
E
Sr/Ca (mmol/mol)
Distance across valve (mm)

The following graphs are all from specimens of *Liothyrella concentrica* from Trig M, Eocene of North Otago, New Zealand. In TMLIO1, TMLIO2, TMLIO3, TMLIO4 and TMLIO5 each graph represents the following:

A) Mg/Ca across a transverse section.

B) Al/Ca across a transverse section.

C) Ca/Ca across a transverse section.

D) Mn/Ca across a transverse section.

E) Sr/Ca across a transverse section.

TMLIO1

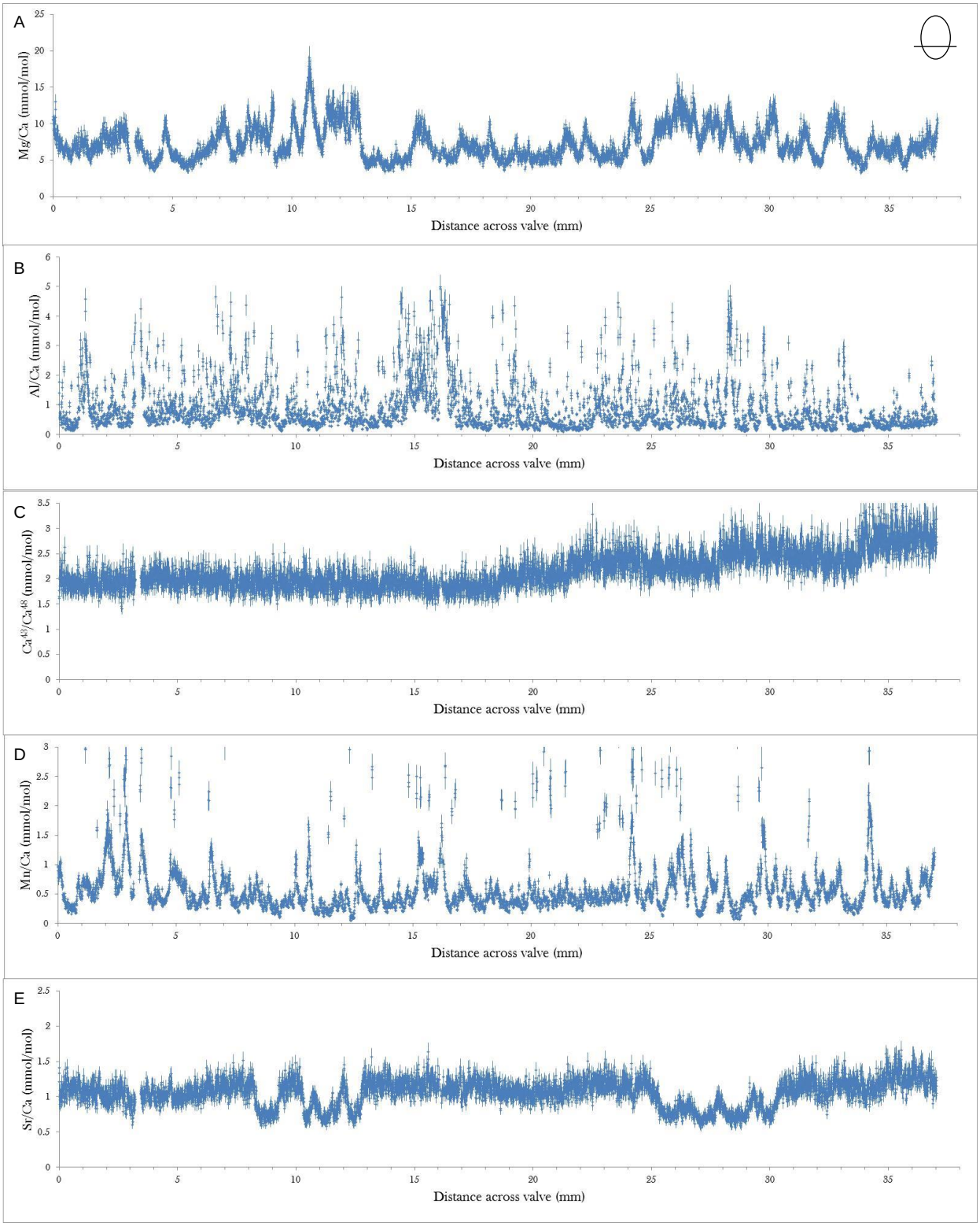
A
Mg/Ca (mmol/mol)
Distance across valve (mm)
B
Al/Ca (mmol/mol)
Distance across valve (mm)
C
Ca43/Ca48 (mmol/mol)
Distance across valve (mm)
D
Mn/Ca (mmol/mol)
Distance across valve (mm)
E
Sr/Ca (mmol/mol)
Distance across valve (mm)

TMLIO2

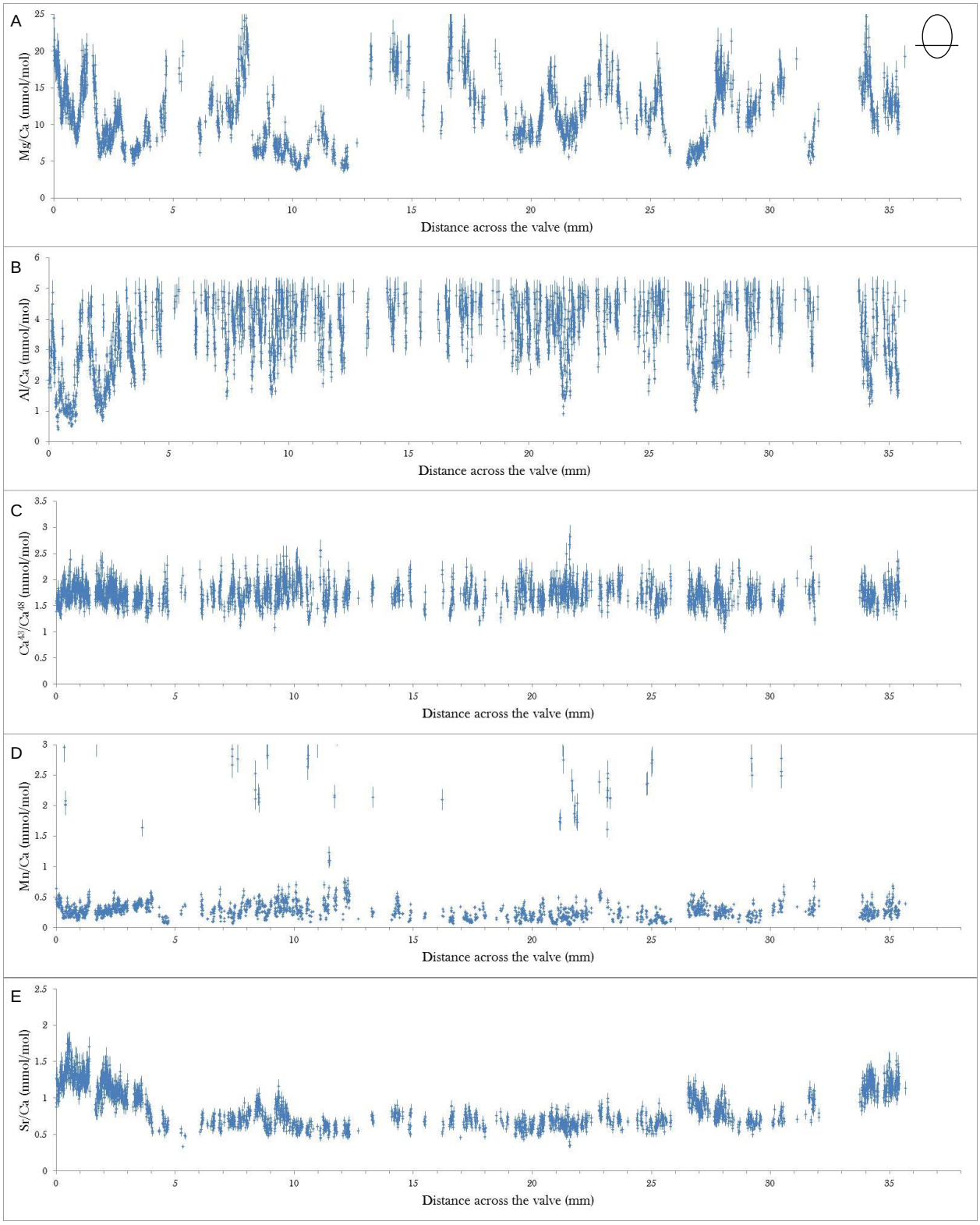
A
Mg/Ca (mmol/mol)
Distance across the valve (mm)
B
Al/Ca (mmol/mol)
Distance across the valve (mm)
C
Ca43/Ca48 (mmol/mol)
Distance across the valve (mm)
D
Mn/Ca (mmol/mol)
Distance across the valve (mm)
E
Sr/Ca (mmol/mol)
Distance across the valve (mm)

TMLIO3

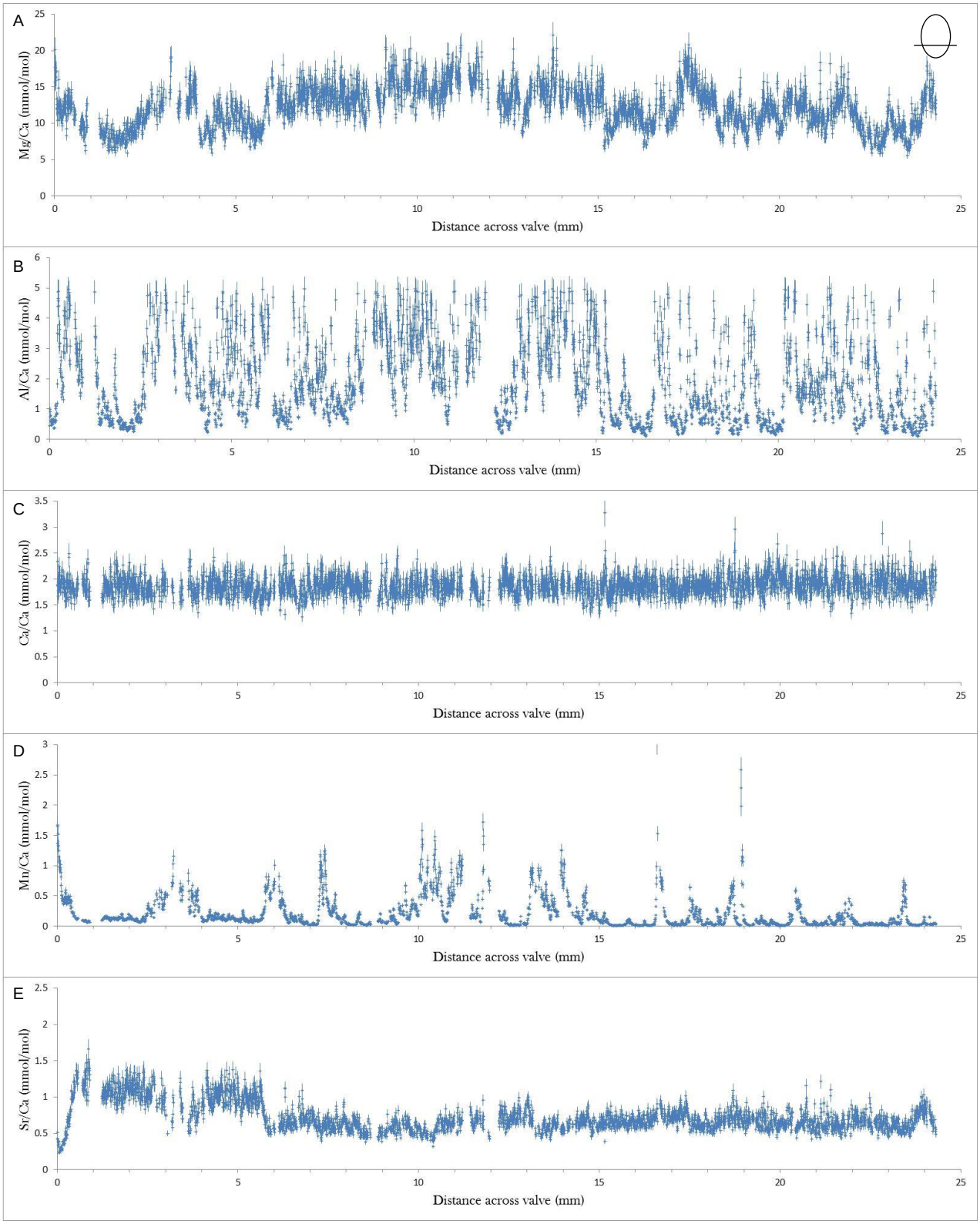
A
Mg/Ca (mmol/mol)
Distance across valve (mm)
B
Al/Ca (mmol/mol)
Distance across valve (mm)
C
Ca/Ca (mmol/mol)
Distance across valve (mm)
D
Mn/Ca (mmol/mol)
Distance across valve (mm)
E
Sr/Ca (mmol/mol)
Distance across valve (mm)

TMLIO4

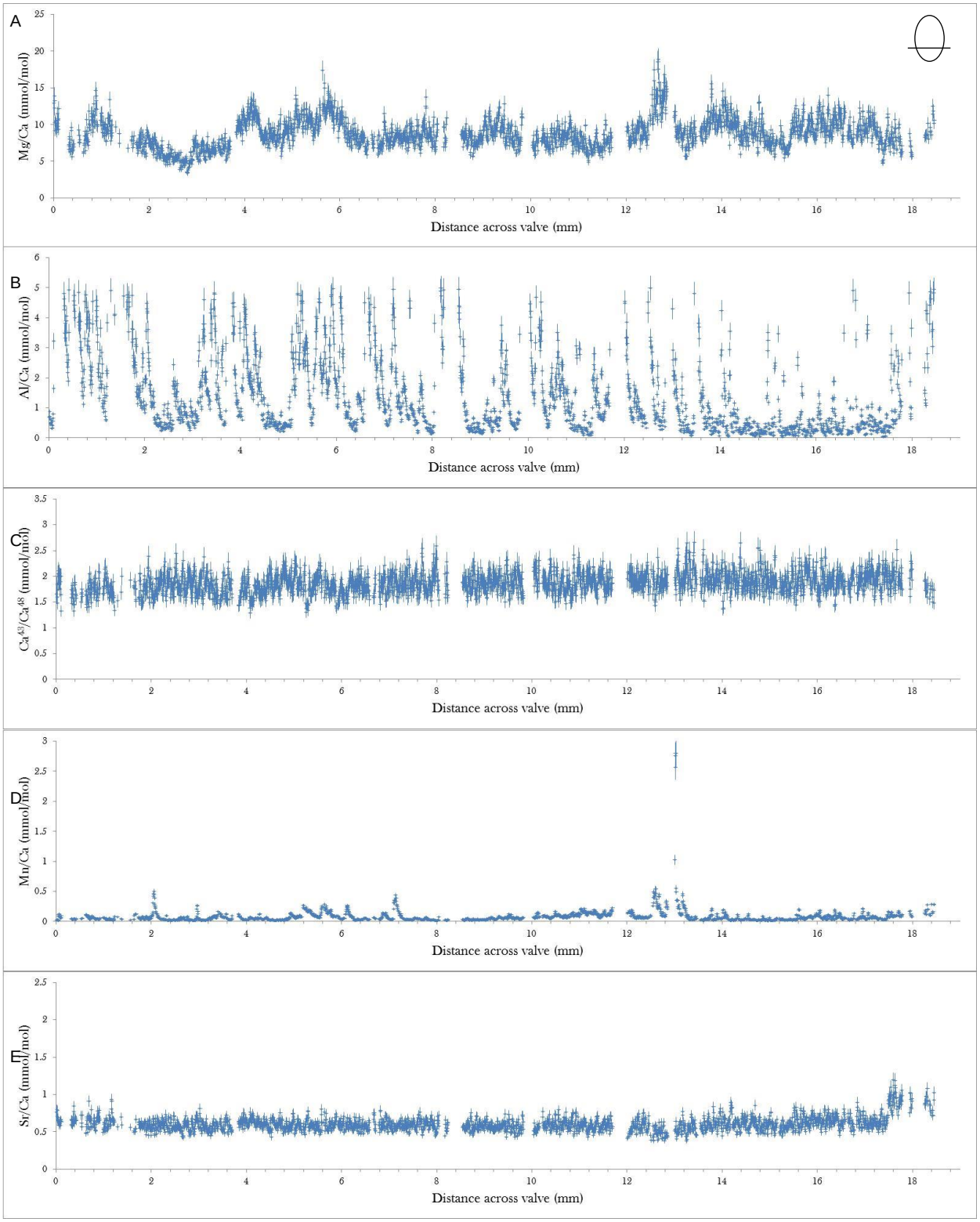
A
Mg/Ca (mmol/mol)
Distance across valve (mm)
B
Al/Ca (mmol/mol)
Distance across valve (mm)
C
Ca^{43}/Ca^{48} (mmol/mol)
Distance across valve (mm)
D
Mn/Ca (mmol/mol)
Distance across valve (mm)
E
Sr/Ca (mmol/mol)
Distance across valve (mm)

TMLIO5

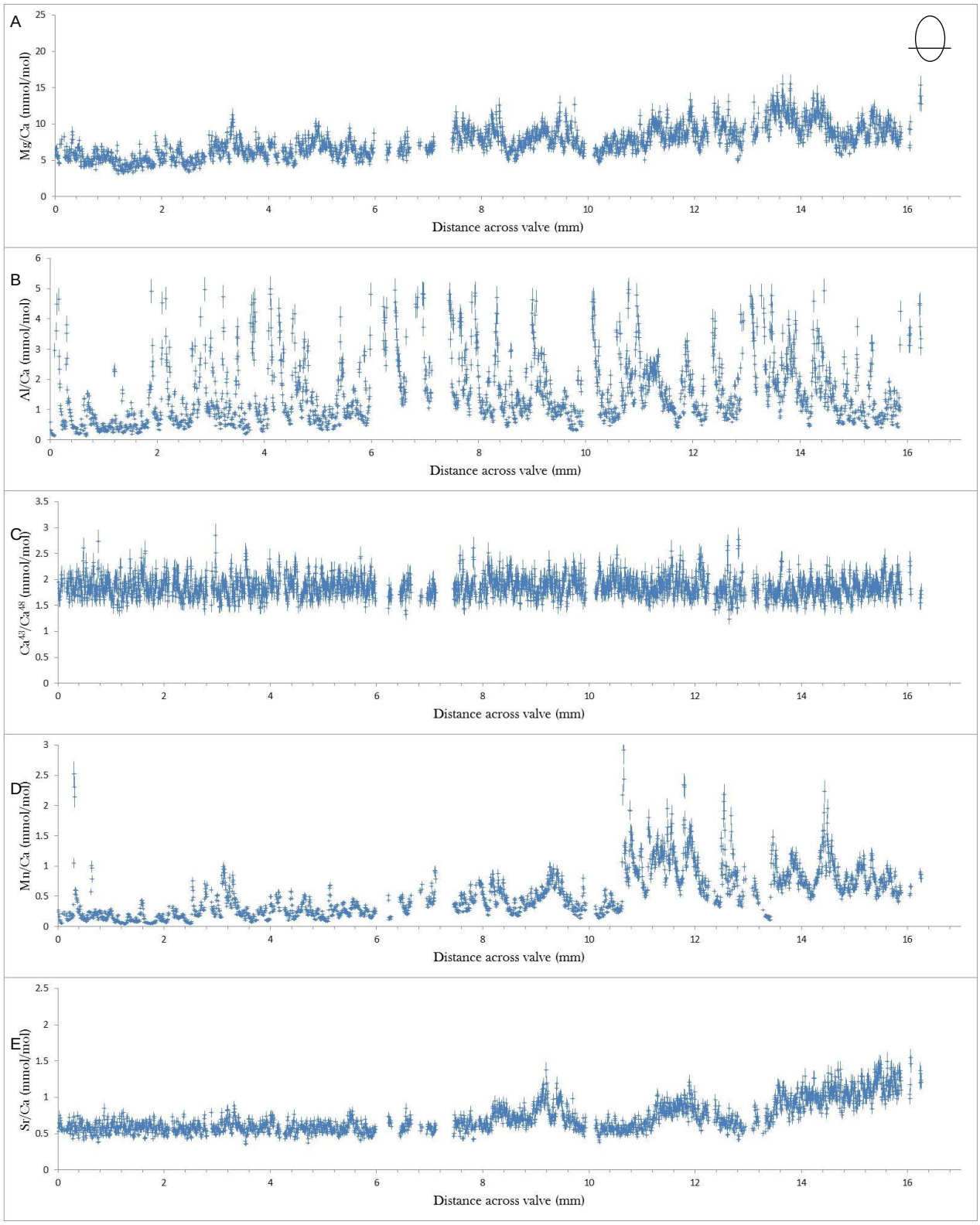
A
Mg/Ca (mmol/mol)
Distance across valve (mm)
B
Al/Ca (mmol/mol)
Distance across valve (mm)
C
Ca43/Ca48 (mmol/mol)
Distance across valve (mm)
D
Mn/Ca (mmol/mol)
Distance across valve (mm)
E
Sr/Ca (mmol/mol)
Distance across valve (mm)

The following graphs are all from specimens of *Terebratulina suessi* from Trig M, Eocene of North Otago, New Zealand. In TMTER1, TMTER2 and TMTER3 each graph represents the following:

A) Mg/Ca across a transverse section.

B) Al/Ca across a transverse section.

C) Ca/Ca across a transverse section.

D) Mn/Ca across a transverse section.

E) Sr/Ca across a transverse section.

TMTER1

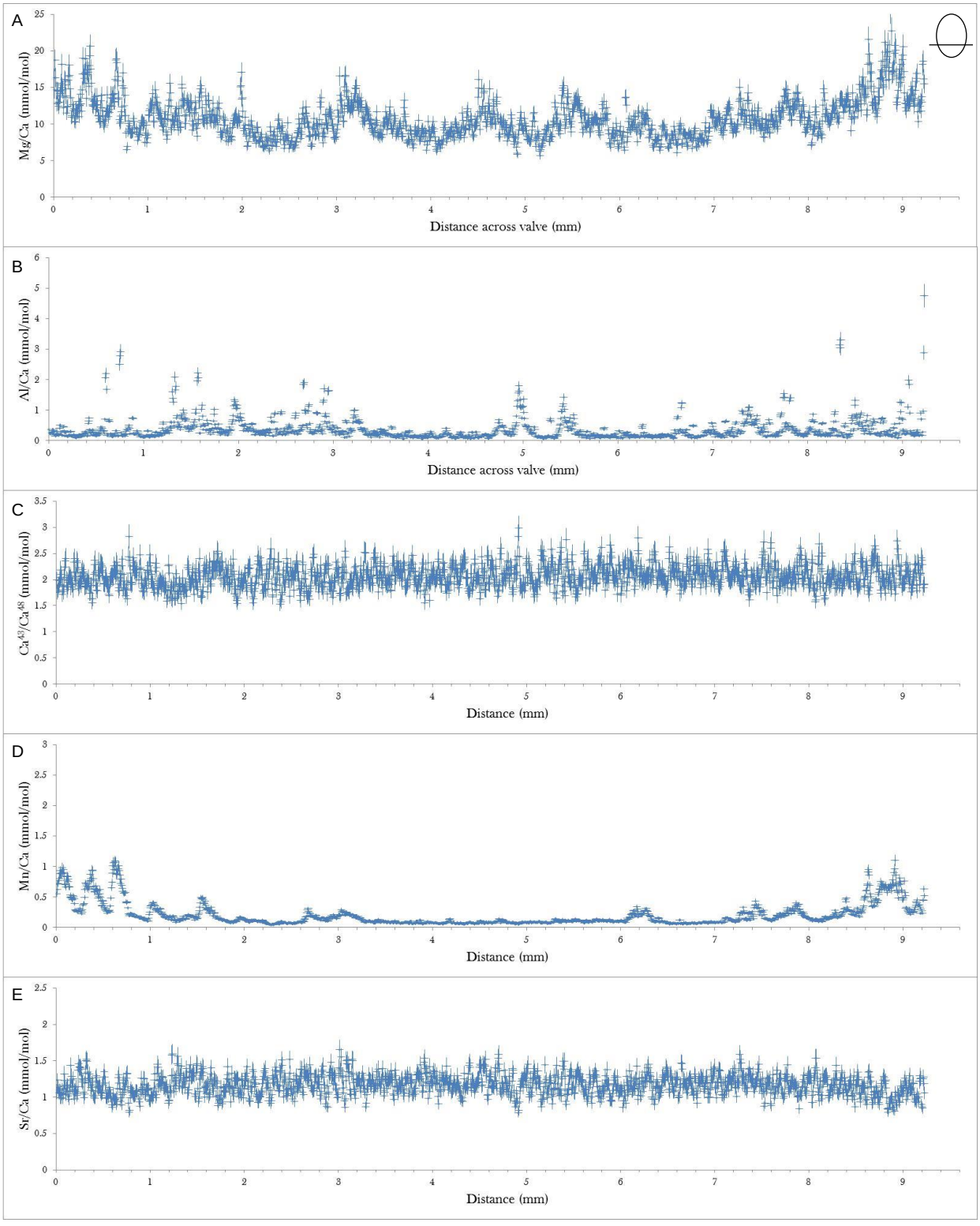
A
Mg/Ca (mmol/mol)
Distance across valve (mm)
B
Al/Ca (mmol/mol)
Distance across valve (mm)
C
Ca43/Ca48 (mmol/mol)
Distance (mm)
D
Mn/Ca (mmol/mol)
Distance (mm)
E
Sr/Ca (mmol/mol)
Distance (mm)

TMTER2

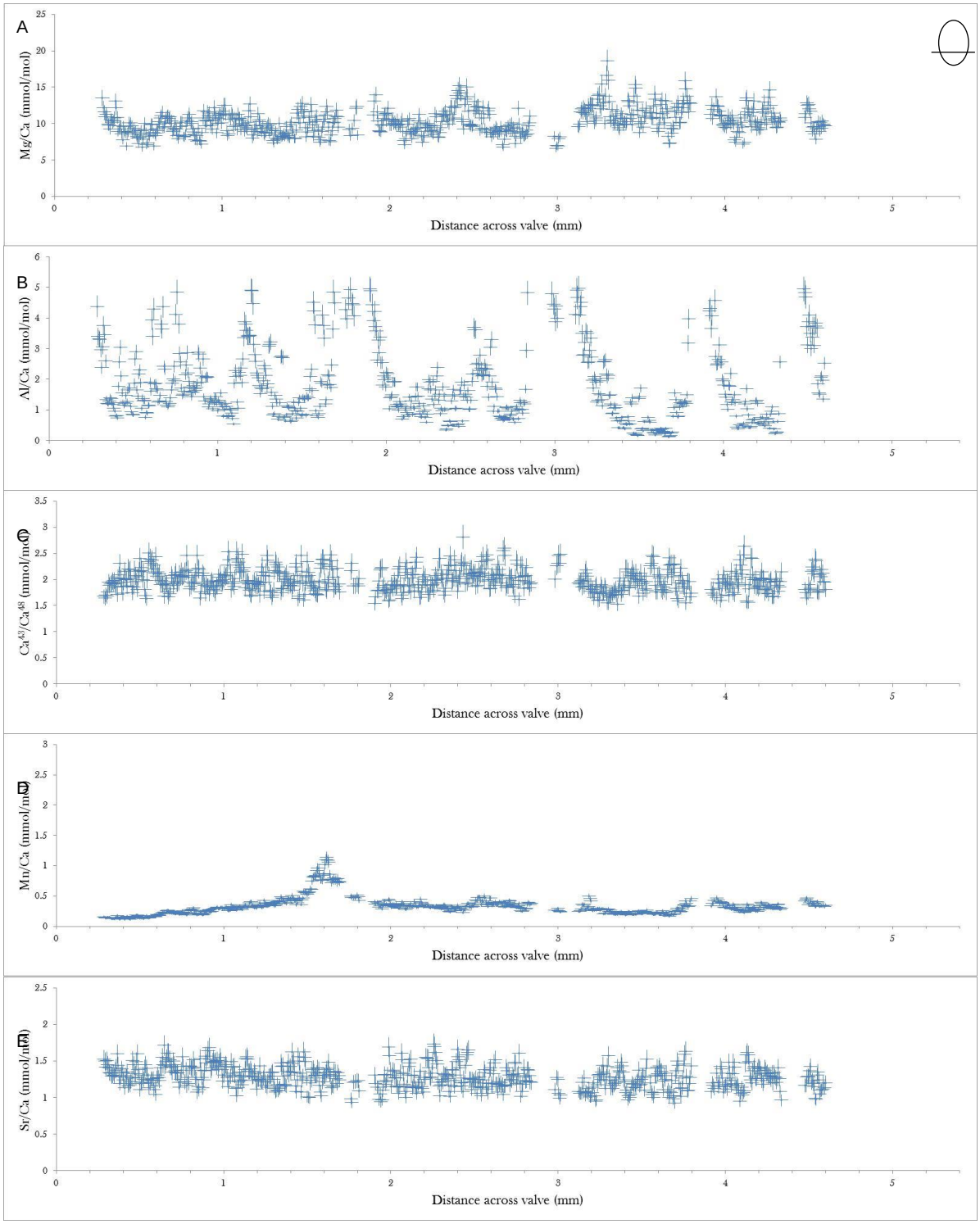
A
Mg/Ca (mmol/mol)
Distance across valve (mm)
B
Al/Ca (mmol/mol)
Distance across valve (mm)
C
Ca43/Ca48 (mmol/mol)
Distance across valve (mm)
D
Mn/Ca (mmol/mol)
Distance across valve (mm)
E
Sr/Ca (mmol/mol)
Distance across valve (mm)

TMTER3

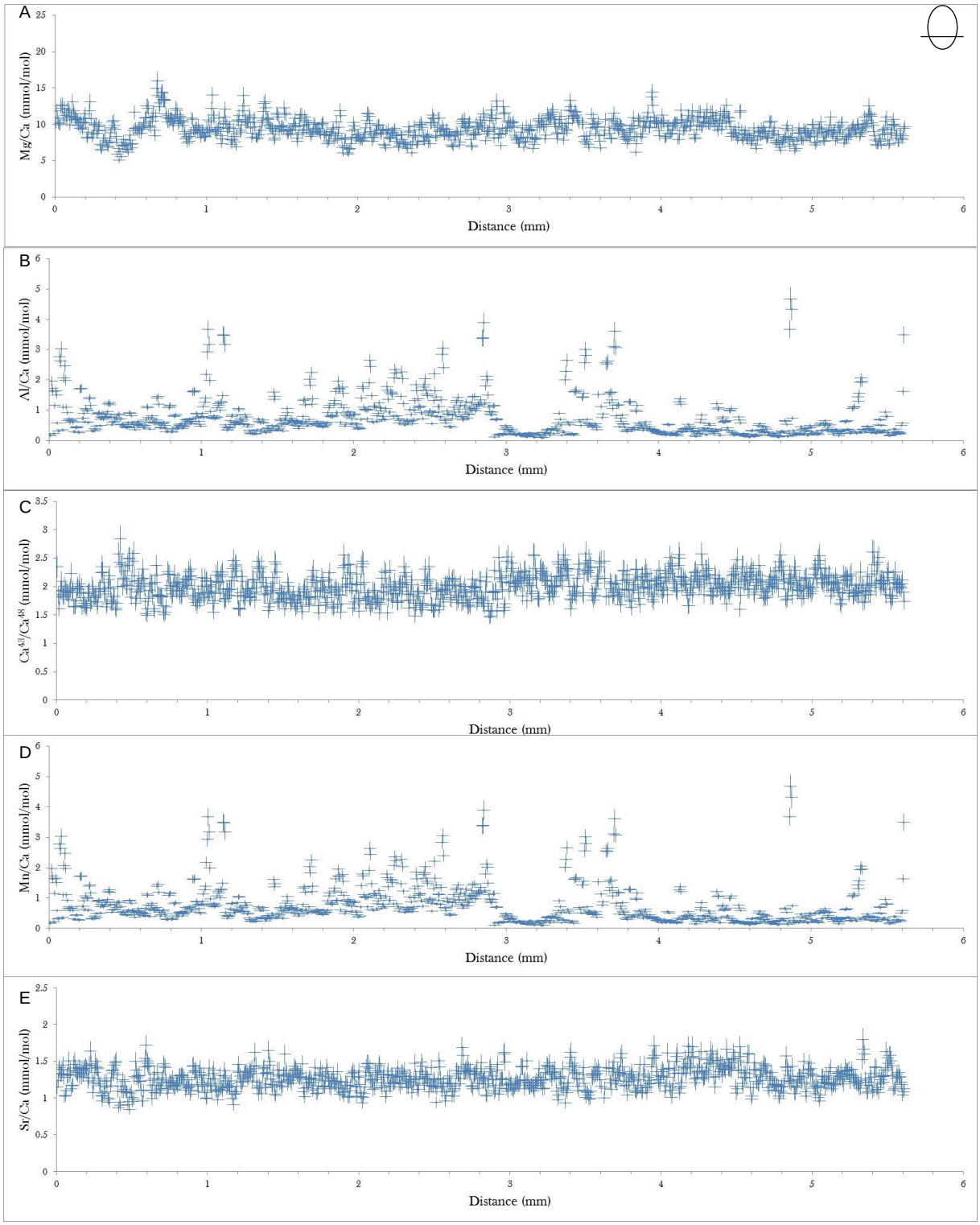
A
Mg/Ca (mmol/mol)
Distance (mm)
B
Al/Ca (mmol/mol)
Distance (mm)
C
Ca43/Ca48 (mmol/mol)
Distance (mm)
D
Mn/Ca (mmol/mol)
Distance (mm)
E
Sr/Ca (mmol/mol)
Distance (mm)

Appendix 4

The following graphs are all from specimens of *Atrypa* from North of Nyhamn, Lower Silurian of Gotland, Sweden. In NNY1 and NNY2 each graph represents the following:

A) Mg/Ca across an ontogenetic section.

B) Al/Ca across an ontogenetic section.

C) Ca^{43}/Ca^{48} across an ontogenetic section.

D) Mn/Ca across an ontogenetic section.

E) Sr/Ca across an ontogenetic section.

In NNY3 the each graph represents the following:

A) Mg/Ca across a transverse section.

B) Al/Ca across a transverse section.

C) Ca^{43}/Ca^{48} across a transverse section.

D) Mn/Ca across a transverse section.

E) Sr/Ca across a transverse section.

NNY1

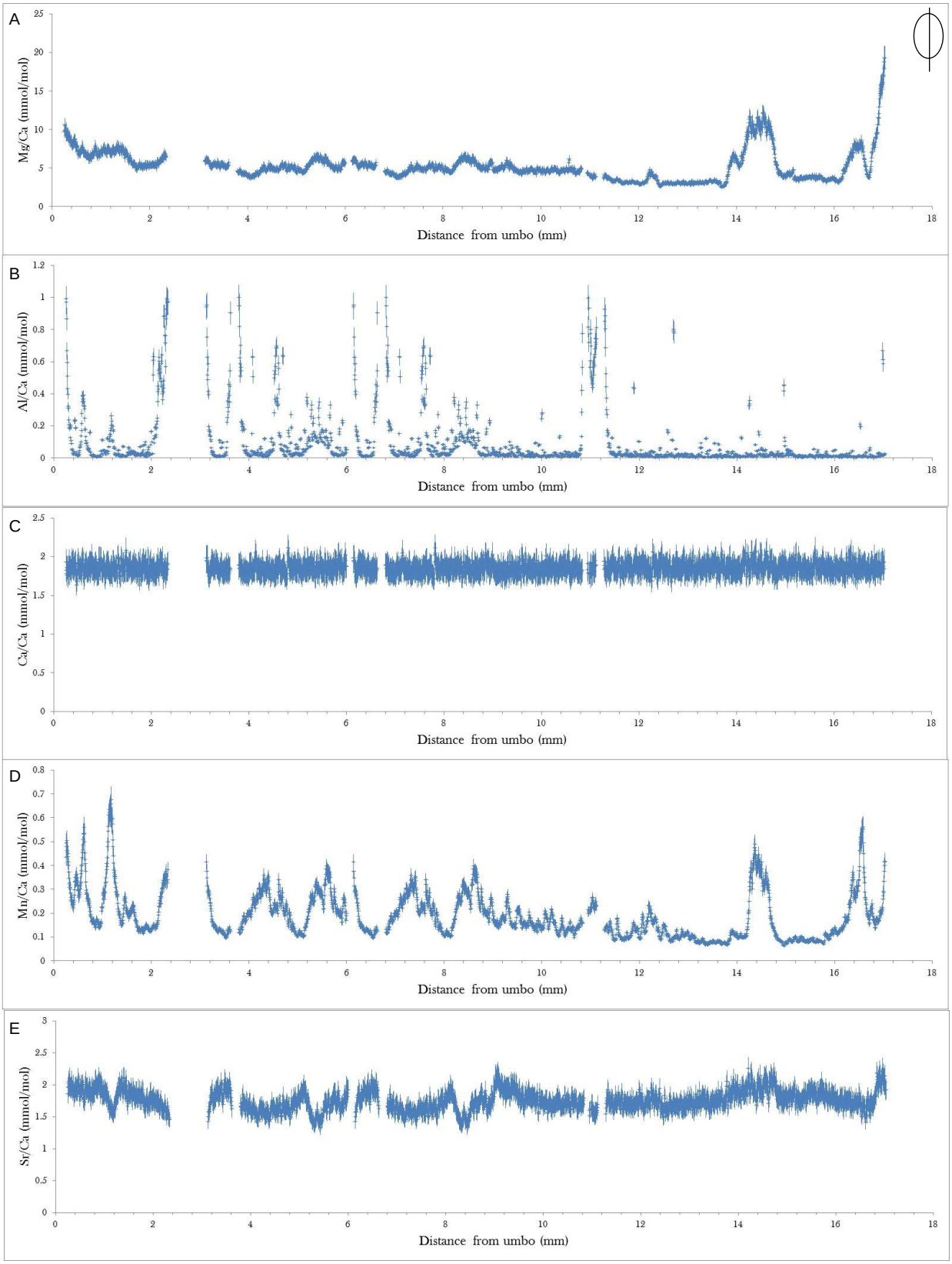
A
Mg/Ca (mmol/mol)
Distance from umbo (mm)
B
Al/Ca (mmol/mol)
Distance from umbo (mm)
C
Ca/Ca (mmol/mol)
Distance from umbo (mm)
D
Mn/Ca (mmol/mol)
Distance from umbo (mm)
E
Sr/Ca (mmol/mol)
Distance from umbo (mm)

NNY2

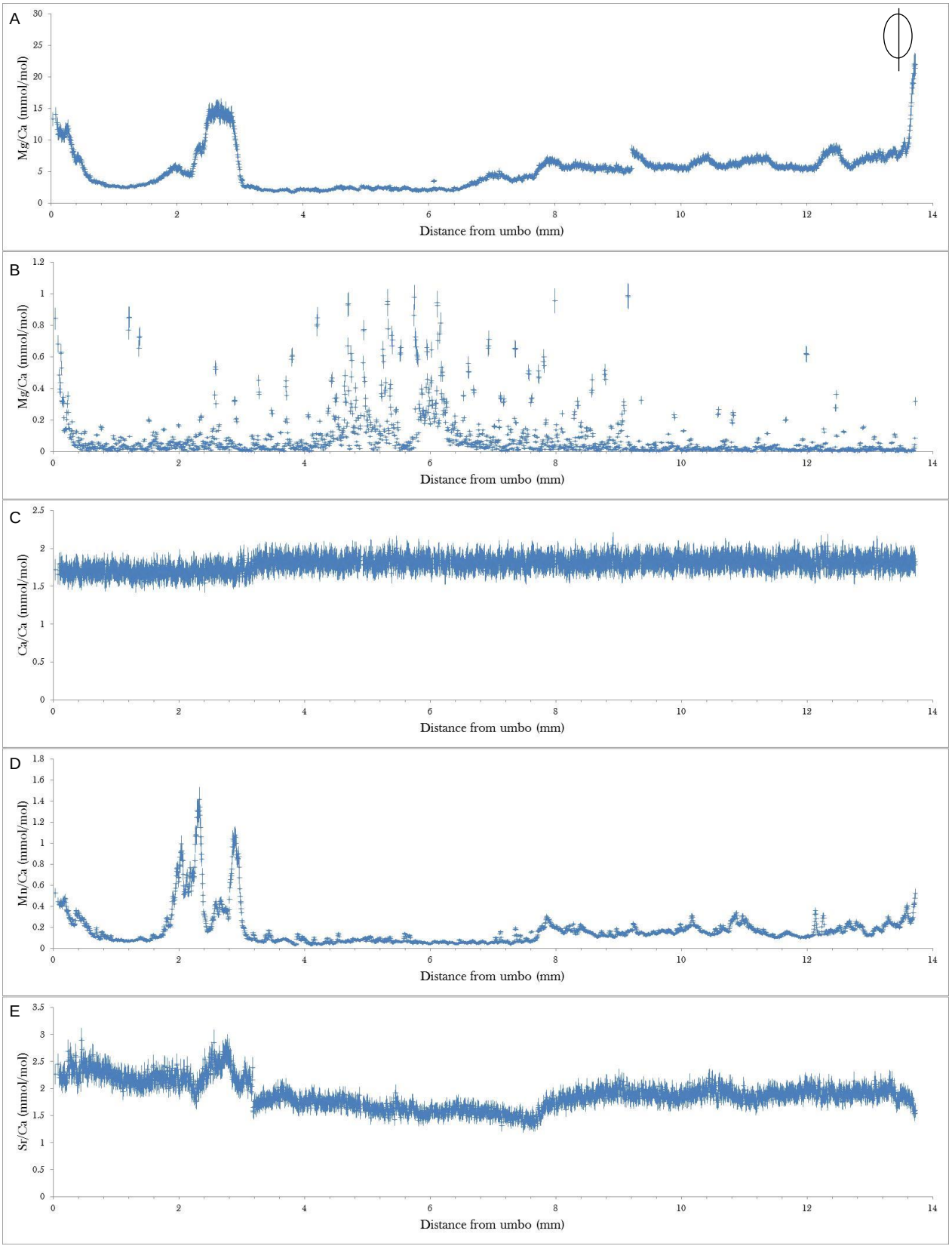
A
Mg/Ca (mmol/mol)
Distance from umbo (mm)
B
Mg/Ca (mmol/mol)
Distance from umbo (mm)
C
Ca/Ca (mmol/mol)
Distance from umbo (mm)
D
Mn/Ca (mmol/mol)
Distance from umbo (mm)
E
Sr/Ca (mmol/mol)
Distance from umbo (mm)

NNY3

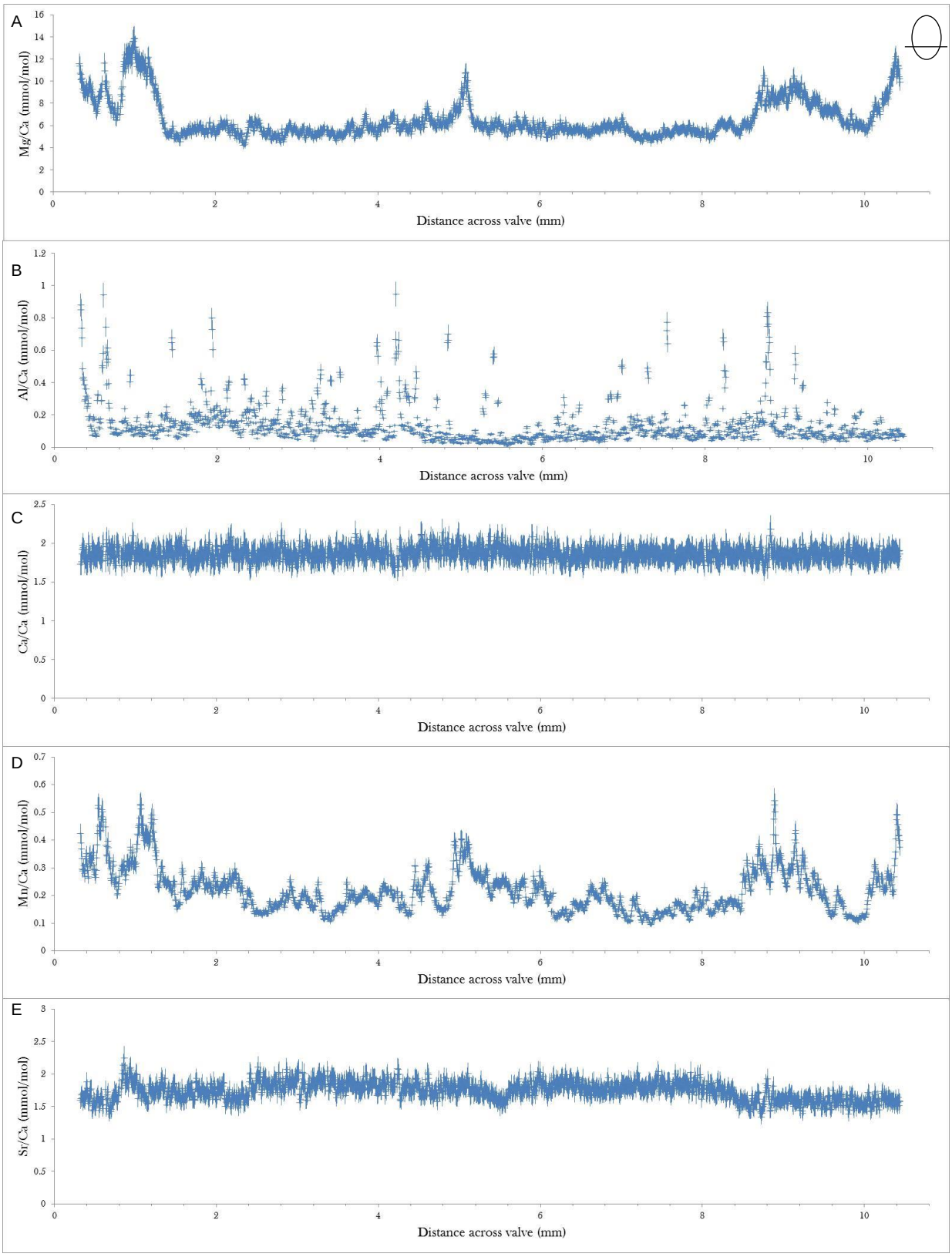
A
Mg/Ca (mmol/mol)
Distance across valve (mm)
B
Al/Ca (mmol/mol)
Distance across valve (mm)
C
Ca/Ca (mmol/mol)
Distance across valve (mm)
D
Mn/Ca (mmol/mol)
Distance across valve (mm)
E
Sr/Ca (mmol/mol)
Distance across valve (mm)

The following graphs are all from specimens of *Atrypa* from North of Nyhamn, Lower Silurian of Gotland, Sweden. In NYH1 and NYH2 each graph represents the following:

A) Mg/Ca across an ontogenetic section.

B) Al/Ca across an ontogenetic section.

C) Ca^{43}/Ca^{48} across an ontogenetic section.

D) Mn/Ca across an ontogenetic section.

E) Sr/Ca across an ontogenetic section.

In NYH3 the each graph represents the following:

A) Mg/Ca across a transverse section.

B) Al/Ca across a transverse section.

C) Ca^{43}/Ca^{48} across a transverse section.

D) Mn/Ca across a transverse section.

E) Sr/Ca across a transverse section.

NYH1

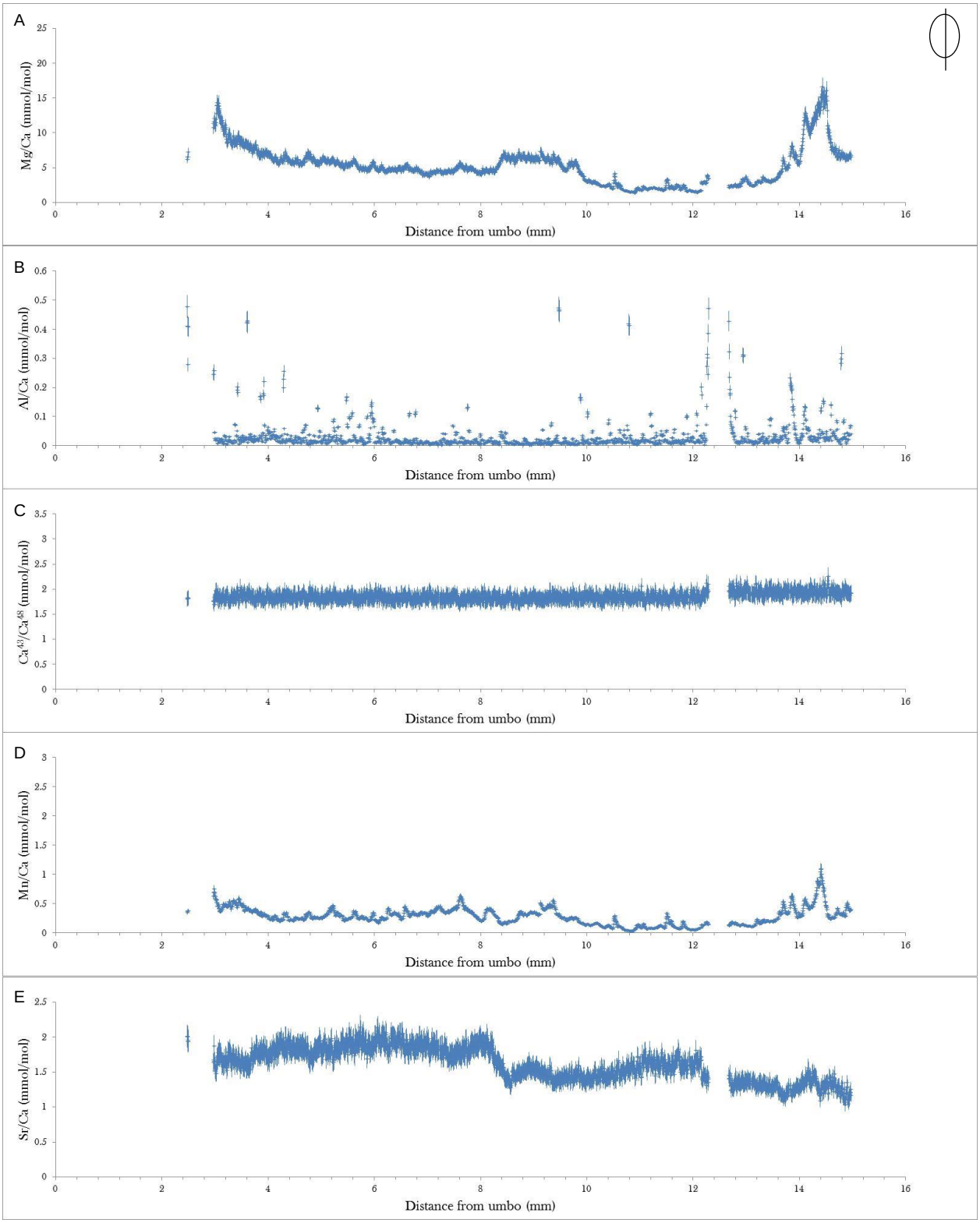
A
Mg/Ca (mmol/mol)
Distance from umbo (mm)
B
Al/Ca (mmol/mol)
Distance from umbo (mm)
C
Ca^{43}/Ca^{48} (mmol/mol)
Distance from umbo (mm)
D
Mn/Ca (mmol/mol)
Distance from umbo (mm)
E
Sr/Ca (mmol/mol)
Distance from umbo (mm)

NYH2

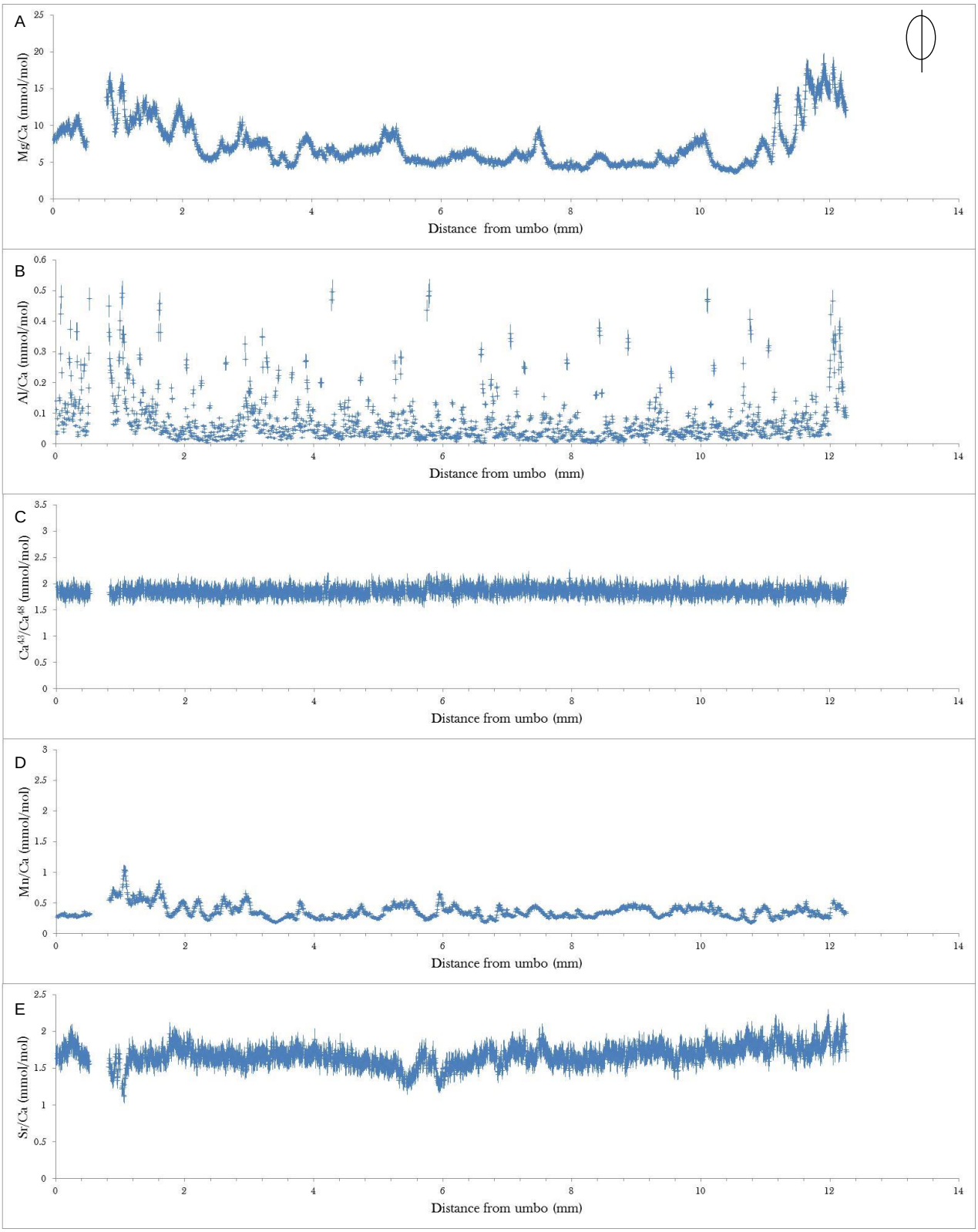
A
Mg/Ca (mmol/mol)
Distance from umbo (mm)
B
Al/Ca (mmol/mol)
Distance from umbo (mm)
C
Ca^{43}/Ca^{48} (mmol/mol)
Distance from umbo (mm)
D
Mn/Ca (mmol/mol)
Distance from umbo (mm)
E
Sr/Ca (mmol/mol)
Distance from umbo (mm)

NYH3

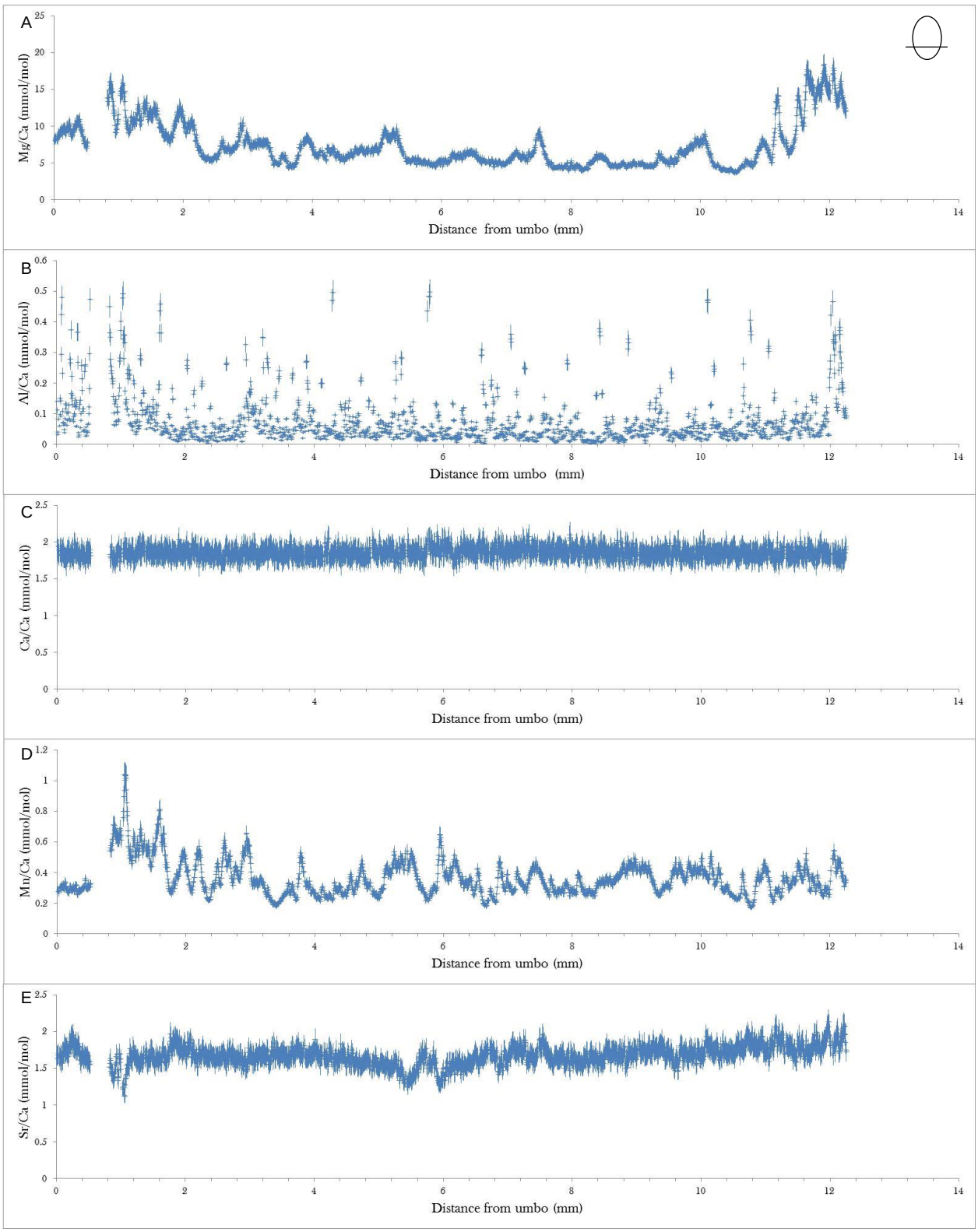
A
Mg/Ca (mmol/mol)
Distance from umbo (mm)
B
Al/Ca (mmol/mol)
Distance from umbo (mm)
C
Ca/Ca (mmol/mol)
Distance from umbo (mm)
D
Mn/Ca (mmol/mol)
Distance from umbo (mm)
E
Sr/Ca (mmol/mol)
Distance from umbo (mm)

The following graphs are all from specimens of *Atrypa* from Ireviken 3, Lower Silurian of Gotland, Sweden. In IRE1 and IRE2 each graph represents the following:

A) Mg/Ca across an ontogenetic section.

B) Al/Ca across an ontogenetic section.

C) Ca^{43}/Ca^{48} across an ontogenetic section.

D) Mn/Ca across an ontogenetic section.

E) Sr/Ca across an ontogenetic section.

In IRE3 the each graph represents the following:

A) Mg/Ca across a transverse section.

B) Al/Ca across a transverse section.

C) Ca^{43}/Ca^{48} across a transverse section.

D) Mn/Ca across a transverse section.

E) Sr/Ca across a transverse section.

IRE1

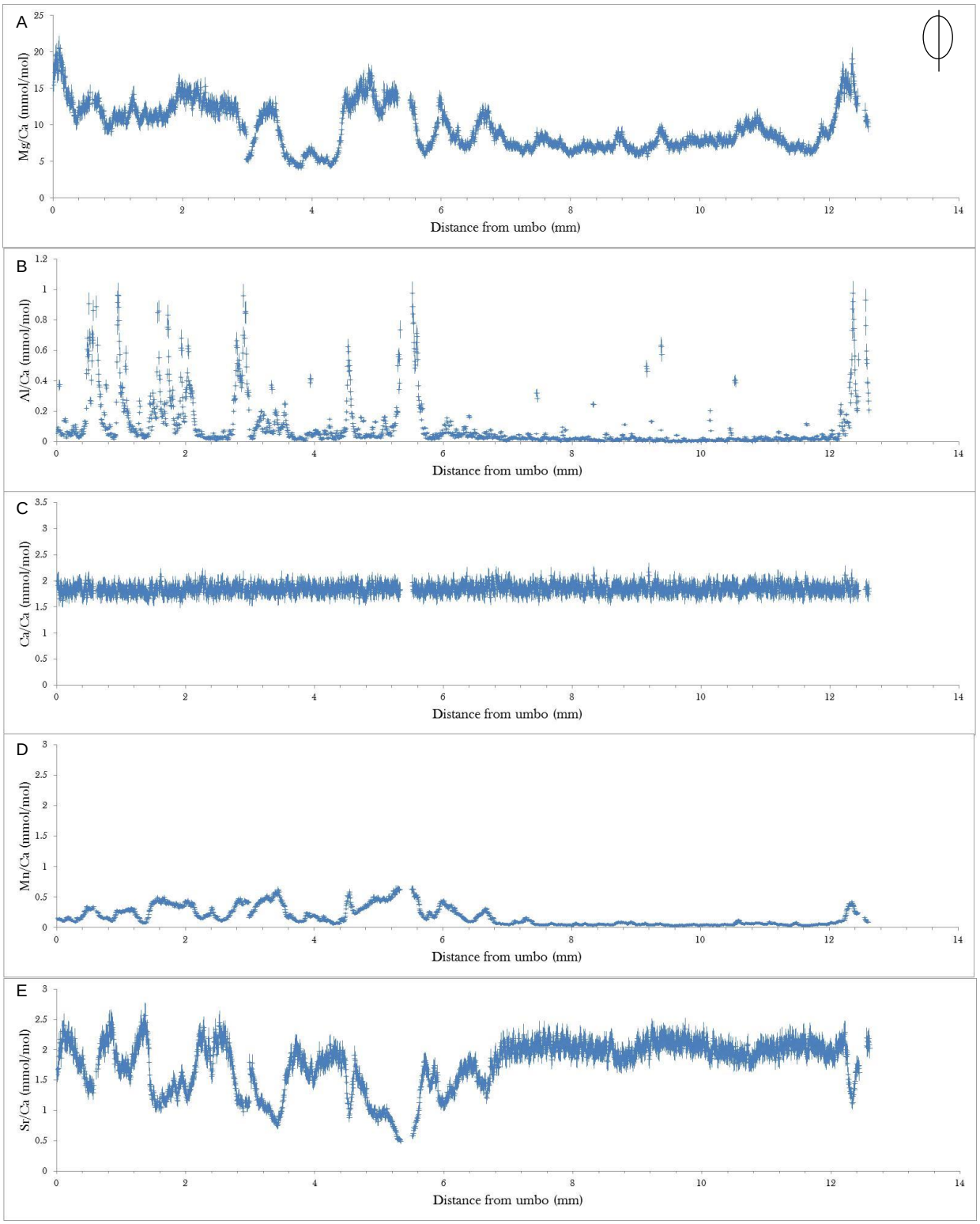
A
Mg/Ca (mmol/mol)
Distance from umbo (mm)
B
Al/Ca (mmol/mol)
Distance from umbo (mm)
C
Ca/Ca (mmol/mol)
Distance from umbo (mm)
D
Mn/Ca (mmol/mol)
Distance from umbo (mm)
E
Sr/Ca (mmol/mol)
Distance from umbo (mm)

IRE2

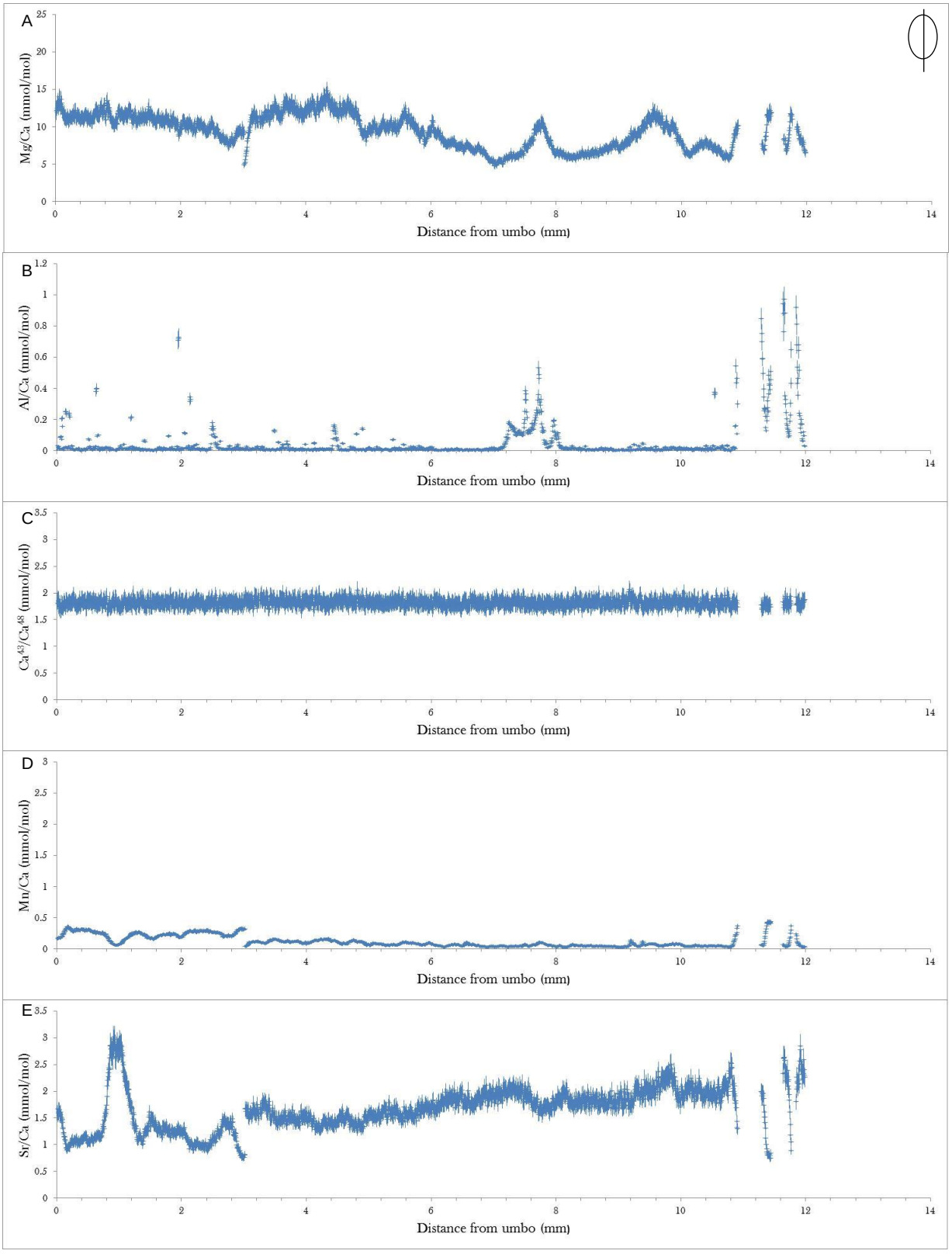
A
Mg/Ca (mmol/mol)
Distance from umbo (mm)
B
Al/Ca (mmol/mol)
Distance from umbo (mm)
C
Ca43/Ca48 (mmol/mol)
Distance from umbo (mm)
D
Mn/Ca (mmol/mol)
Distance from umbo (mm)
E
Sr/Ca (mmol/mol)
Distance from umbo (mm)

IRE3

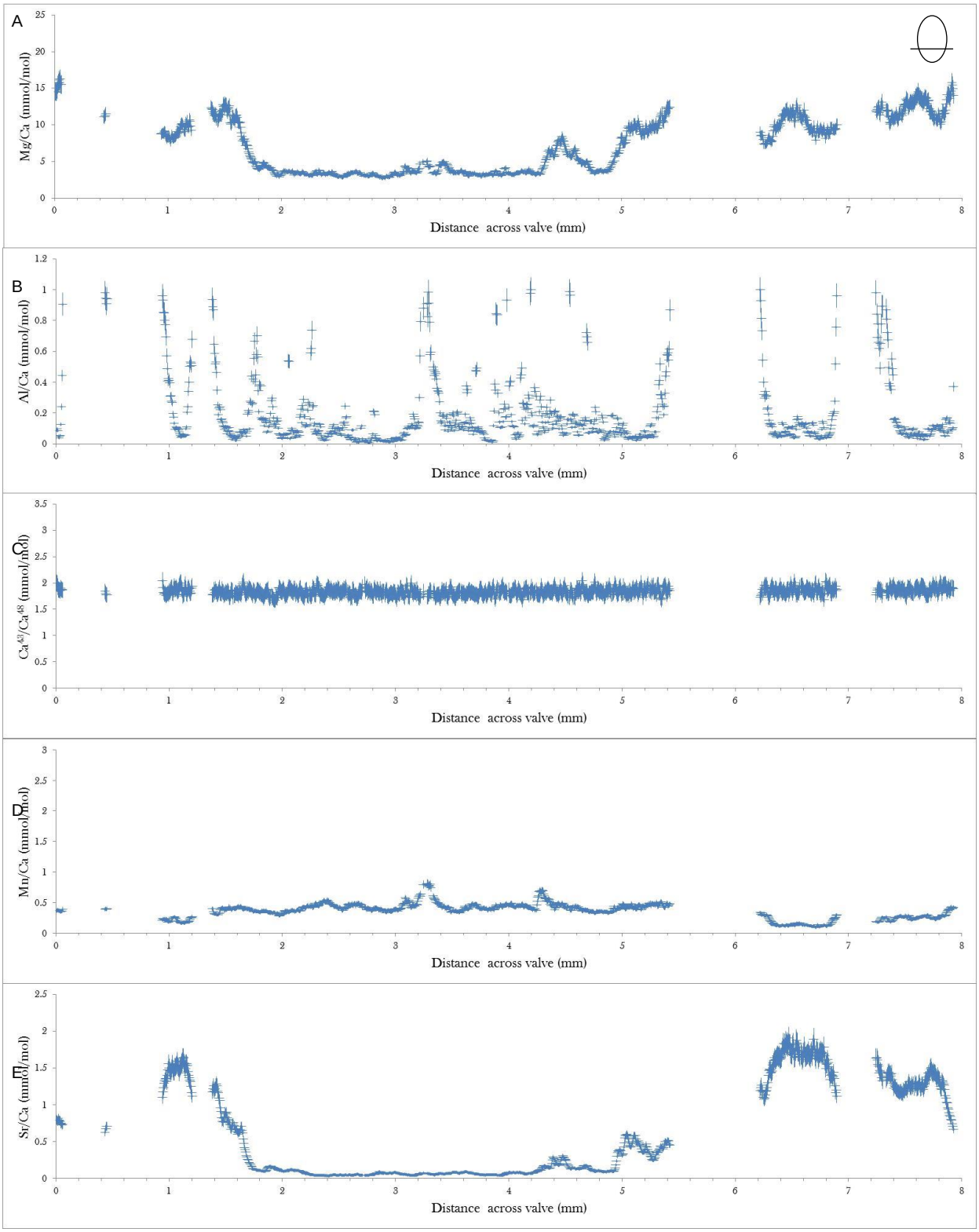
A
Mg/Ca (mmol/mol)
Distance across valve (mm)
B
Al/Ca (mmol/mol)
Distance across valve (mm)
C
Ca43/Ca48 (mmol/mol)
Distance across valve (mm)
D
Mn/Ca (mmol/mol)
Distance across valve (mm)
E
Sr/Ca (mmol/mol)
Distance across valve (mm)

The following graphs are all from specimens of *Atrypa* from Ygne, Lower Silurian of Gotland, Sweden. In YGNE1 and YGNE2 each graph represents the following:

A) Mg/Ca across an ontogenetic section.

B) Al/Ca across an ontogenetic section.

C) Ca^{43}/Ca^{48} across an ontogenetic section.

D) Mn/Ca across an ontogenetic section.

E) Sr/Ca across an ontogenetic section.

In YGNE3 the each graph represents the following:

A) Mg/Ca across a transverse section.

B) Al/Ca across a transverse section.

C) Ca^{43}/Ca^{48} across a transverse section.

D) Mn/Ca across a transverse section.

E) Sr/Ca across a transverse section.

YGNE1

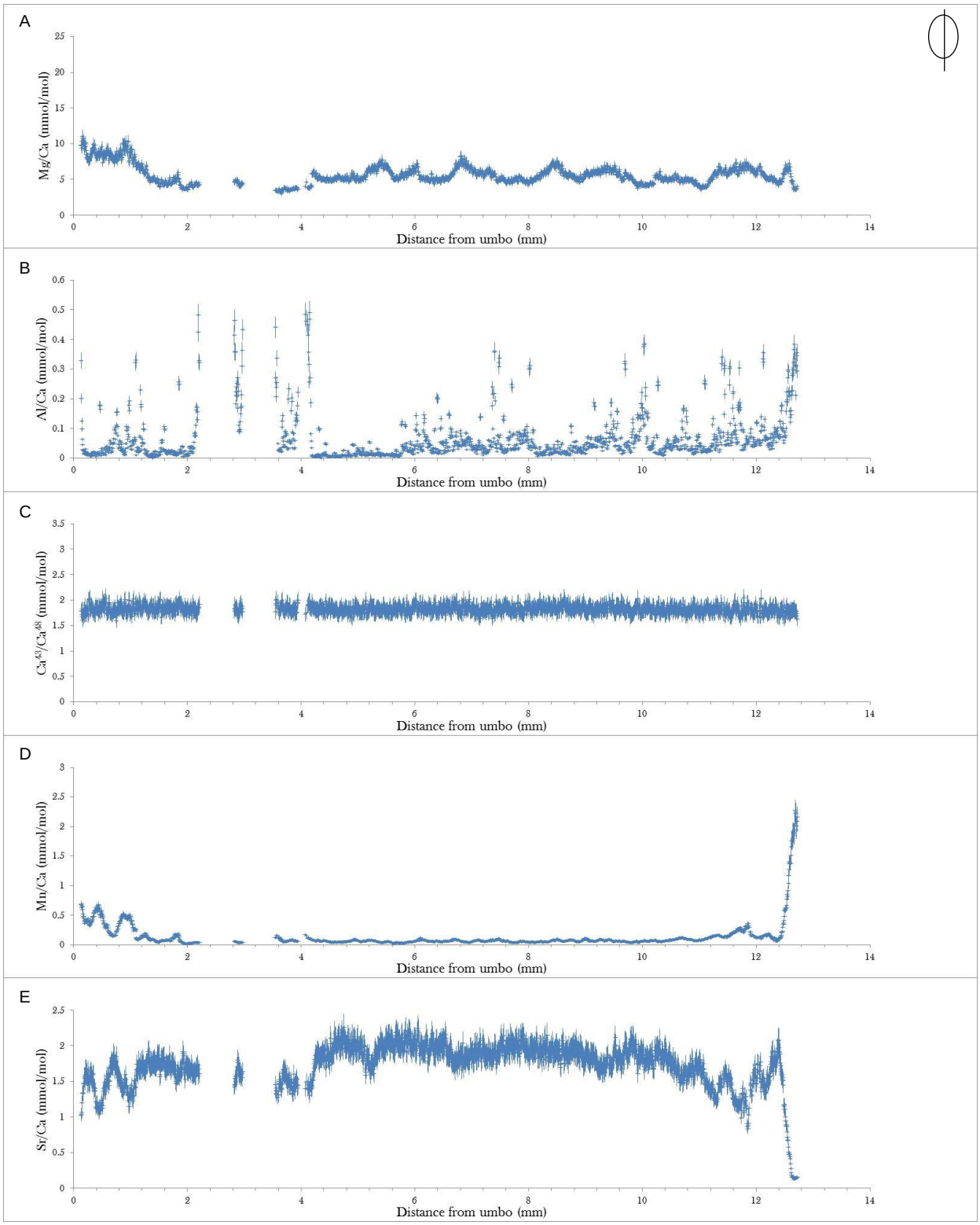
A
Mg/Ca (mmol/mol)
Distance from umbo (mm)
B
Al/Ca (mmol/mol)
Distance from umbo (mm)
C
Ca43/Ca48 (mmol/mol)
Distance from umbo (mm)
D
Mn/Ca (mmol/mol)
Distance from umbo (mm)
E
Sr/Ca (mmol/mol)
Distance from umbo (mm)

YGNE2

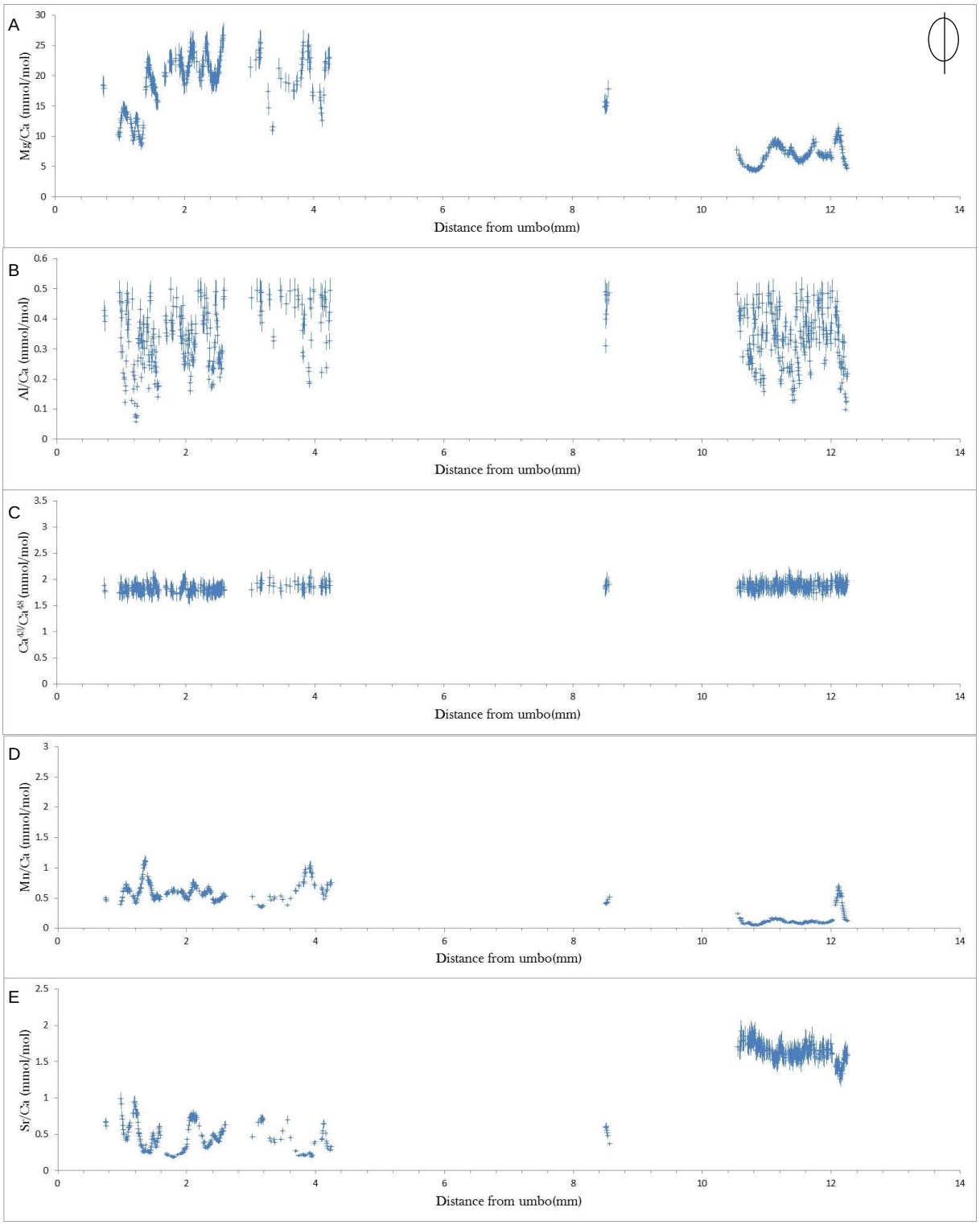
A
Mg/Ca (mmol/mol)
Distance from umbo(mm)
B
Al/Ca (mmol/mol)
Distance from umbo(mm)
C
Ca^{43}/Ca^{48} (mmol/mol)
Distance from umbo(mm)
D
Mn/Ca (mmol/mol)
Distance from umbo(mm)
E
Sr/Ca (mmol/mol)
Distance from umbo(mm)

YGNE3

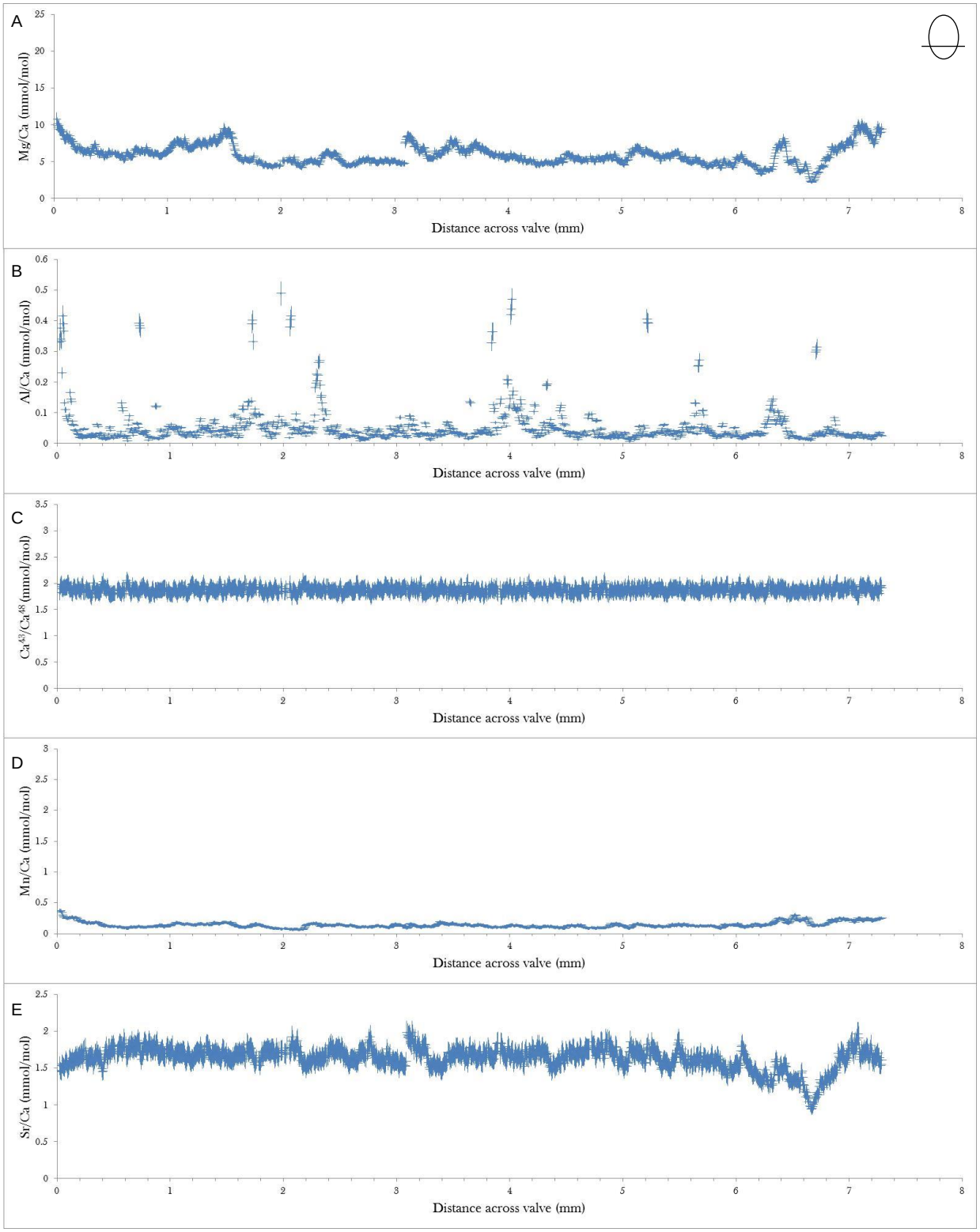
A
Mg/Ca (mmol/mol)
Distance across valve (mm)
B
Al/Ca (mmol/mol)
Distance across valve (mm)
C
Ca^{43}/Ca^{48} (mmol/mol)
Distance across valve (mm)
D
Mn/Ca (mmol/mol)
Distance across valve (mm)
E
Sr/Ca (mmol/mol)
Distance across valve (mm)